Université de Montréal

Pharmacokinetic/pharmacodynamic relationship of pulmonary administration methods for milrinone: A translational approach

par
Paul Gavra

Faculté de Pharmacie

Thèse présentée à la Faculté des Études Supérieures
en vue de l'obtention du grade de
Philosophiae Doctor en Sciences Pharmaceutiques
Option pharmacologie

Août 2016

Résumé

Suite à l'interruption de la circulation extracorporelle (CEC) chez les patients qui subissent une chirurgie cardiaque, le rétablissement de la circulation sanguine au niveau du poumon cause souvent une hypertension pulmonaire qui, à son tour, peut engendrer des complications au cœur droit. Pour traiter cette hypertension, la milrinone, un inhibiteur de la phosphodiestérase 3 (PDEIII) est souvent donnée par voie intraveineuse. Par contre, cette administration cause également une hypotension systémique qui peut nécessiter l'administration d'agents vasoactifs. Une administration de la milrinone par nébulisation a donc été adoptée, ciblant ainsi directement les poumons [1]. En cas d'urgence, la milrinone peut être injectée ou atomisée directement au niveau de la trachée.

Lors de chirurgies cardiaques nécessitant une CEC, un protocole expérimental s'avère souvent difficile à respecter chez le patient. En effet, les contraintes temporelles, les nombreux médicaments co-administrés et le stress physique causé par la chirurgie sont autant de facteurs qui peuvent biaiser une étude dont le but est caractériser l'effet pharmacologique de la milrinone. Il s'est donc avéré important, en premier lieu, de quantifier les effets des artéfacts reliés aux manipulations chirurgicales sur notre biomarqueur, soit le ratio de la pression systémique moyenne sur la pression pulmonaire moyenne. Chez le porc, nous avons observé des changements de 30-50% au niveau des pressions systémiques moyennes, soit le double des changements au niveau des pressions pulmonaires pour le même artéfact. La durée moyenne de tous les effets, des artéfacts, (au niveau systémique et pulmonaire conjointement) fut de 4.5±2.5 min (n=152). Dû au biais potentiel apporté par ces artéfacts, l'utilisation d'un modèle animal dépourvu de manipulations chirurgicales s'est avérée être pleinement justifiée.

En second lieu, la voie pulmonaire étant une voie d'administration non homologuée pour la milrinone, le site optimal de déposition pulmonaire permettant un effet local maximal n'a pas été identifié. La milrinone cible la PDEIII au niveau des muscles lisses vasculaires. Ainsi, l'effet anti-hypertensif local de la milrinone se situe au niveau des artères musculaires côtoyant l'arbre trachéobronchique. Nos études se concentrent sur les nébulisations par simple jet (SJ), par mèche vibrante (VM) ainsi que sur les administrations d'urgence, soit l'instillation (ITI) et l'atomisation (ITA) intratrachéale. De ce fait, nous avons conduit des études *in vitro* pour caractériser la taille des particules générée par les deux formes de nébulisation, qui est un facteur influençant la déposition pulmonaire. Nous avons aussi tenté, grâce à des études *in et ex vivo*, de démontrer une différence d'efficacité entre les deux méthodes de nébulisation. Les études *in vitro* ont permis, de quantifier la dose se rendant au poumon, soit la dose inhalée, et ont démontré une différence au niveau de la distribution de la taille des particules des gouttelettes générées par les deux nébulisations. Les résultats indiquent une taille de particules plus fine, visant préférentiellement la zone alvéolaire pour la nébulisation par mèche vibrante. Ils indiquent aussi une plus grande dose inhalée pour la nébulisation par mèche vibrante mais de façon surprenante, en tenant compte de la dose inhalée par le patient, une meilleure relaxation pulmonaire par simple jet. En plus d'une meilleure oxygénation suite à l'administration de la milrinone, nos études démontrent une sensibilité de 20 fois plus grande, tel que démontrée par le IC50 de la relaxation à l'acétylcholine, et un effet de relaxation près de 25% supérieur chez la nébulisation par simple jet

En troisième lieu, la relation pharmacocinétique (PK) et pharmacodynamie (PD) de la milrinone par nébulisation n'a pas été caractérisée en absence d'artéfacts chirurgicaux et encore moins pour les voies d'urgence. Suite au développement d'un modèle d'hypertension pulmonaire sans manipulations chirurgicales, nous avons déterminé une relation concentration/effet (PK/PD) pour les méthodes d'administration pulmonaire et comparé leurs efficacités après correction pour la dose réellement inhalée, déterminée par collecte urinaire. Cette dernière étude démontre un EC_{50} de

l'impact de la milrinone sur le ratio des pressions artérielles systémiques moyennes sur les pressions artérielles pulmonaires plus faible suite à l'administration de la milrinone par simple jet ainsi qu'une augmentation de ce ratio de près 40%.

Les résultats obtenus au cours de ces études suggèrent l'administration par simple jet semble plus efficace. Par conséquent, un meilleur jugement clinique pourra être appliqué lors de la méthode d'administration ainsi que de la dose utilisée de la milrinone.

Mots-clés : milrinone; inhalation; intratrachéale; nébuliseur; pharmacocinétique; pharmacodynamie; hypertension pulmonaire; circulation extracorporelle; chirurgie cardiaque; *in vivo*; *in vitro*.

Abstract

Following weaning from cardiopulmonary bypass (CPB), the cardiac surgery patients undergoing a procedure are often faced with the pulmonary reperfusion syndrome which may lead to pulmonary hypertension condition which, in turn, is likely to precipitate right ventricular dysfunction. Milrinone, a phosphodiesterase type 3 inhibitor (PDEIII) is used, among others, to facilitate CPB weaning in patients by reducing the severity of pulmonary hypertension through vasodilation. Milrinone is typically given intravenously. However, this mode of administration is frequently associated with systemic hypotension which may require administration of vasoactive agents. Administration of milrinone throughnebulization has therefore been developed, targeting the lungs directly and avoiding systemic hypotension. In case of emergency, milrinone may even be injected directly into the trachea or even possibly atomized intratrachealy. In this thesis we will describe an experimental protocol where the administration of milrinone through inhalation was studied.

Unfortunately, experimental protocols during surgeries requiring CPB are often challenging due to time and procedural constraints. Indeed, the signal-to-noise ratio makes it difficult to isolate the effect of a specific intervention. The effect of the other administered medications and the physical stress of surgery may result in potentially incomplete or biased pharmacological studies. This aspect is the basis of the first portion of the thesis. The identification and and the quantification of the surgical manipulation artifacts on our main biomarker, the mean systemic pressure over the mean pulmonary pressure, was our first objective. In our first study, following our experimentation, we witnessed a 30-50% changes on systemic pressures and these changes were twice those observed on pulmonary pressures for the same artefact. Pooled durations of all effects on both mAP and mPAP averaged 4.5±2.5 min (n=152). These changes fully justified the creation of a new model due to the potential biais of the artefacts.

Secondly, as nebulization is a novel way to administer milrinone, the pharmacokinetic-pharmacodynamics (PK-PD) relationship has not been completely characterized. Even less information is available for the emergency routes. Milrinone targets PDEIII in vascular smooth muscle, thus the local antihypertensive effect of milrinone is most likely to occur at the level of muscular arteries alongside the tracheobronchial tree. We studied four methods of administration: simple jet (SJ), vibrating mesh (VM) nebulization, intratracheal instillation (ITI) and atomization (ITA). In addition, the optimal pulmonary deposition and absorption site for maximum local effect remains as of yet unknown. We have strived to identify the factors influencing the lung deposition of milrinone through nebulization and part of the work discussed in this thesis is aimed at characterizing the amount of milrinone deposited on the various sections of the tracheobronchial tree by the mentioned methods. Through in and ex vivo studies we have investigated the differences in efficacy of the two nebulization methods. We have found each method to generate a significantly different deposition pattern and as such, influencing lung deposition. Our results show that VM targets the lower airways and alveoli, whereas SJ targets preferably the higher and middle airways. Our study also shows a higher inhaled dose for VM but surprisingly a better dose-related efficacy for SJ. Indeed, in addition to a better oxygenation, our study shows, as demonstrated by the acetylcholine-induced relaxation IC_{50}, a 20 times higher sensitivity and a 25% higher maximum relaxation following simple jet nebulization.

Subsequently, following the development of a pulmonary hypertension model devoid of surgical manipulations and, by association, artefacts, we have determined a urinary-dose-corrected PK/PD relationship for the nebulization and emergency methods of milrinone administration. We explored the methods of intratracheal bolus and atomization and compared their efficacy to those of nebulization. This study shows a lower EC_{50} of milrinone impact and an almost 40% increase of the mean systemic arterial pressure over mean pulmonary arterial pressures ratio following simple jet adminstrationThe information

obtained by these studies offers the potential to aid clinicians in making a more informed judgment in the use of milrinone.

Keywords : milrinone; inhalation; intratracheal; nebulizer; pharmacokinetics; pharmacodynamic; pulmonary hypertension; cardiopulmonary bypass; cardiac surgery; *in vivo*; *in vitro*.

Table of contents

Table List

Figures List

Equation list

Abbreviations

Δt	min	Time inerval
A, B, α et *β*	---	Pharmacokinetic macroconstants
ACI	---	Andersen cascade impactor
Ach	---	Acetylcholine
ADH	---	Antidiuretic hormone
ADME	---	Absorption, distribution, metabolism, elimination
AMP	---	Adenosin monophosphate
AMPc	---	Cyclical adenosin monophosphate
ANP	---	Atrial natriuretic petide
ATP	---	Adenosine triphosphate
AUC	ng ml^{-1} min^{-1}	Area under the curve
AV	---	Atrioventricular
BK		Bradykinin
C	ng/ml	Plasma concentration
Cl	L/h	Clairance
C_{last}	ng/ml	Last sample concentration
Cl_R	L/h	Renal clairance
C_{max}	ng/ml	Concentrations plasmatiques maximales
CO	---	Cardiac output
CPB	---	Cardiopulmonary bypass
CV	%	Coefficient of variation

D	---	Dose
E_0	---	Baseline effect
EC_{50}	ng/ml	Concentration producing 50% of effect
ECD	µm	Effective cutoff diameter
ELS	---	Extended least squares
E_{max}	---	Maximum effect
ET-1	---	Endothelin
$e^{-\alpha t}$	---	Distribution phase
$e^{-\beta t}$	---	Elimination phase
F	---	Bioavailability
GLS	---	Generalized least squares
GTP	---	Guanosine triphosphate
HPLC	---	High performance liquid chromatography
I_0	---	Baseline inhibition
I_0	---	Baseline inhibitory effect
IC50	ng/mL	Half maximal inhibiting concentration
IL-6	---	Interleukine-6
iMil	---	Inhaled milrinone;
iNO	---	Inhaled nitric oxide;
$iPGI_2$	---	Inhaled prostacyclin
ITA	---	Intratracheal atomization
ITI	---	Intratracheal instillation
IV	---	Intravenous
k_{10}	min^{-1}	Elimination constant
k_{12}, k_{21}	min^{-1}	Transfer constant constants

k_e,	min^{-1}	Elimination constant
LLOQ	ng/ml	Lower limit of quantification
Log P	---	Octanol/water partition coefficient
LV	---	Ventricule gauche/Left ventricule
MAD	µm	Mean aerodynamic diameter
mAP	mmHg	Mean arterial pressure
mPAP	mmHg	Mean pulmonary artery pressure
MS/MS:	---	Tandem mass spectrometry
MS	---	Mass spectrometry
NO	---	Nitric oxide
OAT	---	Organic anion transporter
OATP	---	Organic anion transporting polypetide
OCT	---	Organic cation transporter
OF	---	Objective function
OLS	---	Ordinary least squares
PA	mmHg	Pulmonary arterial hypertension
PAP	mmHg	Pulmonary arterial pressures
PD	---	Pharmacodynamic
PDEIII	---	Posphodiesterase III
PG	---	Prostaglandin
PGI_2	---	Prostacyclin
P-gp	---	Acid p-glycoprotein
PH	---	Pulmonary hypertension
PK	---	Pharmacokinetic/pharmacokinetics

pKa	---	Acid dissociation constant
PM	g/mol	Molecular weight
PPM	---	Patient-prosthesis mismatch
PVR	$dyn \cdot sec \cdot cm^{-5}$	Pulmonary vascular resistance
Q	mL/min	Blood flow
RV	---	Right ventricule
SA	---	Sinoatrial
SJ	---	Simple jet nebulizer
SMC	---	Smooth muscle cell
t	min	Time
t_0	min	Time zero
$t_{1/2\,\alpha}$	min	Distribution half-life
$t_{1/2\,\beta}$	min	Elimination half-life
$t_{1/2}$	min	Apparent half-life
t_{last}	min	Time of last sample
t_{max}	min	Time of maximum effect
TNF-α	---	Tumor necrosis factor
TXA_2	---	Thromboxane A_2
UV	---	Ultraviolet
V_1	L	Central compartment volume
V_2	L	Peripheral compartment volume
V_d	L	Apparent volume of distribution
VEGF	---	Vascular endothelial growth factor
VIP	---	Vasoactive intestinal peptide
VM	---	Ultrasonic vibrating mesh nebulizer

WLS	---	Weighted least squares
γ:	---	Hill coefficient
λ_z	min^{-1}	Elimination constant

Dragi mei parinţii,

Aceste sunt aripile ce mi-aţi dat pentru a zbura. Vă mulţumesc.

Acknowledgements

To my directors

First and foremost, I would like to thank my director, Dr. France Varin. You welcomed me into your laboratory and, amongst all the hypotheses, theories, discussions, vials and life lessons, you made a space for me to call a second home. From day one, you've guided every step of my way and helped mould the critical thinking that allowed me to become the scientist and human being that I am today. Words will never be able to express how thankful I am for your supervision and tutelage.

I would also like to thank my co-director, Dr. André Y. Denault for his tremendous help during the span of my doctorate. Dr. Denault, your innovation, determination and implication are truly inspiring. I have never left your office without the feeling that I could accomplish everything. Our meetings have always pushed me to delve deeper into the subject and your optimism has been a remarkable source of encouragement.

To my colleagues.

We have shared much over the span of our work together and the memories and bonds that we've made are a testimony to how much we've grown since we first met. Francois Gaudreault, you were my colleague, my teacher and the lessons that I've learned from you, I will carry for years to come. Anne Nguyen, thank you for all the discussions, thank you for all the nights working together, thank you for so many other reasons. Fady Thomas, my first supervisor, thank you for our work together and thank you for your friendship. Thank you Véronique for all the lovely moments. Thank you Natasha and Hélène for your hard work. Johanne Couture, thank you for everything you've taught me throughout the years. Your advice helped shaped the work ethic that I have today. Thank you Dr. Théoret for your supervision and help at the CHU Sainte Justine. These projects would not have succeeded without your contribution.

Thank you Christiane and Audrey from the CHU Sainte-Justine as well for your availabilities and contributions to these projects. Thank you Marie-Pierre Mathieu for your wonderful technical help at the Montreal Heart Institute.

To the Université de Montréal

I would like to express my thanks to the members of the Faculté de Pharmacie of the Université de Montréal. The administrative and technical support provided created the beneficial work environement required for the success of doctoral endeavours.

Funding agencies

I am thankful also for the grants which made this research possible The funding provided by the Groupe de Recherche Universitaire sur le Médicament was key in securing the material need for the experiments.

To my family

I would like to thank my parents, whose support made my graduate studies possible. Their sacrifices allowed me to pursue a higher education and their unwavering care throughout the years gave me the will to move forward.

To my friends

Thank you for your patience and for believing in me. Richy, palabras no pueden expresar cuanto te agradezco tu apoyo. Gracias por todo.

To the members of the jury,

Thank you for your time and for being part of the jury. I am thankful for your input and for the scientific dialogue that we about to share.

Foreword

This thesis was performed through funds from the Groupe de recherche universitaire sur le médicament (Fonds de recherche en santé du Quebec). The studies were conducted under the supervison of Dr. France Varin of the Université de Montréal Faculty of Pharmacy. This project was part of an ongoing cooperation between Dr. Varin's laboratory and Dr. André Y. Denault (co-director) and Dr Perrault's animal surgery laboratory at the Montreal Heart Institute (MHI). The long-term objective of the MHI team is the optimization of vasoactive drug use in cardiac surgery requiring cardiopulmonary bypass.

The thesis is divided into the following three main sections: a general introduction (Section I), followed by the main body of research works (Section II), and a general conclusion (Section III). The first section covers an introduction to the principles of heart and lung anatomy and cardiopulmonary bypass as well as basic concepts related to pulmonary hypertension, pulmonary drug administration, inhaled particle deposition theories, chromatography basics and a reminder of the basic concepts of pharmacokinetics and pharmacodynamics as well as modeling principles. The second section consists of four scientific articles resulting from research. Finally, the last section is a general discussion of the results and research perspectives.

SECTION I: INTRODUCTION

CHAPTER 1. Cardiovascular physiology

1.1. Introduction

In order to perform cardiac surgery, the heart has to be still. In order to maintain adequate circulation in the rest of the body during cardiac surgery, cardiopulmonary bypass (CPB) is currently used. During CPB, all the organs will be perfused except the heart and the lung. Consequently at the end of cardiac surgery, during the reperfusion period, significant vascular consequences can occur and in some patients, reperfusion injury can be lethal [2, 3]. The treatment of these conditions is however based on the anatomical and physiology concepts of the cardiovascular system, the respiratory system and, of course, their interaction. In the following chapter, we will both define and address the normal physiology of the cardiorespiratory system so as to set up a better understanding of the factors playing into the treatment of the pulmonary hypertension generated by the reperfusion syndrome and, by extension, cardiopulmonary bypass.

1.2. Heart and circulation

The most devastating consequence of pulmonary hypertension is, through the small, low-pressure pulmonary circulation, its effect on the right heart [4]. In turn, this effect impacts in many ways the higher-pressure systemic circulation. As such, it is impossible to approach only the pulmonary paradigm without an overview of the “heart of the matter”.

1.2.1. Heart structure

The heart, biomechanical motor that keeps us going, is divided into two separate pumping chambers, ushering blood into two distinct circulations at different pressures. These movements require specific timing, coordination of a neural network, heart valves, vascular supply, connective tissue and muscle cells. The different heart structures are lined with a very smooth and simple squamous

epithelium layer called endocardium, the smoothness of which acts as prevention of abnormal blood clotting. The heart anatomy (Figure 1) may be separated in the four cardiac chambers (two atria and two ventricles) and the valves separating them from each other as well as from the two circulations to which the chambers are connected.[5] When blood passes into one of the atria or from atrium to ventricle, it flows through four cardiac valves; the tricuspid, mitral, aortic and pulmonary valves. The annulus is the fibrous ring which holds together these four cardiac valves. By the means of interdigitated connective tissue, the bases of these valves mesh into the annulus and are thus interconnected.

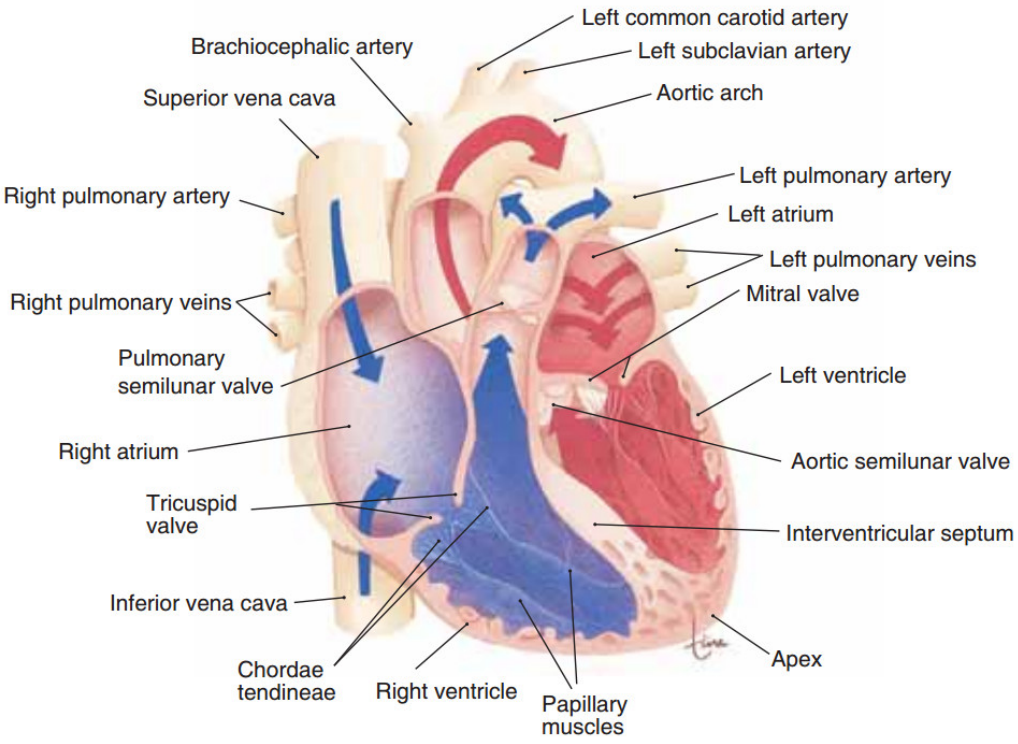

Figure 1: Frontal section of the heart, in anterior view, showing internal structures. With permission from Scanlon [5].

The cardiac atria are mainly the filling chambers of the heart. They are two thin-walled low pressure reservoirs. The right atrium receives the whole venous return from the body by means of the superior and inferior venae cavae that respectively drain the upper and lower bodies. The left atrium receives blood from the small pulmonary circulation through the four pulmonary veins. The left atrium also produces a hormone called the atrial natriuretic peptide which is highly involved in blood pressure maintenance. It decreases the reabsorption of sodium ions by the kidneys, therefore boosting fluid excretion. This elimination of sodium also increases water elimination, which, in turns, lowers blood volume and consequently, blood pressure.

The ventricles are the actual pumps which keep the blood flowing. By contracting, each of the ventricles pushes blood into either the small, pulmonary circulation for the right ventricle or into the larger systemic circulation from the left ventricle. In this thesis, as previously mentioned in the hypertension section, the main clinical outcome is directly related to the right ventricle and the thickening of its wall due to pulmonary-hypertension-induced cellular hypertrophy. When blood passes into, or from one chamber to another, it passes almost inevitably through one of the four cardiac valves. The foremost purpose of these valves is stopping potential blood backflow. The cardiac valves are shown in Figure 2:

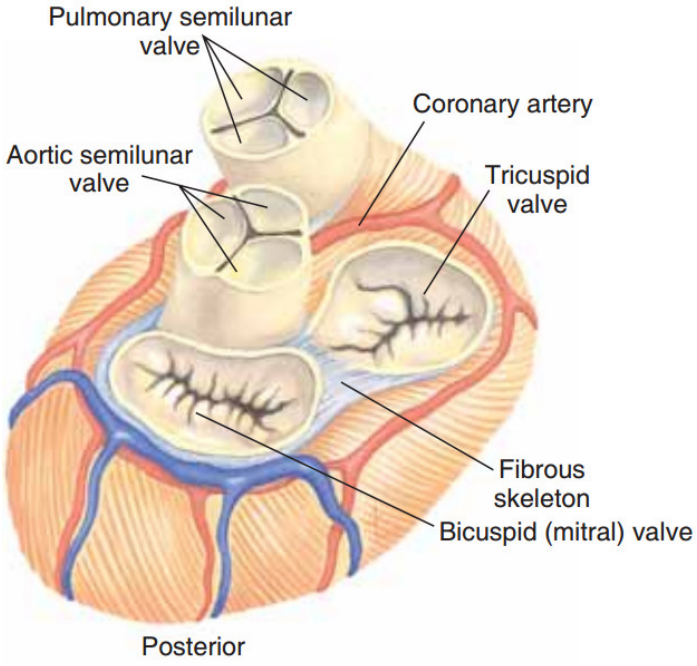

Figure 2: Heart valves in superior view. With permission from Scanlon [5].

As blood drains from the venae cavae, it reaches the right atrium and subsequently makes its way into the right ventricle via the right atrioventricular valve, also known as the tricuspid valve. It is so named for the three connective-tissue-reinforced endothelium flaps which make up the valve. Once the ventricle begins its contraction, the pressure generated closes the tricuspid and the blood is diverted towards the small circulation after passing through the pulmonary semilunar valve. After re-oxygenation of the blood by passage through the lungs, it returns to the left atrium and into the left ventricle through the left atrioventricular valve, most commonly known as the mitral valve that is made of two endothelium cups. Again, as the left ventricle contracts, the pressure generated closes the mitral valve and the blood is diverted into the systemic circulation.

The heart wall is composed of three layers. Firstly, the epicardium, also named visceral pericardium, is a thin serous membrane that covers the heart. The

second layer is the myocardium which is the thick muscular middle layer and third one is, as mentioned previously, the endocardium which is the squamous inner-layer of endothelial cells. The cardiac muscular cells are quite unique as they show features of both smooth and skeletal muscle. Unlike skeletal muscle, they are mononucleated while still exhibiting skeletal muscle striations. The cellular membranes at the end of the cells fold and fit into the folds of adjacent cells. These interlocking folds, named intercalated disks, are distinctive of cardiac muscle histology. These discs contain so-called gap junctions which have the property of low resistance, thus allowing freer diffusion of ions and, consequently, electrical impulse. The properties of these muscular cells are what keep the electrical activity and spontaneous contraction through a lifetime of heartbeats. Cardiomyocytes exhibit excitability, contractility, rhythmicity and conductivity.

The heart is intricately innervated by both the sympathetic and parasympathetic systems (Figure 3) to respectively either increase heart rate and contractility or conversely, decrease the heart rate through the vagus nerve. The action potential enters the heart through the sinoatrial (SA) node which then transmits to the atrioventricular (AV) node, followed by depolarization of the Purkinje fibers. Chamber contraction order is based on the electrical impulse transfer speed of the different parts of the cardiac autonomous nervous system.

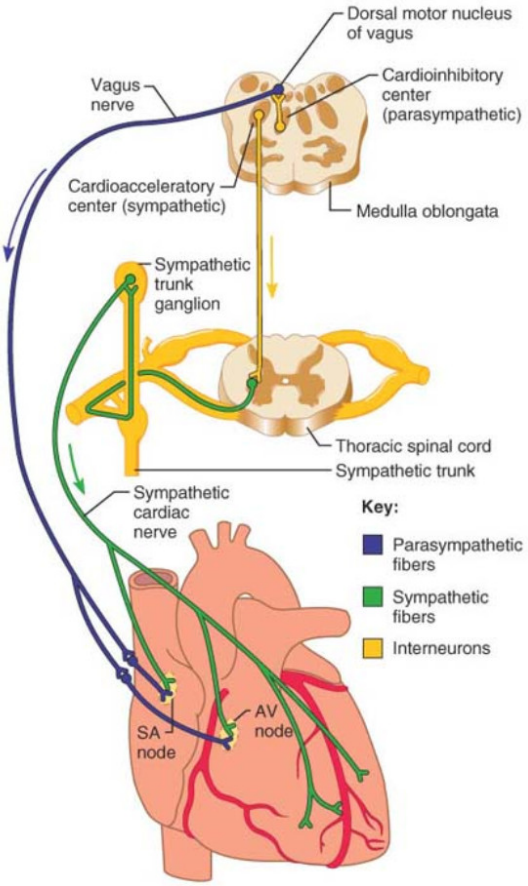

Figure 3: Autonomic innervation of the heart. With permission from Marieb [6].

1.2.2. Systemic vasculature

Systemic vascular anatomy is very variable, depending on the part of the body. The ranges are very wide in terms permeability (e.g. hepatic sinusoids versus brain-blood barrier) size (e.g. capillaries versus aorta). This range translates into varying thicknesses of the three sheaths which compose all vessels: adventitia, media and intima, which will be discussed in detail in section 2.3.5.

1.2.3. Hemodynamics

Blood flow is an extremely complex system regulated by many parameters, both mechanical and/or biochemical. These parameters are aortic and venous pressures and vessel resistance, viscosity, length and radius of vessel. These parameters are regrouped by Poiseuille's law which characterizes vascular flow.

$$F \propto \frac{\Delta P \times r^4}{\eta \times L}$$

Equation 1: Poiseuille's Law. F: blood flow; : pressure gradient; r: vessel radius; η: viscosity; L: length of the vessel.

Blood pressure is the force which blood flow exerts on the walls of the vessels through which it flows. When a measure is taken, two numbers are determined: the systolic and diastolic pressure, the former always being the highest. To keep these numbers within normal ranges, several factors are involved, including of course the strength of the pump itself. Firstly, venous return, which is the amount of blood returning to the heart via the two venae cavae regulates through Starling's Law (which states that the more cardiac fibers are distended, the more they will subsequently contract) the force at the end of a systole. Another factor to be accounted for is the skeletal muscle pumps. This factor involves in particular deep-leg venous return and could be best described as the pumping of venous blood content towards the heart through the contraction of surrounding skeletal muscles.

Blood flow is inversely proportional to vessel resistance, at the capillary level. Two major factors in vascular hemodynamics are both peripheral resistance and large artery elasticity. Peripheral resistance can be seen as a container holding the full volume of blood. Indeed, the smaller the container, the greater the pressure exerted by the body of liquid held within. Large artery elasticity may be

seen as the recoil from the left ventricular contraction which helps lower systolic pressure and raise diastolic.

Viscosity of blood also factors into blood flow. This viscosity depends highly on the presence of blood proteins, mainly albumin as well as the hematocrit.

Lastly, hormonal control is summarized in Figure 4. The adrenal medulla secretes epinephrine and norepinephrine, both of which have an effect through direct stimulation of vasoconstriction, thus raising blood pressure. On the other hand, hormonal control through aldosterone, antidiuretic hormone and atrial natriuretic peptide has an indirect effect on blood pressure as it generates change mainly through changes in blood water content and volume.

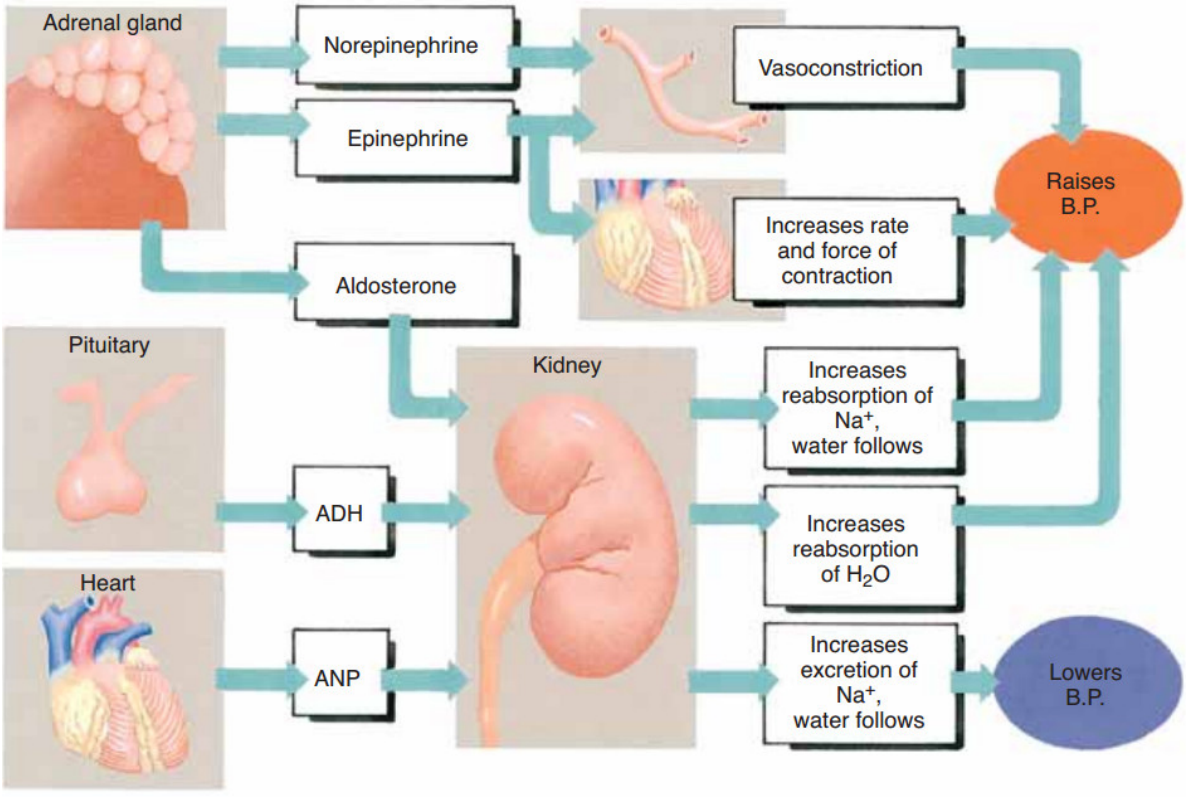

Figure 4: Hormones that affect blood pressure. Where ADH: anti-diuretic hormone, ANP: atrial natriuretic peptide and B.P.: blood pressure. With permission from Scanlon [5].

1.3. Lungs

When discussing a highly complex organ, such as the respiratory tract, it might be thought convenient to firstly compartmentalize it into different sections. The anatomical units making up the luminal part of the lungs can be divided into the large airways, such as the nose, mouth pharynx, larynx trachea and main bronchi, the smaller airways such as the smaller bronchi and bronchioles and lastly, the respiratory acini which are made up by the terminal bronchioles, alveoli ducts and alveoli. Running parallel to the luminal respiratory part and interweaving with the airways structure's mucosa are the vascular networks making up the pulmonary and bronchial circulations.

1.3.1. Airways structure

The respiratory tract can be roughly divided into two major parts. Firstly, the upper respiratory tract may be identified, which is made up of the portions outside the thoracic cavity: the nose, pharynx, larynx and the upper part the trachea. Secondly, the lower airways are made up of the parts inside the chest cavity, the tracheobronchial tree which begins with the lower trachea, the bronchi, bronchioles and alveoli. The tracheobronchial tree is made up of 23 generations (Figure 5) beginning at the trachea and ending with the alveolar sacs.

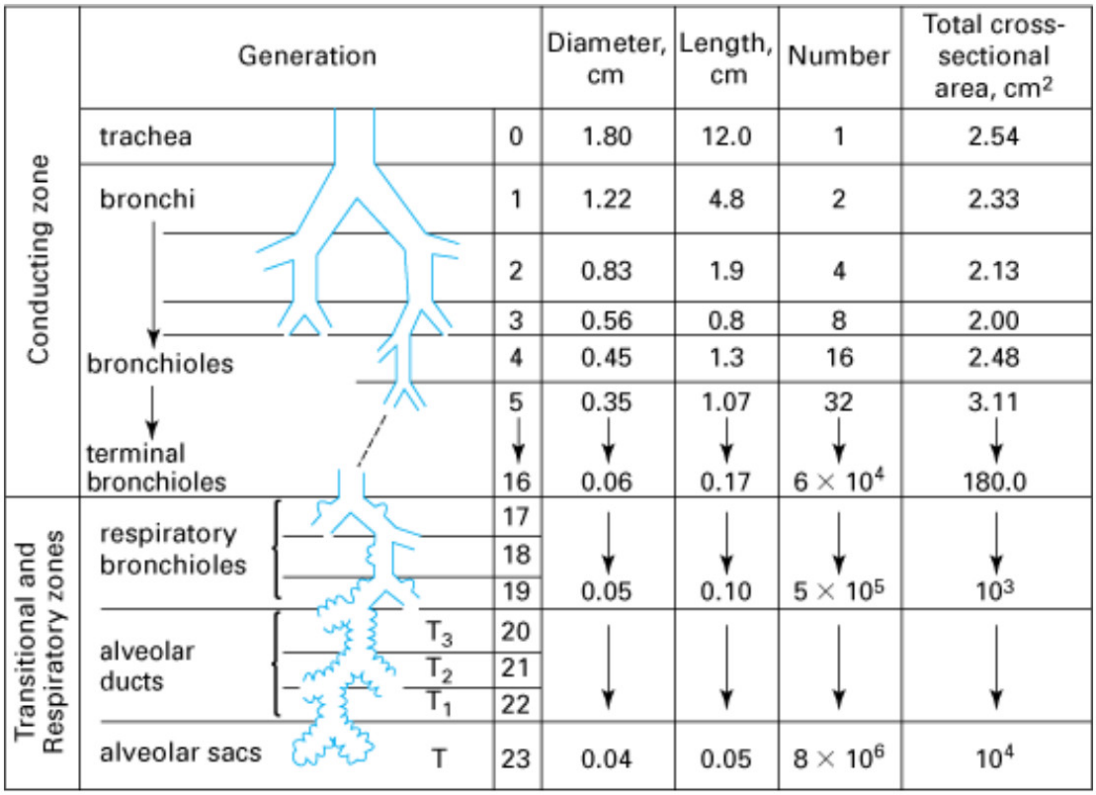

Figure 5: Schematic representation of airway branching in the human lung with approximate dimensions. With permission from Levitsky [7].

1.3.2. Upper airways

The nose is the entry and exit point of air in the respiratory tract. Made of cartilage, the nose's nostrils are equipped with hairs whose role is to halt the progression of dust. The nasal mucosa is made up of ciliated epithelium and mucus-producing goblet cells. The ciliated cells continuously displace the mucus towards the nasopahrynx, oropharynx and pharynx in view of it later being swallowed, leading to the destruction of the bacteria it may contain by means of the hydrochloric acid present in the stomach. By passing through the nostrils, air is not only filtered of major particulates, but also warmed by the rich vasculature and humidified [7].

Stemming from the larynx is the flexible cartilaginous tube called the trachea. In humans, about 20 C-shaped cartilages prevent the trachea from collapsing upon itself [8]. The cartilages are surrounded by muscular tissue and the inner walls are covered with mucus produced by goblet cells and mucous glands. This mucus is constantly moved towards the larynx in view of deglutition [8].

1.3.3. Middle and lower airways

The trachea branches at the carina into the first generation bronchi which further divide into the three right-lobar and two left-lobar bronchi. The lobar bronchi further arborize 15 to 20 times in a dichotomous fashion into an extensive network of segmental and subsegmental bronchi up until the terminal bronchi which is the final generation of the tracheobronchial tree before the beginning of the respiratory region. The daughter/mother branch ratio for branches with a diameter greater than 1 mm is 0.76 whereas, in 1 mm and lower branches, the ratio increases to 0.87 [9].

Alveoli are the functional units of the lung where gaseous exchange occurs. Disposed in the form of clusters, these units are held together by connective tissue whose elasticity is necessary for exhalation. The area of all these functional units combined is around 75 square meters. Alveolar walls are made up of type I cells which are simple squamous epithelium. The air-side of alveoli is coated with a thin layer of a fluid. This serous liquid, which approaches a total intrapulmonary volume of 10-30 mL is absolutely necessary for gaseous exchange as gases need dissolution for the exchange to occur.[6] Mixed in the tissue fluid can be found a lipoprotein named pulmonary surfactant which is secreted by alveolar type II cells. Its role is to reduce the liquid's surface tension and prevent alveolar collapse [8].

Normal gas exchange (Figure 6) involves the absorption of an adequate quantity of O_2 and an externalization of a suitable amount of CO_2. For an average individual, this translates into a ventilation rhythm of 12-15 breaths per minute with a ventilation volume of 500 ml of air.[8] Typical pulmonary blood flow is

equivalent to cardiac output which, in an average individual is around 5 L/min. Contrary to the high hydrostatic pressure generated in high resistance systemic arteries (85 mmHg), the thin and elastic pulmonary arteries generate pressures of 15 mmHg. Due to the change in total-vessel lumen area between the higher lungs and the respiratory section, the transit time of blood in the alveolar-adjacent capillaries is slow and averages 0.75 sec. This transition time allows time for the gaseous exchange where the blood O_2 pressure increases from 40 to 100 mmHg and CO_2 pressure decreases from 45 to 40mmHg [7].

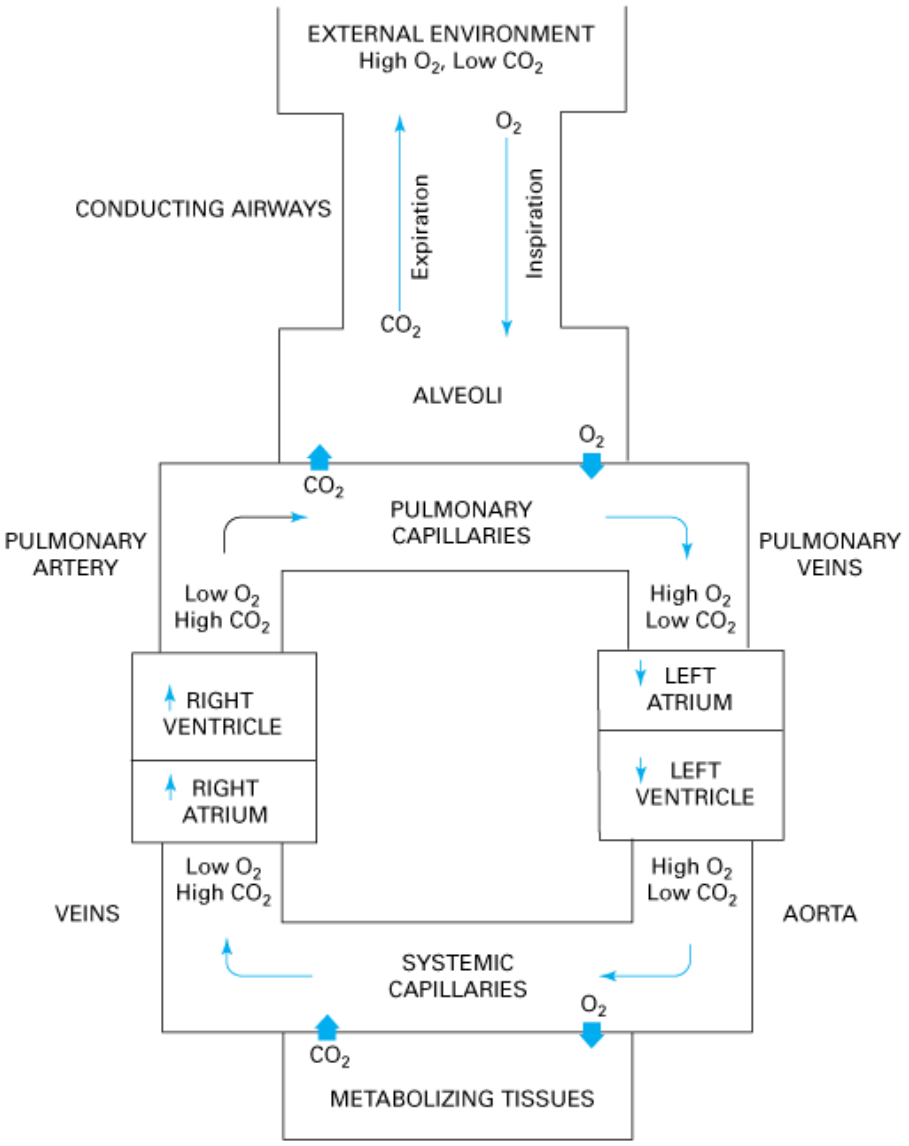

Figure 6: Schematic representation of gas exchange between the tissues of the body and the environment. With permission from Levitsky [7].

1.3.4. Cells

The trachea and main bronchi epithelium is a pseudostratified epithelium made up of many types of cells as described below (Figure 7).

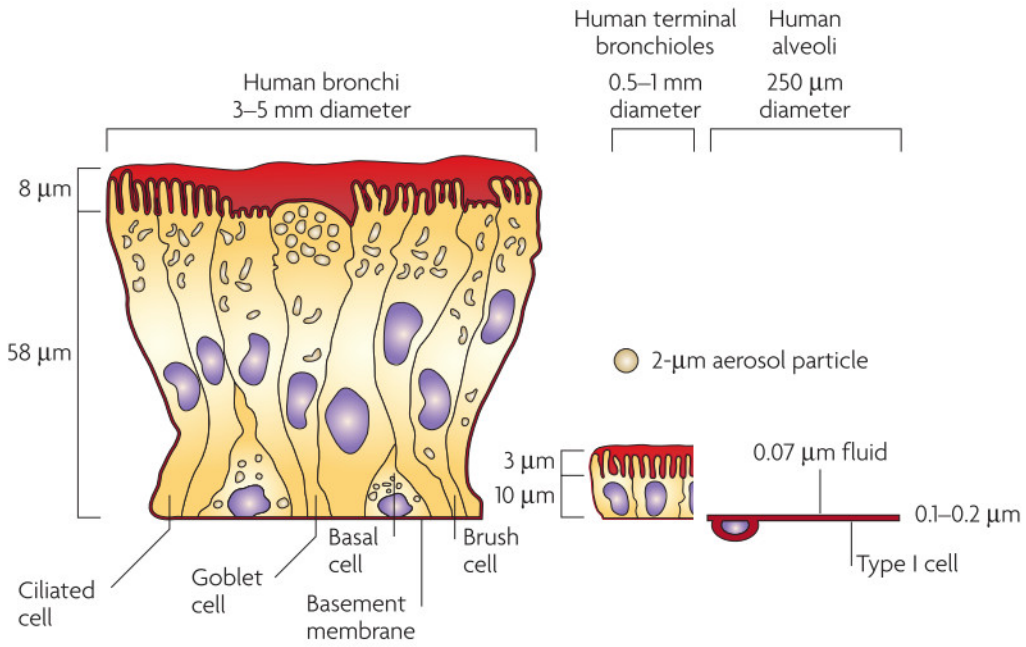

Figure 7: Comparison of the lung epithelium at different sites within the lungs. With permission from Patton [10].

Ciliated cells are columnar epithelial cells, which is a cell type characterised by its height being greater than its width [11]. The apical region of these cells is covered with cilia, whose role is the displacement of mucus. Goblet cells, like ciliated ones, are also part of the columnar epithelial cell type. Their main purpose is the production and secretion of mucins, which are major component of pulmonary mucus. These cells' cytoplasm is in great part occupied by mucin-containing vesicles [11]. Mucins are released through both merocrine and apocrine secretion. In addition to the baseline secretions of these cells, production may be increased in the presence of external factors such as particulates or microorganisms [10].

Basal cells, part of the basal lamina, basal cells are yet undifferentiated cells. Though little is known about the mechanisms of differentiation of these cells, their role is to replenish the surface layers of ciliated and mucous cells of the pulmonary epithelium [8].

Mast cells are cells of which the main function is the release of cytokines and chemokines which play a critical role in allergic responses. These chemical mediators include, but are not limited to histamine, serotonin, heparin and eosinophil chemotactic factor [8].

Clara cells located mostly in bronchioles, their function is a secretory one. In addition, they contain cytochrome P450 isoenzymes which play a role in drug metabolism.

Pneumocytes are cells make up the lining of the alveoli, thus participating in gas exchange control. Type I cells cover up over 95% of the alveolar surface of the lungs. They have a 25 nm thickness, which is critical in gaseous exchanges. Their role is to provide a barrier as thin as possible while still remaining permeable to O_2 and CO_2. Type II cells cover the remaining 5% of alveolar surface. However, conversely to surface, in terms of cell number, type-II cells represent 60% of the cells lining the alveoli. Their main purpose is to produce and secrete surfactant phospholipids [8].

Finally, alveolar machophages are relatively large cells which possess the capacity for engulfing local or foreign through endocytosis (phagocytosis for solid matter or pinocytosis for liquids). Freely moving between vessels and tissues through extravasation, they also participate actively in cellular communication through the use of cytokines, most notably the pro-inflammatory ones: tumor necrosis factor alpha, interleukin 1, 6, 8 and 12. They also play a role in pulmonary drug clearance through their endocytotic capabilities [9].

1.3.5. Airways vasculature

Certainly, the main focus of airway vasculature is to reach the tracheobronchial respiratory region and allow gaseous exchanges between the blood and the luminal side of the lungs. However, that is not its only function. Indeed, two circulations are thus distinguished: firstly, the pulmonary circulation whose aim is the aforementioned exchange and, secondly, the bronchial circulation which

nourishes the tracheobronchial tree. The interactions and anastomoses between the two can be seen in Figure 8.

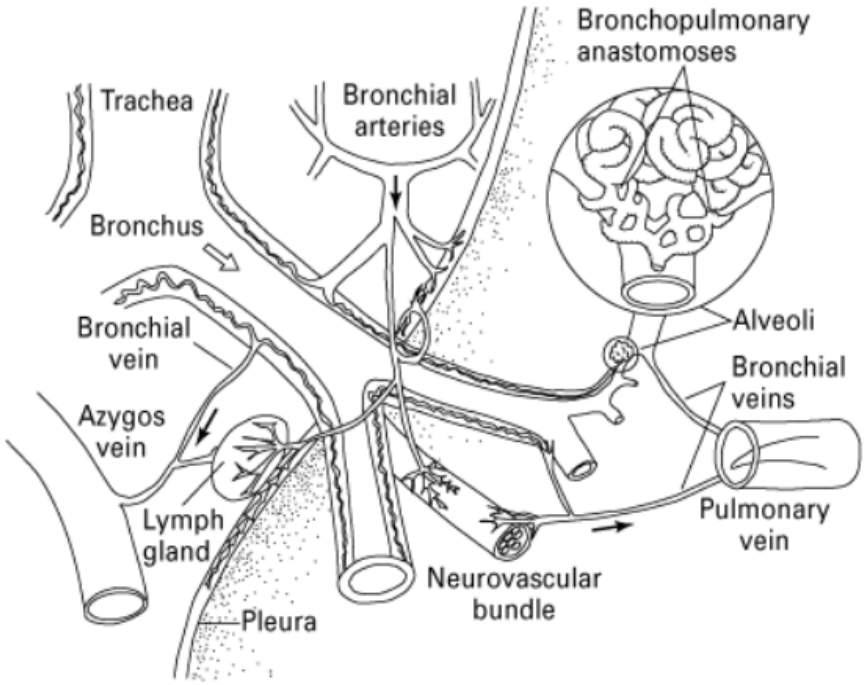

Figure 8: Illustration of the main anatomic features of the bronchial circulation. With permission from Levitsky [7].

In normal subjects, most of the venous return will circulate into the pulmonary circulation. Venous blood will pass through the pulmonary artery, branching out through the pulmonary parenchyma and returning to the main systemic circulation by passing through the left ventricle and atrium, with the scope of oxygenation. Many exceptions occur however as some subjects exhibit intracardiac and/or intrapulmonary shunting and some are afflicted with congenital anomalies. The bronchial circulation's aim is to supply the lung parenchyma with nutrients through an extensive capillary bed circulating through the bronchial walls. All intrapulmonary structures related to the bronchial

circulation drain into the pulmonary veins. As such, these two circulations have extensive anastomoses that mix together oxygen-rich and less-rich blood [12]. However, the perihilar region (region around main bronchi and pulmonary arteries and veins) drains to the azygos system [13]. The bronchial circulation accounts to roughly one percent of the cardiac output.

Both these circulations are, to varying degrees, made up of the standard vascular tunics which can be seen in Figure 9.

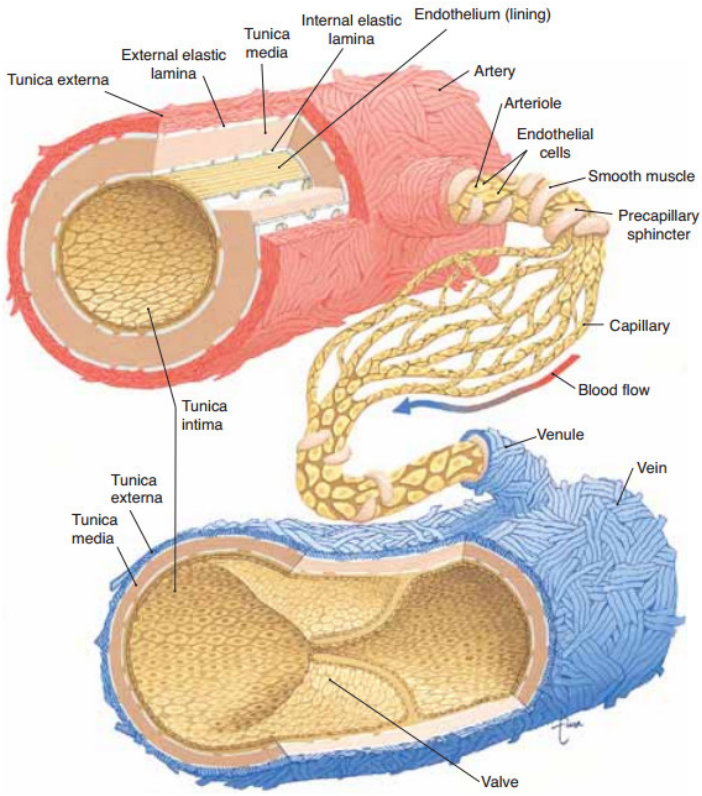

Figure 9: Structure of an artery, arteriole, capillary network, venule, and vein. With permission from Scanlon [5].

1.3.6. Vasculature composition

The adventitia is commonly known to be the collagen-rich elastic sheath surrounding blood vessels. It is considered a scaffold through which intermesh fibroblasts, perivascular nerves, nourishing vessels and a wide array of cellular populations such as, but not limited to macrophages, T-cells, B-Cells and mast cells while aiding in the regulation of lumen size through smooth muscle tone (Figure 10). It has also been shown to participate in signaling related to remodelling purposes [14].

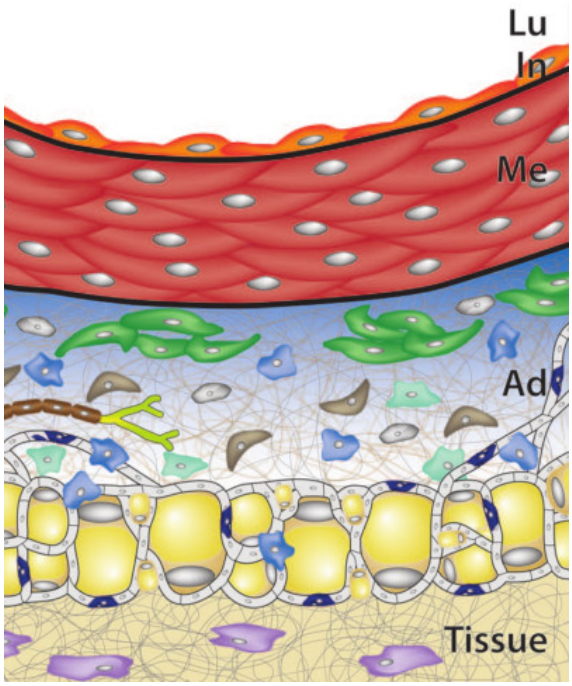

Figure 10: The arterial adventitia. Tissue represents the conjunctive tissue scaffold. Where Lu: vascular lumen; In: intima; Me: media; Ad: adventia; Tissue: conjunctive tissue scaffold. With permission from Majesky [14].

Whether in the pulmonary or systemic circulation, the tunica media is seen as the muscular layer of blood vessels. It is made up almost entirely of smooth muscle cells, positioned concentrically in lamellae around the intimal layer. It is

within this layer that contraction occurs through the action of several receptors and mediators (Figure 11).

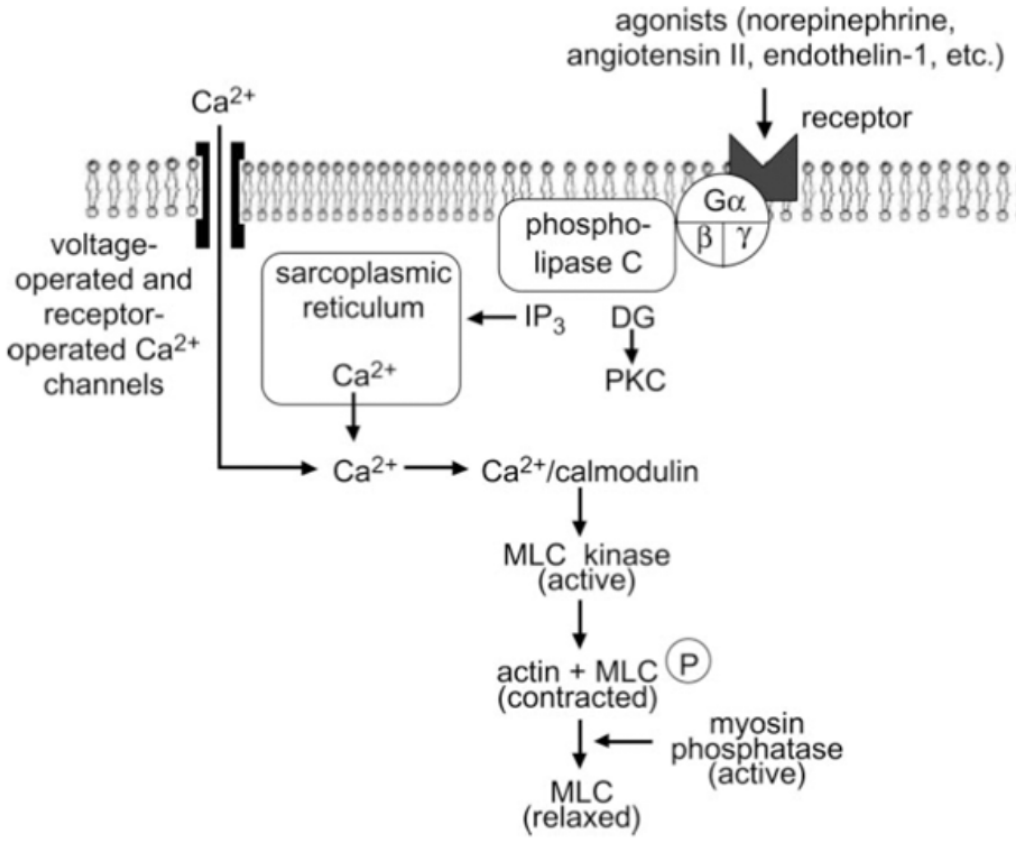

Figure 11: Regulation of smooth muscle contraction. Where G: G-protein; α, β and γ; G-protein subunits; DG: diacylglycerol; IP_3: inositol 1,4,5-trisphosphate; Ca^{2+}: calcium; PKC: phosphokinase C; MLC: myosin light chain. Following stimulation, either by an influx of calcium or the presence of an agonist which acts through phosphatidylinositol 4,5-bisphosphate, there is a release of calcium from the sarcoplasmic reticulum which phosphorylates myosin light chain kinase which initiates the contraction of the smooth muscle cell. Adapted with permission from Webb [15].

The intima is the part of the vessel that is actually in contact with the blood [5]. It is composed of squamous epithelium called endothelium from which many different vasoconstrictors and vasodilators which mediate the modulation of

vascular resistance in the pulmonary system are derived [14]. Impairment in the hemodynamic regulation of the airway vasculature can lead to a multitude of pathologies, including pulmonary hypertension.

As the tracheobronchial tree's anatomy evolves with each passing branch generation, so does the vascularisation around it. Indeed, the composition and thickness of the different sections making up the pulmonary arteries changes with tracheobronchial depth. Furthermore, arterial matches tracheobronchial caliber as both jointly decrease in diameter. The pulmonary circulation is made up, initially, of elastic arteries, transitioning into muscular ones and ending with the capillary network. The walls of the larger arteries (≥ 1000 μm in diameter) are made up mostly of elastic lamellae, few smooth muscle cell (SMC) and collagen fibrils [14]. As the caliber of arteries decreases, the elasticity decreases and the percentage of smooth muscle mass increases, up until arteries with a 40 to 50 μm diameter.

Indeed, larger arteries with a diameter greater than 3200 μm are considered elastic, between 3200-2000 μm, they are transitional between elastic and muscular and, when having an internal diameter between 1000-50 μm, they are muscular [12]. Subsequently, SMC in arteries progressively diminishes in quantity and, when approaching the capillary bed structure, a single smooth muscle cell may remain in the artery wall [12].

1.3.7. Neural and humoral control of pulmonary vasculature

Pulmonary vessels are innervated by both sympathetic and parasympathetic fibers of the autonomic nervous system. However, when compared to systemic vasculature, the innervation is sparser. Larger elastic vessels tend to show more innervation than small muscular ones and no innervation is witnessed for vessels lower than 30 μm in diameter. The stimulation of the sympathetic nerves of the airways causes vasoconstriction by the release of certain neurotransmitters, including norepinephrine, neuropeptide Y, and substance P. The catecholamines epinephrine and norepinephrine both increase pulmonary

vascular resistance when injected into the pulmonary circulation. Histamine, found in the lung in mast cells, is a pulmonary vasoconstrictor. Certain prostaglandins and related substances, such as $F_{2\alpha}$, E_2 and thromboxane, are also pulmonary vasoconstrictors, as is endothelin (ET-1), a 21 amino acid peptide synthesized by the vascular endothelium. In addition, alveolar hypoxia and hypercapnia also cause pulmonary vasoconstriction. At the opposite, parasympathetic stimulation results in acetylcholine and vasoactive intestinal peptide release, leading to vasodilatation and increased mucosal blood flow. The β-adrenergic agonist isoproterenol, nitric oxide, and certain prostaglandins (PG), such as PGE_1 and PGI_2 (prostacyclin), are additional pulmonary vasodilators. In the following section, we will explore how CPB and the reperfusion injury can alter the normal pulmonary vasculature physiology.

CHAPTER 2. Cardiopulmonary Bypass and Pulmonary Hypertension

Cardiopulmonary bypass in action at the Montreal Heart Institute

Cardiopulmonary bypass (CPB), the heart lung machine has been viewed as one of the foremost medical advances of the 20th century [16]. Indeed, thanks to this procedure, cardiac surgical corrections are now common. Roughly 2000 surgeries involving CPB are performed worldwide per hour [16]. In Canada, specifically, there are 36 000 heart surgeries performed yearly, of which 8000 are performed in Quebec [4]. This medical advance having permitted scalpel entry within the cardiac walls is, however, not without risks. The CPB procedure has been shown to have a profound effect on pulmonary vasculature.

2.1. Methodology, functioning and pathophysiological consequences

CPB management has, through the ages, evolved into a highly complex labyrinth of tubing as can be seen in Figure 12.

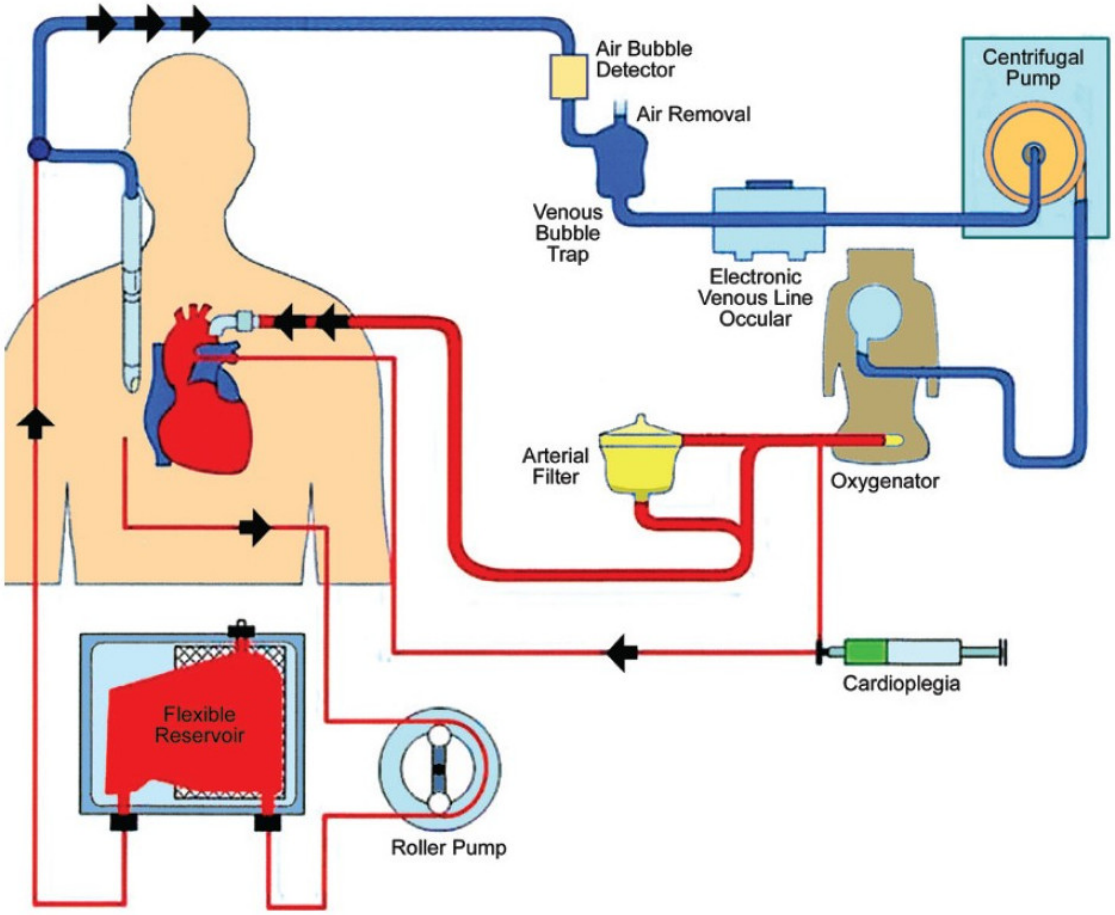

Figure 12: Components of cardiopulmonary bypass. Taken from Aslati [17].

In rough terms, this method implies the transport of blood from the vena cavae and the right atrium, into a venous reservoir through an oxygenation chamber where gaseous exchange is allowed via a membrane interface. Inside this membrane interface chamber is also added the anesthesia mixture. Subsequently, blood is warmed or cooled at will and then redirected to the aorta.

There are several types of consequences associated with this procedure.

Physiological. Following the extensive interaction with foreign materials and substances, CPB exerts an important toll on the outcome of surgery. Indeed, CPB duration was shown to be a significant factor in predicting the clinical outcome of cardiac [18].

Structural. CPB is associated with an increase in pulmonary vascular permeability, resulting in enhanced extravascular water and edema, which causes endothelial and epithelial damages [19].Other changes related to CPB are: thickening of the alveolar septa, vascular congestion, mitochondrial swelling of the alveolar epithelial cells, vacuolation of endothelial cells, blood vessel congestion, and diffuse alveolar damage [20].

Serological. The diversion of blood results in the activation of an inflammatory response through the activation of neutrophils and the release of a multitude of mediators. The activation of neutrophils leads to free radical production, degradation of the interstitium by the proteinases contained in their granules and increased levels of circulating catecholamines [21]. As will be covered in a later section, some mediators have been claimed to play an important role in pulmonary hypertension (PH) following CPB, including ET-1, lysosomal enzymes, interleukin-6 and anaphylatoxins [20, 21]. Most of the effects related to the physiological damages caused by the CPB procedure can be traced back to the blood/biomaterial interactions. Protein adsorption onto the inner surface of materials joint with platelets reaction, intrinsic coagulation activation, fibrinolytic activity and complement activation are at the core of the damaging CPB effect on vasculature [22]. Everything starts with an initial adsorption of a protein layer on the surface of the biomaterials, particularly fibrinogen, albumin and gamma-globulin. This layer of proteins induces platelet adhesion and aggregation which, as erythrocytes and leukocytes are gradually trapped in fibrinogen, is followed

by the formation of a thrombus. This same protein adsorption also leads to activation of the intrinsic coagulation pathway involving the participation of the contact proteins factor XII, factor XI, HMWK (definer) and prekallikrein [22]. In addition an important part of the blood/biomaterial interactions includes the activation of the complement system, notably anaphylatoxins C3a, C4a and C5a which mediate the chemotactic, adhesive and phagocytic responses of leucocytes in the inflammatory process.

These physiological changes and activations within the blood result in a possibly disastrous effect on the lungs called the reperfusion syndrome (Figure 13) where the pulmonary pressures surge, leading to pulmonary hypertension, an increase in cardiac post-charge and, potentially, to right-heart failure [23, 24].

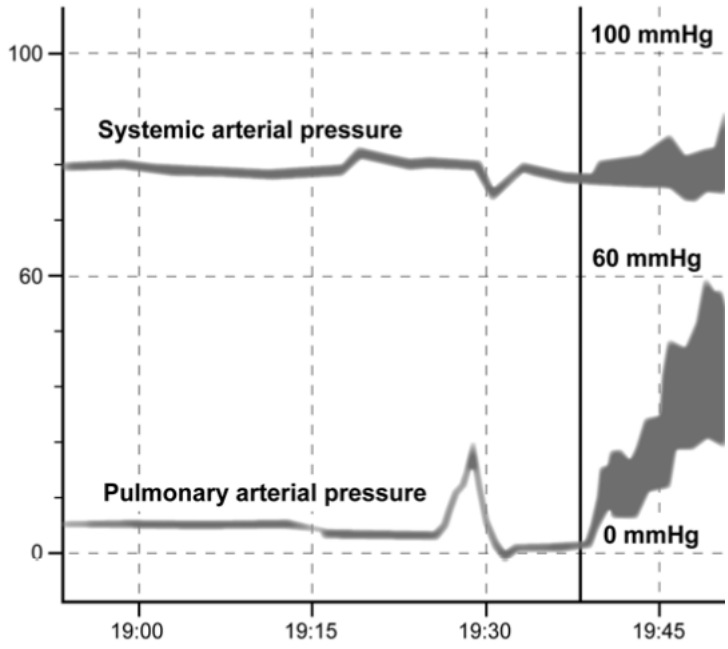

Figure 13: Systemic and pulmonary artery pressure during cardiopulmonary bypass (CPB). At the end of CPB shortly following reperfusion significant increase in pulmonary artery pressure is observed in relation to the systemic pressure. With permission from Denault et al [4].

2.2. Pulmonary hypertension

Depending on the basis of mechanisms, the World Health Organization classifies pulmonary hypertension into five specific groups, as can be seen in Table I.

Table I: Current clinical classification of pulmonary hypertension.

1. Pulmonary arterial hypertension (PH)
    - 1.1. Idiopathic
    - 1.2. Familial
    - 1.3. Associated with
        - 1.3.1. Collagen vascular disease
        - 1.3.2. Congenital systemic-to-pulmonary shunts
        - 1.3.3. Portal hypertension
        - 1.3.4. Human immunodeficiency virus infection
        - 1.3.5. Drugs and toxins
        - 1.3.6. Other (thyroid disorders, glycogen storage disease, Gaucher disease, hereditary hemorrhagic telangiectasia, hemoglobinopathies, chronic myeloproliferative disorders, splenectomy)
    - 1.4. Associated with substantial venous or capillary involvement
        - 1.4.1. Pulmonary veno-occlusive disease
        - 1.4.2. Pulmonary capillary hemangiomatosis
        - 1.5. Persistent pulmonary hypertension of the newborn
2. Pulmonary hypertension with left-sided heart disease
    - 2.1. Left-sided atrial or ventricular heart disease
    - 2.2. Left-sided valvular heart disease
3. Pulmonary hypertension associated with lung diseases and/or hypoxemia
    - 3.1. Chronic obstructive pulmonary disease
    - 3.2. Interstitial lung disease
    - 3.3. Sleep-disordered breathing
    - 3.4. Alveolar hypoventilation disorders
    - 3.5. Long-term exposure to high altitude
    - 3.6. Developmental abnormalities
4. Pulmonary hypertension due to chronic thrombotic and/or embolic disease
    - 4.1. Thromboembolic obstruction of proximal pulmonary arteries
    - 4.2. Thromboembolic obstruction of distal pulmonary arteries
    - 4.3. Nonthrombotic pulmonary embolism (tumor, parasites, foreign material)
5. Miscellaneous
    - Sarcoidosis, histiocytosis X, lymphangiomatosis, compression of pulmonary vessels (adenopathy, tumor, fibrosing mediastinitis)

Adapted with permission from Mcgoon [25].

Pulmonary arterial hypertension (PH) is defined as a mean pulmonary artery pressure superior to 25 mmHg at rest, or to 30 mmHg during exercise [26]. This type of pulmonary hypertension also comprises idiopathic PH, which is a disease of unknown cause, and can just as much lead to right ventricular failure because of the elevation in pulmonary artery pressure as the other groups [27]. The other conditions making up Group I of the World Health Organization table have very similar histological appearances.

2.2.1. Vascular pathways involved in pulmonary hypertension

The histology of pulmonary arteries in patients with PH shows a higher vessel wall thickness, and an unusual layering characterized by thickening of the intimal layer and wall architecture irregularities such as intimal fibrosis [28]. Indeed, though stemming from several underlying causes, PH comprises a group of clinical and pathophysiological entities with comparable features. The chief vascular alterations in PH result in hemodynamic alterations from thrombosis, increase of endothelial and smooth-muscle cells and vasoconstriction. Regardless of the underlying cause of HP, there are many cellular mechanisms (Figure 14) acting together in the maintenance of the disease.

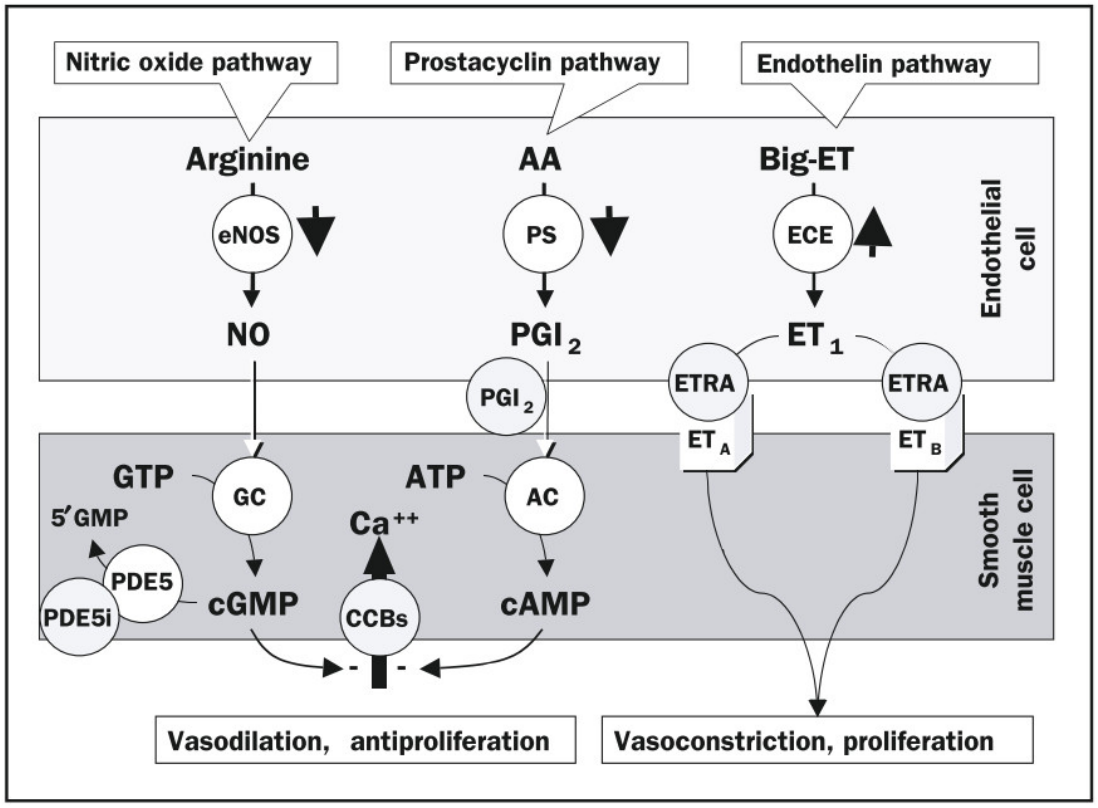

Figure 14: The three mechanistic pathways known to be disturbed in patients with pulmonary arterial hypertension. The points at which drug treatment affects these mechanistic processes are shown in gray circles.

AA: arachidonic acid; CCB: calcium channel blocker; ETRA: endothelin receptor antagonist (eg, bosentan [dual], ambrisentan, and sitaxsentan [receptor A selective]); PDE5i: phosphodiesterase 5 inhibitor (eg, sildenafil). Left, The nitric oxide (NO) pathway. Nitric oxide is created in endothelial cells by type III (ie, endothelial) NO synthase (eNOS), which in pulmonary arterial smooth muscle cells (PASMCs) induces guanylate cyclase (GC) to convert guanylate triphosphate (GTP) to cyclic guanylate monophosphate (cGMP). Cyclic GMP is a second messenger that constitutively maintains PASMC relaxation and inhibition of PASMC proliferation by ultimately reducing inward flux of calcium

ions (Ca++). Cyclic GMP is removed by the PDE5 enzyme to yield the inactive product 5′GMP. Patients with PH have reduced expression and activity of eNOS. Middle, The prostacyclin pathway. The production of prostaglandin I2 (PGI2 [ie, prostacyclin]) is catalyzed by prostacyclin synthase (PS) in endothelial cells. In PASMCs, PGI2 stimulates adenylate cyclase (AC), thus increasing production of cyclic adenosine monophosphate (cAMP) from adenosine triphosphate (ATP). Cyclic AMP is a second messenger that constitutively maintains PASMC relaxation and inhibition of PASMC proliferation. Patients with PH have reduced expression and activity of PS. Right, The endothelin (ET) pathway. Big- (ie, pro-) ET is converted in endothelial cells to ET1 (a 21–amino acid peptide) by endothelin-converting enzyme (ECE). ET1 binds to PASMC ETA and ETB receptors, ultimately leading to PASMC contraction, proliferation, and hypertrophy. Endothelin 1 also binds to endothelial cell ETB receptors (not illustrated). Patients with PH have increased expression and activity of ECE. With permission from McGoon [25].

Nitric Oxide (NO) is a highly potent vasodilator and inhibitor of platelet activation and smooth-cell proliferation. The impairment of the NO pathway, contributing to pulmonary vasodilatation, can also be a cause of PH. This mediator activates a signaling cascade in the endothelial cell that results in smooth muscle cell relaxation [29]. It has also been shown that inhalation of NO by PH patients produces selective pulmonary vasodilatation, and thus enables a diminution of pulmonary vascular resistance. No change in systemic vascular resistance is observed because NO is rapidly sequestrated and inactivated by hemoglobin [30].

Prostacyclin (PGI_2) and Thromboxane A2 (TxA_2) are derivatives of arachidonic acid produced by endothelial cell. PGI_2 shows a three-way activity as vasodilator, as platelet activator and proliferation inhibitor [31, 32]. On the contrary, TxA_2 is a platelet aggregator and a vasoconstrictor. In PH, it was found that the balance between these two vascular effectors was shifted towards TxA_2 [32] as shown by metabolite dosing in urine; thus indicating that this imbalance is part of the underlying causes of PH [32]. As will be discussed later, shifting the balance towards prostacyclin is one of the current treatment options being developed. Indeed, when administered by inhalation, prostacyclin was shown to be efficient in decreasing pulmonary artery pressure by inducing vasodilatation in patients with PH [33].

Endothelin-1 is a potent arterial and venous vasoconstrictor involved in the development of PH as can be seen in Figure 15. It can affect vascular resistance by binding to ET_A receptors located on vascular smooth muscle cells and inducing vasoconstriction. ET_B receptors, expressed on vascular endothelial and smooth muscle cells, reduce pulmonary ET-1 clearance through downregulation of ET-1 cleaving enzyme, also increasing vasoconstriction. However, in contrast, ET_B receptor stimulation increases the release of NO and prostacyclin [34-36]. In addition to its vasoconstrictor effects, ET-1 possesses a stimulating effect on vascular smooth muscle cells, leading to architectural changes in the vascular walls and increased muscularisation.

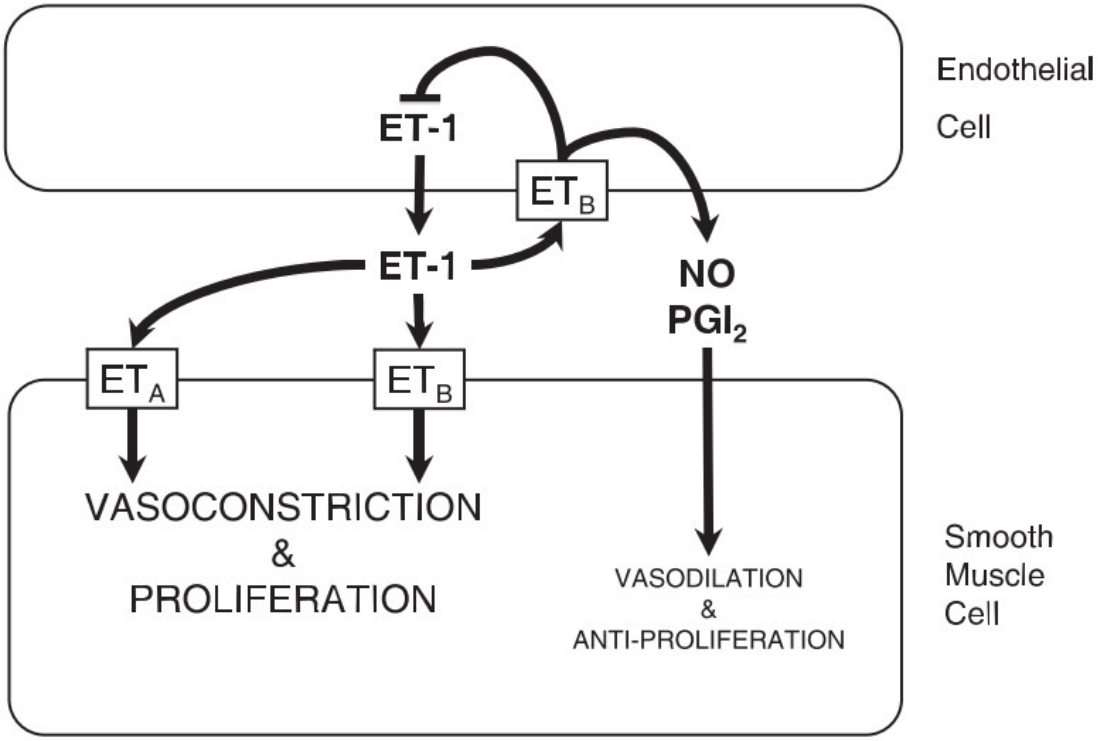

Figure 15: Endothelin-1 (ET-1) signaling pathway in the regulation of pulmonary vascular tone.

Big ET-1 is cleaved to ET-1 by endothelin-converting enzyme (ECE) in endothelial cells. ET-1 binds its specific receptors ETA and ETB with differential effects. Binding of ET-1 to ETA or ETB on smooth muscle cells leads to vasoconstrictive and proliferative effects. ETB are tran- siently expressed on endothelial cells after birth; binding of ET-1 to ETB on endothelial cells leads to downregulation of ECE activity and increased production of nitric oxide (NO)and prostacyclin (PGI2), which lead to vasodilation and antiproliferation. Adapted with permission from Steinhorn [34].

Serotonin (5-hydroxytryptamine, 5-HT) has an overall vasoconstriction action while also promoting smooth-muscle cell hyper- trophy and hyperplasia [34].
Adrenomedullin is a very present vasodilator in the lung as shown by the high mRNA concentration in the organ. Such a presence suggests a possible role in

the homeostasis of lung pressure [26, 29, 31]. Furthermore, plasma levels increases of this peptide are proportionally correlated with the mean pressure of the right atria [37].

Vasoactive intestinal peptide (VIP) is an effective vasodilator, thus decreasing pulmonary artery pressure. It lowers smooth-muscle cell proliferation and inhibits platelet activation [29, 31].

Vascular endothelial growth factor (VEGF) was found, among others, to underlie the expansion of endothelial cells, particularly within vascular lesions [29, 31].

In summary, although these effectors haven't been directly linked to the pathogenesis of PH, their circulating concentration changes have certainly been linked to its pathophysiological consequences. These changes and their links to PH factors are summarized in Table II. Patients suffering from PH show an abnormal release of vasoconstrictors and vasodilators by the epithelium. As seen, the vascular epithelium plays a central role in the regulation of pulmonary vascular tone by releasing vasodilators, such as NO and PGI_2, and vasoconstrictors, such as ET-1.

Table II: Mediators of pulmonary vascular responses in pulmonary arterial hypertension.

Vasoconstriction	Cell Proliferation	Thrombosis
Increased TxA_2	Increased VEGF	Increased TxA_2
Decreased PGI_2	Decreased PGI_2	Decreased PGI_2
Decreased NO	Decreased NO	Decreased NO
Increased ET-1	Increased ET-1	
Increased 5-HT	Increased 5-HT	Increased 5-HT
Decreased VIP	Decreased VIP	Decreased VIP

Where TxA_2: thromboxane A 2; PGI_2: prostaglandin I_2 (prostacyclin); NO: nitric oxide, ET-1: endothelin-1; 5-HT: 5-hydroxytryptamine (serotonin); VEGF: vascular endothelial growth factor; VIP: vasoactive intestinal peptide; Adapted with permission from Farber [31].

2.3. Clinical View of Pulmonary Hypertension

In cardiac surgery, PH may be classified more directly as pre-capillary, capillary or post-capillary. This straightforward classification method is based on the site of the underlying cause. Typically, in a surgical context, PH tends to be post-capillary as the underlying cause is usually left-ventricular. Pre-capillary PH is characterized by dysfunction limited to the arterial side of the pulmonary circulation, while post-capillary hypertension causes abnormalities in the venous circulation, between the capillary bed and the left atrium [38]. The myocardial dysfunction resulting from elevated pulmonary pressure, both pre- and post-capillary, can be explained by the critical role of pulmonary circulation in the

regulation of afterload and preload as, among others, the high pulmonary artery pressure increases right ventricle (RV) afterload, causing possible right heart failure [39, 40].

2.3.1. Diagnosis and mechanism

Pulmonary hypertension may be diagnosed before surgery. X-rays may show a possible enlargement of the right ventricle or the electro cardiogram may indicate irregular rhythms hinting at right heart modifications. Conclusive diagnosis may be performed through right heart catheterization or transoesophageal echocardiography. It may be pre-existing, such as PH secondary to valvular disease, or is can appear due to mechanical failure resulting from post-CPB pulmonary reperfusion syndrome [4]. In the case of patient-prosthesis-mismatch, PH may even persist following the surgery [4]. Common PH mechanisms are illustrated in (Figure 16).

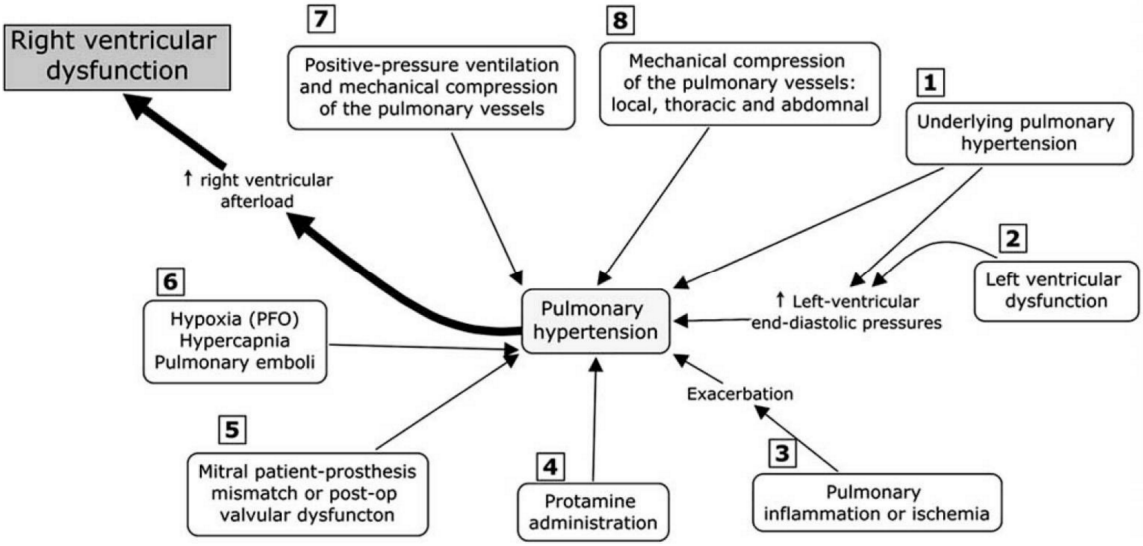

Figure 16: The most common mechanisms that could induce pulmonary hypertension in cardiac surgery. Where PFO: patent foramen ovale. Taken with permission from Denault [4]

Left ventricular systolic or diastolic dysfunction and mitral of valvular disease either pre- or postoperative are the most common causes of PH [38]. Pulmonary inflammation, arising through pulmonary microvascular damage and modification of cytokines and vascular mediators occurring possibly during or at the end of CPB exacerbates pre-existing PH. Through complement activation and vasoconstriction, protamine can also contribute to the emergence or deterioration of intra and post-operative PH [41]. A surgical cause of PH may be mitral patient-prosthesis mismatch. Hypoxia, hypercapnia and pulmonary embolisms can occur before, during or after surgery. In addition, PH itself can cause RV dysfunction which in turn increases RV pressures and consequently can lead to opening up a patent foramen ovale which is a right-left shunt present in 30% of the population [42]. The opens of this shunt exacerbates hypoxia by lowering oxygenation. PH may also be caused by physical factors such as positive-pressure ventilation which distends capillaries, leading to lung hyperinflation and mechanical compression caused by blood or air in the pleural cavity, known as hemothoraces and pneumothoraces respectively.

2.3.2. Pulmonary hypertension treatment

Pulmonary hypertension treatment is based on the etiology of the hypertension, hence the importance of the pathophysiology involved.

2.3.2.1 Non-pharmacological and pharmacological approach

The non-pharmacological approach is directed to the cause of the PH for example, in the case of valvular pathologies, there is the option of surgical intervention. These interventions can indeed help control the hypertension. However, unlike the surgical option, no curative pharmacological treatment exists, only symptomatic. Several agents have been studied, as shown in Table III

Table III: Randomized controlled trial in the treatment of pulmonary hypertension in adult cardiac surgery.

	Author	Country	Date	Agents Used	Design	N	Inclusion criteria	Primary End-Point
1	Fattouch *et al*.	Italy	2006	$iPGI_2$ *vs* iNO vs intravenous vasodilators	RCT Unicenter	58	MVR + PHT before the end of CPB	Hemodynamic
2	Ocal *et al*.	Turkey	2005	iPGI2 *vs* NTG	RCT Multicenter	68	CABG with protamine reaction after CPB	Hemodynamic
3	Stafford *et al*.	USA NC	2005	Heparinase *vs* protamine	Non-inferiority clinical trial design Multicenter	167	CABG on + off pump after CPB	Bleeding
4	Fattouch *et al*.	Italy	2005	$iPGI_2$ *vs* iNO *vs* intravenous vasodilators	RCT Unicenter	58	MVR + PHT in the intensive care unit	Hemodynamic
5	Hache *et al*.	Canada	2003	iPGI2 *vs* placebo	RCT Unicenter	20	PHT before CPB	Hemodynamic
6	Solina *et al*.	USA	2001	iNO *vs* milrinone	RCT Unicenter	62	PHT after surgery	Hemodynamic
7	Feneck *et al*.	UK	2001	Milrinone *vs* dobutamine	RCT Multicenter	120	CO < 2 L/min/m et PAOP > 10 mmHg after cardiac surgery	Hemodynamic
8	Solina *et al*.]	USA	2000	iNO *vs* milrinone	RCT Unicenter	45	PHT after surgery	Hemodynamic
9	Schmid *et al*.	Switzerland	1999	iNO *vs* NTG *vs* PGE_1	Crossover Unicenter	14	PHT after surgery	Hemodynamic
10	Hachenberg *et al*.	Germany	1997	Enoximone *vs* dobutamine+NTG	RCT Unicenter	20	HTP in MVR before and after surgery	Hemodynamic

Where CABG: coronary artery bypass graft; CO: cardiac output; CPB: cardiopulmonary bypass; iNO: inhaled nitric oxide; $iPGI_2$: inhaled prostacyclin; MVR: mitral valve replacement; NO: nitric oxide; NTG: nitroglycerin; OR: operating room; PAOP: pulmonary artery occlusion pressure; PGE_1: prostaglandin E_1; PGI_2:

prostacyclin; PHT: pulmonary hypertension; RCT: randomized controlled trial; UK: United Kingdom; USA: United States of America. Adapted with permission from Denault [4].

These studies explore the use of antihypertensive and hypotensive agents such as nitric oxide, prostacyclin, nitroglycerin, dobutamine in order to alleviate and reduce the possible complications of PH, in particular RV failure

2.3.2.1. Major consequence of pulmonary hypertension: right ventricle failure

Although no curative treatment exists, in the case of RV failure, patient management involves the use of loop diuretics, potassium-sparring agents, metazolone supplementation so as to reduce intravascular volume and facilitate preload management [25]. The use of inotropic support is also common with digoxin and intravenous (IV) milrinone. Pharmacological aid can also target the molecular pathways underlying the pulmonary hypertension, specifically aiming at the vascular level. Calcium channel blockers, prostacyclin analogues, endothelin receptor and phosphodiesterase (both 3 and 5) antagonists are the main avenues of treatment. Prevention of PH represents a promising strategy to prevent RV failure before it even appears. To date, very few studies have addressed this issue and one of the potential avenues constitutes the prevention of the pulmonary reperfusion syndrome. In this regard, both iPGI2 [24]and inhaled milrinone [23, 43] have been demonstrated to prevent CPB-induced endothelial dysfunction, in an animal model. A pilot randomized controlled trial conducted by Hache *et al.* in patients with preoperative PH concluded that iPGI2 was superior to placebo in reducing PH and was also associated with lower requirements for vasoactive support [33].

2.4. Pulmonary hypertension animal models

PH can be induced in animals by several methods in order to study the characteristics of this disease. Hypoxic pulmonary hypertension is one of the easiest to perform and can be induced by prolonged exposition to hypoxic conditions. This results in pulmonary vasoconstriction followed by arteriolar remodeling and thickening of the arterial wall (Figure 17) [44].

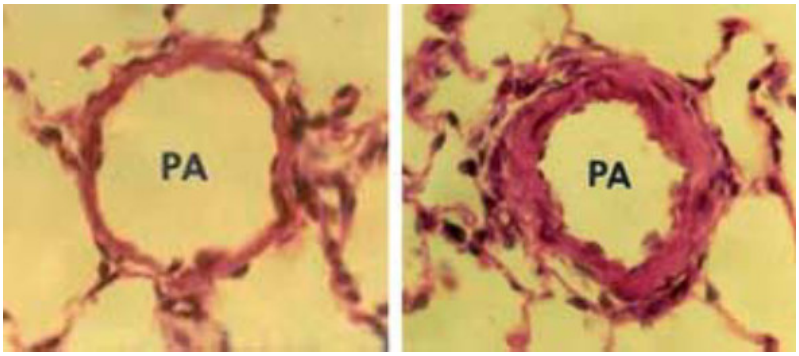

Figure 17: Rat pulmonary arterioles, left, normal, right, after two weeks of hypoxia. Taken with permission from Naeije [45].

Another highly used option is the use of monocrotaline, which is a compound from the alkaloid family and which has the potential to cause PH in animals through its selective toxic effect on pulmonary vasculature. It selectively targets pulmonary vasculature as it is activated by liver oxydases and the lungs represent the first major vascular bed following liver passage [45]. It produces endothelial necrosis with pulmonary edema, leading to elevated pulmonary artery pressure and right ventricular hypertrophy. Other chemical damage-induced PH models are alpha-naphthyltiourea and bleomycin whose side-effects are deep-lung inflammation, edema and muscular vasculature remodeling. There are also methods of generating PH though the use of endogenous molecules such as VEGF or thromboxane A2 [35, 46]. A more physical method to induce PH is through the use of microspheres or embolizations to apply

physical damaged to the capillary bed [47]. In other animal models, PH can be secondary to shunt cardiopathy caused by surgical manipulation [48]. The use of genetically modified animals is another alternative to provoke PH in animal models [45, 49].

A less common pulmonary hypertension model is though induction of hypercapnia. The effect of hypercapnia on pulmonary pressures has been described by several human [50, 51] and animal [52-55] studies. The main physiological characteristic of hypercapnia is the presence is a higher quantity of CO_2, circulating dissolved in the blood stream. This increase in CO_2 results in higher circulating levels of HCO_3^- (carbonic acid) which in turns decreases blood pH causing systemic acidosis [51]. Uncompensated, this acidosis causes a decrease in systemic resistances and increases cardiac output [56]. It also increases the QT interval, heart rate and subsequently systemic blood pressures [51]. Compensated however, the systemic hemodynamic effects of hypercapnia are reduced or nullified [55]. Moderate compensation of hypercapnic acidosis could thus generates a potentially generate an adequate model for pulmonary hypertension. Pulonary pressures increase proportionally to the inspired CO2 fraction, making the hypertension titratable [57].

Out of several potential candidates, swine is considered a good animal model to study PH during CPB [58]. The anatomy and physiology of the porcine heart share many characteristics with that of humans and similarities between humans and swine have been recognized on the basis of their anatomic and physiologic features. For example, the blood distribution, the blood supply to the conduction system, the appearance of the myocardium and the wound healing characteristics are similar in both species [23, 45, 58, 59]. In addition

2.4.1. Prevention of Pulmonary Hypertension in Cardiac Surgery

Pulmonary hypertension is a potentially fatal condition. Death to PH most often occurs following RV failure or arrhythmias related to right heart wall stress [25]. This condition can lead to the cardio-intestinal syndrome resulting from intestinal edema and hepatic congestion [60].

CHAPTER 3. Milrinone

3.1. Physicochemistry and Mechanism of Action

Milrinone (1,6-Dihydro-2-methyl-6-oxo-[3,4′-bipyridine]-5-carbonitrile) (Figure 18) is a vasodilator, positive inotropic agent derived from the parent drug amrinone, which belongs to the bipyridine chemical family.[61, 62] This compound, sold under lactate form (pH 4), has a logP of 1.17 and pKa of 9.67.

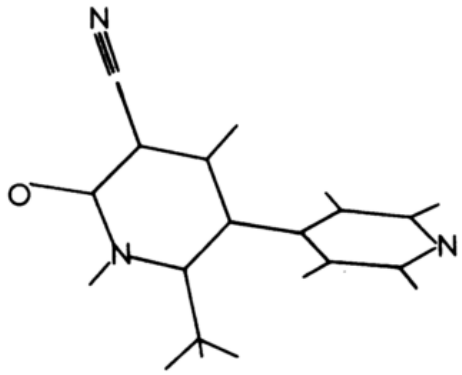

Figure 18: Chemical structure of milrinone. Taken with permission from Mylotte [63].

Milrinone exerts its effect by inhibiting the phosphodiesterase type III (PDEIII) enzyme, which is responsible for cyclic adenosine monophosphate (cAMP) hydrolysis. This action results in an increase in cAMP intracellular concentrations in the vascular smooth muscle cells and cardiomyocytes. [64, 65] In the cardiomyocytes, the rise in intracellular cAMP results in an increased influx of calcium in the cell, leading to an enhanced intracellular calcium concentration, which in turn increases cardiac contractility. However, in the smooth muscle cell (Figure 19), the increased intracellular cAMP concentration leads to vasodilatation by decreasing calcium concentration in the cell [66].

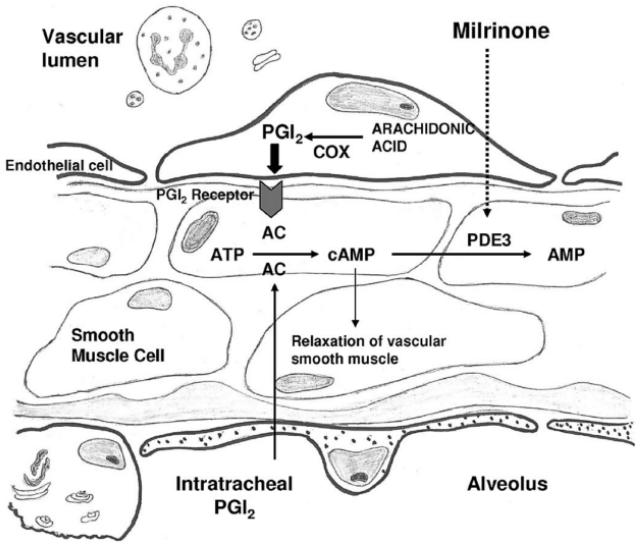

Figure 19: Signal transduction pathway of PGI2–cAMP system. PGI2 and milrinone increase cAMP by different mechanisms and hence combination of these two therapies will greatly increase cAMP levels enhancing the relaxation of the vascular smooth muscle. COX, cyclo-oxygenase; AC, adenylate cyclase. Taken with permission from Rashid [67].

Studies showed that intravenous administration of milrinone leads to left ventricular afterload reduction, increased cardiac output, reduction in total peripheral resistance, [68] reduction of pulmonary artery pressure, pulmonary vascular resistance, and increased cardiac index without any change in myocardial oxygen consumption [69, 70]. Because of its beneficial effects on the cardiovascular system, milrinone has become an attractive option for the treatment of patients undergoing cardiac surgery.

As mentioned previously, the use of cardiopulmonary bypass (CPB) is associated with a multitude of post-operative complications. The administration of milrinone before cardiac surgery could therefore be used to limit these injurious mechanisms.

3.1. Milrinone pharmacokinetics

Following 10-125 µg/kg in human volunteers, milrinone was shown to have a volume of distribution of 0.32 L/kg and a total body clearance of 0.32 L/kg/h and a half-life of 50 minutes.[61] The volunteer clearance suggests an active secretion mechanism. Following 0.2-0.7 µg/kg IV infusions in congestive heart failure patients, milrinone had a volume of distribution of 0.45 L/kg, a total body clearance of 0.14 L/kg/h and a half-life of 2.4h. The oral route (F = 0.79-0.85) showed similar mean clearance values (0.4 L/kg/h) but a higher mean volume of distribution (0.56 L/kg) [61]. In patients undergoing CPB, pharmacokinetic parameters were similar to congestive heart failure patients[71]. Milrinone is chiefly excreted unchanged in urine as only 12% of it is metabolized into O-glucuronide. About 70% of milrinone circulates protein-bound [61].

3.2. Clinical use

3.2.1. Intravenous milrinone

Initially, milrinone was used intravenously for its inotropic properties in congestive heart disease. Then its hypotensive properties made it an alternative for pulmonary hypertension. In a clinical context, milrinone, even administered intravenously, was shown to be effective in facilitating weaning from CPB. However, IV milrinone as a treatment for CPB-weaning does involve a certain risks for patients, such as an increased myocardial oxygen consumption, impaired platelet function and severe systemic hypotension [72].

3.2.2. Inhaled milrinone

It was shown by a several studies that inhaled milrinone may have Inhaled milrinone is thus a compound that possesses a lot of advantages without systemic side effects.

In a context of cardiac surgery in adult patients, milrinone administered by inhalation has been proven effective for the treatment of HP, as it shows a

selective action on pulmonary vasculature [23, 73]. Inhaled milrinone causes a pulmonary-selective vasodilatation, and a reduction in mean pulmonary artery pressure and pulmonary vascular resistance in patients with pulmonary hypertension [73, 74] and without causing systemic hypotension [73, 74]. Several studies were performed on the efficacy on milrinone inhalation in the treatment and prevention of pulmonary hypertension (Table IV)

Table IV: Clinical use of inhaled milrinone.

Author	Date	Type	n	Population	Groups	Timing	Type of nebilizer	Dosage	Data collection	Results
Haraldsson	**2001**	Observational	20	Cardiac surgical patients with post-op PH (mPAP >25 mmHg and PVR >200 dyn·s/cm5)	Part I: iMil (3 doses), Part II: iPGI2 vs. iPGI2 + iMil	post-op (ICU)	Jet	Part I: 3 mg iMil (3 incremental doses: diluted 0.25 mg/ml, diluted 0.5 mg/ml, 1mg/ml) over 30 min (3 subsequent 10 min periods). Part II: iPGI2 (10 ug/ml) over 10 min + (iPGI2 (10 ug/ml) + iMil (1 mg/ml)) over 10 min.	Bsl, after each 10 min periods and 20 min after end inhalation.	iMil (1 mg/ml) ↓mPAP (6%), ↓PVR (20%), ↓TPG (15%), ↓PVR/SVR (17%) & all values returned to bsl 20 min after end inhalation. iPGI2 had similar vasodilator effects but iMil + iPGI2 potentiated (PVR, SV) & prolonged >20 min (mPAP, PVR, TPG). No systemic hypotension in all groups.
Sablotzki	**2005**	Observational	18	Heart transplant candidates with/without PH (mPAP >30mmHg)	PH vs. no PH	per-diagnostic (right heart catheterization)	Ultrasonic	2 mg iMil (diluted in 3 ml) within 15min (25-50 ug/ml).	Bsl, 10, 30, 60 min after start inhlation.	In PH group ↓mPAP, ↓PVRI (25%), ↓TPG after 10 min & ↓PCWP, ↑RVEF after 30 min. mPAP and PVRI values returned to bsl after 30 min. In non-PH group ↑PCWP. No systemic hypotension in all groups.
Lamarche	**2007**	Retrospective	70	Cardiac surgical patients under CPB with PH	Pre- vs. Post-CPB	pre-/post-CPB	Jet	5 mg iMil (1 mg/ml) over 5 min (50-80 ug/kg).	After CPB	iMil pre-CPB ↓mPAP, ↓CPB reinitiation, ↓DSB, ↑LV FAC. iMil post-CPB ↑mPAP, ↓mAP/mPAP ratio. Both groups ↓mAP, ↑HR, ↑CI, ↓PaO2/FiO2. No systemic hypotension in all groups. CPB time, cross clamp time and iMil pre-CPB identified as potential DSB risk factor.
Wang	**2009**	Randomized Controlled Trial	48	Cardiac surgical patients under CPB with PH (mPAP >25mmHg) and post-op PH (mPAP >25 mmHg & PVR >200 dyn·s/cm5)	iMil vs. IV Mil	post-op (ICU)	Jet	24 mg iMil (1 mg/ml) over 4 h. IV Mil bolus 50 ug/ml + infusion 0.5 ug/kg/min for 4 h.	0, 1, 2, 3, 4 h after start inhalation and 15, 30, 45, 60 min after end inhalation.	iMil ↑PaO2/FiO2, ↓Qs/Qt. IV Mil ↓mAP and ↓SVR after 2-4h (induced systemic hypotension; n = 2). Both groups ↓mPAP, ↓PVR and ↑CI. mPAP and PVR values returned to bsl after 60 min end inhalation.
Hegazy	**2010**	Randomized Controlled Trial	92	Cardiac surgical patients with PH (sPAP >30 mmHg or mPAP >25 mmHg)	iMil vs. iPGI2	pre-CPB	Jet	5 mg iMil (1 mg/ml) over 5 min (50-80 ug/kg). 5 ml iPGI2 (15 ug/ml) over 5 min.	0, 15 min after end inhalation and 15, 30 min post-CPB weaning and at arrival to ICU.	In both groups ↓PVR, ↓mPAP, ↑CI, ↑HR and ↑RVEF after CPB weaning and at arrival to ICU. No systemic hypotension in all groups.
Singh	**2010**	Randomized Controlled Trial	35	Cardiac surgical patients (children <12yr) with PH (mPAP >30 mmHg)	iMil vs. iNTG	pre-CPB (pre-anesthesia)	Jet	iMil or iNTG (diluted in 3ml) over 10 min (50 µg/kg) after pulmonary vasodilatation by 100% oxygen for 10 min.		In both groups ↓sPAP, ↓dPAP, ↓mPAP, ↓PVRI, ↓SVRI and ↑Qp/Qs. No systemic hypotension in all groups.
Guo	**2011**	Randomized Controlled Trial	30	Cardiac surgical patients under CPB	iMil vs. placebo	pre-op	NA	5 mg iMil (diluted in 5 ml) per 8 h two days pre- op.	0, 30 min post-aortic unclamping and 0, 24, 72, 168 h post-op.	In both groups ↑ all factors plasma levels post-CPB. In iMil group PVR, OI, TNF- alpha, IL-6, MDA and venous/arterial ratio leucocyte count were lower post-op.
Gong	**2012**	Randomized Controlled	30	Cardiac surgical patients under CPB	iMil vs. placebo	pre-CPB (pre-	Ultrasonic	15 ml iMil (0.1%) over 15 min.	0 min, imm. pre-CPB and 0, 24 h post op.	In both groups ↑ all factors plasma levels post-CPB and 24 h post-op. In iMil group Il-6, TNF-alpha, MMP-9 were lower at the end of surgery.
Denault	**2014**	Randomized Controlled Trial	21	Cardiac surgical patients with PH (sPAP >30 mmHg or mPAP >25 mmHg)	iMil vs. placebo	pre-CPB	Jet	5 mg iMil (1 mg/ml) over 5 min (50-80 ug/kg).	0 min, end inhalation, 20 min after end inhalation (pre-CPB), post-CPB and at chest closure.	iMil ↓PVR. In control group ↑ right-sided cavity dimensions (↑RVEDA, ↑RADt and ↑TAPSE). No systemic hypotension in all groups.
Buckley	**2007**	Case report	1	Patient with acute PH	IV treprostinil + iNO + iMil	ICU (added salvage therapy)	Jet	iMil (diluted 0.5 mg/ml) at flow rate 2 L/min (4mg/h) in addition to iNO 20 ppm and treprostinil 2 ng/kg/min for 3 days. iMil decreased to 1 mg/h over 24 h on day 4 and tapered off until	Every hour on day 1 and daily thereafter until day 9.	iMil ↑SvO2 (12%) within 10 min starting inhalation. No systemic hypotension or HR effect.
Carev	**2010**	Case report	2	Cardiac surgical patients with severe PH (sPAP 80-90 mmHg and mPAP 40-50+	IV Mil + iMil	post-op (ICU)	Jet	iMil (diluted 0.5 mg/ml) at rate 0.3 ml/min over 70 min in addition to IV Mil 0.5-0.75 ug/kg/min and NTG 1-3 ug/kg/min.	Bsl and 0, 12, 24 h after end inhalation.	↓PVR (40-43%), ↓mPAP (6-8%) after inhalation and ↓PVR (32-39%), ↓mPAP (2-25%), ↑mAP/mPAP (16-41%) 24 h after inhalation. No systemic hypotension.
St-Pierre	**2014**	Case report	1	Cardiac surgical patients with PH (mPAP 74 mmHg)	iMil + iPGI2	pre-CPB	Jet	5 mg iMil (1 mg/ml) over 5 min (50-80 ug/kg) in addition to 75 ug iPGI2.	Bsl, during, after (pre-CPB) inhalation and post-CPB.	↓PVR (9-40%), ↓mPAP (12-41%) during and after inhalation and post-CPB (max effect). No systemic hypotension.

Bsl, baseline; CPB, cardiopulmonary bypass; CI, cardiac index; dPAP, diastolic pulmonary pressure; DSB, difficult separation from bypass; FiO2, fraction of inspired O2; HR, heart rate; ICU, intensive care unit; IL-6, Interleukin-6; iMil, inhaled milrinone; iNO, inhaled nitric oxide; iNTG, inhaled nitroglycerin; iPGI2, inhaled prostacyclin; LVFAC, left ventricular fractional area change; mAP, mean artery pressure; MDA, malondialdehyde; MMP-9, metaloproteinase-9; mPAP, mean pulmonary artery pressure; OI, oxygenation index; PaO2, arterial O2 tension; PCWP, pulmonary capillary wedge pressure; PH, pulmonary hypertension; PVR, pulmonary vascular resistance; PVRI, pulmonary vascular resistance index; Qs/Qt, intrapulmonary shunt fraction; RADt, tranverse dimensions of the right atria; RVEDA, right ventricular end diastolic area; RVEF, right ventricular ejection fraction; sPAP, systolic pulmonary artery pressure; SV, stroke volume; SvO2, venous oxygen saturation ; SVR, systemic vascular resistance; SVRI, systemic vascular resistance index; TAPSE, triscupid systolic annular plane excursion; TPG, transpulmonary gradient. Taken with permission from Nguyen.

In these studies, when milrinone is used as a treatment for HP, both pulmonary vascular resistance (PVR), and pulmonary arterial pressure (PAP) decreased [74].

When inhaled milrinone was administered pre-CPB in prophylaxia to at-risk patients undergoing cardiac surgery, the same decreases in in pulmonary vascular resistence and pulmonary arterial pressure [65] were observed without any reported case of systemic hypotension. In addition, pre-CPB milrinone inhalation was associated with a decrease in difficult CPB weaning [65] and lower plasma levels of pro-inflammatory cytokines such as IL-6 and TNF-α [75, 76]. These prophylactic effects linked to inhaled milrinone administration observed in patients also support the previously observed results in CPB swine models [23].

CHAPTER 4. Pulmonary administration and deposition

4.1. Nebulization

Inhalation is a well-known and use administration method for several medications. For proper inhalation, the aerodynamic diameters of drug particles should be found within certain ranges. As such, specific tools have been developed to successfully and efficiently deliver formulations to human lung airways. A major research concern in pulmonary drug delivery is the utilization of physical or chemical mechanisms, to improve the performance and delivery of these tools, among which, are nebulizers [77].

4.1.1. Nebulizer types

Air-Jet Nebulizers (Figure 20)

This type of nebulizer, is the oldest and most common one. It uses a secondary pressurized gas stream with a 2-10ml/min flow to transform a liquid suspension into a large array of particle sizes. They are considered more cumbersome and difficult to use because of the need for the secondary stream which reduces portability and added tubing [78]. In addition as these devices require a gas source which is often oxygen flow. Therefore their final effect on pulmonary vasculature may be influence by the administration of oxygen which is a pulmonary vasodilator. These nebulizers have also been known to show lower delivery efficiency than their counterparts and high residual volume.

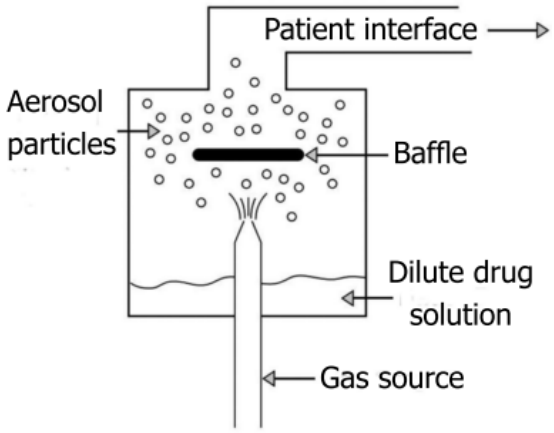

Figure 20: Typical structure of air jet nebulizers. Adapted with permission from Kleinsteuer [79, 80].

Ultrasonic wave nebulizers (Figure 21) use a high frequency (1-3MHz) vibrating piezoelectric crystal to nebulize medication. Ultrasonic nebulizers produce less noise and, when compared with jet nebulizers, have a faster drug delivery. There is no need for additional gas source However, the heat generated produced during nebulization places certain restrictions on the medication to be nebulized. Much like their jet counterparts, these nebulizers are known to have high residual volumes [77].

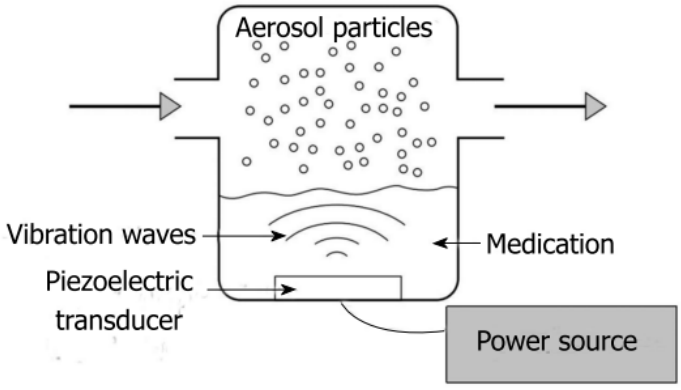

Figure 21: Typical structure of ultrasonic mesh nebulizers. Adapted with permission from Kleinsteuer [79, 80].

Ultrasonic vibrating mesh nebulizers (Figure 22) are considered a more advanced generation. These nebulizers generated a predominantly fine distribution of particles and are considered silent, highly performant and leaving a reportedly low residual volume and delivering 2-3 times more medication than jet nebulizers [77]. They transfer the liquid through vibrating micro-holes thus generating a breathable mist. Unlike ultrasonic nebulizers, mesh nebulizers are not known to have heat-imposed medication restrictions. They do not require additional gas flow.

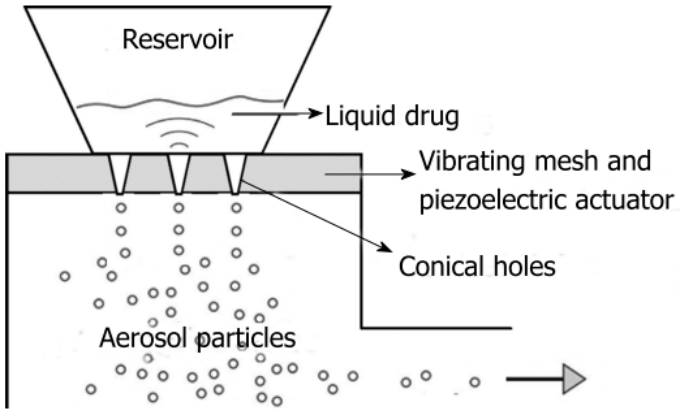

Figure 22: Typical structure of ultrasonic mesh nebulizers. Adapted with permission from Kleinsteuer [79, 80].

4.2. Particle size distribution

An aerosol is usually considered to be a double phase system consisting of a finely partitioned particulate matter floating in a gaseous medium. The particles may be solid, liquid or even the two conjointly. These particles have a wide array of size ranges and their deposition pattern is fully dependent on factors such as the gaseous medium and the physical forces that affect it (Figure 23) [81].

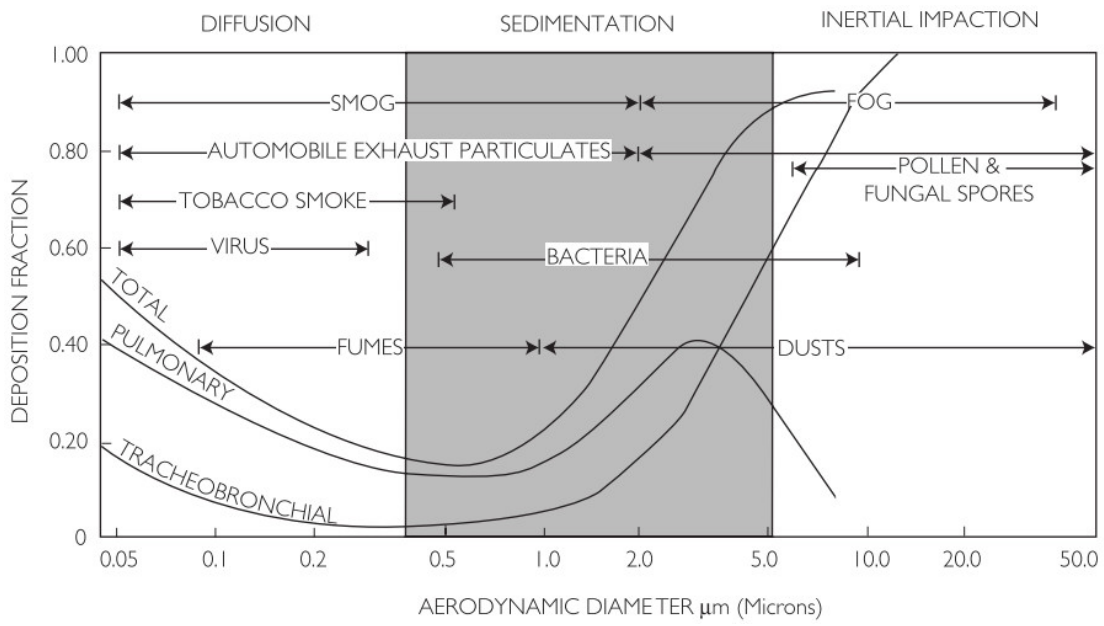

Figure 23: Relationship between particle size and lung deposition.

With permission from Labiris [81].

In the case of inhalation, there are the added factors inherent to the intrapulmonary environment. There are several methods with which to produce aerosols, nebulization is one of the technique. These methods most often generate clouds of so-called polydisperse distributions, meaning that the quantity of particles of certain aerodynamic diameters generated will follow a normal distribution of sizes around a mean or a median. As can be seen in Figure 23, these ranges of size result in a heterogeneous cloud where particles have different probabilities of deposition in different regions within the lung.

4.1. Deposition mechanisms

Particles can be deposited through three major mechanisms that affect deposition on the mucosae of different tracheobronchial tree generations. These are impaction, sedimentation and Brownian diffusion as illustrated in the

following Figure 24 representing intrathoracic pathways after passing the upper airways.

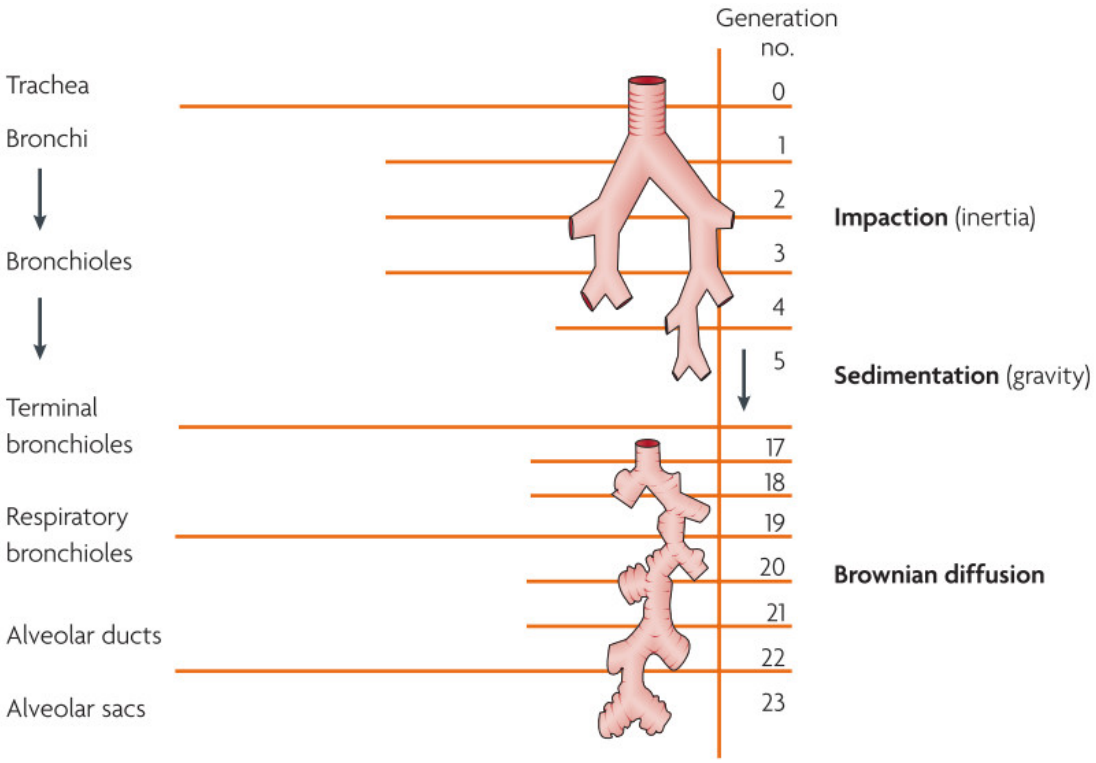

Figure 24: Factors that determine the deposition of inhaled particles. Taken from Patton [10].

4.1.1. Inertial impaction

Firstly, in the first ten generations, where air velocity is highest, particles deposit mostly through inertial impaction (Equation 2) by the sheer force of the aerosol particle colliding with the tracheobronchial tree mucosae. The majority of particles above 10 μm have a high probability of deposition in the oropharyngeal region, particularly in the larynx if the drug is administered through the mouth. [8] This portion of the administered dose is collected by the ciliary cells and transported towards the digestive system where it stands a chance of being absorbed through the gastrointestinal tract [9].

$$I \propto V_p \times V_\alpha \times \sin(\frac{\theta}{rg})$$

Equation 2: Inertial impaction. Under gravitational acceleration (g), the probability (I) of a particle being deposited is proportional to the terminal settling velocity (Vp) of the particle times the velocity of the airstream (Va) and inversely proportional to the radius (r) of the airway

Meaning that the greater the aerosol particle, the great the settling velocity, the greater the bend angle θ and the smaller the airway radius, the higher will be the probability of deposition by inertial impaction.

4.1.2. Sedimentation

It is the deposition of particles under the simple act of gravitational forces. In the region where sedimentation occurs, a decrease of air velocity is observed due to the increase in tracheobronchial volume. Indeed, as the airways subdivide, the space from all bronchi and bronchiole increases. As such, once a particle reach a certain settling velocity within that space, its deposition is attributed to the force of gravity and the resistance of the air that surrounds. This settling velocity (Vt) may be calculated through Equation 3 [9].

$$V_t = (\sigma - \varrho) \times \frac{g \times d^2}{18\gamma}$$

Equation 3: Sedimentation. γ: air viscosity; σ: particle density; ϱ: air density; d: particle diameter.

As the particles become smaller a correction factor (Cunningham) must be added to adjust the air-drag of particles of this size [9, 82].

4.1.3. Brownian diffusion

When reaching very small sizes, such as tens or thousands of a micrometer, the main mechanism of deposition becomes Brownian diffusion. At this point, particles are so small that they are affected and displaced by the random movement of gaseous molecules. Furthermore, at this size, the density of the particles themselves are no longer taken in to account as a factor for deposition [9]. This displacement of particles by molecules (Λ) can be described by the following Equation 4 [9].

$$\Lambda = \frac{R \times T \times C \times t}{N \times 3 \times \pi \times \gamma \times d}$$

Equation 4: Brownian diffusion. R : gas constant; T: temperature; C: Cunningham's number; t: particle residence time; N: number of molecules per gram of air; γ: air viscosity and d: particle diameter.

Contrary to sedimentation, this mechanism of deposition increases with the decreasing size of particles as their size is inversely proportional to their displacement by gaseous molecules. The higher the displacement implies the higher probability of deposition.

4.1.4. Airway geometry

These mechanisms describe a probability of deposition in certain conditions, but of course, they are all three dependent on the anatomical makeup of the air passages. Indeed, airway geometry is variable from a patient to another and has a very significant influence on the site of particle deposition. [83]. The geometry of the airway bifurcation is unique to each individual. Even though mother branches divide into two daughter branches as described in the Weibel model, the angle at which they are formed is variable [84]. Thus, each patient has a tracheobronchial tree that potentially occupies and ventilates certain regions inside the lungs more than others. This peculiarity certainly

accounts for the high interindividual variability of the inhalation route of administration.

4.1.5. Aerodynamic diameter

As mentioned in the mechanism section, one of the most important factors is the particle aerodynamic diameter, and its velocity. In fact, the particle diameter determines the site of deposition[85] . According to previous studies, particles ranging from 1 to 3 um in diameter deposited mainly in the alveolar region, those of 3 to 5 um deposited uniformly throughout the lung, while those larger than 5 um were found to deposit predominantly in the large conductive airways [9, 86]. We can see in Table V a summary of particle deposition sites according to particle size.

Table V: Deposition of monodisperse merosols in the aerodynamic size range 1 to 8 μm.

Particle aerodynamic diameter (μm)	Percentage deposition in:			Percentage "total" deposition	Percentage exhaled
	Oropharynx	Tracheobronchial zone	Alveoli		
1	0	0	16	16	84
2	0	2	40	42	58
3	5	7	50	62	38
4	20	12	42	74	26
5	37	16	30	83	17
6	52	21	17	90	10
7	56	25	11	92	8
8	60	28	5	93	7

Adapted from Stahlhofen [87, 88].

A decrease in particle size results in a greater percentage of particle deposition in the alveolar region. An increase in particle diameter enhances oropharyngeal deposition [87]. Several mechanisms are responsible for particle deposition in the lungs. For particles in the size range of 1 to 10 um, inertial impaction and gravitational sedimentation can occur. The former takes place when relatively large particles (superior to 1 um diameter) deposit in the oropharynx or at bifurcations of the airways as the air changes direction. On the other hand, the gravitational sedimentation may arise in small conductive airways and alveoli, where particles deposit onto the airway surfaces during slow breathing. [88]

4.1.6. Other factors

There are of course other factors which directly, though to a lesser extent, affect aerosol deposition. The breathing pattern plays an important role, because a rapid inhalation increases the probability of deposition in the oropharynx and large conductive airways, while a slow inhalation allows a large number of particles to penetrate in the peripheral parts of the lungs. [78, 89]The shape of the particle will also affect deposition in some measure. Ellipsoidal shapes, when compared to spherical shapes, have a higher mass for the same

maximum aerodynamic diameter. [9]. Another secondary factor to take into account is hygroscopicity. Some material will have a tendency to absorb more water than others. As such, under the 99.99% humidity conditions of the lungs, the use of different mediums may incur a change in the size of the aerosol particles. [9]. An example is the doubling of aerosol particles of hypertonic saline as it absorbs humidity during itsmovement in the tracheobronchial tree.

4.1.7. Cascade impaction

Thus, the characterization of the aerodynamic diameter of pharmaceutical aerosols is required to predict lung deposition of the substance, as the site of deposition is, as discussed earlier, highly influenced by particle size. Particles with an aerodynamic diameter superior or equal to 5um deposit in the oropharynx and tracheobronchial region, whereas particles in the range of 1 to 3 um deposit in majority in the pulmonary region [90, 91]. However, to identify the particle size distribution range of particles in polydisperse clouds, a technique called cascade impaction is needed. It can be used for quality control of drugs and delivery systems, and for size and distribution characterization [92].

4.1.7.1. Operating principles

A typical cascade impactor is made up of several stages which serve as size-separating sieves for incoming clouds of particles. The size of these sieves decreases at each level, thus having each stage capture particles down to the size of its specific sieve. The defining measurement for each stage is referred to as a cutoff diameter. As can be seen in Figure 25, the cumulative collection efficiency curves follow a sigmoid pattern of collected particles around $d_{50\%}$, the cutoff mark.

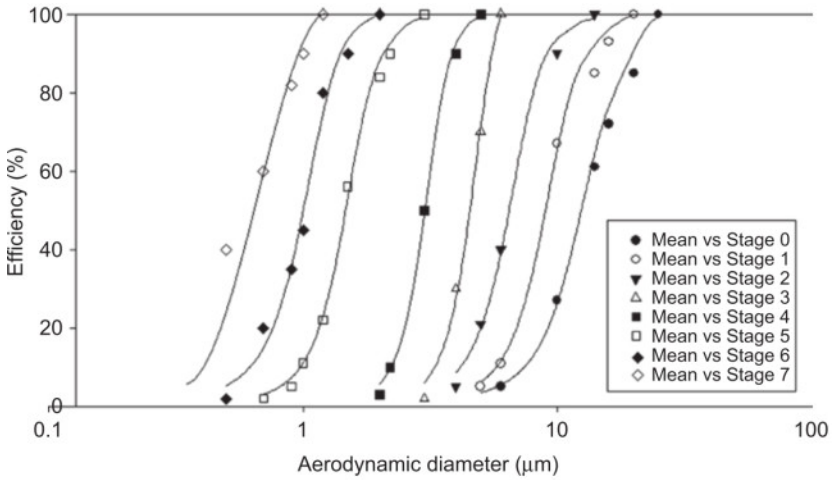

Figure 25: The calibration curves of the ACI at an inhalation flow rate of 15 L min−1 at room temperature. Taken with permission from Abdelrahim [93].

Much like the quantal response curves used to represent efficacy, the sigmoid can also be thought of as a Gaussian distribution of particles sizes centered on the Theoretical cutoff aerodynamic diameter of that particular stage. Ideally, the sigmoids associated to each stage of the impactor should not overlap.

Impactors consist of an air stream, pumped by a vacuum, containing aerosolized particles passing through multiple stages of decreasing nozzle diameter [92-96] . The collection plate below each stage collects the larger particles, while the smaller particles with low inertia are carried by the air stream. Those particles will eventually deposit in subsequent stages with the decrease in orifice diameter, which causes an increase in air velocity and particle inertia [90] . Each impaction plate is characterized by an effective cut-off diameter (ECD), representing the size at which 50% of the particles entering are retained on that stage. The active pharmaceutical ingredients can be quantified by high-performance liquid chromatography (HPLC), and these data may then be used to establish the efficiency curve of the impactor. The use of the impactor can also provide information about the fine particle fraction, or “respirable mass”,

which represents the mass of particles below a given cut-off diameter that can reach the lung [97] . Basically, when particles pass into each stage of the impactor, they either impact on the stage or remain caught in the airstream and continue their route to the next stage (Figure 26).

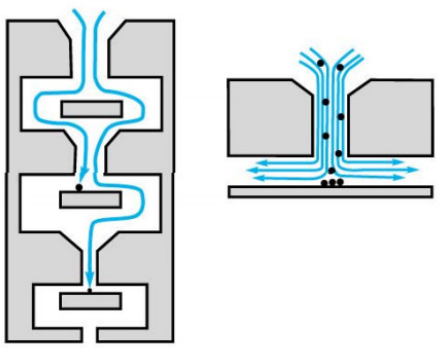

Figure 26: Impactor stage deposition. http://www.copleyscientific.com/files/ww/articles/Cascade%20Impactors.pdf

The smaller a particle, the higher is the probability of it passing through to later stages of the impactor. As each stage stops particles of specific sizes (aerodynamic diameters), the quantity of drug collected from that stage, normalized by the total dose, is representative of the fraction of particles of the polydisperse cloud which have those sizes. As such, it is possible to relate the deposition of a certain size of particle on a certain impactor stage (in vitro) to a Theoretical deposition in certain areas of the tracheobronchial tree (in vivo) (Figure 27).

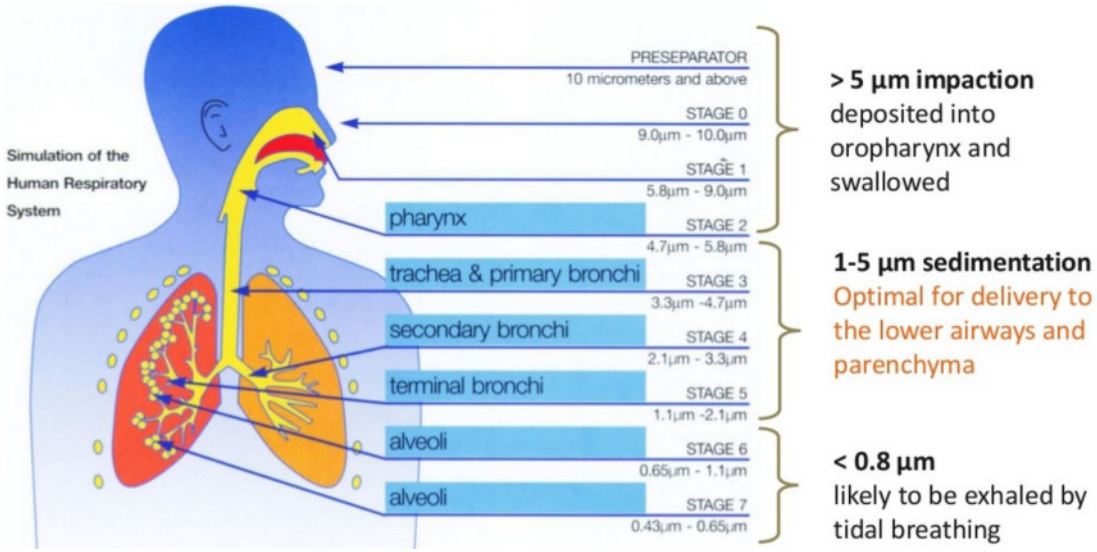

Figure 27: Relationship between Andersen 8-stage CI cut sizes at 28.3 L/min and likely particle deposition in the respiratory tract. Adapted with permission from Le [98].

Thus, it becomes possible to target specific part of the tracheobronchial tree using methods that generate clouds of polydisperse aerosols of certain aerodynamic diameters [94].

4.1.7.2. Types of cascade impactors

Several types of impactors have been developed, but the most widely used are firstly the Andersen cascade impactor (ACI) as seen in the following Figure:

Figure 28: Andersen 8-stage impactor. Taken with permission from Copley Scientific. http://www.copleyscientific.com/files/ww/brochures/Inhaler%20Testing%20Brochure%202015_Rev4_Low%20Res.pdf

Secondly, we have the current gold standard, the Next Generation Impactor (NGI)

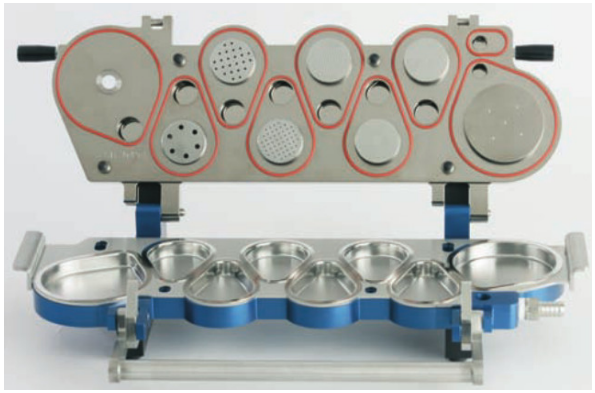

Figure 29: New generation cascade impactor. Taken with permission from Copley Scientific.

http://www.copleyscientific.com/files/ww/brochures/Inhaler%20Testing%20Brochure%202015_Rev4_Low%20Res.pdf

The ACI is made of eight stages, and the airflow is set at 28,3 L/min while the NGI is a horizontal seven stages impactor with the possibility of having an airflow reaching 100 L/min. The NGI was specifically designed to make up for the shortcomings of other types of impactors, notably, the ACI. This can be seen in the kurtosis of the particle distribution around the cut-off diameter. Research has shown that the NGI collection efficiency curves show lesser overlap between one stage to another than the ACI and most notably, the NGI shows less inter-stage loss [95] . However, due to its horizontal configuration, particles have a higher probability of undergoing a bounce effect when inside the NGI. [99]. This issue is however minimized through the use of specific coating. One of the major drawbacks of impactors in general is the need for the methodology to be performed at low temperature to avoid the evaporation of aerosol particles when adhering to the impactor walls. This, of course reduces the possibility of reproducing the intrapulmonary heat and humidity environment.

CHAPTER 5. High performance liquid chromatography and tandem mass spectrometry

5.1. High performance liquid chromatography

The basic principles underlying HPLC are separation, identification and quantification of molecules. This technique is commonly used in the pharmaceutical field. It separates compounds by elution of a liquid (mobile phase) on a column constituted of a solid support (or stationary phase). The physicochemical principles at the basis of the separation highly rely on the type of column used.

The central element of the HPLC system is the analytical column which consists of a metal tube, a few mm in diameter and of variable length (5 to 25 cm) containing the stationary phase. With increased column length usually comes an increase in compound separation, but also in analysis time. A smaller diameter limits the diffusion and allows for smaller injection volumes of samples, however it is easier to reach the maximal capacity of the column. The column is filled with a stationary phase composed of a solid support made up of particles of microporous 3-10 µm silica and an inert carrier. The size of the support particles and its porosity result in exchange surfaces of many hundreds of square meters per gram [100] .

Due to the characteristics of these columns, HPLC pumps must be able to produce and sustain high pressures (around 300 bar). They must be able to produce a pulse-less adjustable flow (usually between 0 and 10 ml/min) that remains constant under different condition of pressure or viscosity of the mobile phase. Injection of samples must be rapid to avoid disrupting the system pressure or mobile phase flow [100] .

5.1.1. Regular or reverse phase chromatography and mobile phase

Regular HPLC implies that the stationary phase is polar and the mobile phase is apolar. In this situation, the column has a tendency to hold back polar compounds. "Reversed phase", on the other hand is when the stationary phase is nonpolar and the mobile phase is polar, thus retaining mainly nonpolar compounds. A reversed phase column consists of silica particles to which were grafted 4 to 18 carbon fatty acid chains or aromatic compounds according to the level of hydrophobicity desired [100] .

Reverse phase HPLC is based on a principle of molecule partition between stationary and mobile phases. The partition coefficient of a particular compound depends on the mobile phase polarity which, in reverse phase, is rather polar. It is generally constituted of an aqueous buffer adjusted to a specific pH and, of a mixture of solvents such as methanol, acetonitrile and tetrahydrofurane [101] . The resulting mobile phase determines the retention time of the eluting molecule analyzed. Just as mobile phase polarity is controlled, so is polarity of the molecule, through ionization. The buffer pH is adjusted according to the pKa of the molecule so as to maintain it in an ionized state, be it basic or acidic. The mobile phase composition is not necessarily a constant throughout a run. The percentage of solvent may change as a function of time, either abruptly or gradually according to different patterns of gradient. Such a versatility is quite useful for detection, peak separation and cleaning of the injected sample. Finally, the final viscosity of the mobile phase has also to be taken into account and kepts as low as possible to reduce the internal pressure of the system [101].

5.1.2. Detection

Since physicochemical properties of endogenous and exogenous differ, passage through the column will enable separation of the molecules. Following that separation, molecules will need to be detected and quantified. The most routinely used method of detection is ultraviolet (UV) where the detector emits a

specific wavelength (185-450 nm) at which the molecule absorbs. The remaining light is then compared to a reference beam and using Beer-Lambert's Law, absorption is calculated. Eluted peaks absorbing at this wavelength exhibit a Gaussian form (Figure 30) [101].

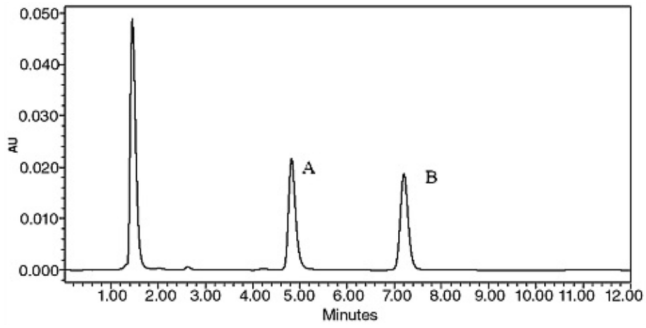

Figure 30: Typical chromatogram for sildenafil 1µg/mL (A) and internal standard 0.5 µg/mL (B) in human plasma. Taken with permission from Quintero [102] .

This degree of absorption expressed as absorbance unit coupled with that gathered from a calibration curve, generates an interpolated concentration value. This methodology implies proportionality between the area under the curve of the peak and the amount injected. The height of peak may also be used as it also should be proportional to the injection amount. The Gaussian peak form is an ideal situation as in some cases it is possible to observe skewness of peaks or changes in kurtosis.

5.2. Mass spectrometry

Ultraviolet detection, though universally accessible, is highly prone to interferences with the solutes of interest and often impedes analysis and results in wasting valuable biological material and time. A more complex but reliable method of detection is mass spectrometry (MS) and, more so, tandem mass spectrometry (MS/MS). The initial phase of mass spectrometric analysis is the production of gas phase ions of the compound through the use of an ionizing

electrospray flowing through a sheath of gas (usually nitrogen, process shown in Figure 31) [103].

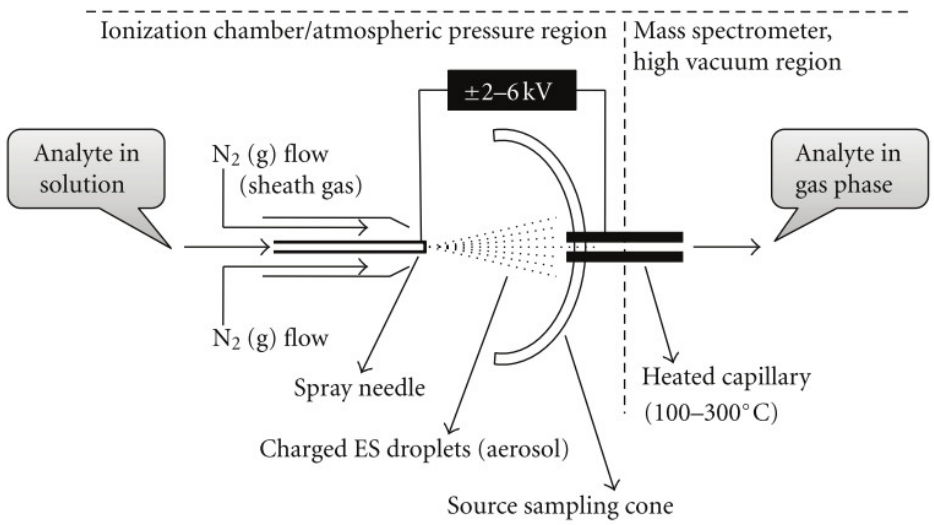

Figure 31: A schematic representation of the electrospray ionisation ion source. Taken with permission from Banerjee [104].

These ions subsequently fragment into primary product ions with distinct chemical properties. Each of these primary product ions can be further broken down and so on and so forth. In the case of tandem spectrometry, the term implies two fragmentations, the first into product ions, of which the abundance characterized, followed by a second fragmentation of the product ions. The mass spectrometer then distinguishes the fragments of ions according to the mass/charge ratio *(m/z)* of its components and thus builds a full spectrum map of the fragmentation by plotting the abundance of these *m/z* ratios (Figure 32) [103, 104].

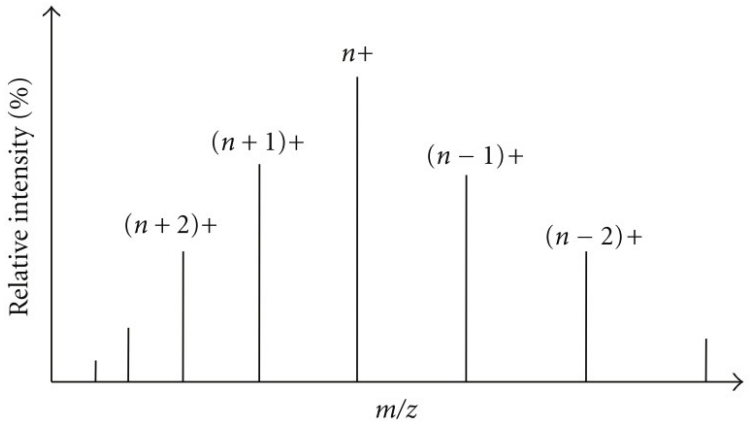

Figure 32: A typical representation of the electrospray ionisation mass spectrum in positive ion mode. Taken from Banerjee [104] .

The intensity of the signal is then plotted against its respective m/z ratio. As the composition of each fragment is highly specific and reproducible, the *m/z* ratio is as well. This process of mass spectrometry is summarized in Figure 33.

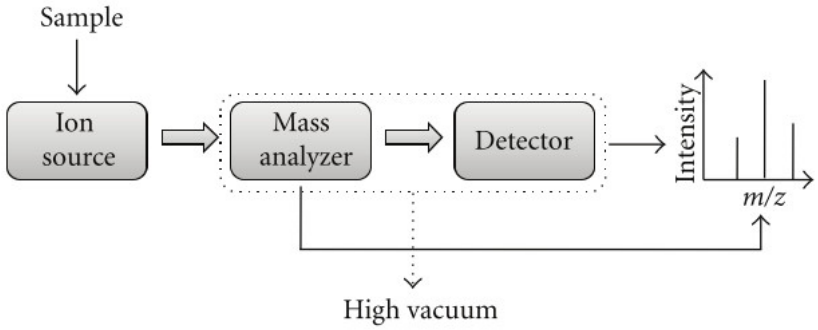

Figure 33: The basic components of the electrospray ionisation mass spectrometer. Taken from Banerjee [104].

The nominal mass is calculated using the mass of the predominant isotope of each element composing the ion. However, the exact masses of isotopes are not exact whole numbers. They are slightly different from the summed mass values of their constituent particles that are protons, neutrons and electrons. These differences, which are called the mass defects, are equivalent to the

binding energy that holds these particles together. Consequently, every isotope has a unique and characteristic mass defect [103] . The monoisotopic mass, which takes into account these mass defects, is calculated by using the exact mass of the most abundant isotope for each constituent element [103].

The mass spectrometer's functions are to transform the sample into product ions in the ionization source, use their mass/charge ratio to separate them in the mass analyser, fragment them further and analyze the resulting fragments in a second analyser, detect the ions produced by the second fragmentation and measure their abundance with the detector that converts the ions into electrical signals and finally process the signals from the detector that are transmitted to the computer [103, 104].

CHAPTER 6. Drug pharmacokinetics

6.1. Transmembranary movement

To produce its pharmacological effect, a drug must achieve a sufficient concentration at its site of action. This concentration depends of course on the administered dose but also on the speed and degree of its absorption. The absorption of a drug, independently of the route of administration is a resultant of its passage into the systemic circulation, after having crossed one or more cellular membranes. The speed at which this transfer is carried out is a function of the nature of the membrane involved and the physicochemical properties of the drug.

The cell membrane is a bilayer of amphipathic nature. It's hydrophobic on the inside due to its non-polar groups such as fatty acid chains or lecithin. On the outside, the cell membrane is hydrophilic due to its polar groups like glycerol and phosphatidylcholine [105]. The membrane structure is neither continuous nor permanent but fluid. The elements are arranged in slats that slide over each other. According to Singer and Nicolson's mosaic model, proteins occupy part or all of the thickness of the membrane. The surface proteins confer a negative charge to the membrane surface and Mg^{++} and Ca^{++} cations are set to stabilize the membrane. This creates an aqueous environment at the membrane surface which becomes a limiting factor for the very fat-soluble substances.

Passage through this membrane of protein-unbound molecules is determined by well-defined mechanisms, firstly, the rate of passive diffusion, both through micropores and well as through dissolution through the membrane itself which can be summarized under Fick's Law [106].

$$\frac{dQ}{dt} = \frac{D \cdot S \cdot \Delta C}{\varepsilon}$$

Equation 5: Fick's law. D: coefficient of diffusion; S: membrane surface; ΔC: concentration gradient; ε: membrane thickness [105].

There are several types of diffusion: simple, passive and specialized.

Simple diffusion. The cell membrane is dotted with aqueous micropores or cavities providing more polar molecules with exchanges between intracellular and extracellular mediums. No direct evidence shows their presence, the existence of these pores is explained by the fact that the very small molecules pass through faster than expected by the laws of passive diffusion. In addition to micropores, small polar molecules can also borrow the transcellular route. In general, only polar substances whose molecular weight is less than 300 daltons diffuse transcellularly and most drugs have a higher molecular weight higher than 300.

Passive diffusion. The physicochemical factors affecting passive diffusion are liposolubility, molecular weight and acid dissociation constant. Liposolubility is the primary factor affecting the rate of transfer. It depends on the oil/water partition coefficient of the drug which is shifted towards lipophilicity or hydosolubility through the drug's chemical structure. The presence of alkyl, phenyl, sulfur or halogen groups increase lipophilicity whereas the presence of hydroxyl, acid, ester and quaternary ammonium groups increase hydrosolubility. Molecular weight plays very little if the molecule has a molecular weight of under 1000 Da. On the other hand, the molecules of high molecular weight are generally more liposoluble and according the Fick's law, the net effect is generally slower membrane transfer speed, and even for a fat soluble molecule. Passive diffusion is also affected by the dissociation constant (pKa) of the drug in question. Jointly with the surrounding environment pH, it determines the proportion of the drug in non-ionized (NI) form and therefore the fraction of drug available for transfer as the non-ionized fraction diffuses much faster, if not exclusively. The transfer speed of drug molecule is proportional to the gradient of concentration of the non-ionized diffusible form between both sides of the membrane (eg. blood/cell) [105].

Specialized transport. The second major is specialized transport which moves molecules from one side of the membrane to the other through the means of transmembranary carrier proteins. This transport can be further divided into passive and active transports. Both subdivisions, as they use carriers as transport vehicles and as these carriers are in limited numbers, are subject to the principles of saturation and competition. The rate of transport dA/dt follows a Michaelis Menten kinetic of the form:

$$\frac{dA}{dt} = \frac{V_{\max} \cdot A}{K_d + A}$$

Equation 6: Michaelis Menten. A: amount of molecules; K_d: ligand-transporter dissociation constant; $V_{max,}$: maximum transport speed [105].

Passive transport of molecules follows the direction of their transmembrane concentration gradient and does not require energy. Active transport, on the contrary, does necessitate energy and transports molecules against their concentration gradient. These carriers are relatively unspecific and will serve as either cellular influx of efflux transports. Some influx transporters will specifically transport anionic substances such as OATP and OAT (organic anion transporting polypeptide and organic anion transport, respectively) while others, such as organic cation transporters (OCT) will transport cationic substances. Others are even less specific as the sodium-taurocholate cotransporting polypeptide. Efflux transporters are one of the exit ways of the cell. P-glycocoprotein (P-gp) is the most known member of the efflux transporters. Member of the ABC (ATP-binding cassette) family, P-gp transporters are ubiquitously distributed throughout the body and highly present at the blood-brain barrier [107, 108]. They are specifically located on the apical side of the cell and are responsible for the efflux of lipophilic compounds into the lumen. Their presence has been linked to the resistance mechanisms of several

antineoplasic agents. These membrane transporters play an important role in the absorption, distribution and elimination of internal and external products.

6.2. Absorption

To enter the system, with the exception of intravenous administration, the drug firstly needs to be absorbed. There are as many routes of absorption as there are ways of administering the drug. Some are parenteral, enteral, and others are topical. Intravenous, intramuscular and subcutaneous routes are the most common parenteral routes. As they are introduced directly in the extracellular liquid, maximum plasma concentrations are reached very quickly.

Enteral routes imply that the drug will have to cross an epithelium before reaching the systemic circulation. The most commonly used and studied one is the oral route. The degree and rate of absorption is modulated by several factors: disintegration of the pharmaceutical formulation, drug dissolution in gastric fluid, gastric emptying rate, intestinal peristalsis, surface of the intestinal mucosa, drug/intestinal wall interaction and absorption and finally intestinal perfusion. A comprehensive description of the oral route is not in the scope of this thesis, the physiological, physicochemical concepts underlying these modulating factors can be transposed to the pulmonary route.

Gastrointestinal drug absorption is a phenomenon that begins inside the mouth with the sublingual vasculature, followed by passage through the stomach which is a 1.5L container filled with acidic fluid (pH 1-3) permitting usually very little absorption. However, this gastric fluid does favors the absorption of acidic molecules. After dissolution in the gastrointestinal fluid, the drug will be absorbed even faster if the form is predominantly unionized and fat-soluble, a situation which is dependent, as mentioned, on the inherent pKa of the molecule and the ambient pH [109]. Gastric fluid then empties through the pyloric sphincter into the small intestines. This gastric emptying rate adds to the variability of oral administration as it slows down through meals. The small intestine is the next section and, thanks to the multiple folds in the mucosa and the presence of microvilli, has a surface area of 300 m^2 with a pH oscillating

between 5 and 6. The fraction entering the portal circulation is then brought to the liver where it possibly undergoes hepatic metabolism [109, 110] . This loss of drug following a first passage through the liver is called first pass effect and will be further discussed in the metabolism section. After clearing the liver the remaining fraction is considered bioavailable and will distribute to all tissues

6.2.1. Pulmonary absorption

Amongst the many topical routes of administration one of great importance, specifically in the context of this thesis is the pulmonary route. There are several benefits arising from delivering drugs to the lungs: fast onset of action, high local concentration and increased selectivity and good systemic delivery of drugs with poor oral bioavailability. Once the drug has dissolved into the 10-30 mL of pulmonary surfactant fluid, it will rapidly spread through local diffusion and be available for absorption. If this diffusion occurs at an alveolar level, absorption speed is even comparable to intravenous administration (Figure 34).

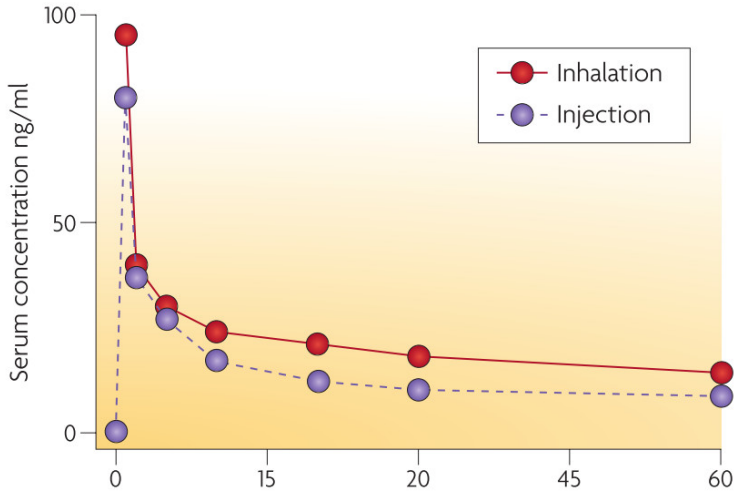

Figure 34: Inhaled morphine (dose = 8.8 mg) compared with intravenous injection (dose = 4 mg) in human volunteers. Taken from Patton [10].

The total pulmonary surface area available for drug absorption is around 75 m^2 and this route of administration bypasses the liver first-pass effect, increasing the systemic bioavailability of highly extracted drug [86]. Thus, pulmonary administration offers great potential for fast systemic delivery of small-molecule therapeutics.

The site for optimal absorption is not clear yet though. For the high-molecular-mass immunoglobulins of the IgG class (150 kDa), evidence suggests that the best place for absorption might be in the larger airways where receptor-mediated transcytosis of IgG occurs [111, 112]. Small hydrophobic molecules are thought to be rapidly absorbed (within seconds) throughout the lungs by passive diffusion and paracellular routes through the plasma membrane [113] and by specific transporters (Table VI) or via the tight junctions [113].

Implication pour milrinone?

Table VI: Summary of drug transporter expression in human lungs.

Protein Name	Expression in Human Lungs	Cellular Distribution	Cellular Localisation
ABC transporters			
P-gp	Moderate	Bronchial/bronchiolar epithelium	Apical
		Alveolar epithelium (contradictory data)	Apical
		Alveolar macrophages	
		endothelium	
MRP1	High	Bronchial/bronchiolar epithelium	Basolateral
		Alveolar macrophages	
MRP2	No or low	Bronchial/bronchiolar epithelium	Apical
MRP3	Low or high	Unknown	
MRP4	Moderate	Unknown	
MRP5	High	Unknown	
MRP6	Moderate	Unknown	
MRP7	Moderate to high	Unknown	
MRP8	Low or high	Unknown	
MRP9	Low or high	Unknown	
BCRP	Low or high	Airway epithelium	Apical
		Seromucinous glands	
		Small capillaries	
SLC transporters			
OCT1	Contradictory data	Tracheal/bronchial ciliated cells	Apical/cytoplasmic
OCT2	Contradictory data	Tracheal/bronchial ciliated cells	Apical
		Basal cells	Entire membrane
OCT3	Contradictory data in airways	Basal cells	Entire membrane
		Airway smooth muscles	
		Endothelium	
OCTN1	Yes	Tracheal epithelium	Apical
		Alveolar macrophages	Cytoplasmic
OCTN2	Yes	Airway epithelium	Apical
		Alveolar epithelium	Apical
PEPT1	Low	Bronchial epithelium	Unknown
PEPT2	High	Airway epithelium	Apical
		Type II pneumocytes	Cytoplasmic
		Endothelium	Apical?
OAT1	No		
OAT2	Contradictory data	Unknown	Unknown
OAT3	No		
OAT4	No		
SLCO transporters			
OATP1A2	No		
OATP1B1	No		
OATP1B3	No		
OATP1C1	No		
OATP2B1	Yes	Unknown	Unknown
OATP3A1	Yes	Unknown	Unknown
OATP4A1	Yes	Unknown	Unknown
OATP4C1	Yes	Unknown	Unknown
OATP5A1	No		
OATP6A1	No		

Adapted with permission from Bosquillon [114].

Interestingly, apical-to-basal electrical resistance across the epithelium, which is a measure of the tightness of cell junctions, seems to decrease from a maximum in the trachea to a minimum in the distal airways before returning to a high value in the alveoli [10].

6.2.2 Inhalation versus Instillation

The pulmonary administration of drugs represents many advantages, because of the lung's large surface area, its important vascularization, its extremely thin epithelium, and the bypass of liver first-pass effect [115]. Those characteristics make the inhalation route ideal for a rapid onset of action, the administration of low doses, and thus less systemic side effects [88].

The two common administration methods are inhalation, where the drug is transformed into a breathable mist and intratracheal administration where the drug is given as a bolus instilled inside the trachea. In addition, using specific atomization devices, the drug may also be sprayed intratracheally. Some studies compared aerosol administration with intratracheal bolus in animals, and came to the conclusion that aerosols enable a much faster absorption [116, 117]. This is most likely due to a greater proportion of the aerosolized drug reaching the alveolar region or, if the instilled drug reaches the alveoli, a different intra-alveolar (Figure 35).

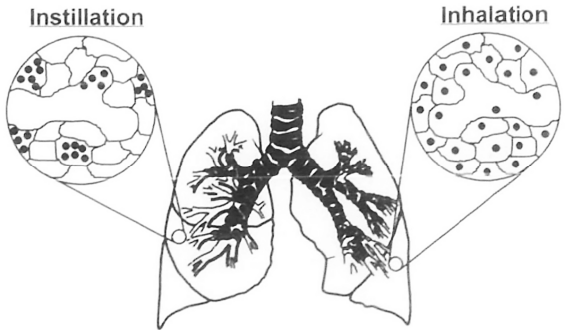

Figure 35: Differences in particle distribution following an instillation or inhalation exposure, (dark dots) illustrating the

decreased homogeneity of an instilled dose in the alveolar region. Taken with permission from Osier [118] .

Particles inhaled as aerosols show a more uniform distribution in the lung than when they are administered by intratracheal injection. [117, 119] By comparison, instillation delivery is highly variable and depends on the anatomical makeup of the individual's lung as well as their positioning and the method of instillation (Figure 36) [117].

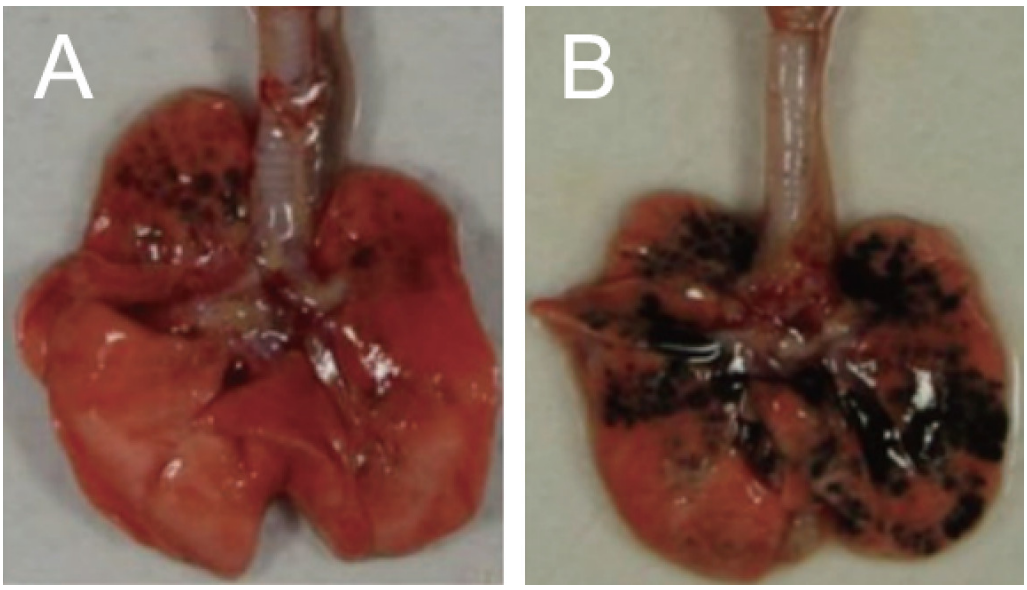

Figure 36: Macroscopic features of lungs after high speed bolus administration of an india ink suspension in horizontally positioned rats using a standard gavage needle (A) and an aerosolizing microsprayer (B). Adapted with permission from Hasegawa-Baba [120].

The previous figure shows the intrapulmonary distribution difference between a simple instillation through a gavage needle and intrapulmonary aerosolization through amicrosprayer. In addition, instillation of drugs is a topical administration where the molecules are potentially absorbed through the pulmonary epithelium

at any level of the tracheobronchial tree. Transmembranary absorption at higher levels of the tracheobronchial tree also follows Fick's law, implying an inversely proportional to the thickness of the membranes to be crossed.

6.3. Distribution

Once a drug is absorbed or enters the systemic circulation, it begins distributing itself throughout the body. This distribution will mainly be affected by its physico-chemical properties and the affinity of membrane transporters towards it. For example, it may either remain in the blood, or it may be distributed in specific organs and/or fatty tissue. The volume of distribution of a drug is based on the concept of a ratio between the total amount of drug in the body and its plasma concentration. The resulting number represents a fictitious volume in which the amount of drug is evenly distributed. This method of calculating the volume of distribution (Vd) results in distribution values often difficult to reconcile with our anatomy, eg chloroquine would distribute in a volume of 200 L/kg. This is why this volume is called an "apparent" volume of distribution. Though, up to 40L, it may represent actual liquid volumes inside the body e.g. 5L for representing the blood compartment, more often than not, this volume remains conceptual, representing the extent at which the drug has left the vascular compartment [109]. This situation occurs because the majority of PK studies use central compartment sampling as their reference point. A better representation of reality would be obtained by taking into account organ tissue/plasma partition coefficients as commonly done through physiologically-based PK.

For a drug to be distributed in the body, it must be able to leave the vascular compartment. It will then diffuse into the interstitial space and subsequently pass through membranes, entering cells where it will dissolve in their water content. The speed and extent of distribution will depend on its molecular weight, its liposolubility (represented by its partition coefficient) and its nonionized fraction at pH 7.4. A large molecular weight, high hydrophilicity and high ionized fraction are all factors that will reduce the volume of distribution of a drug. The extent of

distribution will depend greatly on the presence of influx and efflux transporters such as OCTs, OATs and P-gp [114].

To achieve distribution to the tissues, the drug must also reach the said tissues. Plainly, well perfused tissues will receive large amounts of the drug very quickly, and tissues less well perfused, will receive the drug later and more slowly. If tissue perfusion decreases, the distribution rate to those specific tissues will also decrease [109].

6.3.1. Plasma protein binding

When the drug enters the bloodstream, it is brought into contact with plasma proteins to which it reversibly binds, producing an equilibrium state between the concentration of free and bound drug. It becomes important at this point to differentiate between free and bound drug concentrations, which are the detected concentrations of the drug and which vary over time and free and bound fractions which represent the free and bound concentrations of drug when related to the total (free + bound) concentration and that, ideally, should remain constant, in a linear system [109].

Acidic drugs, such as oral antidiabetic agents, anticoagulants, diuretics, anticonvulsants, non-steroid anti-inflammatory medication and some antibiotics preferentially bind to the 69000 Dalton plasma albumin [121]. Drugs of a basic nature, such as beta-blockers, calcium channel blockers, antiarrhythmic medication, morphine, salbutamol and tricyclic antidepressants bind preferably to the 40000 Dalton α_1-glycoprotein acid [122, 123]. Drug binding to plasma proteins is subject to binding affinity to the particular plasma protein, represented by the constant of affinity, K_a, and the number of protein binding sites [109]. The binding of a drug to plasma proteins prevents the release of the drug from the vascular compartment and thus limits its distribution. For example, if 80% of the plasma concentration of a drug is bound to plasma proteins, only 20% of the concentration which represents the free drug can leave the vascular compartment and has a chance to distribute within the tissues and bind to its

target. Only free plasma drug molecules that diffuse or are transported outside the vascular compartment to the interstitial space are exposed to tissue proteins to which they can bind, just like plasma proteins, according to an affinity constant ($K_{at)}$. Equilibrium between the free and bound concentrations is rapidly reached, inside or outside the vascular compartment. Each one is highly dependent on the protein affinity constants on each side and the free fraction maintains equilibrium. A stronger K_a might lead to a small V_d whereas a stronger K_{at} might lead to a higher V_d.

6.3.2. Lung distribution

The lung plays an important part in the distribution and accumulation of a variety of endogenous and exogenous compounds. Several lipophilic basic amines, such as imipramine, propranolol, lidocaine, fentanyl, and verapamil undergo a heavy first pass effect following pulmonary tissue uptake. This phenomenon forms a slowly diffusible and displaceable drug pool which distributes mainly through simple diffusion followed by pulmonary tissue binding and possibly alveolar macrophage implication [124]. This distribution and uptake are dependent on the same principles as distribution in other parts of the body, namely lipophilicity, ionization, facilitated transport and plasma and tissue binding affinities.

6.4. Metabolism and hepatic clearance

The metabolism of a drug is mainly a process leading to an increase in hydrosolubility, allowing more polar metabolites to be evacuated in aqueous media, such as urine and/or bile. Multiple organs are known to have drug metabolism functions and, in order of importance, they are: the liver, intestines, brain, lungs, kidneys and skin. Even if this section covers mostly liver functions, the metabolism principles are applicable in the same fashion to any other organ with perhaps a change in the amount of the enzymes involved. Anatomically, the liver receives 75% of its blood volume through the portal vein and blood incoming from the intestines by way of the splanchnic veins and 25% from the

hepatic artery [6]. The liver is a true powerhouse of metabolism as it not only contains large amounts of enzymes capable of biotransformation, but is also highly perfused at a rate of 1500 ml/min or 30% of cardiac output [6]. Thus, it receives large quantities of endogenous or exogenous molecules very rapidly and subsequently clears them to different degrees. The definition of clearance of a drug is the volume of blood from which that drug is completely removed per unit time. This term reflects the ability of the body or even of a specific organ to eliminate the drug from the blood perfusing it. As such clearance is the most appropriate term to refer to the elimination of a substance in the body. The liver's ability to metabolize a molecule, thus essentially clearing it depends on three factors: a) the intrinsic ability of the enzyme system to process the molecule, b) plasma protein binding, and c) hepatic plasma flow [109]. Liver biotransformation of a drug, or the transformation of a mother molecule into daughter molecules also known as metabolites occurs when the substrate is able to reach the enzymes in the hepatocytes. Access to intracellular enzymes is achieved by passive diffusion as the anatomic formation of blood vessels into sinusoids facilitates it or via membrane transporters like the OATs and OCTs, for ionized molecules [125]. The drugs then undergo either phase I or II metabolism. The hepatic lobule, as can be seen in Figure 37 is arranged in a hexagonal fashion, with blood flowing from its apexes to its center.

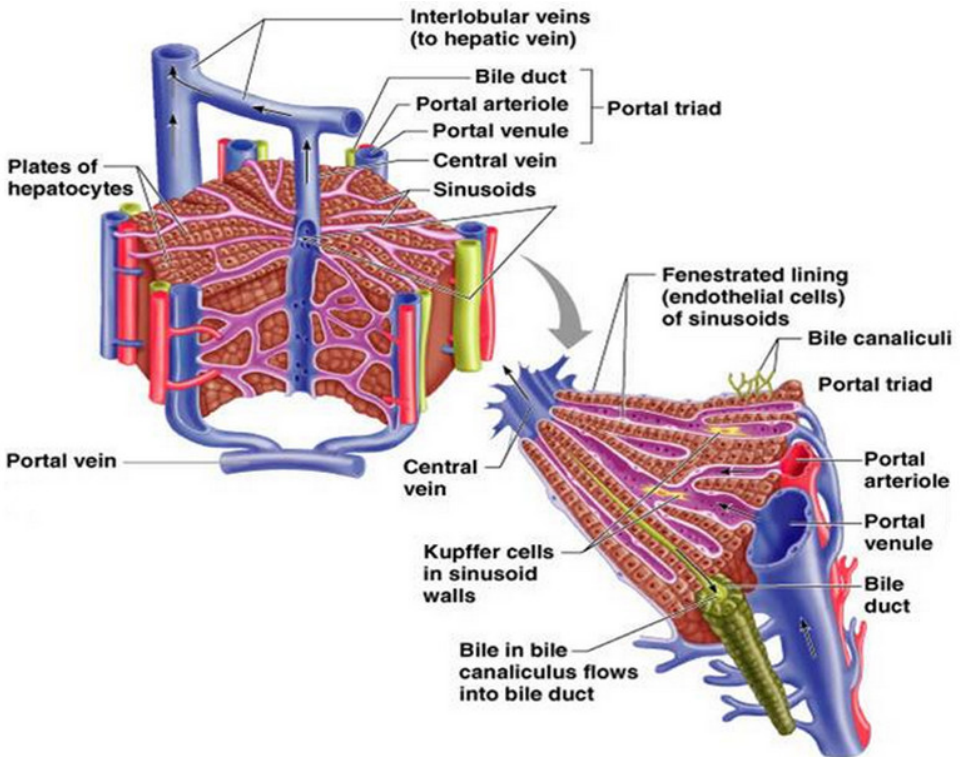

Figure 37: Schematic view of the cut surface of the liver, showing the hexagonal nature of its lobules and an enlarged view of a small portion of one liver lobule, illustrating the components of a portal triad (portal tract region), bile canaliculi, and Kupffer cells in the sinusoid walls. Arrows indicate the direction of blood and bile flow Adapted with permission from Marieb [6].

6.4.1. Phase I metabolism

Phase I are irreversible catabolic reactions, namely, oxidation, reduction, deamination, dealkylation, hydrolysis and, hydroxylation. Many enzymes perform this phase I metabolism, however one of the most common enzyme family is the cytochrome P-450 isoenzyme family. These isoenzymes may be induced or inhibited following pre-treatment with another drug or they can be a site for competitive (concentration-reversible) or non-competitive (conformation-changing/ allosteric) inhibitions [109, 126].

6.4.2. Phase II metabolism

Phase II reactions can occur following, or not, phase I reactions. They are carried out in a pH or enzyme-reversible fashion by transferases such as glucuronide transferases (resulting in glucuronidation), sulfotransferases (resulting in sulfatation), glutathione transferases (resulting in glutathione conjugation) and N-acetyl-transferases (resulting in acetylation) [127]. The most common phase II reaction in the liver being glucuronidation.

6.4.3. Hepatic clearance

The activity of the enzyme system is defined by its intrinsic clearance which reflects the maximum capacity of the said system to metabolize a substrate. Drug plasma protein binding becomes a limiting factor in metabolism when drug affinity for plasma protein, K_a , is greater than drug affinity for the enzyme responsible for intrinsic clearance (Clint). When the converse situation arises, the equilibrium shifts towards an enzyme-bound state and thus does not impede metabolism. Hepatic clearance (CL_h) is of course related to both the enzymatic ability of the liver to extract that specific drug and the liver blood flow. It follows the principles of the following equation:

$$CL_h = E_h \times Q_h$$

Equation 7: Hepatic clearance. CL_h: hepatic clearance; E_h: liver drug extraction coefficient; Q_h: hepatic blood flow.

Figure 38: Example of hepatic extraction and clearance. Where Cl_h: hepatic clearance; E_h: liver drug extraction coefficient; Q_h: hepatic blood flow.

The extraction coefficient can further be characterized by the addition of coefficients representing plasma protein binding and intrinsic clearance, representing the well-stirred hepatic clearance model [109, 128].

$$Cl_h = Q_h \times E_h = \frac{Q_h \times fu_b \times Cl_{int}}{Q_h + fu_b \times Cl_{int}}$$

Equation 8: Well-stirred clearance model. Where E_h: liver drug extraction coefficient; Q_h: hepatic blood flow; fu_b: fraction unbound; Cl_{int}: intrinsic clearance.

As such, both the intrinsic clearance and the hepatic blood flow rate can, in some cases, become a limiting factor to hepatic clearance. When drug intrinsic clearance is much lower than hepatic flow rate, the Cl_h of this drug is greatly limited by its intrinsic clearance and drug binding to plasma proteins and

changes in blood flow bring insignificant changes to hepatic clearance. Due to these characteristics, this substance is called flow-independent and the inhibition or induction of the enzyme systems involved in the metabolism of the drug and/or the changes in the plasma protein binding of the drug are highly important for clearance. On the contrary, when drug intrinsic clearance is much greater than the flow rate, a situation arises mathematically where the hepatic clearance depends mainly on changes in blood flow and clearance, and this drug is called flow-dependent.

6.4.4. First pass effect

When a drug is given orally, it will generally reach the systemic circulation after passing the liver, lungs and heart for a first time [110]. Following this first passage it will be distributed to all organs through arterial distribution. During that first passage of the drug, a more or less important fraction of the dose may almost inevitably be extracted by these organs though metabolism, or in the case of the enterocytes, metabolism and efflux transporters. The amount of drug that reaches the systemic circulation can be much less than the dose administered. and the fraction extracted represents the first-pass effect. The importance of the first passage through an organ is directly related to the drug intrinsic clearance by that organ, which is to say that the greater the Cl_{int}, the lower the amount of drug that reaches the systemic circulation and by definition, the lower the bioavailability. Oral administration of a high Cl_{int} or flow-dependent drug has a higher probability of resulting in a lower bioavailability. Examples of such drugs are: the bioavailability of calcium channel blockers being 45%, beta-blockers, 40%, antidepressants, 45%, morphine, 45% and lidocaine, 30%.

6.4.5. Lung metabolism

The does not express the full range of isoenzymes present in the liver [129]. Indeed, different expression patterns occur in the lung (Table VII).

Table VII: Overview of the expression of metabolic enzymes detected in lung tissue.

	Isoform	mRNA expression	Protein expression	Metabolic activity	Comment
Phase I enzymes	CYP1A1	Yes	Yes	Yes	Only in smokers, decrease to normal levels within 2 months after cessation of smoking
	CYP1A2	Disparate data	Disparate data	Not reported	
	CYP1B1	Yes	Yes	Yes	Induced by smoking
	CYP2A6	Yes	Disparate data	Not reported	
	CYP2A13	Yes		Not reported	No clear report on activity
	CYP2B6	Yes	Yes	Yes	Splicing variant, previous 2B7
	CYP2C	Disparate data		Yes	
	CYP2D6	Yes	Yes	Disparate data	
	CYP2E1	Yes	Yes	Yes	
	CYP2F1	Yes		Not reported	
	CYP2J2	Yes	Yes	Yes	Strongly expressed, possible endogenous role
	CYP2S1	Yes	Yes	Unclear	
	CYP3A4	Yes	(Yes)		Protein detected in 20% of investigated samples
	CYP3A5	Yes	Yes	Yes	
	CYP4	Yes		Unclear	
	FMO	Yes			Varied expression among isoforms
Phase II enzymes	UGT	Yes	Yes	(Yes)	Varied expression among isoforms, generally low metabolic capacity
	GST	Yes		Yes	
	Esterases	Yes		Yes	High metabolic capacity
	Epoxide hydrolase	Yes		Yes	Low metabolic activity
	Peptidases			Yes	High metabolic capacity
	SULT	Yes		Yes	High metabolic capacity

Adapted with permission from Olsson [11].

As an example, while CYP3A4 is the main isoenzyme expressed in human liver, lung expression was only found in 20% of the investigated subjects [130]. Lung CYP enzymes are mainly located in the Clara cells and the alveolar type II cells [131]. As the lung is the only organ through which the entire cardiac output passes; due to this high pulmonary blood flow, the metabolic capacity of the lung should not be ignored. For instance, with a cardiac output of 5 l/min and 30%

removal of a compound, the pulmonary clearance is 1.5 l/min. This could be compared to the maximal clearance of a compound completely metabolized in the liver which corresponds to a hepatic blood flow of 1.6 l/min [132].

6.5. Elimination

Elimination is the final phase in drug kinetics. Elimination can occur through hair, nails, sweat, but most predominantly through bile and urine. The free drug, circulating in the blood at equilibrium with the protein-bound fraction, is the only form available for elimination.

Biliary excretion of anionic or cationic substances necessitates active transport. It is a saturable process that can easily be inhibited by another substance which competes for the same transport system. Given the small bile flow of 750mL per day[133], biliary excretion of a drug is rarely the major elimination pathway. However, during a single liver pass, a drug may undergo a phase I reaction and the resulting metabolite, a phase II reaction, thus generating a second highly polar metabolite of higher molecular weight which, in turns, can be substrate for bile transporters. This situation explains why some drugs have very low circulating levels following oral administration. Drugs excreted into bile may also be reabsorbed in the gastrointestinal tract, thus increasing their elimination half-life.

The main elimination organ is the kidney [109]. Drug reaches the kidneys through the afferent arteriole, from where the unbound fraction may be filtered through the glomerular membrane of the nephron, one of the circa 6 million functional structures making up each kidney [6]. Once in the proximal tubule, the filtered molecules are joined by the molecules entering the nephron through tubular secretion. As the drug makes its way forward, the changes in pH might allow the reabsorption phenomenon to take place.

6.5.1. Glomerular filtration

Glomerular filtration rate (GFR) is a passive process which involves the free drug molecules passing through the basal membrane of the glomerulus, much

like through a sieve. Under a positive hydrostatic pressure gradient, glomerular filtrate is formed at a rate of approximately 120ml/min. This porous glomerular membrane allows passage for only the molecules whose molecular weight is below 65000 Daltons[109], thus excluding macromolecules such as albumin, globulins, and other plasma proteins. This filtration rate is also a function of the renal blood flow and in situations where blood is decreased, such as heart failure, there is also a decrease in renal excretion.

6.5.2. Tubular secretion

Tubular secretion (TS) is an active phenomenon that depends on membrane transporters found in the apical and basal membranes of the epithelial cells of the proximal tubule. Free drug from the blood may, through carriers or by passive diffusion under a concentration gradient pass into the epithelial cells and further, into the tubular lumen. The probability of secretion is dependent of the drug's affinity towards these carriers [110].

6.5.3. Tubular reabsorption

Tubular reabsorption (TR) can be an either passive or active transport phenomenon. Most often, it is passive and it involves the return of the drug from the tubular lumen towards the vascular compartment. This phenomenon occurs at the distal tubule level. Tubular reabsorption usually depends on the existence of a concentration gradient, the physicochemical properties of the drug and urine pH. The concentration gradient is usually kept since one of kidneys' functions is concentrating urine. The physicochemical properties involve the level of lipophilicity of the drug and the unionized form fraction [110].

Renal clearance (CL_R) of a substance is overall defined by the following equation:

$$Cl_R = GFR \times fu_b + TS - TR$$

Equation 9: Renal clearance. GFR: fraction unbound; fu_b: fraction unbound.

Both kidney disease and age have a negative impact on the three phases, glomerular filtration, tubular secretion and tubular reabsorption [134]. As such, both of these conditions can lead to changes in the pharmacological response to drugs eliminated by the kidney.

6.6. Drug effect

These phases of pharmacokinetics are more or less simultaneous. As soon as absorption begins, so does distribution and very shortly after, elimination. In parallel to these is of course drug effect. One of the basic premises of pharmacokinetics is that there is an underlying relationship between the concentration of a drug at the site of action and the effect shown by subject. In some cases, the relationship between concentration and effect is direct, whereas in other cases, there is a time delay between them. The response to stimulation by an agonist may also be reversible, or not. The most common relationship is described by the agonist/ receptor complex formation described by the Hill equation (Equation 10), also known as a sigmoid Emax model.

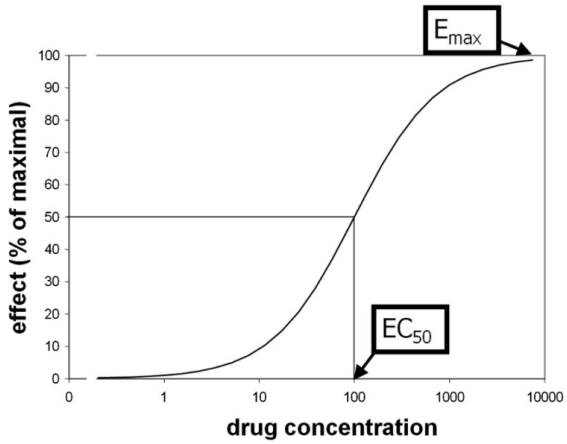

Figure 39: Illustration of EC50 and Emax. Taken with permission from Black [135].

This model describes the relationship between agonist response and agonist concentration according to the maximal effect potentially generated. The Hill coefficient, known as γ describes the abruptness with which the effect develops [136].

$$response = \frac{E_{max} \times C_R^{\gamma}}{EC_{50}^{\gamma} + C_R^{\gamma}}$$

Equation 10: Hill equation. E_{max}: maximum effect potentially generated; EC_{50}: drug concentration generating 50% of the effect C_R and, the concentration of drug at the receptor; γ: Hill coefficient.

It is also possible to incorporate a baseline effect, thus generating the following equation:

$$response = baseline \pm \frac{E_{max} \times C_R^{\gamma}}{EC_{50}^{\gamma} + C_R^{\gamma}}$$

Equation 11: Hill equation with baseline. E_{max}: maximum effect potentially generated; EC_{50}: drug concentration generating 50% of the effect C_R and, the concentration of drug at the receptor; γ: Hill coefficient; baseline: predetermined response baseline.

In the case of an indirect relationship, there is a significant difference in emergence of the response in contrast to that of the drug. In such situations, mostly due to tissue equilibrium delay, two effect values are observed for the same drug plasma concentration, one at increasing concentrations shortly after drug administration and another, for the same concentrations during drug elimination phase. When plotting effect versus concentration, it is possible to witness this situation by observing a hysteresis loop (Figure 40). In this case, as the effect is modelled as a structurally different virtual compartment, it is related to the central compartment by a constant called Ke_0 which describes the delay between the appearance of concentration and response [137]. This constant is critical in describing the onset and offset of pharmacological response of drug exhibiting hysteresis loops.

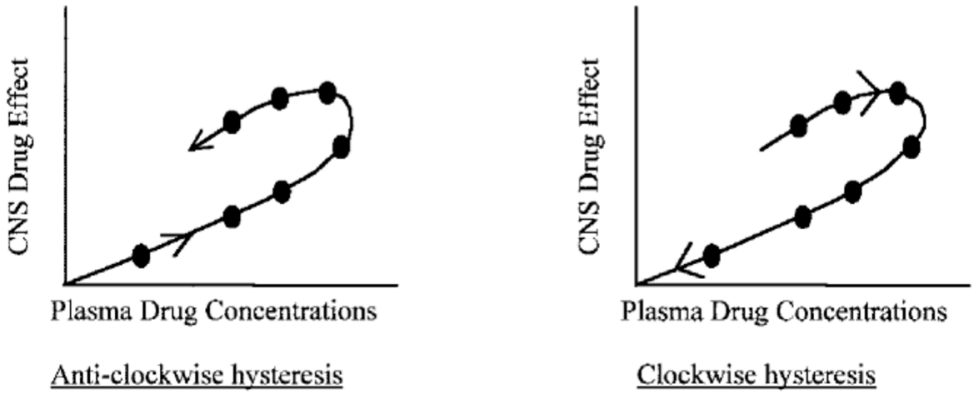

Figure 40: Types of hysteresis. Adapted with permission from Ghoneim [138].

CHAPTER 7. Modeling

Pharmacokinetics is stated as a science dedicated to the investigation of absorption, distribution, metabolism and elimination of drugs. One of the prerequisites for this type of analysis is the availability of methodologies that characterise in a quantitative fashion the movement of drugs within the body and thankfully, many such choices exist.

Proper characterisation of drug action combines the principles of both pharmacokinetics and pharmacodynamics. PK/PD modeling is a powerful tool for making the link between drug kinetics and the corresponding effect. The ability to describe or even as going as far as to predict effect variations according to the measured blood levels is a linchpin in drug development.

The PK/PD approach has seen a phenomenal evolution beginning with visual analysis of hand-drawn curves and stemming all the way through to highly complex minimisation algorithms for the objective function and minimisation/characterization of inter and intra-individual variability for population pharmacokinetics. The scope of all PK/PD modelling, no matter how complex, is the best determination possible of PK (Cl, V_d, $T_{1/2}$, T_{lag}) and PD (k_{e0}, E_{max}, EC_{50}) parameters in view of patient treatment optimization. There is a well-known quote in pharmacokinetic modeling: “All models are wrong, but some are useful.” (George E.O. Box) It denotes the potential apport which modeling may bring.

Usually modeling starts with individual data set analysis which, in turn, requires rigorous collection of data to describe all PK phases. These are sine qua non conditions for the initial determination of pharmacokinetic parameters such as: Cl, V_d, AUC, C_{max}, T_{max} and $T_{1/2}$. This information is important for establishing regimens promoting the efficacy and safety of the drug. Moreover, PK and/or PD models can be used to simulate new data from changes in conditions related to drug administration (dose, dosage) or the patient's condition (physiological or pathological).

Estimation of pharmacokinetic parameters may be derived from several types of analysis, among which the most common are non-compartmental and compartmental.

7.1. Non-compartmental analysis

Non-compartmental analysis is considered model-independent as, unlike compartmental analysis, there is no designation of a fixed number of compartments describing the kinetics of the drug. There are few major assumptions: the body is regarded as a single space in which the drug is administered, where sampling is performed and where elimination occurs. This analysis method uses simple algebraic equations that allow a robust and presupposition-free descriptive approach of the phenomena observed.

When plasma concentrations (C) are plotted against time on a semi-logarithmic graph, the terminal slope (3-4 observations about 2-4 half-lives) corresponds to the constant rate of elimination (k_e) which is also denoted λ_z (Figure 41).

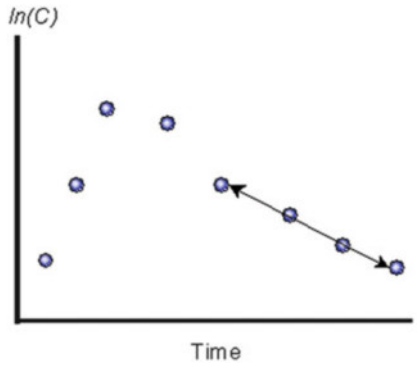

Figure 41: Semilog plot demonstrating the estimation of λz. The terminal data points are fit by log-linear regression to estimate the slope. Taken from Gabrielsson [139].

The area under the curve (AUC) of the plasma concentrations (C) versus time (t) denotes the total exposure to the drug and is representative of the dose. This AUC ($AUC_{0 \rightarrow tlast}$) is computed throughout the sampling period, t_0 until the time of the last sample (t_{last}) (Equation 12) [139].

$$AUC_{0 \rightarrow t} = \sum_{i=1}^{n} \left[\frac{C_i + C_{(i+1)}}{2} \cdot (t_{(i+1)} - t_i) \right]$$

Equation 12: Area under the concentration-time curve until time of last sample. C_i: concentration at time i; t_i: time

It involves summing the areas of a large number of trapezoids whose base corresponding to the time interval between samples. The more intervals, the higher the estimation accuracy. In a linear system, i.e. a system where the clearance remains unchanging, drug exposure is proportional to the administered dose (Equation 13) [140].

$$AUC_{0 \rightarrow \infty} = \frac{F \cdot D}{Cl}$$

Equation 13: Relationship between area under the concentration-time curve and clearance. Where Cl: clearance; F: bioavailability; D: dose.

Where AUC 0 → ∞ represents the area under the curve from drug administration (t_0) to time infinity (t_∞). The partial area calculated from the last sample t_{last} to t_∞ is calculated as follows:

$$AUC_{\text{tlast} \rightarrow \infty} = \frac{C_{last}}{k_e}$$

Equation 14: Extrapolated area under the concentration-time curve. Where k_e: elimination constant; C_{last}: concentration measured in the last sample.

As such, the full AUC is defined by the following equation:

$$AUC_{0\rightarrow\infty} = \sum_{i=1}^{n}\left[\frac{C_i + C_{(i+1)}}{2} \cdot (t_{(i+1)} - t_i)\right] + \frac{C_{last}}{k_e}$$

Equation 15: Overall area under the concentration-time curve. C_i: concentration at time i; t_i: time k_e: elimination constant; C_{last}: concentration measured in the last sample;

The same approach may be use to describe the AUC of not only concentration, but also effect, so as to obtain a quantitative reference of the overall effect of a drug.

In contrast to the predictive nature of non-compartmental analysis, compartmental PK and PD analysis relies on a series of mathematical expressions to describe and predict the time course of the effect in response to administration of a drug. A representation of compartmental versus non-compartmental analysis can be seen in Figure 42.

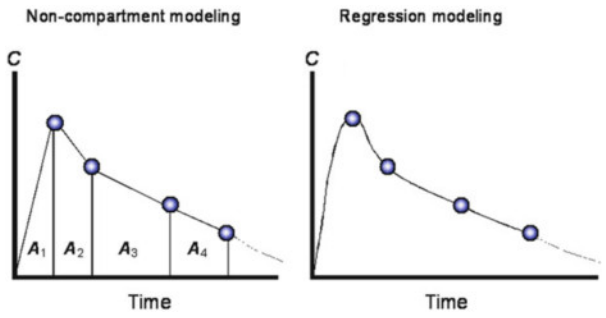

Figure 42: Comparison of NCA and nonlinear regression modeling. Left and right respectively. A_1, A_2, A_3, and A_4 represent partial areas calculated by the trapezoidal rule. Taken from Gabrielsson [139].

7.2. Compartmental analysis

Compartmental analysis is a quantitative approach that reduces the body to one or more compartments so as to establish a structural model that adequately explain the observed changes. A compartment may be defined as a virtual space in which a drug (active ingredient) is homogeneously distributed. Generally, structural models consist of one, two or at most three compartments to describe the observed data. The first compartment, central compartment, conceptually represents all the highly perfused tissues such as liver, kidneys and lungs, which are considered in direct equilibrium with the systemic circulation. The second and third compartments, more peripheral, are attributed to other less perfused tissue such as fat, muscle and skin. All the aforementioned compartments each have an apparent volume in which the drug distributes. This distribution is managed by rate constants of exchange between the compartments (Figure 43).

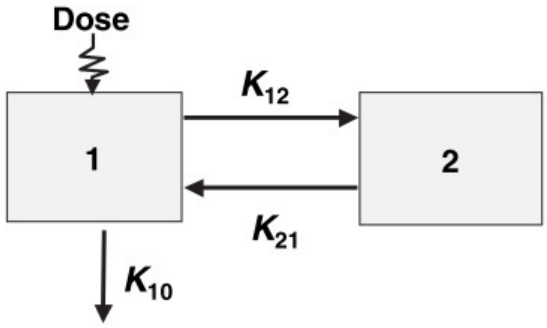

Figure 43: A schematical representation of a bi-compartmental model showing the capacity of elimination (K_{10}), and processes of distribution (K_{12}) and redistribution (K_{21}). Adapted with permission from Toutain [141].

These rate constants, also known as micro-constants, jointly with the amounts in each compartment can be set up in a system of differential equations of inputs and outputs whose integrated solution mathematically describes the evolution of plasma or peripheral drug concentrations over time (Equation 16).

$$\frac{dX_1}{dt} = K_{21} \times A_2 - K_{12} \times A_1 - K_{10} \times A_1$$

$$\frac{dX_2}{dt} = K_{12} \times A_1 - K_{21} \times A_2$$

Equation 16: Differential equations generated from a bi-compartmental model. X: compartmental drug concentrations; A: compartment amounts; K: intercompartmental constants

The integrated solution of this system of differential equations will generate macro-constants (A, B, α and β) which describe the temporal evolution of plasma drug concentrations [134]:

$$\hat{C}_p = A \cdot \mathrm{e}^{-\alpha t} + B \cdot \mathrm{e}^{-\beta t}$$

Equation 17: Bi-compartmental integrated equation. Where $\hat{C}_p$: predicted concentrations in the central compartment at time t; A predicted concentration at time 0 for the distribution phase; B predicted concentration at time 0 for the elimination phase; α: growth rate constant of the distribution phase; β: growth rate constant of the elimination phase

Therefore, the primary basis on which stands a compartmental model is its capacity to correctly estimate the parameters that compose its mathematical equation from the available observed data. To resolve such estimations, software containing nonlinear modeling iterative algorithms have been developed. However, as can be seen in Figure 44, it remains a challenge to accurately represent reality.

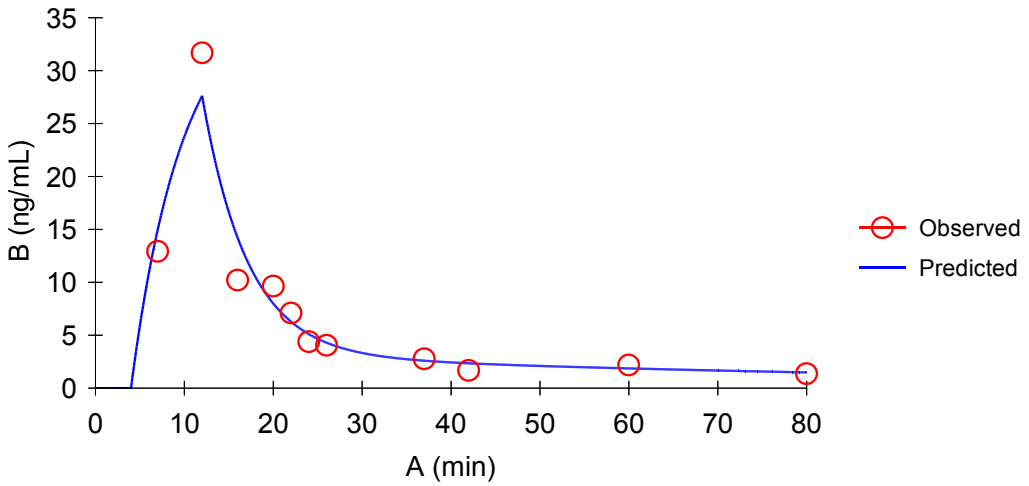

Figure 44: Modeling example. Modeled in Winnonlin®.

In the above example we have a pharmacokinetic model with two compartments following intravenous infusion showing the observed and predicted data. Several factors come into play for successful modeling such as among others, optimal sampling and compartment number.

Usually, the more compartments are added to the model, the closer it will fit the data and yield a perfect model. However, overparametrization of the model will bring about a situation of correlation between several parameters thus not providing clear information about the function of each [142]. Overparametrization may also be witness in the condition number of the analysis. This number gives insight on the extent of the difficulty with which the derivate system converged towards a solution and, by association, to the stability of the system.

7.2.1. Objective Function and Minimization

Though there are many algorithms available, a very common one is the minimisation of the objective function (OF). As can be seen in Figure 45, the OF is a numerical and quantifiable representation of the residuals between that

which was predicted and that which was actually observed, in other words, the fitting of predicted data to observed concentrations [142].

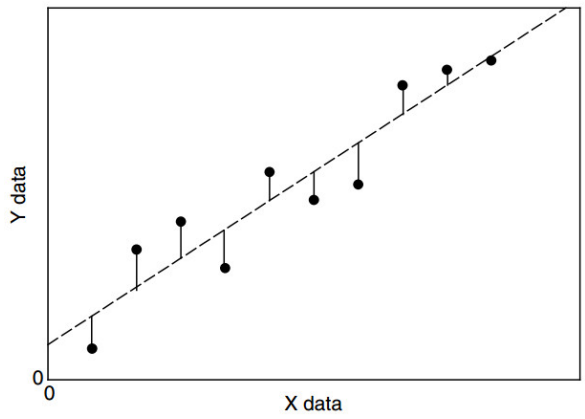

Figure 45: Illustration of the concept of least squares linear regression. The dashed line minimizes the squared deviation (indicated by solid lines) between the observed data and the predicted value. Taken with permission from Bonate [142].

The OF is mathematically defined as the sum of least squares between the observed (obs) and predicted (pred) as shown in the following equation:

$$OF = \sum_{i=1}^{n} W_i(obs_i - pred_i)^2$$

Equation 18: Objective function equation. Where obs_i: data observed at time i; $pred_i$: data predicted at time i.

The main OF minimisation algorithms are: ordinary least squares (OLS), weighted least squares (WLS) or generalized least squares (GLS) and the extended least squares (ELS) or maximum likelihood [140, 142]. These methods differ from each other mostly in terms of the weight applied to each function.

7.2.2. Model quality appreciation

When finally reaching the point of selecting the final model, many other factors come into consideration. There are several visual inspection criteria and statistics to review in order to affirm that the model estimates acceptably the observed data. Diagnostic plots are available to verify the quality of the fitting and the choice of weight. Coefficients of variation give an indication towards the accuracy of fit and possible overparametrization. The correlation matrix assesses the possible correlation between parameters. As mentioned, the condition number gives insight on the stability of the system. Finally, the F-Test and Akaike and Schwarz Criterions will help decide between competing models [142].

CHAPTER 8. Research hypotheses and objectives

8.1. Working hypotheses

The main research hypotheses of this thesis are that:

- Each type of pulmonary administration (SJ, VM, ITI, ITA) generates a characteristic particle size distribution
- Particle size distribution will affect pulmonary deposition and, in turn milrinone hemodynamic effect on the mAP/mPAP ratio.
- Milrinone systemic absorption will depend on the balance between tracheobronchial vs alveolar deposition
- Milrinone plasma concentrations can be used to predict, and eventually optimize its beneficial effect on the mAP/mPAP ratio.

For doing so, a comprehensive research approach comprising animal back-translational studies as well as complementary *in vitro* and *ex vivo* studies was carried out. The first research section involved firstly the identification and quantification of the surgical artefacts affecting PK/PD determination of milrinone. Secondly, a new HPLC-MS/MS method was developed in order to compensate for the lack of specificity and specificity of a previous method. They were followed by *in vivo* studies which compared the *in vivo* and *ex vivo* efficacy of the simple jet and vibrating mesh nebulizer. Lastly and most importantly, a new hypercapnic animal model was developed and was used to determine the PK/PD of four types of pulmonary administrations for milrinone.

8.2. Specific objectives

Objective 1: To confirm the need for an animal model without surgical stress.

The PD biomarker used for milrinone PK/PD modeling is the mAP/mPAP ratio. Previous experience shows that the hemodynamic repercussion of surgical manipulations on this biomarker can bias the characterization of the pharmacological effect of milrinone.

The specific objective was:

I. To quantify the duration and amplitude of the effect of each hemodynamic artefact caused by surgical manipulations during CPB preparation.

Objective 2: To develop a milrinone-specific and sensitive bioanalytical method

Development of bioanalytical methods allows the quantification of drug plasma levels when PK studies are executed. Depending on the efficiency of extraction, chromatographic separation and detector, a wide array of molecules may potentially be simultaneously quantified. Previous work in our laboratory provided a milrinone quantification analytical method, however, in cardiac patients undergoing surgery polymedication cannot be stopped and, the method exhibited a lack of specificity for milrinone.

The specific objective was:

I. To optimize and validate an analytical HPLC-MS/MS method with a specificity and sensitivity (LOQ <1.25 ng/mL) in a small volume of bilogical sample

Objective 3A: To compare the performance of simple jet and vibrating mesh nebulizers

Nebulizers are the most common tool for the administration of inhaled milrinone. Two types are commonly used, simple jet and the ultrasonic vibrating mesh. These two nebulizers are thought to produce inhaled mists of different sizes, a factor which affects pulmonary milrinone deposition and possibly effect.

The specific objectives were to assess the differences between the two nebulizers:

I. To determine, using a cascade impactor, the dose emitted by these nebulizers.
II. To quantify the dose delivered to the entry port of the impactor (inhaled dose).
III. To assess the particle size distributions of each nebulizer.

Objective 3B. To compare the *in-vivo* hemodynamic and *ex-vivo* efficacy of milrinone administration through simple jet and vibrating mesh nebulizers

I. Determine in vivo efficacy of the nebulizations through their impact on the hemodynamic parameters of swine undergoing cardiopulmonary bypass
II. To compare the relaxation profiles to acetylcholine and bradykinin of arteries having received milrinone through one of the two nebulizations

Objective 4: To determine a PK/PD model for milrinone administered through simple jet and vibrating mesh nebulizations and through intratracheal bolus and atomization.

Several clinical studies report that inhaled milrinone has the ability to reduce pulmonary pressures without affecting systemic pressures. Despite the beneficial effects reported for inhaled milrinone, no study has characterized the PK/PD relationshop of the pulmonary route. In addition to nebulization, in emergency cases, milrinone may also be administered through an intratracheal

bolus. However, the intratracheal bolus has the downside of unpredictable absorption, so an intratracheal atomization method is proposed.

The specific objectives were:

I. To develop a hypercapnic pulmonary hypertension model devoid of surgical artefacts.

II. To determine the PK/PD relationship for the four pulmonary milrinone administration methods.

III. To confirm via the urinary excretion of milrinone, changes in metabolism and bioavailability of the pulmonary route of administration.

SECTION II: BODY OF WORKS

CHAPTER 9. Manuscript #1: Impact of Surgical Procedure Artefacts on the Hemodynamic Parameters of an Isoflurane-Anesthetized Swine Cardiopulmonary Bypass Model.

Paul Gavra[1], B.Sc., André Y. Denault[2], M.D., Ph.D., Cristian Rosu[2], M.D., Louis P. Perrault[2], M.D., Ph.D. and France Varin[1], B.Pharm., Ph.D.

[1]Faculty of Pharmacy, Université de Montréal, Montréal, Canada
[2]Montreal Heart Institute, Montréal, Canada

Running title: Bypass Procedures on Hemodynamic Parameters

Corresponding author:
France Varin, B.Pharm, Ph.D.
Faculté de pharmacie, Université de Montréal,
C.P. 6128, Succursale Centre-Ville,
Montréal, QC, Canada H3C 3J7.
Phone : +15143437016
E-mail : france.varin@umontreal.ca

Current status : Published in Archives of Clinical and Expermental Surgery

Abstract

Objectives: This study quantifies cardiopulmonary bypass preparation artefacts on mean systemic arterial pressures (mAP), mean pulmonary arterial pressures (mPAP) and their ratio (mAP/mPAP) in order to assess the usefulness of this ratio as a pharmacodynamic marker for pharmacokinetic/pharmacodynamic modeling studies.

Materials and Methods: Fifteen anesthetized swine were monitored every minute before initiation of cardiopulmonary bypass. Percent relative changes from pre-artefact values (Δ%) were used during anesthesia induction and stabilization (Δ% minute-1 reduction rates). In addition, in some animals, amplitude and duration were recorded for the following procedures: sternotomy, pulmonary artery catheter installation, purse-string sutures and cardiac cannulations.

Results: Isoflurane 5% anesthesia induction effect on mAP, lasted on average 5.3±2.0 minutes at 5.9±1.9 Δ% minute-1. Isoflurane 2% anesthesia stabilization effect on mAP lasted on average 36.0±8.0 min at 0.8±0.9 Δ% minute-1. During stabilization, no change in mAP/mPAP was observed ($p=0.68$). Average amplitudes of artefacts on mAP were 30-50 Δ%; almost twice those observed for mPAP and mAP/mPAP for the same manipulations ($p<0.05$). Pulmonary artery catheter installation artefacts lasted longer than those of other procedures ($p<0.05$). Average artefact duration was 4.5±2.5 minutes ($n=160$).

Conclusions: In isoflurane-anesthetized swine, mAP/mPAP ratio remains constant during anesthesia stabilization, unlike mAP and mPAP individually. Moreover, the ratio shows potential as a pharmacodynamic biomarker for pharmacokinetic/pharmacodynamic studies involving CPB.

Key words: Cardiopulmonary bypass, anesthesia, surgical artefacts, mAP/mPAP, swine

Introduction

Every year, worldwide, 1-1.25 million adult cardiac surgeries are performed [1], the majority of these requiring a cardiopulmonary bypass (CPB). Surgical preparations for this procedure are associated with physical stress. During that period, lungs and heart are bypassed and neither is perfused. At the end of surgery, the patient is weaned from CPB and normal circulation is restored. Upon weaning from CPB, a pulmonary reperfusion syndrome can cause pulmonary hypertension [2] which, in turn, might be associated not only with difficult weaning but also with right ventricular dysfunction and poor post-surgery prognosis [3, 4]. Consequently, treatment and prevention of the pulmonary hypertension would be expected to reduce the severity of the pulmonary reperfusion syndrome.

To better study pulmonary hypertension and/or potential pharmacological treatment avenues, adult swine CPB models have been developed [5, 6]. They provide insight on some key hemodynamic parameters such as the mean systemic arterial (mAP) and mean pulmonary arterial pressure (mPAP). The ratio of these two measures (mAP/mPAP) has been suggested as a biomarker for both pulmonary hypertension severity and selective pulmonary drug effect [7] which makes it an excellent candidate for pharmacokinetic/pharmacodynamic (PK/PD) relationship modeling. Monitoring of the mAP/mPAP ratio identifies conditions where mPAP decreases while mAP remains constant, thus indicating both the drug's local pulmonary effect and its lack of systemic hypotension. This ratio is already being used in human cardiac surgery as it has been identified as a significant predictor of post-operative outcome [8]. Most importantly, this ratio was also found not to be influenced by the induction and maintenance of general anesthesia in cardiac patients [9] thereby strengthening its use as a possible PK/PD descriptive tool. Prophylactic interventions, such as nebulized drugs, are currently being investigated as potential treatment options for pulmonary hypertension [6, 7, 10]. These are administered before the beginning of CPB to

exert their preventive antihypertensive effect locally on the lungs. However, as the drug is administered in time-constrained operating room conditions, their pharmacological effect often coincides with CPB preparation artefacts which, in turn, affect the ratio. Monitoring and quantifying the changes incurred on the ratio by surgical artefacts, in absence of any drug, is necessary in view of interpreting a PK/PD relationship obtained in the presence of both preparation artefacts and drug effect. Moreover, knowledge of artefact duration is important in order to properly design PK/PD protocols. Such a study is practically not feasible in surgical patients. Hence, the adult swine CPB model was used to replicate human CPB preparations e.g. isoflurane anesthesia induction (AI), anesthesia stabilization (AS) as well as surgical procedures: sternotomy, pulmonary artery catheter (PAC) installation, cardiac cannulations (CC) and purse-string suturing (PSS). This study was undertaken specifically to quantify the amplitude and duration of the CPB preparation-related mAP, mPAP and ratio artefacts in a swine CPB model. The overall goal is to provide a better understanding of how CPB-related preparations affect mAP, and mPAP values and more importantly, their ratio, a potential biomarker to be used in the PK/PD modeling of medication intended for pulmonary hypertension.

Material and methods

Animals

This observational study was performed on fifteen, 3-month old castrated male 35 kg Landrace swine undergoing two separate research projects. The experimental procedures were approved by the institutional Animal Care Committee (*Comité de déontologie animale de l'Institut de cardiologie de Montréal*) in accordance with the recommendations and guidelines on the care and use of laboratory animals issued by the Canadian Council on Animals (institutional committee numbers: 2010-73-2, 2010-73-3).

Animal preparation

Prior to entry in the operating room, animals were sedated with 2.2 mg kg^{-1} xylazine (Boeringer Ingelheim, Burlington, Ont, Canada) and 33-44 mg kg^{-1} ketamine hydrochloride (Ayerst Veterinary Laboratories, Guelph, Ont, Canada) intramuscularly. General anesthesia (Abbott Laboratories Limited, St-Laurent, QC, Canada) was induced with 5% isoflurane (AI) using mask ventilation. The animals were then intubated and ventilated at 15-18 breaths per minute and 6-8 mL kg^{-1} using a 0.66 inspired oxygen fraction. Subsequently, the electrocardiogram (ECG) electrodes, oxygen sensor and a rectal thermometer were installed. In aseptic conditions, the left femoral artery and the right femoral vein were then cannulated to install the mAP sensor and a central venous catheter, respectively. Cannulations were also performed on the internal right carotid and the external and internal right jugular veins. Isoflurane concentration was then lowered to 2% for anesthesia maintenance, marking the start of the AS period. A median sternotomy followed by a sternal retraction were then performed. A pulmonary arterial catheter (PAC, Edward Lifesciences, Irving, Ca, USA) was then positioned in the pulmonary artery through the internal right jugular vein cannula to monitor the mPAP. Correct positioning of the PAC was confirmed using pressure-waveform identification. Heparin was then given at 300 IU kg^{-1} (Leo Pharma, Inc, Ajax, Ont, Canada) preceding surgical manipulations.

CPB surgical manipulations

The first protocol (n=4), animals were scheduled to undergo coronary bypass procedures. Hemodynamic data collection was stopped after the AS period. Therefore, only AI, AS and PAC installation measures were available from these animals.

The second protocol (n=11), animals were scheduled to undergo CPB. Two PSS were placed on the aorta and one on the right atrium. The sutures were followed by aortic and subsequently atrial cannulation using 22F and 29/29F

double-staged cannulas (DLP, Inc, Grand Rapids, Mich, USA) respectively. Once surgical manipulations were finished, CPB was initiated and data acquisition stopped.

Hemodynamic measurements

The mAP and mPAP were monitored at one minute intervals using a Solar® 8000M patient monitor (Milwaukee, WI, USA), printed at the end of each experiment using a Marquette PRN50 digital writer (Milwaukee, WI, USA). AI and AS periods were determined using mAP pressure reduction rates (% minute^{-1}). The AI period was considered to start at the beginning of mask ventilation (before mAP signal acquisition) and to end when isoflurane was changed from 5 to 2%. The time between 5% isoflurane induction and mAP signal acquisition was kept as short as possible but was dependent on cannulation time. The AI pressure reduction rate was calculated as follows:

$$\text{Equation 1: } AI\ rate = \frac{\frac{mmHg_I - mmHg_L}{mmHg_I} \times 100}{T_{mmHg_L} - T_{mmHg_I}}$$

Where $mmHg_I$ is the initial mAP pressure value obtained at time T_{mmHg_I} after signal acquisition and $mmHg_L$ is the last value of the AI period obtained at time T_{mmHg_L}.

The beginning of the AS period was the isoflurane 5 to 2% concentration changing point. A constant mAP (within 5%) for more than 4 minutes was considered indicative of the AS period's end. Consistent patterns of pulmonary pressure decreases during the AS period were sometimes not available as they depended on how many trials were made before successful installation of the PAC. When PAC installation time was longer than the stabilization timeframe, pulmonary artery pressure was already stabilized under 2% isoflurane anesthesia conditions (n=9) leaving five animals for mPAP AS rate determination. The AS pressure reduction rates for mAP and mPAP were calculated similarly to the AI rates using Equation 1. During the AS period, care

was taken to calculate the mPAP rate using pressures at times devoid of any surgical interference.

For CPB-related surgical procedures, times corresponding to the beginning and end of each procedure were noted during surgery. Because sternotomy was carried out before installation of the PAC, mPAP data for it were not available. The amplitude of the artefact (Δ) expressed as a percent relative change from pre-artefact value (Δ%) of each surgical procedure was calculated for the mAP, mPAP and ratio, as follows:

$$\text{Equation 2: } \Delta\ \% = \frac{mmHg_S - mmHg_{PS}}{mmHg_{PS}} \times 100$$

Where $mmHg_S$ is the maximum pressure value recorded during a surgical stress and $mmHg_{PS}$ is either the pre-artefact (PSS, CC) or post-artefact (PAC) pressure value. Pre-artefact values were recorded one minute before beginning the procedure while post-artefact values, at the end of the PAC installation artefact. The PAC installation artefact ended when mAP pressures either showed a return to anterior reduction rates or were constant (within 5% variation) for more than 4 minutes. Post-artefact pressure values were used to calculate PAC installation artefact as no mPAP pre-artefact values were available.

For each surgical procedure, duration of the hemodynamic artefact was calculated as the difference between the onset time of the artefact and the time of return to its pre-artefact value. The beginning and end of each surgical procedure was also noted. To mimic an operating-room setting, all procedures were carried out without deliberate pause for return to pre-artefact value. For each animal, 3 PSS and 2 CC were performed. PSS were performed at short time intervals thus sometimes generating merged pressure spikes. Merged pressure spikes were counted as a single PSS.

Statistical analysis

Descriptive statistics are presented as mean ± standard deviation. Changes in amplitude (Δ%) and durations of artefacts (min) on the following hemodynamic parameters: mAP, mPAP and ratio for each surgical manipulation were compared using SPSS 16.0.1 (SPSS Inc, Chicago, Il, USA). First, normality of distribution of data was assessed by means of the Shapiro-Wilk test. In comparisons involving all three hemodynamic parameters, normally distributed values were analyzed using one-way ANOVAs and followed by a Tukey's post-hoc test. Non-normally distributed data were analyzed using the Kruskal-Wallis test followed by a Mann-Whitney U test. Non-paired t-tests or Mann-Whitney U tests preceded by Levene variance tests were performed for mAP vs mPAP AS durations and also for ratios during vs after AS. Statistical significance was set at $p<0.05$.

Results

A typical progression of surgery and the hemodynamic changes associated with isoflurane induction and stabilization is represented in Fig.1 and with the different manipulations in Fig.2. The animal “n” differed between hemodynamic parameters as well as between surgical procedures. For the second protocol, complications were observed in 2 out of 11 animals: one died immediately after sternotomy during the (AS period) and the other did not tolerate prolonged isoflurane anesthesia (data recording ended after the AS period and before surgical manipulations).

During the AI period, only mAP was available as the pulmonary artery catheter had yet to be installed. Mean elapsed time between beginning of induction and mAP signal acquisition was 16±10 minutes (n=15) and first recorded values for mAP averaged 89±31 mmHg. The AI period lasted on average 5±2 minutes (n=8), during which a reduction in mAP was observed at a rate of 5.9±1.9 Δ% $minute^{-1}$. For some animals (n=6), preparations were too lengthy to determine the AI rate as these animals had already reached the AS period when first recorded data was available.

The AS period was found to be of similar durations (p=0.077) for systemic and pulmonary pressures, respectively, 36±8.0 (n=11) and 25.0±14 (n=5) min after mAP signal acquisition. Due to the length of arterial/venous cannulation procedures and PAC installation, mAP and mPAP rates were characterized in 11 and 5 animals respectively. Using initial AS pressure values, mAP and mPAP pressure reduction rates were 0.8±0.9 and 0.2±0.2 Δ% min^{-1}, respectively and there was an overall reduction of 17.6±6.6 (p=0.03) and 17.1±7.1 Δ% (p=0.04) for mAP and mPAP. Beginning and end-AS mean ratio values were similar.(p=0.68).

Percent relative change from pre-artefact values and duration of hemodynamic changes caused by each CPB-related surgical procedure, are summarized in

Table 1. Often, due to the close timing of manipulations, the multiple aortic PSS artefacts translated as only one single hemodynamic artefact for a total of 22. During sternotomy, Δ% were observed for mAP in only 5 animals and were highly variable (32±37 Δ%). The remaining animals did not show any artefact resulting in a highly variable overall effect (9.9±23 Δ%, n=13).

The artefact amplitudes caused by each surgical manipulation on mAP and mPAP were compared. Mean mAP changes caused by PAC installation (Δ%: 47), PSS (Δ%: 41) and CC (Δ%: (-)34), were all three significantly greater than those observed for mPAP (Δ%: 14, 21 and (–)21, respectively; $p<0.05$). Similarly, significant differences in mAP vs ratio Δ% were observed (Δ%: 22, 25 and (–)25, for PAC installation, PSS, and CC, respectively; $p<0.05$). In contrast, no significant difference was found in mPAP vs ratio Δ% for PAC installation, PSS and CC.

Artefact durations on the hemodynamic parameters were also analyzed. The PAC installation mAP artefact (8.3 min) lasted significantly longer than PSS (4.2 min) and CC (4.4 min) mAP artefacts ($p<0.05$). Again, PAC installation ratio artefact (7.4 min) lasted significantly longer than PSS (4.4 min) and CC (3.7 min) ratio artefacts ($p<0.05$). Overall mean artefact duration of all pooled data (all surgical manipulations on all hemodynamic parameters) was 4.5±2.5 minutes (n=160).

Discussion

This study confirms, in the swine model, that the ratio remains stable during induction and stabilization of general anesthesia, as documented in patients. In addition, this study documents both the amplitude and duration of the hemodynamic changes caused by standard CPB-related surgical procedures. These findings should be taken into account in studies that aim at determining drug-related hemodynamic effects in cardiac patients undergoing cardiac surgery with CPB. As such, this information will help not only design studies, reduce bias and enable a better characterization of the net pharmacological effect, but also help in the analysis of ongoing studies. Robitaille *et al* [9] showed that, during general anesthesia, patients' systemic and pulmonary pressures decreased proportionally, resulting in an unchanged ratio. Their study was conducted in a context of general anesthesia induced by a drug combination of fentanyl/sufentanyl, midazolam and isoflurane. In swine, no change was observed in the ratio during induction and stabilization, thus concurring with their results even with the sole use of isoflurane. Since isoflurane is a common anesthetic for this animal species [11], our results can be generalized to a broader range of experimental models. Indeed, in absence of surgical manipulation, the ratio seems a reliable hemodynamic marker that doesn't fluctuate with the degree of anesthesia.

Systemic and pulmonary pressures took up to 45 minutes to stabilize after lowering isoflurane from 5 to 2%. Therefore, by utilizing the ratio, it would be possible to start PD data sampling before complete stabilization, resulting in a considerably shorter experimentation time.

Surgery is an acute physical stress known to elicit several endocrine responses, in particular during CPB-related procedures. The sympatho-adrenal response involves physiological vasopressor surges [12] resulting in hypertension and possibly tachycardia [13]. Previous swine studies [14, 15] have documented the evolution of hemodynamic artefacts as well as plasma concentration changes of

several biochemical markers of pain and inflammation at pre-determined time points: before, during and after esophageal and inguinal soft tissue surgeries. Potts *et al* [12] were able to model and describe individual mAP artefacts as pressure spikes related to vasoactive amine bolus inputs. The present study monitored continuously the hemodynamic parameters during CPB procedures and quantified the amplitude of each hemodynamic change related to a specific surgical artefact in view of calculating their areas under the curve for application in future PK/PD studies.

Our results show that the amplitude and duration of surgical procedure artefacts on mAP and the mPAP differed significantly one from the other. Variations in systemic pressures observed during surgical manipulations were to be expected as they involved surgical stress and, in the case of the PSS and CC, direct contact with the heart and/or aorta. In regards to PAC installation, the ensuing large mAP artefact could be attributed to pulmonary artery contact [16]. The resulting vasoconstriction could explain the high variability observed for mAP artefacts.

Overall, CPB-related surgical procedures caused on average a 40 % mAP change from pre-artefact values which is higher than the 20% increase suggested by Potts *et al* [12] most probably because of the nature of the stress. Nursing procedures such as endotracheal tube suctioning do not generate as much stress as surgical procedures. The 40 Δ% on mAP is approximately twofold higher than that observed for mPAP and the ratio. Even though pulmonary pressures usually show very small variability due to their low-pressure nature [17], our results suggest that surgical manipulations do affect the pulmonary circulation. Consequently, use of the aforementioned hemodynamic parameters as markers for modeling within 7 minutes of a surgical manipulation would introduce a large vasopressor artefact in the area under the curve of any hemodynamic parameter. If manipulation artefacts are accounted for, the most useful hemodynamic parameter for PK/PD modeling is, in our opinion, the ratio. It demonstrates minimal amplitude artefacts while still reflecting changes in both mAP and mPAP.

Limitations

Given the observational nature of this study, no attempt was made to modify animal preparation, anesthetic procedures or timing of surgery manipulations. Firstly, lengthy animal CPB-related procedures, especially PAC installation time which resulted in, reduced availability of pulmonary data during AS period. Secondly, depending on surgical conditions and/or animal responsiveness, amplitudes and durations of hemodynamic artefacts were greatly variable and sometimes overlapped, inflating the measured artefact and its variability. As this situation is highly representative of intra-operative clinical protocols, this might also be perceived as strength. Furthermore, animals used in this study were healthy, relatively young adults and without previous surgeries, whereas a typical patient undergoing CPB would be subject to several previous health issues, notably, pre-existing pulmonary hypertension, which could certainly affect the hemodynamic reaction to surgical procedures.

Conclusion

Monitoring mAP/mPAP ratio throughout the CPB preparations enabled characterization of the amplitude and duration of surgical procedures' artefacts. This information is necessary when designing and analyzing data from PD studies involving cardiovascular agents as these artefacts modify the PD biomarker used to assess efficacy. Our study also reinforces the use of the ratio as a PD biomarker because, while remaining informative on pulmonary drug effect, its sensitivity to surgical artifacts appears minimal.

Acknowledgements

This research was supported by Fonds de recherche du Québec - Santé (FRQS) and Groupe de recherche universitaire sur le médicament de l'Université de Montréal (GRUM). The authors would like to acknowledge the invaluable help of Marie-Pierre Mathieu and Stéphanie Blanchet from Dr. Perrault's laboratory.

Tables

	Sternotomy (S)	Pulmonary Artery Catheter (PAC)	Purse-string Sutures (PSS)	Cannulations (CC)
mAP (n)	(13)	(13)	(22)	(16)
Δ pressure (%)	9.9 ± 23	47 ± 33*	41 ± 19#	-34 ± 14†
Artefact duration (min)	6.6 ± 4.6	8.3 ± 3.7‡	4.2 ± 1.7	4.4 ± 1.8
mPAP (n)		(10)	(22)	(16)
Δ pressure (%)		14 ± 8	21 ± 11	-21 ± 11
Artefact duration (min)		6.0 ± 2.3	3.9 ± 1.4	3.7 ± 1.8
mAP/mPAP (n)		(10)	(22)	(16)
Δ ratio (%)		22 ± 13	25 ± 14	-25 ± 10
Artefact duration (min)		7.4 ± 4.3††	4.4 ± 1.8	3.7 ± 1.1

Table 1: Hemodynamic mean changes caused by each surgical procedure and their duration

Mean changes (Δ), expressed as percentages of pre-artefact values. mAP: mean systemic arterial pressure; mPAP: mean pulmonary arterial pressure; mAP/mPAP: mean systemic arterial pressure over mean pulmonary arterial pressure ratio; n: number of animals.

* p = 0.001 and 0.045 vs PAC mPAP and mAP/mPAP Δ% respectively;

p = 0.001 and 0.001 vs PSS mPAP and mAP/mPAP Δ% respectively;

† p = 0.004 and 0.004 vs CC mPAP and mAP/mPAP Δ% respectively;

‡ p = 0.012 and 0.012 vs PSS and CC mAP artefact duration respectively;

†† p = 0.001 and 0.001 vs PSS and CC mAP/mPAP artefact duration.

Figures

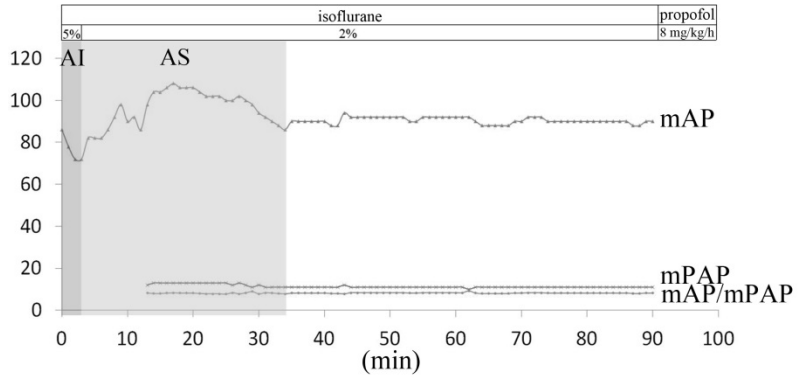

Figure 1: Changes in mean systemic arterial pressure in mmHg (mAP), mean pulmonary arterial pressure (mPAP) and mean systemic arterial pressure over mean pulmonary arterial pressure ratio (mAP/mPAP) during anesthesia induction with 5% isoflurane (AI) and anesthesia stabilization with 2% isoflurane (AS) in a swine from the first protocol.

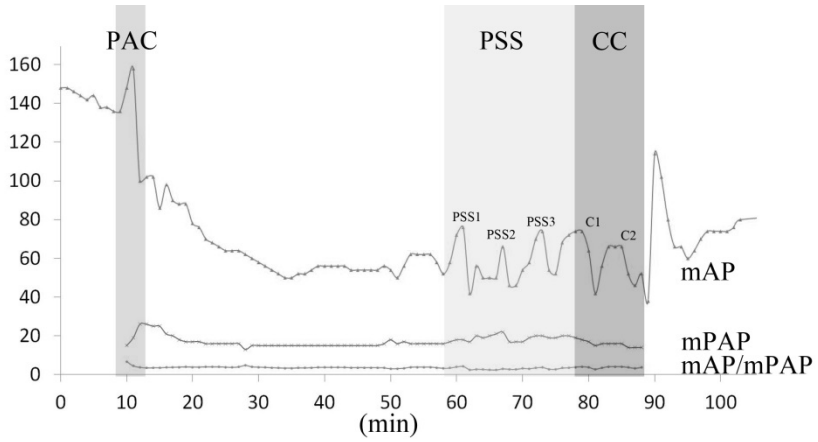

Figure 2: Progression of hemodynamic parameters and surgical procedures' artefacts in a swine from the second protocol. Changes in mean systemic arterial pressure in mmHg (mAP), mean pulmonary arterial pressure in mmHg (mPAP) and mean systemic arterial pressure over mean pulmonary arterial pressure ratio (mAP/mPAP) are shown during pulmonary artery catheter insertion (PA), purse-string sutures (PSS): PSS1 and PSS2 aortic sutures; PSS3 auricular suture; and cardiac cannulations (CC) C1: aortic cannulation; C2: auricular cannulation.

References

1. Herbertson M. Recombinant activated factor VII in cardiac surgery. Blood Coagul Fibrinolysis. 2004;15:S31-2.
2. Balanos GM, Talbot NP, Dorrington KL, Robbins PA. Human pulmonary vascular response to 4 h of hypercapnia and hypocapnia measured using Doppler echocardiography. J Appl Physiol. 2003;94:1543-51.
3. Maclean MR, Johnston ED, McCulloch KM, Pooley L, Houslay MD, Sweeney G. Phosphodiesterase isoforms in the pulmonary arterial circulation of the rat: changes in pulmonary hypertension. J Pharmacol Exp Ther. 1997;283:619-24.
4. Denault A, Deschamps A, Tardif JC, Lambert J, Perrault L. Pulmonary hypertension in cardiac surgery. Curr Cardiol Rev. 2010;6:1-14.
5. Hubert M, Salazkin I, Desjardins J, Blaise G. Cardiopulmonary bypass surgery in swine: a research model. J Exp Anim Sci. 2003;42:135-49.
6. Fortier S, DeMaria RG, Lamarche Y, Malo O, Denault A, Desjardins F, *et al*. Inhaled prostacyclin reduces cardiopulmonary bypass-induced pulmonary endothelial dysfunction via increased cyclic adenosine monophosphate levels. J Thorac Cardiovasc Surg. 2004;128:109-16.
7. Lamarche Y, Malo O, Thorin E, Denault A, Carrier M, Roy J, *et al*. Inhaled but not intravenous milrinone prevents pulmonary endothelial dysfunction after cardiopulmonary bypass. J Thorac Cardiovasc Surg. 2005;130:83-92.
8. Hentschel T, Yin N, Riad A, Habbazettl H, Weimann J, Koster A, *et al*. Inhalation of the phosphodiesterase-3 inhibitor milrinone attenuates pulmonary hypertension in a rat model of congestive heart failure. Anesthesiology. 2007;106:124-31.
9. Robitaille A, Denault AY, Couture P, Belisle S, Fortier A, Guertin MC, *et al*. Importance of relative pulmonary hypertension in cardiac surgery: the

mean systemic-to-pulmonary artery pressure ratio. J Cardiothorac Vasc Anesth. 2006;20:331-9.

10. Aubin M-C, Laurendeau S, Mommerot A, Lamarche Y, Denault A, Carrier M, *et al*. Differential effects of inhaled and intravenous sildenafil in the prevention of the pulmonary endothelial dysfunction due to cardiopulmonary bypass. J Cardiovasc Pharmacol. 2008;51:11-7.
11. Greene Sa, Benson GJ, Tranquilli WJ, Grimm Ka. Effect of isoflurane, atracurium, fentanyl, and noxious stimulation on bispectral index in pigs. Comp Med. 2004;54:397-403.
12. Potts AL, Anderson BJ, Holford NH, Vu TC, Warman GR. Dexmedetomidine hemodynamics in children after cardiac surgery. Paediatr Anaesth. 2010;20:425-33.
13. Desborough JP. The stress response to trauma and surgery. Br J Anaesth. 2000;85:109-17.
14. Eisold S, Mehrabi A, Konstantinidis L, Mieth M, Hinz U, Kashfi A, *et al*. Experimental study of cardiorespiratory and stress factors in esophageal surgery using robot-assisted thoracoscopic or open thoracic approach. Arch Surg. 2008;143:156-63.
15. Schoffmann G, Winter P, Palme R, Pollak A, Trittenwein G, Golej J. Haemodynamic changes and stress responses of piglets to surgery during total intravenous anaesthesia with propofol and fentanyl. Lab Anim. 2009;43:243-8.
16. Moore JP, Hainsworth R, Drinkhill MJ. Phasic negative intrathoracic pressures enhance the vascular responses to stimulation of pulmonary arterial baroreceptors in closed-chest anaesthetized dogs. J Physiol. 2004;555:815-24.
17. Kittnar O. Cardiac preload: hemodynamic physiology during thoracic surgery. Curr Opin Anaesthesiol. 2011;24:21-3.

CHAPTER 10. Manuscript #2: A specific and sensitive HPLC-MS/MS micromethod for milrinone plasma levels determination after inhalation in cardiac patients.

Paul Gavra[*], Anne QN. Nguyen[*], Yves Théorêt[†], Catherine Litalien[†], André Y. Denault[††] & France Varin[*]

*Faculty of Pharmacy, Université de Montréal, Montréal, Canada
† Unité de Pharmacologie Clinique, CHU Ste-Justine, Montréal, Canada
††Montreal Heart Institute, Montréal, Canada

Correspondence: France Varin, Faculty of Pharmacy, Université de Montréal, P.O. Box. 6128, Succursale Centre-Ville, Montréal, QC, Canada H3C 3J7.
E-mail : france.varin@umontreal.ca
Short Title: HPLC-MS/MS micromethod for plasma milrinone in cardiac patients
This research was supported by Fonds de la recherche en santé du Québec (FRSQ) and Groupe de recherche universitaire sur le médicament de l'Université de Montréal (GRUM). A studentship was granted by the Canadian Institutes of Health Research to Anne QN Nguyen.

Current status: Published in Therapeutic Drug Monitoring

Abstract

Background: Milrinone administered through inhalation is an emerging method aimed at specifically reducing pulmonary hypertension without affecting systemic pressures. Its administration has been shown useful both in patients undergoing cardiac surgery and for persistent pulmonary hypertension of the newborn. These populations are prone to receive many concomitant medications and/or blood sampling may require a low volume quantification method. In order to address these issues in view of pharmacokinetic studies, this paper aims to develop and validate a specific and sensitive analytical assay using HPLC and MS/MS detection for the quantification of milrinone plasma concentrations after inhalation in patients undergoing cardiac surgery.

Methods and Materials: Plasma samples (50 µL) were extracted using ethyl acetate. Milrinone was separated on a C18 analytical column at 50°C. The mobile phase consisted of methanol and 10 mM ammonium acetate (45:55 v/v). The electrospray was operated in the negative ionization mode and monitored the following mass transitions: m/z 212.1 → 140.0 at 36 eV for milrinone and m/z 252.1 → 156.1 at 32 eV for olprinone.

Results: Calibration curves followed a quadratic regression in the concentration range of 0.3125–640 ng/mL. The lower limit of quantification is 0.3125 ng/mL and is based on a low plasma volume of 50 µL. Mean drug recovery and accuracy were ≥ 72.3% and 96.0%, respectively. Intra- and inter-day precision (CV%) was ≤ 7.4 % and ≤ 11.5%, respectively. The specificity allowed milrinone quantification in the multidrug administration conditions of cardiopulmonary bypass.

Conclusions: This validated micromethod proved to be highly sensitive and specific while using a low volume of plasma. Its low volume and its lower limit of quantification indicate that this approach is suitable for further characterisation of milrinone pharmacokinetics in both adults (inhalation) and neonates.

Introduction

Cardiopulmonary bypass (CPB) is associated with a multitude of post-operative complications[1-4]. During CPB, in addition to blood/CPB apparatus interactions[5,6], lungs are minimally perfused and at weaning, may undergo ischemia-reperfusion injury that can eventually lead to pulmonary hypertension[7]. Compared to intravenous administration, inhaled milrinone has a more selective action on pulmonary vasculature with no systemic hypotension[8,9]. Results in patients given inhaled milrinone before cardiac surgery indicate plasma concentrations below 10 ng/mL shortly after weaning from cardiopulmonary bypass[10], and often under the lower limit of quantitation (LLOQ) 10 hours after inhalation (unpublished results). Thus, to fully characterize the elimination phase of inhaled milrinone, an improved sensitivity is required. Also revealed, due to the many concomitant medications given before, during and after CPB, chromatographic interferences were often observed at milrinone retention time, making quantification impossible. Therefore, a higher degree of specificity was also deemed necessary.

Milrinone, is also a possible treatment for several conditions in pediatric populations ranging from neonates to children. Milrinone is currently given intravenously to neonates in the case of persistent pulmonary hypertension of the newborn (PPHN). This life-threatening condition affects 2-6 infants in 1000[11] and 10% of all preterm and term neonates that require neonatal intensive care[12]. Use of intravenous milrinone has been shown to offer advantages in PPHN[13,14], when combined with inhaled nitrous oxide. Although inhaled milrinone could represent an interesting alternative, current pharmacokinetic data in neonates[15] remains quite limited.

Inhaled milrinone is also emerging as a treatment option for children with pediatric pulmonary hypertension due to acyanotic congenital heart disease

which, when leading to right heart failure, is a leading cause of mortality and morbidity in cardiac patients[16]. Furthermore, milrinone was recently tested in the context of post-surgical support for neonates after cardiovascular surgery[17].

Milrinone now appears as a pediatric treatment option that would greatly benefit from pharmacokinetic characterization and dose optimization. For doing so, a low plasma volume analytical method and a higher degree of sensitivity are required. in particular for inhaled milrinone studies.

Few analytical methods for the determination of milrinone in human plasma have been published using HPLC-UV10,[18-20]. The LLOQ (based on 1 mL of plasma) reached with UV detection is approximately 1 ng/mL and, most importantly, lacked the high specificity required in cardiac patients. More recently, an HPLC-MS/MS assay[21] was proposed for therapeutic drug monitoring of milrinone given as an intravenous infusion in pre- or post-surgical cardiac patients. While the specificity issue was solved, the sensitivity reached (0.66 ng/mL) was not high enough, especially for its application in neonates. The aim of this report is to propose a validated HPLC-MS/MS micromethod for determination of milrinone plasma levels that achieves both a high sensitivity and selectivity.

Material and Methods

Chemicals and Reagents

Milrinone was kindly supplied by Sandoz (Boucherville, QC, CAN). Olprinone hydrochloride, the internal standard (IS), was purchased from Toronto Research Chemicals (Toronto, ON, CAN). HPLC grade methanol, ethyl-acetate (Fisher Scientific, Nepean, ON, CAN) and ammonium acetate (Sigma Aldrich, St. Louis, MO, USA) were used.

Standard Solutions and Buffers

Ammonium acetate 10 mM was prepared daily from a 2M stock solution. Stock solutions (1 mg/mL) of pure milrinone standard were prepared in methanol and stored at −20° C. Working solutions (10 000, 1000, 100 ng/mL) were prepared extemporaneously in water. A stock solution of the IS (10 000 ng/mL) was prepared in water, aliquoted and stored at −20° C. Working solutions (1000 ng/mL water) were prepared when needed.

Calibration and Quality Control Samples

Twelve milrinone concentration standards, 0.3125 (LLOQ), 0.625, 1.25, 2.5, 5, 10, 20, 40, 80, 160, 320, 640 ng/mL and a blank plasma sample were used to establish plasma calibration curves. The samples were prepared extemporaneously by serial 1:1 dilutions using previously screened blank plasma. Quality control (QC) samples were prepared by spiking blank plasma with milrinone stock solutions to obtain final concentrations of 0.5 2, 50, 100 and 500 ng/mL. Calibration curves were fitted to a quadratic regression using a weighted least square regression ($1/y^2$ nominal) with the Agilent MassHunter Workstation Data Acquisition software (Version B.04.01, Agilent Technologies, Santa-Clara, CA, USA).

Plasma Sample Preparation

In 1.5 mL conical polypropylene microtubes, 25 µL of IS was added to 50 µL of plasma. Subsequently, 500 µL of ethyl acetate was added, followed by horizontal agitation for 2 minutes (Eberbach, Ann Arbor, MI) and 4 min centrifugation. Then, 400 µL of the supernatant were evaporated (Speedvac Plus model SC210A; Savant Instruments, Farmingdale, NY). Prior to HPLC-MS/MS analysis, samples were reconstituted in 25 µL of mobile phase and vortexed for 10 seconds. Samples were then transferred to vials and 5 µL injected.

HPLC-MS/MS Analysis

Chromatographic Conditions

The HPLC system was an Agilent 1200 (Agilent Technologies, Santa Clara, CA, USA) which consisted of an autosampler (Hi-ALS SL4), a column oven (TCC SL), a degasser and a binary pump (Bin pump SL). Separation of analytes was performed on a Zorbax Eclipse XDB-C18 (4.6 x 150 mm 5 µm) protected by a security cartridge system and using an isocratic mobile phase (methanol:10 mM ammonium acetate; 45:55 v/v) with a flow of 1 mL/min. Injection volume was 5 µL. Running time was of 2.6 min with overlap for flushing and syringe filling. The C-18 column was kept at 50°C.

Mass Spectrometry Conditions

All analyses were performed on an Agilent 6460 triple quadrupole mass spectrometer equipped with an electrospray ion source (Agilent Technologies, Santa Clara, CA, USA). The ion source was operated in negative mode with nozzle voltage of -500 V. Compound-dependent parameters are listed in Table 1. Other mass spectrometer parameters were set as follows: the drying gas (nitrogen) temperature was 275°C with a flow of 5 L/min; the nebulizer pressure was 45 PSI; the sheath gas had a temperature of 325°C with a flow of 11 L/min. Capillary voltage was 3500 V. All data were acquired, analyzed and processed with the Agilent MassHunter Workstation Data Acquisition software. An example

of milrinone and olprinone chromatogram extractions using their respective optimal transitions can be seen in Fig. 1. Retention times for milrinone and olprinone were 2.02 and 2.19, respectively.

Assay Validation

Specificity was tested by obtaining blank drug-free plasma samples from healthy subjects and from patients immediately before inhalation of milrinone (pre-dose). Samples from healthy subjects and patients were assayed to determine whether endogenous plasma components or anesthesia medication cause interference at the retention times of the analyte or IS. To this end, chromatograms of blank samples of both healthy subjects and patients were compared to milrinone and olprinone-containing samples. Blank plasma samples from four previously tested patients that exhibited interfering compounds under our previous assay conditions[10] were re-assayed. Interactions with the analyte or IS were ruled out. Linearity was assessed by 10 12-point calibration curves covering the expected clinical range (0.3125–640 ng/mL) on 10 separate days. Sensitivity was evaluated by observing the inter-day variability of 10 LLOQ calibration standards over 10 different days. Recovery was assessed by comparing the peak heights of milrinone spiked prior to and after extraction for six replicate sets of samples spiked at 2.5 and 100 ng/mL. Recovery of the IS was also determined by comparing the peak heights of four extracted samples with the 100% value determined using *in vitro* samples. Intra-assay precision and accuracy were assessed in plasma as follows: 0.5, 2, 50, 100 and 500 ng/mL QC concentrations were assayed in replicates of 6. All samples were assayed on the same day and their back-calculated concentrations determined from the calibration curve prepared the same day. Inter-assay precision and accuracy were assessed in the following way: 2, 100 and 500 ng/mL QC concentrations were assayed in duplicate for the first set of five calibration curves and 0.5 and 50 ng/ml QC concentrations were assayed in duplicate for the second set of five calibration curves. One curve with its respective QC samples was assayed per

day for a total of 10 calibration curves over 10 different days. Precision was expressed as the coefficient of variation (C.V. %) and accuracy as the percent bias (%). Accuracy was determined by comparing the calculated concentration of the extracted milrinone plasma standard with the nominal concentration of milrinone.

Stability

Short-term stability (5h) was verified in four replicates of plasma standards at 2 and 500 ng/mL thawed at room temperature and kept at this temperature for 5h before analysis and comparison to fresh samples. Injector stability (24h) was verified in four replicates of plasma standards at 2 and 500 ng/mL injected in two different runs, 24 hours apart with two different calibration curves. To test freeze-thaw cycle stability, four calibration standards were prepared and frozen at -70˚C for 24h. Those samples were then thawed at room temperature and analyzed alongside fresh samples of the same concentration. Samples were refrozen under the same conditions and freeze-thaw cycle repeated one more time before reanalysis. Stability of extracts (2 and 500 ng/mL), stored in the refrigerator or the autosampler for 24h was also tested. Results were compared with those obtained for the freshly prepared samples.

Clinical Application to Cardiac Patients Undergoing Cardiopulmonary Bypass

This method was developed to determine milrinone plasma concentrations in cardiac patients after a 5 mg dose (Milrinone Lactate 1 mg/ml; Pharmaceutical Partners of Canada Inc., Richmond Hill, ON, CAN) inhaled over a 20 min period. Following ethics committee approval and permission from Health Canada, informed and written consent was obtained from all participating subjects. Blood samples were obtained before starting inhalation (time zero), during inhalation, and up to 10 hours after inhalation. Samples were kept in an ice-water bath for less than 10 min before centrifugation. Plasma was immediately flash-frozen on

dry ice and stored at −70° C until analysis. Milrinone plasma concentration-time profile obtained in one patient is shown in Fig. 2.

Results and Discussion

Method optimization

The current method was developed taking advantage of the sensitivity and specificity provided by mass spectrometry. Compared to Nguyen et al.[10], several changes were made for method optimization. Required volume of plasma was reduced to 50 µL, optimizing the use of clinical samples and facilitating pharmacokinetic studies in children and neonates. In absence of a deuterated or C-13 milrinone IS, which may be considered suboptimal, the former IS (amrinone) was changed to olprinone due to subject-related variations that induced a systematic bias when comparing patient samples to calibration standards. Using olprinone as IS, within assay precision was acceptable (CV : 13.88 %, n = 21). Furthermore, to reduce the costs incurred for milrinone extraction, the SPE was changed to a liquid-liquid extraction. In preliminary analyses, liquid-liquid extraction using ethyl acetate/dichloromethane (4:1 v/v) showed no advantage. The mobile phase was simplified from ACN:THF-NaH_2PO_4 buffer pH 3 (gradient ranging from 10:90 to 40:60,) to methanol:10 mM ammonium acetate (isocratic 45:55 v/v). These changes result in a method that has, to our knowledge, the lowest LLOQ for plasma milrinone quantification: 0.3125 ng/mL. This LLOQ was necessary for quantifying milrinone plasma levels up to 10 hours post-dose.

Assay Validation

Extracted MRM signals of milrinone and olprinone from a cardiac patient blank, a low calibration standard (0.3125 ng/mL, LLOQ), a medium calibration standard (80 ng/mL) and cardiac patient sample (610 min) are shown in Fig. 3. Both clinical and calibration samples were shown to be free of any interference with milrinone. Prior to the current method, milrinone specificity during CPB was a major drawback. When necessary during CPB, support medication had to be administered to patients, generating chromatographic interference during HPLC-

UV analysis. No such difficulties were observed with the current method due to the benefits of mass spectrometry quantification. Indeed, patients from an ongoing study showing chromatographic interferences were successfully reanalyzed; an example is shown in Fig. 4.

The 10 milrinone calibration curves (0.3125 to 640 ng/mL) were fitted to quadratic regressions and showed a coefficient of determination (r^2) of 0.9954 ± 0.0024 (n = 10). The LLOQ showed mean inter-assay precision and accuracy bias of 5.97% and 0.65% (n = 10), respectively, indicating acceptable sensitivity. Mean recoveries of milrinone for the 2.5 and 100 ng/mL concentrations were 78.0 ± 2.1% and 78.9 ± 6.6 % (n = 6), respectively.

Precision and Accuracy

Intra and inter-assay precision and accuracy results can be found in Table 2. Pooled QCs and LLOQ over the 10 days showed that accuracy averaged 98.25% and ranged from 96.00 to 101.09 (n = 60). Intra- and inter-day precisions (CV%) were ≤ 3.02% and ≤ 11.42%, respectively.

Stability

Sample short-term stability (5h) showed accuracy ranging from 90 to 102%. Injector stability samples (24h) showed accuracy ranging from 92 to 106%. Freeze-thaw cycle stability samples showed accuracy ranging from 94 to 103% after two freeze-thaw cycles. For stability of extracts stored in the refrigerator or autosampler for 24h, no significant difference was observed when compared with values obtained from freshly prepared samples.

Clinical Application

Cardiac Patients Undergoing Cardiopulmonary Bypass.

Milrinone plasma concentration-time profile obtained in one patient (Fig. 2) shows a maximum concentration of 40.63 ng/mL occurring 10 min after starting milrinone inhalation. Ten hours after inhalation, milrinone plasma levels were

0.33 ng/mL, just above the LLOQ. With the current method, full characterization of the terminal half-life was achieved.

Persistent Pulmonary Hypertension of the Newborn

The pharmacokinetic study of McNamara et al[15] used an assay with a LLOQ of 10 ng/mL and using 100 µL of plasma allowing six blood samples of 800 µL per neonate. The current method, with a LLOQ of 0.3125 ng/mL and using 50 µL of plasma would, by allowing additional samples, a thorough characterization of milrinone overall pharmacokinetics. In addition, it would also allow for the determination of single dose pharmacokinetics and further exploration of milrinone use as a treatment option for PPHN.

Acyanotic congenital heart disease and newborns undergoing cardiovascular surgery

Currently, no studies have characterized inhaled milrinone pharmacokinetics in a pediatric population. Singh et al. explored the efficacy of milrinone in this particular condition and showed a 14.9% decrease in mean pulmonary arterial pressures. Such pharmacodynamic studies would greatly benefit from concentration-response profiles if one wished to optimize drug administration. In the case of post-operative support, intravenous milrinone was shown to be beneficial[17]. Inhaled milrinone has yet to be tested for this indication and would be a possible research avenue. However, the sensitivity of Pellicer et al.'s assay (LLOQ: 2 ng/ml) would not allow adequate characterization of inhaled milrinone terminal half-life. Even more than for adults, plasma exposure following milrinone inhalation in pediatric and/or neonatal studies is expected to be fairly low. Therefore, the current HPLC-MS/MS method offers the required sensitivity and specificity to provide adequate characterization of inhaled milrinone pharmacokinetics in this population.

Conclusion

A highly sensitive and specific HPLC-MS/MS assay for inhaled milrinone was developed that utilizes a low-cost rapid extraction procedure for a low sample volume (50 µL), is milrinone-specific in a cardiac surgery context and has good sensitivity (LLOQ: 0.3125 ng/mL). This validated assay allows adequate determination of milrinone plasma levels after its administration by inhalation in patients undergoing CPB surgery and fulfills the need for a low volume and sensitive method in pediatric and even neonate pharmacokinetic studies.

Acknowledgements

This research was supported by Fonds de recherche du Québec-Santé (FRQS) and Groupe de recherche universitaire sur le médicament de l'Université de Montréal (GRUM). A studentship was granted by the Canadian Institutes of Health Research to Anne QN. Nguyen. The authors would like to acknowledge the invaluable support of Christiane Drouin from the Department of biochemistry du Centre Hospitalier Universitaire Ste-Justine. The authors are grateful to Fondation des Gouverneurs de l'Espoir and Lions Clubs International for the gift of the LC-MS/MS.

Tables

Table 1 MRM transitions and fragmentation parameters used for the quantification of milrinone using olprinone as the internal standard.

Compound name	MRM m/z transition	Dwell	Fragmentor (V)	Collision energy (eV)	Polarity
Olprinone	252.1 → 156.1	200	120	36	Positive
Milrinone	212.1 → 140.0	200	115	32	Positive

Table 2 Intra-assay and inter-assay precision and accuracy.

		Concentration (ng/mL)		Precision	Accuracy
	n	Nominal	Measured mean ± SD	Coefficient of variation (%)	Bias (%)
Intra-assay					
	6	0.5	0.51 ± 0.02	4.33	1.45
	6	2	1.92 ± 0.10	4.96	-2.60
	6	50	48.49 ± 3.57	7.36	-3.02
	6	500	504.21 ± 12.22	2.42	0.84
Inter-assay					
	10	0.3125	0.32 ± 0.02	5.97	0.65
	10	0.5	0.48 ± 0.03	6.12	-4.00
	10	2	1.95 ± 0.08	3.94	-2.68
	10	50	48.11 ± 3.57	5.21	-3.78
	10	100	98.24 ±11.22	11.42	-1.76
	10	500	505.43 ± 6.64	1.71	1.09

Figures

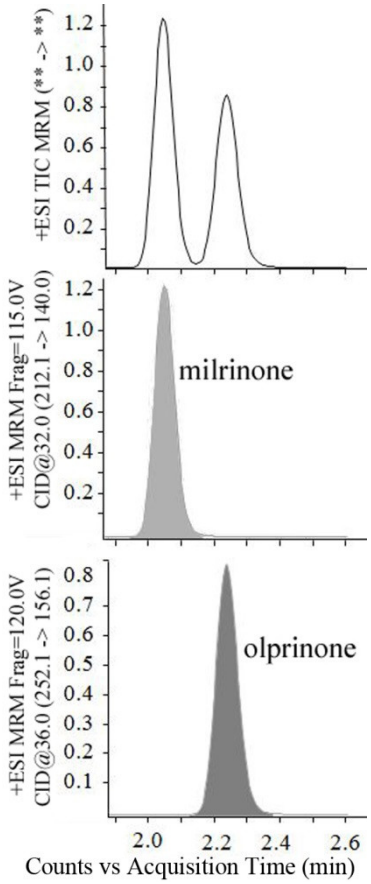

Fig. 1 Initial chromatogram and extracted MRM signals of milrinone and olprinone from an extracted QC sample (100 ng/mL).

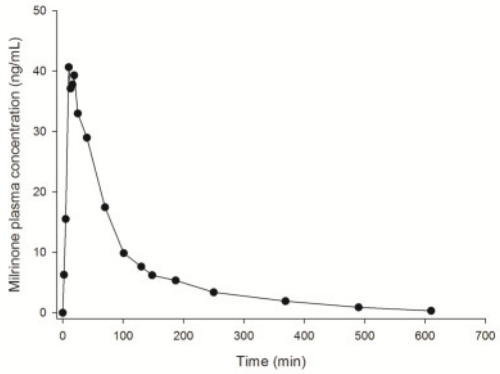

Fig. 2 Milrinone concentration-time profile in a patient having received a dose of 5 mg of milrinone by inhalation over 20 min.

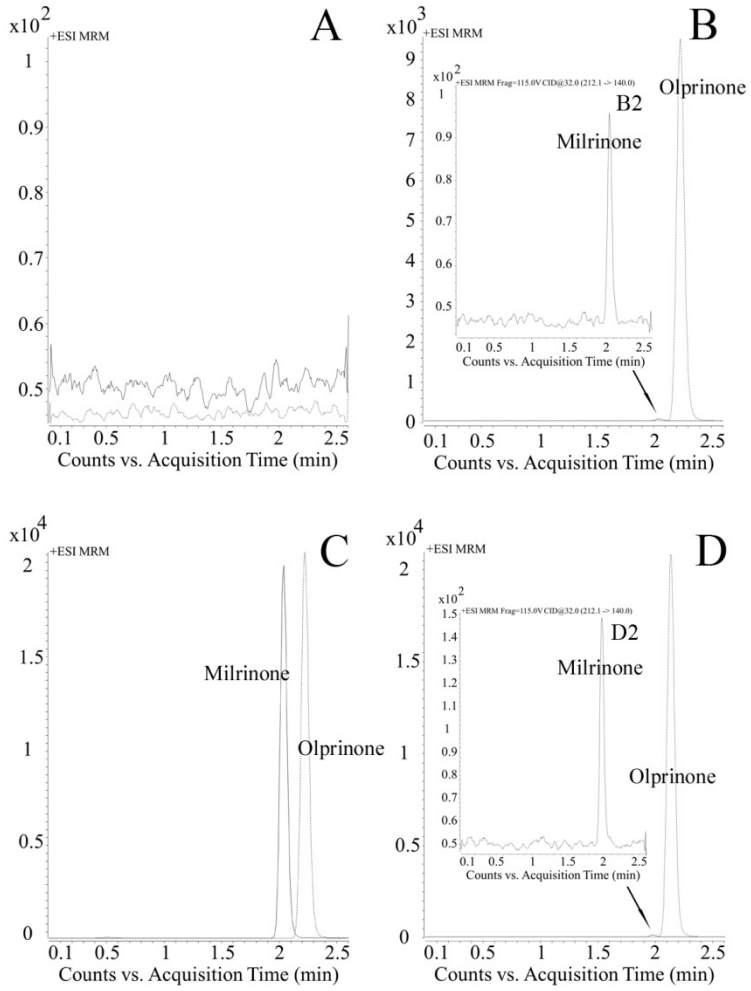

Fig. 3 Overlaid extracted milrinone (212.1 -> 140.0) and olprinone (252.1 -> 156.1) MRM signals from (A) a blank cardiac patient plasma sample (B), a plasma calibration standard sample, LLOQ (0.3125 ng/mL), (C) a plasma calibration standard sample (80 ng/mL) and (D) a cardiac patient plasma sample 610 minutes after an inhalation of 5 mg of milrinone dose over 20 minutes (0.3344 ng/mL). B2 and D2 inserts are the magnified extracted milrinone (212.1 -> 140.0) MRM signal of the respective samples.

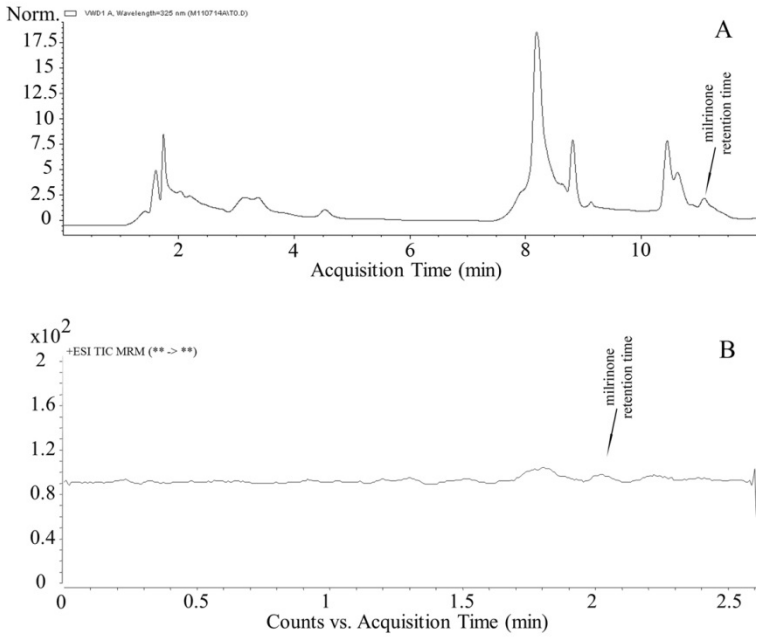

Fig. 4 Comparison of bioanalysis method specificity. A blank plasma sample from the same patient was analyzed (A), using the method of Nguyen et al.[10] and (B) using the current method.

References

1 Denault, A., Deschamps, A., Tardif, J. C., Lambert, J. & Perrault, L. Pulmonary hypertension in cardiac surgery. Curr Cardiol Rev. 2010; 6: 1-14,

2 Gorcsan, J. et al. Assessment of the immediate effects of cardiopulmonary bypass on left ventricular performance by on-line pressure-area relations. Circulation. 1994; 89: 180-190

3 Hind, C. R. et al. Effect of cardiopulmonary bypass on circulating concentrations of leucocyte elastase and free radical activity. Cardiovasc Res. 1988; 22: 37-41

4 Gnanadurai, T. V., Branthwaite, M. A., Colbeck, J. F. & Welman, E. Lysosomal enzyme release during cardiopulmonary bypass. Anaesthesia. 1977; 32: 743-748

5 Courtney, J. M., Sundaram, S., Matata, B. M., Gaylor, J. D. S. & Forbes, C. D. Biomaterials in cardiopulmonary bypass. Perfusion. 1994; 9: 3-10

6 Royston, D. The inflammatory response and extracorporeal circulation. J Cardiothorac Vasc Anesth. 1997; 11: 341-354

7 Urdaneta, F. et al. Treating pulmonary hypertension post cardiopulmonary bypass in pigs: milrinone vs. sildenafil analog. Perfusion. 23: 117-125, doi:10.1177/0267659108094739 (2008).

8 Wang, H., Gong, M., Zhou, B. & Dai, A. Comparison of inhaled and intravenous milrinone in patients with pulmonary hypertension undergoing mitral valve surgery. Adv Ther. 2009; 26: 462-468

9 Sablotzky, A., Czeslick, E. G., Scheubel, R. & Grond, S. Selective pulmonary vasodilation with inhaled aerosolized milrinone in heart transplant candidates. Can J Anaesth. 2005; 52:1076-1082

10 Nguyen, A. Q. N., Théorêt, Y., Chen, C., Denault, A. & Varin, F. High performance liquid chromatography using UV detection for the

quantification of milrinone in plasma: improved sensitivity for inhalation. J Chromatogr B Analyt Technol Biomed Life Sc. 2009; 877: 657-660

11 Walsh-Sukys, M. C. et al. Persistent pulmonary hypertension of the newborn in the era before nitric oxide: practice variation and outcomes. Pediatrics. 2000; 105, 14-20

12 Steinhorn, R. H. Pharmacotherapy for pulmonary hypertension. Pediatr Clin North Am. 2012; 59: 1129-1146

13 McNamara, P. J., Laique, F., Muang-In, S. & Whyte, H. E. Milrinone improves oxygenation in neonates with severe persistent pulmonary hypertension of the newborn. J Cri Care. 2006; 21: 217-222

14 Bassler, D., Choong, K., McNamara, P. & Kirpalani, H. Neonatal persistent pulmonary hypertension treated with milrinone: four case reports. Biol Neonate. 2006; 89: 1-5

15 McNamara, P. J., Shivananda, S. P., Sahni, M., Freeman, D. & Taddio, A. Pharmacology of milrinone in neonates with persistent pulmonary hypertension of the newborn and suboptimal response to inhaled nitric oxide. Pediatr Crit Care Med. 2013; 14: 74-84

16 Singh, R. et al. Inhaled nitroglycerin versus inhaled milrinone in children with congenital heart disease suffering from pulmonary artery hypertension. J Cardiothorac Vasc Anesth. 2010; 24: 797-801

17 Pellicer, A. et al. Phase 1 study of two inodilators in neonates undergoing cardiovascular surgery. Pediatr Res. 2013; 73, 95-103

18 Edelson, J., Koss, R. F., Baker, J. F. & Park, G. B. High-performance liquid chromatographic analysis of milrinone in plasma and urine. Intravenous pharmacokinetics in the dog. J Chromatogr. 1983; 276, 456-462

19 Oddie, C. J., Jackman, G. P. & Bobik, A. Analysis of milrinone in plasma using solid-phase extraction and high-performance liquid chromatography. J Chromatogr. 1986; 374, 209-214

20 Brocks, D. R., Spencer, T. J. & Shayeganpour, A. A sensitive and specific high performance liquid chromatographic assay for milrinone in rat and

human plasma using a commercially available internal standard and low sample volume. J Pharm Pharm Sci. 2005; 8, 124-131

21 Chihoho, B. et al. A clinical assay for the measurement of milrinone in plasma by HPLC mass spectrometry. Biomed Chromatogr. 2012; 26, 566-570

CHAPTER 11. Manuscript #3: Use of nebulized milrinone in cardiac surgery; Comparison of vibrating mesh and simple jet nebulizers.

Paul Gavra[1] B.Sc. Maxime Laflamme[2] M.D. MSc, André Y. Denault[2] M.D., Ph.D., Yves Théoret[3], B.Pharm., Ph.D., Louis P. Perrault[2], M.D., Ph.D. and France Varin[1], B.Pharm., Ph.D.

[1]Faculty of Pharmacy, Université de Montréal, Montréal, Canada
[2]Montreal Heart Institute, Montréal, Canada
[3]Unité de pharmacologie Clinique, Hôpital Sainte-Justine

Running title: Vibrating mesh versus simple jet Milrinone nebulization
Keywords: Cardiac surgery ▪ Cardiopulmonary bypass ▪ Milrinone ▪ Pulmonary hypertension ▪ Vibrating mesh nebulization, simple jet nebulization

Corresponding author:
France Varin, B.Pharm, Ph.D.
Faculté de pharmacie, Université de Montréal,
C.P. 6128, Succursale Centre-Ville,
Montréal, QC, Canada H3C 3J7.
Phone : +15143437016
E-mail : france.varin@umontreal.ca

Current status: Published in Pulmonary Pharmacology and Therapeutics

Abstract

Cardiopulmonary bypass triggers an ischemia-reperfusion injury with endothelial dysfunction in the pulmonary circulation which can result in pulmonary hypertension. Inhaled milrinone reduces this reperfusion phenomenon and two methods commonly available for administering it are simple jet and vibrating mesh nebulizations. However, neither their generated milrinone particle size profiles, nor their ability to aid endothelial relaxation have been compared. Simple jet and vibrating mesh particle size distributions of milrinone were verified through cascade impaction and their efficacy was tested on a cardiopulmonary bypass (CPB) swine model. Post-nebulizations, animals underwent 90 min of CPB, followed by 60 min of reperfusion and lung excision. Pulmonary arterial endothelium-dependent relaxations to acetylcholine and bradykinin were then performed on pulmonary vasculature rings and were subsequently modeled as inhibitory Emax functions. *In vitro* studies showed lower emitted and inhaled doses from the simple jet nebulizer and its particle size distribution indicated upper and middle airway targeting. During *in vivo* studies, milrinone pre-treated, unlike saline groups maintained baseline pulmonary pressures up to 30 min post–CPB. *Ex vivo* studies showed better endothelial relaxation of arteries from the two milrinone groups over those from the control group in an administration/pathway-dependent manner, favoring simple jet administration.

Introduction

Cardiopulmonary bypass (CPB) is used in the majority of cardiac surgical procedures. Its role is to divert deoxygenated blood from the right atrium and, after passage in an oxygenator, to pump it back into the aorta. CPB causes a systemic inflammatory response in the entire organism. The organ mostly affected during CPB is the lung since it receives minimal perfusion during surgery and is exposed to the reperfusion injury during separation from CPB [1]. The pulmonary lesions are characterized by an increase in pulmonary capillary permeability, alveolar/arterial oxygen gradient and pulmonary vascular resistance and a decrease in pulmonary compliance [2]. These alterations are explained by endothelial injury in the pulmonary vasculature manifested by a decreased ability for vasorelaxation when endothelial dysfunction is present. This phenomenon can lead to pulmonary hypertension (PH), increased right ventricular (RV) work and in some cases RV failure. Severe RV dysfunction after CPB carries a poor prognosis with a perioperative mortality ranging from 22 to 86% [3–5].

Milrinone, a phosphodiesterase III inhibitor, increases intracellular levels of cyclic adenosine monophosphate (cAMP), induces positive cardiac inotropy and systemic vasorelaxation. Milrinone is used to reduce pulmonary vascular resistance induced by CPB. However, when administered intravenously, the major problem is the high incidence of systemic hypotension. The use of inhaled milrinone has recently been described in animal and human studies and shown to decrease pulmonary artery pressure (PAP) without systemic hypotension [6–9]. Moreover, inhalation of milrinone before CPB has been shown to be superior to intravenous administration in reducing the pulmonary reperfusion syndrome, preventing pulmonary arterial endothelial dysfunction and improving oxygenation in a porcine model [10]. It is commonly nebulized by either simple jet nebulizer (SJ) or vibrating mesh nebulizer (VM).

One of the main parameters used to assess the severity of PH and to evaluate the efficacy of selective pulmonary vasodilatation is the systemic/pulmonary arterial pressures ratio or mean arterial pressure divided by the mean pulmonary artery pressure (MAP/MPAP) [8,11–15]. The antihypertensive efficacy of milrinone on the ratio was thought to be based on nebulizer emitted dose, the dose ultimately delivered to the lungs (inhaled dose) and milrinone distribution within the lungs which is directly related to the particle size distribution of milrinone. However, this hypothesis was never demonstrated.

The objectives of this paper were twofold: first, to compare milrinone *in vitro* nebulizer performance and particle size distribution profiles for the SJ and the VM nebulizers; and second, to study their respective *in vivo* hemodynamic and *ex vivo* efficacy in an animal model.

Material and methods

Experimentation was divided into three major components, the *in vitro* component: emitted, inhaled doses and particle size determination, the *in vivo* component: drug administration and effect assessment followed by the CPB and lastly, the *ex vivo* component: endothelial dysfunction studies performed on pulmonary arteries retrieved from the animals having just underwent the *in vivo* experimentation. Milrinone was nebulized during the *in vitro* and *in vivo* components.

2.1 Solutions and recovery of *in vitro* experimentation

Injectable milrinone lactate solution was kindly provided by Primacor Canada (Primacor; Sanofi-Synthelabo Canada, Inc. Markham, Ontario, Canada). For the *in vitro* tests, five mg of milrinone lactate (1 mg/mL) were used as loading dose for all tests. After complete nebulization, milrinone was recovered from each set-up component by rinsing with NaH_2PO_4 at pH 3.0. Milrinone was also recovered from F1 and F2 filters (Respirgard, Englewood, Colorado, USA) by sonication for 20 min (FS28H water bath, Fisher Scientific, Loughborough, UK).

2.2 In vitro particle size determination

2.2.1 Nebulizers and breathing pattern

A VM (AeronebPro, Aerogen®, Galway, Ireland) and a conventional in-line jet or SJ nebulizer (Salter Labs, Arvin, CA) were used. During all experiments, a breathing pattern of 14 breaths per minute at 240mL/breath, 1:2 inhaled:exhaled ratio, was produced using a BRS 1000 Breath Simulator

(Copley Scientific, Nottingham UK). Particle size determination was performed on a New Generation Cascade Impactor (NGI, Copley Scientific, Nottingham UK). For both inhaled dose (ID) determination and particle size distribution the setup was intended to mimic clinical positioning in a horizontally placed patient. The impactor setup without the breathing pattern component was assembled as described in the Copley instruction manual. The breathing pattern setup is similar to that described in the articles published by Janssens in 2003 and recently Ciciliani in 2017 [16,17].

2.2.2 In vitro determination of emitted and inhaled doses

Nebulizer emitted milrinone dose (ED) was determined using the setup shown on Fig. 1, insert A for the two types of nebulizers (SJ and VM). Following complete dose nebulization, the amount of milrinone deposited on setup components (T-tube and nebulizer) and output filters were analyzed and added to yield the ED. The ED was the sum of the quantities collected from the output filters and the T-Tube. Dose delivered to patient's lungs (inhaled dose, ID) was assessed using the setup illustrated in Fig. 1, insert B

2.2.3 In vitro particle size distribution studies

Particle size distribution experiments were performed using a NGI (Fig. 1, insert C). Prior to each experience, the impactor was coated with a fine layer of silicone (Slipicone, Dow Corning, Midland, Michigan, USA) to prevent particle bounce. The impactor was kept at 6 °C inside the NGI Cooler (Copley Scientific, Nottingham, UK) and the airflow inside the impactor was maintained at 15 L/min. Samples were recovered from each cup corresponding to each of the 7 diameter cut-off levels and the exit and expiratory filters. The airflow was monitored by an airflow meter (Copley Scientific, Nottingham, UK).

2.3 Sample preparation and HPLC analysis

Samples were appropriately diluted with distilled water and 200 µl of internal standard solution (carbamazepine, 2 µg/mL) was added to 800 µl of diluted sample. A 100 µl sample of the mixture was analyzed. Quantification was done using a slight variation of the UV-HPLC method described by Nguyen et al. [18] on a Hewlett Packard 1050 series system set at 225 nm. The mobile phase (flow rate:1.2 mL/min) consisted firstly of 90:10 buffer:acetonitrile. Buffer (pH 3.0) was 21:916 tetrahydrofuran: NaH_2PO4/K_2HPO_4 50 mM. At 2.5 min, there was a stepwise change to 40:60 buffer:acetonitrile. Sample concentration was determined using a daily prepared calibration curves ranging from 9.78 to 20 000 ng/mL of milrinone. Standard curve linearity ($r^2 > 0.99$) was observed by regression using a $1/\hat{y}$ weighting and ≤ 15% between- and within-day coefficients of variation.

2.4 In vivo and *ex vivo* studies

2.4.1 Animals

Eighteen Landrace swine (Montreal, Quebec, Canada) of either sex (ratio 1:1) and weighing 30 ± 5 kg were treated in accordance with the recommendations of the guidelines on the Care and Use of Laboratory Animals issued by the Canadian Council on Animals and approved by the institutional Animal Care and Use Committee.

2.4.2 Experimental groups

Fifteen minutes before CPB initiation, animals from both milrinone-treated groups received a fixed 2.5 mg dose (60–90 µg/kg) of injectable 1 mg/mL milrinone through nebulization, SJ (n = 6) and VM (n = 6) while those of control

group (n = 6) received 2.5 mL saline by VM nebulization. Nominal doses used for *in vitro*and *in vivo* sections are different, however both represent an average weight normalised dose of 70 µg/kg.

2.4.3 Animal preparation

Swine were sedated with intramuscular ketamine hydrochloride (25 mg/kg; Ayerst Veterinary Laboratories, Guelph, Ontario, Canada) and xylazine (10 mg/kg; Boehringer Ingelheim, Burlington, Ontario, Canada). Induction was achieved using mask ventilation with 2% isoflurane (Abbott Laboratories Limited, St-Laurent, Quebec, Canada). Animals were subsequently intubated and mechanically ventilated with a constant 66:34 oxygen:air mixture at 14 breath per minute with a tidal volume of 6–8 mL/kg. Anesthesia was maintained with a propofol infusion during the CPB. A jugular vein and femoral artery were cannulated to obtain a central venous line and arterial pressure, respectively. Arterial and venous blood gases were measured at regular intervals and maintained within physiologic limits. A cystostomy was performed for measurement of urine output. Electrocardiogram was continuously recorded during the procedure. All animals had a pulmonary artery catheter (Swan-Ganz, Edwards Lifesciences, Irving, California, USA) inserted through the jugular vein. Heart rate was continuously monitored from 5 subcutaneous limb electrodes. Blood samples were withdrawn directly from the right and left atria for baseline before CPB, during CPB at 15, 45 and 75 min, after CPB separation and in the reperfusion period at 30 and 60 min.

Arterial and venous blood gases were measured concomitantly and maintained within physiologic ranges by adjusting the ventilation rate and tidal volume at need. Any significant hypotension during the reperfusion period was treated initially with volume resuscitation and, if necessary, with a small bolus (0.05 mg) of epinephrine. At the end of the procedures, animals were sacrificed

through isoflurane overdose, exsanguinated and the heart and lungs were removed for the *in vivo* protocol.

2.4.4 CPB and excision

After median sternotomy, the pericardium was opened for cardiac exposure. A double purse string was made on the proximal ascending aorta and a single purse string on the right atrium. Then heparin (300 IU/kg; Leo Pharma Inc. Ajax, Ontario, Canada) was administered and a blood sample drawn 2 min after from the right atrium, to verify proper anticoagulation by measuring activated coagulation time (ACT) with Hemochron 801 (Technidyne, Dorval, Quebec, Canada). When ACT reached 300 s, the aorta and right atrium were cannulated with 22F arterial and 29F venous double-staged cannulas (DLP, Inc. Grand Rapids, Michigan, USA), respectively. CPB was initiated when ACT was greater than 400 s. Ventilation was stopped throughout CPB period and anesthesia maintained with a continuous infusion of propofol (0.1–0.2 mg/kg/min; Pharmascience, Inc. Montreal, Quebec, Canada). The CPB circuit consisted of a hollow-fiber membrane oxygenator with an incorporated filtered hardshell venous reservoir (Monolyth; Sorin, Irvine, California, USA), a heatercooler, and a roller pump (Sarns 7000, Ann Harbor, Michigan, USA). The circuit was primed with 500 mL of Pentaspan (10% Pentastarch; DuPont Pharma, Inc. Mississauga, Ontario, Canada), 250 mL of lactated Ringer's solution, 5000 IU of heparin, 12.5 g of mannitol and 15 mEq of sodium bicarbonate. After initial stabilization, the pump flow was adjusted to maintain an index of 2.4 L/min/m^2 and assessed on the basis of venous gases to maintain a mixed venous saturation of greater than 60%. The MAP was maintained between 50 and 70 mmHg with Voluven (6% hydroxyethyl starch 130/0.4 in 0.9% sodium chloride, Fresenius, Homburg, Germany). The temperature was allowed to drift to 36 °C. No aortic cross-clamping or cardioplegia was used and the heart was left beating empty. After 90 min of CPB, swine were rewarmed to

normothermia, mechanical ventilation and isoflurane-induced anesthesia were reinstituted, and the animals were weaned from CPB. Normal circulation was restored for 60 min, at which time the animal was exsanguinated into the cardiotomy reservoir.

The heart and lungs were then excised *en bloc* and immediately immersed in a cold 4 °C modified Krebs-bicarbonate.

2.4.5 Pharmacodynamic measures

Hemodynamic parameters, including mAP, heart rate (HR), mPAP, pulmonary artery wedge pressure and cardiac output (CO) by the thermodilution technique, were measured at 3 pre-determined time points during the procedure: after induction (pre-CPB), and at 30 and 60 min after weaning of CPB. The following blood gas information was also taken at the same time points: Arterial partial pressures of carbon dioxide and oxygen ($PaCO_2$ and PaO_2 respectively), PaO_2 to fractional inspired oxygen ratio (PaO_2/FiO_2) and the alveolar/arterial gradient ($AaDO_2$). The MAP/MPAP was also calculated.

2.4.6 Ex vivo arterial relaxation studies

2.4.6.1 Endothelial function

Less than 10 min after *en bloc* heart excision, the primary pulmonary artery was dissected. Branches of second-degree pulmonary arteries were isolated and dissected free of connective and adventitial tissue and divided into rings (4 mm wide, 16 rings per animal) as previously described [15,19]. All rings were placed into organ chambers (Emka Technologies, Inc. Paris, France) filled with 20 mL of modified Krebs-bicarbonate solution continuously heated at 37 °C and oxygenated with a carbogen mixture (95% O_2 and 5% CO_2). The rings were suspended between two metal stirrups, with the upper one connected to an

isometric force transducer connected to a signal amplifier and then allowed to stabilize for 30 min. Data were collected with biologic signal data acquisition software (IOX 1.700; Emka Technologies Inc. Paris, France). Each arterial ring was stretched to the optimal point of its active length-tension curve (3.5 g), as pre-determined by measuring the contraction to 60 mmol/L KCl at different levels of stretch. The maximal contraction of rings was then obtained with the addition of potassium chloride (KCl 60 mmol/L). After obtaining a plateau, all baths were washed twice with modified Krebs-bicarbonate solution, and indomethacin (IND; 10^{-5} mmol/L) was added in each bath to exclude production of endogenous prostanoids. After 45 min, phenylephrine (range 2×10^{-7} mol/L to 3×10^{-6} mol/L) was added to obtain a KCl-induced contraction averaging 50% of the maximal contraction induced by KCl. The nitric oxide (NO)-mediated relaxation pathway was studied by constructing concentration-response curves to acetylcholine (ACh, 10^{-9} to 10^{-5} mol/L; an agonist of M2 receptors coupled to Gi proteins) and bradykinin (Bk, 10^{-12} to 10^{-6} mol/L; an agonist of B_2 receptors coupled to Gq proteins). At the end of the experiment, endothelium-independent relaxations were studied with the use of 10^{-5} mol/L sodium nitroprusside (SNP), an NO donor.

2.4.6.2 Pharmacodynamic modeling

The ACh and Bk concentration-response curves were subsequently normalized as percentages of the phenylephrine-elicited contraction. Each response curve was individually modelled using a pharmacodynamic inhibitory Emax model with the initial effect value (E0) fixed at 100%. Modeling was performed using Phoenix® 6.4.0.768 (Pharsight, Certara, New Jersey, USA).

2.5 Statistical analysis

Descriptive statistics are presented as mean ± standard deviation or (coefficient of variation). First, normality of distribution of data was assessed by means of the Shapiro-Wilk test. In comparisons involving all three methods of administration, normally distributed values were analyzed using one-way ANOVAs and followed by a Tukey's post-hoc test. Non-normally distributed data were analyzed using the Kruskal-Wallis test followed by a Mann-Whitney *U* test. Comparisons involving pre-CPB, 30 and 60 min post-CPB time points were undertaken using repeated measures ANOVAs followed by Bonferroni post-hoc tests. Statistical significance between modeled pharmacodynamic parameters was assessed by linear mixed effects modeling Phoenix® 6.4.0.768 (Pharsight, Certara, New Jersey, USA). Statistical significance was set at $p < 0.05$ and analyses were performed with the computer software SPSS 16.0.1 (SPSS Inc, Chicago, Ilinois, USA).

Results

3.1 In vitro

Amounts of milrinone recovered from components during emitted and inhaled dose determinations are listed in Table 1 as mean values (coefficient of variation). The VM nebulizer delivered 4.60 ± 0.14 mg, significantly more than the SJ one, 2.61 ± 0.6 mg ($p = 0.356$). Out of those emitted doses, 3.001 ± 0.008 for VM and 1.46 ± 0.19 for SJ respectively reached the impactor (inhaled dose). For both types of nebulizers, during the particle distribution analysis (Fig. 2A), the cumulative amount (mg) of milrinone recovered from all impactor components (3.006 ± 0.008 for VM and 1.625 ± 0.118 for SJ) was similar to the respective inhaled doses ($p = 0.999$ for VM; $p = 0.174$ for SJ). The VM nebulizer showed a greater milrinone recovery for the levels 3–7 corresponding to an 8.6 to 1 μm range ($p < 0.05$). When correcting for the inhaled dose (Fig. 2B), the VM nebulizer shows greater recovery for the levels 4 to 6 or 5.4 to 1.4 μm range and the SJ, for the level 1 or above 14.1 μm range.

3.2 In vivo

A total of 18 animals were studied. Four (16.7%) were excluded from the analysis because of premature death before inhalation of milrinone. One succumbed to ventricular fibrillation resulting from prolonged hypotension during induction (SJ group), one presented electromechanical dissociation after sternotomy without any apparent reason (VM group) and two died from hemorrhagic shock due to cannulation problems and innominate vein trauma (VM nebulizer and saline groups). The 14 animals included in the statistical analysis underwent uneventful CPB and 60 min of reperfusion as described earlier. In both milrinone-treated groups, two animals required vasopressor hemodynamic support; one from the SJ nebulizer group and one from the VM

nebulizer, compared to 4 (80%) in the saline group during the reperfusion period.

3.3 Hemodynamic parameters

The hemodynamic variables are summarized in Fig. 3. Baseline values of the five parameters were similar for all three administrations. The MAP decreased only in the saline group. At 30 min post-CPB, MPAP increased only in the saline group and remained significantly higher than pre-CPB 60 min post-CPB. When compared to pre-CPB values, the MAP/MPAP ratio at 30 min post-CPB was significantly lower for the saline group only. At 60 min, the MAP/MPAP ratio was significantly lower from pre-CPB values for all three groups.

3.4 Gas exchanges

Biochemical parameters are summarized in Fig. 4. Baseline values of the four parameters were similar for all three administrations. In the saline group, the 30 min PaO_2/FiO_2 ratio was significantly lower than both pre-CPB and lower than the one observed at 60 min. The paO_2/FiO_2 ratio at 30 min post-CPB was significantly higher in the VM group, when compared to pre-CPB. The $AaDO_2$ increased significantly in the saline group at 30 min. The $AaDO_2$ parameter was significantly lower in both the SJ and VM compared to saline at 30 min but the opposite was observed at 60 min. The $AaDO_2$ in the VM group at 30 min post-CPB, was significantly lower than both pre-CPB and at 60 min.

3.5 Endothelial function and modeling

Mean and individual *ex-vivo* vascular reactivity results to acetylcholine and bradykinin are shown in Fig. 5A and B respectively. Average relaxations

curves of arterial rings to ACh in animals having received five nebulized mL of either saline (A) or milrinone through simple jet (B) (SJ) or vibrating mesh (VM) (C) nebulization. Average relaxations curves of arterial rings to Bk obtained from animals having received five nebulized mL of either saline (D) or milrinone through SJ (E) or VM (F) nebulization. The resulting mean pharmacodynamic sigmoid inhibitory Emax model parameters obtained from each artery (not pooled per animal) are shown in Table 2. Ach relaxation IC_{50} and Δ Imax following simple jet administration were found to be significantly lower and higher respectively than the IC_{50} and Δ Imax of Ach relaxation following saline and VM administrations. When comparing SJ versus VM nebulization, the vasculature of the group having received milrinone through SJ nebulization exhibited a 25% higher maximal relaxation and a twofold increase in sensitivity to ACh, as shown by the higher Imax and lower IC_{50}, respectively. For the Bk pathway, initial contraction to phenylephrine I_0 and Δ Imax following simple jet administration were both significantly higher than the I_0 and Δ Imax of Bk relaxation following saline and VM administrations. Both milrinone administration methods enhanced the Bk relaxation sufficiently to completely overturn the original phenylephrine contraction. However, for this pathway, drug sensitivity was increased sixfold only following VM nebulization.

Discussion

The major findings of this study are that firstly, SJ and VM nebulizations indeed not only deliver a twofold different inhaled dose, but also generate distinct particle-size distribution profiles. Secondly, the *in-vivo*experimentation showed that inhaled milrinone given before CPB, reduces the increases in PAP observed in the control group and improves oxygenation after CPB in a nebulizer-related fashion for up to 30 min. Thirdly, the *ex-vivo* experimentation showed endothelial function amelioration in both ACh- and Bk-dependent relaxation pathways in both groups who received inhaled milrinone. Lastly SJ nebulization not only has a favourable effect on the hemodynamic, oxygenation and endothelial parameters but it was accomplished with almost half of the dose compared to the VM nebulization. This could imply SJ nebulization targets a more appropriate pulmonary area.

4.1 In vitro emitted and inhaled doses and particle size distribution

The vasorelaxation effect of milrinone is due to an arterial smooth muscle relaxation caused by inhibition of the PDEIII enzyme contained in smooth muscle cell (SMC). Thus, the conditions for an efficacious vasorelaxation are twofold: a sufficient presence of SMC and high enough concentrations PDEIII in the tissue. In the lung, tracheobronchial tree airways are paralleled by pulmonary vasculature of similar caliber [20]. The SMC are unequally distributed in all arteries running along the tracheobronchial tree. Arteries with an internal diameter greater than 3200 μm are considered elastic. Elastic vasculature contains little, if no musculature. Between 3200 and 2000 μm, arteries are transitional between elastic and muscular until the 9th branching generation. In this vessel category, muscular content increases. When reaching an internal

diameter between 2000 and 50 µm, they become fully muscular and are considered as resistance vasculature. Subsequently, the quantity of SMC in artery walls progressively diminishes and, when approaching the capillary bed structure, disappears completely to facilitate gas exchanges.

To our knowledge, PDEIII distribution in the SMC of blood vessels adjacent to the tracheobronchial tree, is not yet determined in humans. As such, there is no indication as to the optimal tracheobronchial level where to target milrinone deposition. However, Maclean et al. have quantified the activity of several PDE isoforms throughout the lung vasculature in normoxic and hypoxic rats [21]. In addition to showing different basal activity at different lung depths during normoxia, PDEIII activity during hypoxia was increased by 92% in the main pulmonary branch and 68% in the intrapulmonary artery. Murray et al. [22] also showed that following hypoxia and severe pulmonary hypertension, the statistically significant increase in PDEIII activity found in the first branch of the pulmonary artery, in the intrapulmonary arteries and in the resistance arteries was related to an increase in enzyme synthesis. These findings suggest that these enzymes would be preferentially located in the first branching where smooth muscle cells begin appearing in vascular walls.

In our experimental design we chose a standard breathing pattern frequently used in clinical practice, as different breathing patterns generate different particle size distributions [23]. The addition of breathing patterns in order to simulate clinical conditions are currently emerging in literature [17]. The impactor, however, does require a constant negative pressure to ensure passage of particles through the different levels. The oscillatory breathing pattern generated by the breath simulator did not overtake the negative pressure required for particle separation. To simulate as accurately as possible the clinical situation, the setup included an endotracheal tube. The five mg dose represents the average dose (70 µg/kg) received by an average 70 kg patient. In agreement with literature, our results show that both the SJ and VM nebulizers are highly inefficient in nebulizing the loading dose [24,25]. The dose emitted by the VM nebulizer is twice that of the SJ. This difference is maintained when

comparing the dose delivered to the impactor by the two nebulizers (inhaled dose). With regards to recovered milrinone content for each level, the VM nebulizer generates more particles with a mean aerodynamic diameter (MAD) ranging from 8.6 to 1 μm (retained in the 3–7 impactor levels, Fig. 2). However, after normalization for the cumulative dose collected from all components of the impactor, the VM nebulizer generates more particles ranging from 5.4 to 1.4 μm MAD (collected in the 4–6 impactor levels) while the SJ nebulizer delivers more particles retained on the first impactor level (MAD greater than 14.1 μm).

Taking into account a standard breathing pattern of 14 breaths per minute at 500 mL/breath, the two nebulizers will thus target different pulmonary regions. Indeed, literature indicates that particles with an MAD between 3.30 and 1.36 μm will have a higher probability to deposit along the alveolar region [26] leading to systemic absorption that, in turn, can lead to a reduction of MAP and a non-specific reduction of MPAP without increasing the MAP/MPAP ratio [15]. Particles with an MAD greater than 14.1 μm would normally impact in the oro-pharynx region. However, due to the endotracheal tube which bypasses extrapulmonary regions, the particles with an MAD greater than 14.1 μm are delivered directly to the bifurcation of the trachea into the first-branch bronchi. Thus, losses normally occurring in the mouth, throat and trachea are reduced, leaving a greater than expected amount to potentially reach the trachea. The portion of the nebulized dose impacting on the endotracheal tube and reaching the carina may potentially act as a pseudo-instillation of milrinone, which has been shown to produce a beneficial effect in patients [27]. The caveat with the pseudo-instillation is the negative pressure required for the cascade impactor to function. This negative pressure could potentially draw product deposited unto the endotracheal tube into the first level of the impactor, thus augmenting the inhaled dose. However, both nebulizers undergo the same negative pressure by the impactor. This implies that, *in vitro*, both undergo proportional changes, but relatively to one another, the comparison remains correct. This comparison is highly important as it shows which region is preferably targeted by each by underlining the difference in particle size distribution. This difference may be

significant as a preferentially alveolar deposition could cause a higher systemic versus local absorption and triggering a vasoconstrictive effect [28], and impeding the intended pulmonary relaxation. Hence, in the absolute, the VM nebulizer does indeed deliver the same quantity of milrinone in the higher region as the SJ, however, by delivering more milrinone to the alveolar region, it is also potentially inhibiting vasorelaxation through the higher baroreflex activation.

The hemodynamic effect of milrinone is reported to be relatively short-lived. Following 75 µg/kg given intravenously in a post-cardiac surgery context, pulmonary pressure reduction may be witnessed within minutes and dissipates within 60 min [29]. In addition to the short-lived hemodynamic effect, smooth muscle relaxation due to endothelial dysfunction prevention can be witnessed several hours after administration in swine as previously shown by Lamarche et al. [15], but only for pulmonary administration. As such, both effects should be taken into account when assessing and characterizing the benefits of pulmonary administration whether by SJ or VM nebulizations. In a clinical setting necessitating CPB where the drug is administered before CPB initiation, the difference in drug delivery to a targeted region is additionally relevant due to the interruption of the pulmonary circulation. In the context of a delivery system targeting the upper bronchi and the lower trachea, milrinone deposited in the upper airways possibly diffuses as other drugs [30] through the epithelial paracellular airway walls and reaches PDEIII- containing smooth muscle cells. Reinforcing this possibility is the fact that due to the interrupted pulmonary blood flow, milrinone is not cleared from the site during CPB thus having sufficient time to diffuse and distribute within the pulmonary parenchyma. This interruption of circulation and regional tissue distribution also possibly explain milrinone's reperfusion syndrome prophylaxis effect.

When comparing efficiency/performance of the two nebulization devices, the loading dose does not represent the dose delivered to the patient lungs. Indeed, the emitted dose suggests the need for a loading dose adjustment in both cases, with a greater adjustment required for the SJ nebulizer. With a loading dose adjusted to produce an inhaled dose that is similar for both

nebulizers, the SJ nebulizer, while targeting the higher airways and their adjacent vasculature might deposit milrinone in a more optimal region. However, this optimal region remains a question of debate. Even though pulmonary resistance is controlled by the smaller arteries and arterioles that are adjacent to the lower airways, the PDEIII within these smaller arteries and arterioles show less activity during hypoxic hypertension than the PDEIII located in the upper airways [21] implying perhaps that inherent vasodilation response to pulmonary hypertension occurs in the upper lung regions instead of the lower, thus indicating them as a potential target zone for milrinone.

4.2 In vivo studies

There is a growing interest for milrinone in cardiac surgery, especially when given by inhalation. Our study shows that several parameters exhibited changes between groups. An increase in MPAP after CPB was observed in the control group. These findings were also reported by Morita et al. [31], whose study demostrated a decrease in the MAP/MPAP ratio after CPB. Our study also shows a drop of the ratio for both milrinone groups, however only at 60 min post-CPB. Unlike for the control group, the ratio was not reduced at 30 min post-CPB for both milrinone groups, suggesting a potential prophylaxis against the reperfusion syndrome as observed by other authors [10,15,32]. Furthermore, as suggested by the $AaDO_2$, our study also showed improved oxygenation at 30 min post-CPB following milrinone administration (SJ and VM) when compared to saline.

4.3 Endothelial function

The concentration-effect relationship of bradykinin and acetylcholine on milrinone pre-treated pulmonary vasculature was modelled. In agreement with previous *ex vivo* studies [15], the pulmonary endothelial dysfunction (on

relaxation) caused by CPB was reduced by *in vivo* pre-administration of inhaled milrinone. However, a comparison between the two methods of administering milrinone has not been reported. As such, the endothelial relaxation effects of milrinone administered through SJ nebulization seem to be the result of both ACh and Bk activity whereas through VM, the effects seem to result from specifically only the Bk pathway.

4.4 Limitations

The *in vitro* particle size distribution experimentation has inherent limitations. The characterization of low mean aerodynamic diameter particles requires low temperatures (7 °C) in order to prevent droplet evaporation. These temperatures prevent the use of high humidity as condensation occurs. Also, the impactor required a constant negative pressure which could perhaps have reduced endotracheal tube deposition, potentially affecting the inhaled dose.

For the *in vivo* studies, it cannot be excluded that both nebulizers deliver beyond the dose required to obtain maximum desired effect in Landrace swine; determining the optimal dose would require a dose-ranging study. Furthermore, our swine were young and healthy. An animal model with pre-existing PH or lung disease may have been more suitable to evaluate the effect of CPB and inhaled milrinone. Lastly, CPB differs from clinical situations because of the absence of cardioplegia and protamine use.

4.5 Relevance

Patient profiles in cardiac surgery have changed significantly in the last decades. Population aging has the consequence of increasing disease prevalence and the complexity of health issues. Thus, the incidence of PH is increasing as well and, being associated with higher mortality and morbidity rates [12,33–35], strategies aimed at reducing and controlling it are becoming

necessary. Reducing or preventing CPB-induced endothelial dysfunction may avert PH and its consequences, among which, possibly fatal RV dysfunction. As inhaled milrinone therapy for PH management involves a local, possibly topic effect, determining the optimal deposition becomes necessary in maintaining lung selectivity and drug efficacy. *In vitro*/*in vivo* association is key in forwarding clinical investigation for the use of milrinone in PH prevention and treatment.

Conclusion

Milrinone nebulization using SJ or VM showed positive results in terms of hemodynamic and oxygenation parameters and endothelial function when compared to saline administration in an animal model. In addition, after having characterised the emitted and inhaled doses, particle-size profiles and relaxation efficacy curves of both SJ and VM nebulizers, our study suggest that SJ nebulization, delivers medication to a region where the drug seems to be more efficacious.

Acknowledgements

This work was supported by a grant from The Fonds de recherche du Québec (FQRS) in partnership with the Groupe de recherche universitaire sur le médicament (GRUM). The authors would like to thank Marie-Pierre Mathieu and Audrey Denoncourt for their precious technical help and expertise.

Tables

Table 1 Amounts (mg) recovered of milrinone from all components of the *in vitro* setup.

N = 3	Simple Jet	Vibrating mesh
Emitted dose	2.61 (24)	4.60 (3)*
T-Tube	0.07 (11)	0.01 (10)*
F1	1.21 (16)	2.20 (3)*
F2	1.52 (8)	2.40 (4)*
Inhaled Dose	1.46 (13)	3.00 (0.2)*

*$p < 0.05$.

Table 2 Half-maximal inhibitory concentration, gamma and maximum inhibition of phenylephrine contraction pharmacodynamic-model estimated parameters characterising the sigmoid acetycholine and bradykinine relaxation curves ± standard deviation .

		n	IC_{50} (ng/mL)	γ	Imax (%)
Acetylcholine	Saline	29	$3.4e^{-7}$± $1.8e^{-7}$	9.1 ± 3.2	51.5 ± 4.6
	Simple jet	16	$7.1e^{-8}$ ± $1.4e^{-8}$*	7.8 ± 1.9	75.4 ± 6.4*
	Vibrating mesh	35	$1.4e^{-7}$ ± $1.6e^{-8}$	11.1 ± 3.2	54.6 ± 3.7
Bradykinin	Saline	32	$1.4e^{-9}$ ± $2.1e^{-10}$	7.2 ± 0.4	85.1 ± 2.7*
	Simple jet	26	$1.7e^{-9}$ ± $2.9e^{-10}$	9.3 ± 0.8*	98.7 ± 3.4
	Vibrating mesh	43	$9.2e^{-10}$ ± $1.0e^{-10}$*	8.8 ± 0.8	100.5 ± 2.4

Where IC_{50} is the half maximal inhibitory concentration, γ is gamma and Imax is the maximum inhibition of phenylephrine and n the number of pulmonary artery rings studied. *$p < 0.05$: Significantly different parameter from those of the other two groups.

Figures

Fig. 1 In vitro setups where inserts A: Emitted dose setup, B: Inhaled dose setup, C: Particle size determination setup, Neb: Nebulizer, F1 and F2: Filters, a: flowmeter; b: two-way valve; CD, collected dose; ED, emitted dose; EF, expiratory filter; ETT, endotracheal tube; F, filter; ID: inhaled dose; LD: loading dose; P: syringe port.

Fig. 2 Milrinone percentage of delivered dose recovered from each cascade impactor level and exit and expiratory filters after SJ and VM nebulization. A, nominal recovered milrinone quantities per impactor level, B, inhaled dose-normalized milrinone quantities per impactor level.*$p < 0.05$.

Fig. 3 Hemodynamic parameters.Hemodynamic parameters before, 30 min and 60 min after cardiopulmonary bypass (CPB) in groups receiving inhaled saline, inhaled milrinone via simple jet or vibrating mesh (Abbreviations: MAP: mean systemic artery pressure; MPAP: mean pulmonary artery pressure.*$p < 0.05$.

Fig. 4 Gas exchanges.Gas exchanges before, 30 min and 60 min after cardiopulmonary bypass (CPB) in groups receiving inhaled saline or inhaled milrinone via simple jet (SJ) or vibrating mesh (VM) Abbreviations: pCO_2, partial pressure in carbon dioxide; pO_2, partial pressure in oxygen; PaO_2/FiO_2, ratio of the arterial oxygen partial pressure to fractional inspired oxygen; $AaDO_2$, Alveolo-arterial oxygen gradient. *$p < 0.05$; $^{\dagger}p < 0.05$ when comparing saline to milrinone through VM and SJ administrations.

Fig. 5 Average *ex-vivo* relaxation curves of arterial rings to increasing acetylcholine and bradykinin concentrations.

References

[1] A. Denault, A. Deschamps, J.-C. Tardif, J. Lambert and L. Perrault, Pulmonary hypertension in cardiac surgery, *Curr. Cardiol. Rev.* **6**, 2010, 1–14.

[2] S. Wan, J.L. LeClerc and J.L. Vincent, Inflammatory response to cardiopulmonary bypass: mechanisms involved and possible therapeutic strategies, *Chest* **112** (3), 1997, 676–692.

[3] C.S. Ng, S. Wan, A.P. Yim and A.A. Arifi, Pulmonary dysfunction after cardiac surgery, *Chest* **121** (4), 2002, 1269–1277.

[4] C.L. Reichert, C.A. Visser, R.B. van den Brink, J.J. Koolen, H.B. van Wezel, A.C. Moulijn and A.J. Dunning, Prognostic value of biventricular function in hypotensive patients after cardiac surgery as assessed by transesophageal echocardiography, *J. Cardiothorac. Vasc. Anesth.* **6** (4), 1992, 429–432.

[5] V.G. Davila-Roman, A.D. Waggoner, W.E. Hopkins and B. Barzilai, Right ventricular dysfunction in low output syndrome after cardiac operations: assessment by transesophageal echocardiography, *Ann. Thorac. Surg.* **60** (4), 1995, 1081–1086.

[6] A.Y. Denault, R.G. Pearl, R.E. Michler, V. Rao, S.S. Tsui, R. Seitelberger, M. Cromie, E. Lindberg and A.M. D'Armini, Tezosentan and right ventricular failure in patients with pulmonary hypertension undergoing cardiac surgery: the TACTICS trial, *J. Cardiothorac. Vasc. Anesth.* **27** (6), 2013, 1212–1217.

[7] A. Haraldsson s, N. Kieler-Jensen and S.E. Ricksten, The additive pulmonary vasodilatory effects of inhaled prostacyclin and inhaled milrinone in postcardiac surgical patients with pulmonary hypertension, *Anesth. Analg.* **93** (6), 2001, 1439–1445, table of contents.

[8] Y. Lamarche, L.P. Perrault, S. Maltais, K. Tetreault, J. Lambert and A.Y. Denault, Preliminary experience with inhaled milrinone in cardiac surgery, *Eur. J. Cardiothorac. Surg.* **31** (6), 2007, 1081–1087.

[9] H. Wang, M. Gong, B. Zhou and A. Dai, Comparison of inhaled and intravenous milrinone in patients with pulmonary hypertension undergoing mitral valve surgery, *Adv. Ther.* **26** (4), 2009, 462–468.

[10] J. Zhang, F. Chen, X. Zhao, A. Aoyama, T. Okamoto, T. Fujinaga, T. Shoji, H. Sakai, Y. Cui, T. Bando and H. Date, Nebulized phosphodiesterase III inhibitor during warm ischemia attenuates pulmonary ischemia-reperfusion injury, *J. Heart Lung Transpl.* **28** (1), 2009, 79–84.

[11] A. Robitaille, A.Y. Denault, P. Couture, S. Belisle, A. Fortier, M.C. Guertin, M. Carrier and R. Martineau, Importance of relative pulmonary hypertension in cardiac surgery: the mean systemic-to-pulmonary artery pressure ratio, *J. Cardiothorac. Vasc. Anesth.* **20** (3), 2006, 331–339.

[12] J.C. Bianco, B. Qizilbash, M. Carrier, P. Couture, A. Fortier, J.C. Tardif, J. Lambert and A.Y. Denault, Is patient-prosthesis mismatch a perioperative predictor of long-term mortality after aortic valve replacement?, *J. Cardiothorac. Vasc. Anesth.* **27** (4), 2013, 647–653.

[13] F. Haddad, J. Guihaire, M. Skhiri, A.Y. Denault, O. Mercier, S. Al-Halabi, B. Vrtovec, E. Fadel, R.T. Zamanian and I. Schnittger, Septal curvature is marker of hemodynamic, anatomical, and electromechanical ventricular interdependence in patients with pulmonary arterial hypertension, *Echocardiography* **31** (6), 2014, 699–707.

[14] A.Y. Denault, J.S. Bussieres, R. Arellano, B. Finegan, P. Gavra, F. Haddad, A.Q. Nguyen, F. Varin, A. Fortier, S. Levesque, Y. Shi, M. Elmi-Sarabi, J.C. Tardif, L.P. Perrault and J. Lambert, A multicentre randomized-controlled trial of inhaled milrinone in high-risk cardiac surgical patients, *Can. J. Anaesth.* 63 (10), 2016,1140-1153.

[15] Y. Lamarche, O. Malo, E. Thorin, A. Denault, M. Carrier, J. Roy and L.P. Perrault, Inhaled but not intravenous milrinone prevents pulmonary endothelial dysfunction after cardiopulmonary bypass, *J. Thorac. Cardiovasc Surg.* **130** (1), 2005, 83–92.

[16] H.M. Janssens, J.C. de Jongste, W.C.J. Hop and H.A.W.M. Tiddens, Extra-fine particles improve lung delivery of inhaled steroids in infants*: a study in an upper airway model, *Chest* **123** (6), 2003, 2083–2088.

[17] A.-M. Ciciliani, P. Langguth and H. Wachtel, In vitro dose comparison of Respimat(®) inhaler with dry powder inhalers for COPD maintenance therapy, *Int. J. Chronic Obstr. Pulm. Dis.* **12**, 2017, 1565–1577.

[18] A.Q. Nguyen, Y. Theoret, C. Chen, A. Denault and F. Varin, High performance liquid chromatography using UV detection for the quantification of milrinone in plasma: improved sensitivity for inhalation, *J. Chromatogr. B Anal. Technol. Biomed. Life Sci.* **877** (7), 2009, 657–660.

[19] A. Mommerot, A.Y. Denault, J. Dupuis, M. Carrier and L.P. Perrault, Cardiopulmonary bypass is associated with altered vascular reactivity of isolated pulmonary artery in a porcine model: therapeutic potential of inhaled tezosentan, *J. Cardiothorac. Vasc. Anesth.* **28** (3), 2014, 698–708.

[20] A.A. Frazier, J.R. Galvin, T.J. Franks and M.L. Rosado-De-Christenson, From the archives of the AFIP: pulmonary vasculature: hypertension and infarction, *Radiographics* **20** (2), 2000, 491–524, quiz 530-1, 532.

[21] M.R. Maclean, E.D. Johnston, K.M. McCulloch, L. Pooley, M.D. Houslay and G. Sweeney, Phosphodiesterase isoforms in the pulmonary arterial circulation of the rat: changes in pulmonary hypertension, *J. Pharmacol. Exp. Ther.* **283** (2), 1997, 619–624.

[22] F. Murray, M.R. MacLean and N.J. Pyne, Increased expression of the cGMP-inhibited cAMP-specific (PDE3) and cGMP binding cGMP-specific (PDE5) phosphodiesterases in models of pulmonary hypertension, *Br. J. Pharmacol.* **137** (8), 2002, 1187–1194.

[23] B.K. Gurses and G.C. Smaldone, Effect of tubing deposition, breathing pattern, and temperature on aerosol mass distribution measured by cascade impactor, *J. Aerosol Med.* **16** (4), 2003, 387–394.

[24] D. Hess, D. Fisher, P. Williams, S. Pooler and R.M. Kacmarek, Medication nebulizer performance. Effects of diluent volume, nebulizer flow, and nebulizer brand, *Chest* **110** (2), 1996, 498–505.

[25] E.C. Smith, J. Denyer and A.H. Kendrick, Comparison of twenty three nebulizer/compressor combinations for domiciliary use, *Eur. Respir. J.* **8** (7), 1995, 1214.

[26] J.P. Mitchell and M.W. Nagel, Cascade impactors for the size characterization of aerosols from medical inhalers: their uses and limitations, *J. Aerosol Med.* **16** (4), 2003, 341–377.

[27] E.C. Gebhard, G. Desjardins, C. Gebhard, P. Gavra, A.Y. Denault, Intratracheal milrinone bolus administration during acute right ventricular dysfunction following cardiopulmonary bypass, J. Cardiothorac. Vasc. Anesth..

[28] S. Hirakawa, H. Ito, T. Sahashi, K. Takai and H. Wada, Effects of milrinone on systemic capacitance vessels in relation to venous return and right ventricular pump function, *J. Cardiovasc. Pharmacol.* **19** (1), 1992, 96–101.

[29] J.F. Butterworth, R.L. James, R.L. Hines and R.L. Royster, A pharmacokinetic and pharmacodynamic evaluation milrinone in adults undergoing cardiac surgery, *Anesth. Analgesia* 1995, 783–792.

[30] H.J. Unwalla, G. Horvath, F.D. Roth, G.E. Conner and M. Salathe, Albuterol modulates its own transepithelial flux via changes in paracellular permeability, *Am. J. Respir. Cell Mol. Biol.* **46** (4), 2012, 551–558.

[31] K. Morita, K. Ihnken, G.D. Buckberg, M.P. Sherman and L.J. Ignarro, Pulmonary vasoconstriction due to impaired nitric oxide production after cardiopulmonary bypass, *Ann. Thorac. Surg.* **61** (6), 1996, 1775–1780.

[32] F. Chen, J. Zhang, a. Aoyama, T. Okamoto, T. Fujinaga and T. Bando, Potential for pulmonary protection by nebulized milrinone during warm ischemia, *Transplant. Proc.* **40**, 2008, 3335–3338.

[33] E.M. Boyle, Jr., T.H. Pohlman, M.C. Johnson and E.D. Verrier, Endothelial cell injury in cardiovascular surgery: the systemic inflammatory response, *Ann. Thorac. Surg.* **63** (1), 1997, 277–284.

[34] A.D. Bernstein and V. Parsonnet, Bedside estimation of risk as an aid for decision-making in cardiac surgery, *Ann. Thorac. Surg.* **69** (3), 2000, 823–828.

[35] J.F. Malouf, M. Enriquez-Sarano, P.A. Pellikka, J.K. Oh, K.R. Bailey, K. Chandrasekaran, C.J. Mullany and A.J. Tajik, Severe pulmonary hypertens**s**ion in

patients with severe aortic valve stenosis: clinical profile and prognostic implications, *J. Am. Coll. Cardiol.* **40** (4), 2002, 789–795.

CHAPTER 12. Manuscript #4:Pharmacokinetics and pharmacodynamics of nebulized and intratracheal milrinone in a hypercapnic swine pulmonary hypertension model.

Paul Gavra[*], Yves Théorêt[†], Louis Perrault[††], André Y. Denault[††] & France Varin[*]

* Faculty of Pharmacy, Université de Montréal, Montréal, Canada

[†] Unité de Pharmacologie Clinique, CHU Ste-Justine, Montréal, Canada

[††] Department of Anesthesiology, Critical Care Division, ontreal Heart Institute, Montréal, Canada

Correspondence: France Varin, Faculty of Pharmacy, Université de Montréal, P.O. Box. 6128, Succursale Centre-Ville, Montréal, QC, Canada H3C 3J7.
E-mail : france.varin@umontreal.ca

Current status : In preparation

Abstract

Objectives: Milrinone pulmonary administration is currently used for the treatment of pulmonary hypertension. Several methods are available: simple jet nebulization, vibrating mesh nebulization, intratracheal instillation and intratracheal atomization. This study aims to explore the concentration-effect relationship of milrinone for each of these methods.

Design: Observational open-label pharmacokinetic/pharmacodynamics cohort study

Setting: Hospital animal laboratory.

Participants: Twelve swine.

Interventions: Following hypercapnia pulmonary hypertension, swine were administered equivalent inhaled milrinone doses of 15 or 50 ug/kg through simple jet nebulization, vibrating mesh nebulization, intratracheal instillation and intratracheal atomization.

Measurements and Main Results: Blood and urine samples were taken up to 360 minutes post-administration. Mean systemic arterial pressure/mean pulmonary arterial pressure ratio was monitored continuously. Right heart echographies were taken before and after hypercapnia and post-drug administration. Mean elimination half-lives were similar for the four administrations. Mean percent changes in the ratio were of 37 (60%), 18 (31%), 17 (36%) and 20 (20%), for simple jet nebulization, vibrating mesh nebulization, intratracheal instillation and intratracheal atomization, respectively. Mean maximum plasma concentrations for intratracheal administrations were reached at 8 and 45 min for atomization and instillation, respectively. Significant increases in right atrial diameter and right ventricular end-diastolic area were witnessed during pulmonary hypertension as well as a return to baseline values following milrinone administration.

Conclusions: The intratracheal methods, particularly ITA, showed less hemodynamic effect than nebulizations and, in the case of ITI, unpredictable drug exposure. Nebulization methods on the other hand, especially SJ, suggest better efficacy and sensitivity but are less fit for emergency situations.

Introduction

In an aging population, the prevalence of heart surgeries is substantially increasing and one of its most dangerous complications is the difficult weaning from cardiopulmonary bypass (CPB).[1] Indeed, when difficult weaning from CPB is related to right ventricle failure, the mortality rate associated varies from 22 to 86%.[2-5] Right ventricle failure can result from the pulmonary hypertension (PH) caused by the pulmonary reperfusion syndrome, which is a possible occurrence during weaning.[6] Therefore, it is critical to either treat the PH or, if possible, prevent the reperfusion syndrome.

Intravenous administration of milrinone, a phosphodiesterase III inhibitor that lowers vascular pressure through vasorelaxation, is commonly used in patients with PH and right ventricular dysfunction. However, a downside to intravenous milrinone is the lack of pulmonary vasorelaxation selectivity which stems from systemic milrinone exposure.[7] Off-label pulmonary administration of milrinone was studied and showed pulmonary selectivity with no associated systemic hypotension.[8-10] This selectivity can be assessed by observing changes in the mean systemic arterial pressure (mAP) over the mean pulmonary arterial pressure (mPAP) ratio (mAP/mPAP) which increases when the severity of PH is reduced.[11-13]

Milrinone can be nebulized using either a simple jet nebulizer (SJ)[8], where the liquid is turned into aerosols via a gas vector stream, or nebulized through vibrating mesh nebulizer (VM)[5] via the movement of an ultrasound micro-grill. In emergency circumstances, milrinone can also be administered as an intratracheal instillation (ITI) of a bolus using a simple syringe.[11] This bolus however is known to distribute in an uneven fashion. An alternative devoid of this downside is intratracheal atomization (ITA).[13]

Several studies have shown potential clinical benefits of nebulized milrinone on CPB weaning.[8,14,15] However, the largest multicenter randomized clinical trial to date, while showing beneficial hemodynamic effects, concluded in no significant

impact on CPB weaning clinical endpoints.[5] Despite non-compartmental analyses indicating an adequate systemic exposure and a correlation between PK and PD partial exposures in a subset of patients (n=19), the multicenter study determined a clinically favourable PD response in only 55% of 63 patients.[5] Denault *et al's* study administered inhaled milrinone using a VM, whereas a previous animal study, showing the benefits of milrinone for PH prevention, used a SJ. The latter demonstrated a higher endothelium-related relaxation following milrinone SJ administration when comparing it to both SJ saline and IV milrinone administrations.[8] This contrast underlines the importance of administration methods. In the present report, a non-CPB swine model was chosen to enable a titratable control of PH as opposed to what is observable after CPB. Swine have previously been used in milrinone research[8] due to the similarities between the species' cardiopulmonary system and the human one. This study aims at exploring and describing the pharmacokinetics and pharmacodynamics of milrinone following these four methods of administration in a swine model of hypercapnia PH.

Material and methods

Animals

Twelve 8-week crossbred Landrace-Yorkshire swine, obtained from Marc Lavallée farm (Montreal, QC, Canada), of either sex (ratio 1:1) and weighing 37±10 kg were treated in accordance with the recommendations of the guidelines on the Care and Use of Laboratory Animals issued by the Canadian Council on Animals and approved by the institutional Animal Care and Use Committee (2012-73-01). Swine were housed in pairs in square straw-lined pens, were given access to water and environment enrichment objects and were not subject to restrictive diet until one night before the experiment when animals underwent an overnight fast before experimentation.

Solutions

Injectable milrinone lactate solution (1 mg/mL) was used for all studies and obtained from Sanofi Canada (Montreal, Qc, Canada).

Nebulizers and Breathing Pattern

The nebulizers were a VM nebulizer (AeronebPro, Aerogen®, Galway, Ireland) and a conventional in-line jet or SJ nebulizer (Salter Labs, Arvin, CA). The endotracheal tube mucosal *atomization* device (*MADett*™) was kindly provided by *Wolfe Tory* Medical Inc (Salt Lake City, UT, USA). During all experiments, animals were ventilated optimally according to their weight with a constant 66:34 oxygen:air mixture at 14 breaths per minute with a tidal volume of 6-8 mL/kg.

Animal Preparation

The morning of the experiment, following intramuscular ketamine hydrochloride sedation (25 mg/kg; Ayerst Veterinary Laboratories, Guelph, On, Canada) and

xylazine (10 mg/kg; Boehringer Ingelheim, Burlington, On, Canada) in their cage, they were transported to the laboratory. Anesthesia induction was achieved using mask ventilation with 2% isoflurane (Abbott Laboratories Limited, St-Laurent, Qc, Canada) as isoflurane is the anesthetic of choice for swine.[16] Animals were subsequently intubated and mechanically ventilated. A jugular vein and femoral artery were cannulated to obtain a central venous line and mAP, respectively. A cystostomy was performed for urine collection. Electrocardiogram was continuously monitored from 5 subcutaneous limb electrodes. All animals had a pulmonary artery catheter (Swan-Ganz, Edwards Lifesciences, Irving, California, USA) inserted through the jugular vein. Hemodynamic parameters, including mAP, mPAP, heart rate, O_2 saturation and central venous pressure were measured continuously during the procedure.

Hypercapnia Pulmonary Hypertension

Following 30 minutes of stabilization in normocapnic conditions, PH was induced through titration of an added CO_2 stream. Carbon dioxide flow varied between 0.25 to 1.2 L/min, representing up to 35% of the inhaled mixture. Carbon dioxide was titrated as to precisely double the mPAP observed during normotension, thus yielding a doubled hypertension baseline observed mAP/mPAP ratio. Our model was based on the swine models developed by Lee *et al* and Yavuz *et al*. [17,18]. Blood pH was managed through a 2 ml/min tromethamine IV infusion and *ad hoc* IV boluses in order to palliate changes in hemodynamic parameters. Mild hypercapnic acidosis was however permitted as it is a necessary factor for PH increase.[17-19]

Experimental Groups

Thirty minutes under stable hypercapnic conditions, milrinone lactate was adjusted to deliver a similar high (50 µg/kg) or low (15 µg/kg) target dose through VM, SJ, ITI or ITA and thereby facilitate comparisons of pharmacodynamic data. Three animals were attributed to each group in order to explore the PK and PD. Intratracheal groups (ITA and ITI) were made up of two

animals having received high doses and one having received a low dose whereas nebulization groups (VM and SJ) were made up of two animals having received low doses and one having received a high dose. Doses were based on previous experimentation. The target dose was adjusted by taking into account the mean *in vitro* dose delivered to the lungs after nebulization.[20] The latter represents the fraction of the administered dose that would reach subject's trachea and accounts for milrinone losses within the nebulizers. This fraction was previously estimated as 0.6 for VM and 0.3 for SJ.[20] Nebulization times were recorded. Target doses for ITI or ITA were assumed to be 100% delivered to the lungs. Method and dose were selected the day of the experiment. The experimental protocol is summarized Figure 1.

Pharmacokinetic and Pharmacodynamic Sampling

Blood samples were taken at 1, 2, 3, 4, 5, 9, 15, 21, 30, 60, 120, 240, and 360 minutes after starting milrinone administration. The mAP/mPAP ratios were calculated at each PK sampling time points. Urine samples were collected at 0 and 360 minutes. Samples were kept in an ice-water bath until centrifugation (15 min, 1900g). Plasma was frozen at -70°C until HPLC-MS/MS analysis.[21] Transthoracic echocardiographic examination was performed by a cardiologist with an expertise in echocardiography during the normotensive and hypertensive periods and following milrinone peak effect. Right atrium diameter and right ventricular end-diastolic area were obtained from the apical 4-chamber view.

Pharmacokinetic and Pharmacodynamic Modeling

For PK/PD modeling, a two-step approach was chosen. Milrinone plasma concentrations vs time profiles were individually modeled using a two-compartment pharmacokinetic (PK) model and extravascular input. To ensure a best fit, rate of input differed between administration groups. Nebulizations were best fitted with a zero-order input (k_{01}) with a duration equivalent to nebulization time. Intratracheal administrations were best fitted using a first-order input (ka).

In all cases, a mix-ratio residual model was used. For each animal, the dose used for modeling was the amount of milrinone recovered in urine over 360 min. Following convergence, PK parameters were fixed and PK/PD data modeled using a sigmoid Emax model without effect compartment. Model-estimated parameters were the hypercapnic baseline ratio (E_0), the maximum predicted effect (Emax), milrinone concentration producing 50% of the effect (EC_{50}) and the Hill coefficient (γ). Observed ΔEmax was calculated as the difference between the ratio at the time of maximum effect and the observed hypercapnic baseline ratio of the individual animal, relative (in percentages) to the hypercapnic baseline ratio. Predicted ΔEmax was determined as the model-predicted maximum effect, relative (in percentages) to the model-predicted hypercapnic baseline ratio (E_0) of the ΔEmax and percent fraction of the Emax over, respectively. Modeling was performed using the Phoenix® 6.4.0.768 pharmacokinetic/pharmacodynamic software (Pharsight, Certara, NJ, USA).

Statistical Analysis

Descriptive statistics and results are presented as mean (coefficient of variation). First, normality of distribution of data was assessed by means of the Shapiro-Wilk test. In comparisons involving all four methods of administration, normally distributed values were analyzed using one-way ANOVAs and followed by a Tukey's post-hoc test. Non-normally distributed data were analyzed using the Kruskal-Wallis test with pairwise comparison. Statistical significance was set at $p<0.05$ and analyses were performed with the computer software SPSS 16.0.1 (SPSS Inc., Chicago, Il, USA).

Results

The results obtained from 12 animals were used for the summary analyses. Dosing data for each method of administration are detailed in Table 1. Two animals (ID 4 and 5), from the ITI and ITA groups respectively, experienced hemodynamic instability after return from hypercapnia, which required volume therapy, tromethamine boluses and stopping experimentation at 180 min. For these animals, the elimination constant was estimated with available data and found similar to other animals in their respective groups.

PK/PD Model Selection

One-, 2- and 3-compartment PK models were tested. Coefficients of variation were similar between 1- and 2-compartment models but ten times higher for 3-compartment model. The 2-compartment model showed the lowest Akaike criterion followed by 3-compartment and 1- compartment. The condition number was found to be highest for 3- and lowest for 1-compartment models. Goodness of fit diagnostic graphics were also verified. Weighted residuals showed a curvilinear tendency for the 1-compartment model indicating poor fit whereas both 2- and 3-compartment models showed homoscedasticity. The predicted versus observed identity lines indicated that unlike the 2- and 3-compartment models, the 1-compartment model underestimated higher concentrations and could not predict Cmax adequately. Error models tested were additive and mix-ratio. The mix-ratio error model yielded a better homoscedastic distribution of residuals than the additive error model. Effect modeling was based on a sigmoid Emax model. Linear and indirect relationships between PK and PD were also tested. When testing the Emax model, an effect compartment was also tried but the estimated K_{e0} values were found extremely high indicating that the compartment was unnecessary.

Pharmacokinetic Analysis

Individual full milrinone plasma concentration-time profiles from 0 to 360 minutes are shown in Figure 2. Individual milrinone plasma concentration-time profiles for only the first 20 min are presented in Figure 3 Data is shown as value (coefficient of variation) in Table 2. Peak plasma concentrations ranged from 2 to 107 ng/mL and varied proportionally according to the dose for ITA, SJ and VM but not for ITI. T_{max} for intratracheal administrations were 8 (76) and 45 (64) min for ITA and ITI, respectively. Nebulization T_{max} was observed at the end of nebulization and correlated with nebulization time (r^2=0.64 and 0.99 for SJ and VM, respectively). Resulting pharmacokinetic parameters are listed in Table 2. Correlations between predicted versus observed concentrations were similar for all four modes of administration and data were merged, due to space limitations (Figure 3, left panel). No difference was observed for T_{lag} between methods (p=0.979). Unlike initially estimated inhaled dose, the amount of milrinone recovered in urine correlated better with the plasma concentration-time area under the curve (r^2=0.79, p<0.0001) and were therefore used for PK modeling.

Pharmacodynamic and PK/PD Analysis.

Individual evolutions of the mAP/mPAP ratio as a function of time are presented in Figure 3. Modeled pharmacokinetic/pharmacodynamic parameters are given in Table 2 and predicted versus observed mAP/mPAP ratios for pooled data are shown in Figure 3. Nebulisation E_{max} times are not indicated in Table 2 as nebulization time varied according to milrinone volume administered, which was inherently different between high and low doses. A sigmoid Emax model best fitted the mAP/mPAP ratio vs milrinone plasma concentration curves. Mean overall normocapnic baseline mAP/mPAP ratio was 5.48 (24) Mean overall E_0 was 2.74 (23). Overall γ parameter varied between 1.5 (ID 4, ITI) and 463 (ID 16, VM). The overall predicted ΔE_{max} varied from 13 (ID 6, ITA) to 63% (ID 15, SJ) relative to E_0. Time to maximum effect was variable and longest for ITI administration. For nebulizations, no significant difference was

found between time to Emax and nebulization time (p=0.61 and p=0.51 for SJ and VM, respectively).

Pharmacodynamic Biomarkers

Transthoracic echocardiographic examination was performed during the normotensive and hypertensive periods and following milrinone peak effect in nine pigs. Mean pooled right atrium diameter and right ventricular end-diastolic area were obtained from the apical 4-chamber view. Changes in right heart dimensions can be seen in Figure 4. Right atrium diameter and right ventricular end-diastolic area increased significantly by respectively 18.4(141) and 18.7(127) % and significantly returned to baseline following milrinone administration.

Discussion

This is the first exploratory study comparing four different pulmonary methods of administering milrinone with the aim of determining their potential impact on the PK/PD relationship of the drug. This relationship was explored through the use of a hypercapnia-induced PH animal model. PK/PD modeling of plasma concentrations and mAP/mPAP ratio suggests that these different methods for delivering milrinone to the lungs result in variable drug sensitivity and maximum effect changes.

Several animal PH models exist to study the characteristics of this disease. Among them are hypoxia[22] and pulmonary damage models.[23-25] Hypercapnia has also been demonstrated to increase pulmonary resistance and mean pulmonary artery pressure.[17] The hypercapnia PH model developed herein, though practical because of its flexibility for hypertension titration, was sometimes difficult to manage due to inter-animal CO_2 reaction variability. Despite this variability, both right atrium and right ventricle dimensions increased significantly during the hypertensive period and returned to baseline values when milrinone peak effect was observed confirming both the hypertensive effects of the hypercapnia model as well as the relaxation effect of milrinone, regardless of administration method. However, the variability of the echographic measurements was too high to allow statistically conclusive comparisons between administration methods. In addition, the unpredictability of milrinone T_{max} or of the time to reach maximum effect following intratracheal instillation hindered prediction of the time at which transthoracic echography needed to be carried out in order to characterize morphological heart chamber changes attributed to milrinone E_{max}. This experimental bias explains why this group was excluded from the final analysis. Nonetheless, our results support current knowledge on both the effect of PH on the right cardiac chambers and on milrinone's effect as an afterload reducing agent.[6]

To explore the PKPD relationship of milrinone, we used the same PD biomarker as the one used in a previous clinical trial.[5] The mAP/mPAP ratio is the biomarker of choice to describe the effect of milrinone because it takes into account the changes in both arterial pressures (local pulmonary and systemic)[12], it correlates with the severity of PH and is a good predictor of hemodynamic complications after cardiac surgery.[8,12] This ratio remains an independent predictor of outcome 5 years after aortic valve surgery.[26] It is the hemodynamic variable having the strongest correlation with RV deformation secondary to PH, indicating that the ratio may be regarded as an excellent tool for describing morphological heart changes.[27] Of all methods, ITI showed the most unpredictable kinetics and, in particular, the most variable bioavailability. Indeed, for one animal from ITI group, milrinone peak plasma concentration (15.6 ng/ml) was observed at 120 min. This was however to be expected as this method is highly dependent on administration factors such as subject position, airways morphology, speed of administration and whether or not an air bolus is pushed after the drug dose.[13] In our swine, no air bolus was given after milrinone administration and this possibly contributed to an uneven intrapulmonary distribution which translated into highly variable absorption.

Low circulating concentrations of milrinone were observed following SJ administration. This low bioavailability has been hypothesized previously.[11] Intratracheal administrations (ITI and ITA), while similar one to another, showed a higher bioavailability than nebulizations, as confirmed by higher mean urinary recovery percentages. This intratracheal bioavailability was however lower than expected. In view of the absence of significant milrinone pulmonary metabolism, the bioavailability of these routes was expected to be 100%. Several studies do nonetheless present reduced intratracheal bioavailability.[28-30] This issue was resolved by using urine-recovered milrinone amounts for PK modeling. This solution was deemed acceptable as milrinone systemic exposure and urinary amounts recovery indicated a good correlation.

Mirinone plasma concentration-time profiles following both types of nebulization were best fitted with a zero-order model, implying an instantaneous systemic absorption stopping at the end of nebulization. The modeling software used (Phoenix®) allowed the determination of a potential absorption rate constant even in the presence of an infusion rate (Figure 3). Nevertheless, as expected, the high values of Ka determined for nebulizations indicated an instantaneous absorption; a finding consistent with documented absorption speeds following inhalation.[31,32] In contrast, absorption after an intratracheal bolus was best fitted by using a first-order input rate, estimating the end of absorption at approximately 7.5 min (5 times the average absorption half-life of 1.5 min).

A fairly good agreement was observed for inhaled total body clearance and terminal elimination half-life between the methods of pulmonary administration. Inter-individual variability of PK parameters being high, no significant changes were observed between groups. However, some trends were observed, the most noticeable one being the one for the distribution clearance, Cl_{12}, which was more than twofold faster for nebulization in comparison to intratracheal administrations. As the lung is generally assumed to be part of the central compartment, this finding would suggest a higher pulmonary retention during intratracheal administration, which is compatible with the particle sizes generated. During ITA administration, milrinone is sprayed locally in atomized form (mean aerodynamic diameter ≈30 um, information provided by Wolf Tory Medical Inc.) and as such, a higher portion of particles may potentially undergo tracheobronchial absorption and local distribution at upper pulmonary levels. During ITI, a bolus is introduced within the lungs, thus not generating a particle size distribution (unpublished results) and also preferentially targeting the upper airways. In contrast, during nebulization, smaller mean aerodynamic diameter (≈3-5 μm) particles are generated, thus targeting preferentially the alveolar region.[20,33,34]

To our knowledge, as of yet, there are no single dose inhalation PK values in swine with which to compare, nor in human. Milrinone apparent total body clearance, normalized by body weight and dose recovered in urine, was found to be lower in studied swine than that reported following IV administration in adult patients suffering from congestive heart disease[35,36], but similar to that reported for children.[37]

The complexity of the pulmonary route and its highly variable absorption adds to the challenge of characterizing the pharmacokinetics, pharmacodynamics and the link between the two.[13,31,38] This complexity is enhanced by the fact that inhaled milrinone has to be delivered to its site of action, the endothelial pulmonary vasculature, and more specifically, the smooth muscle containing phosphodiesterase III; the exact distribution of this enzyme in swine pulmonary arteries remains unknown. Moreover, it is not clear whether the almost instantaneous effect of inhaled milrinone results from its diffusion across the pulmonary mucosa, after distribution into the systemic circulation or from both simultaneously.

With regards to pharmacodynamic parameters, the only observed significant difference between the various methods was found for EC_{50}, between ITA and the other three methods. When comparing nebulization methods, SJ indicated the highest sensitivity, despite a twofold lower systemic bioavailability. These results are consistent with previous research showing a higher post-CPB endothelial relaxation efficacy for milrinone administration through SJ than through VM administration.[20] No significant difference was found between time to Emax and nebulization time reinforcing the assumption that systemic absorption is instantaneous after nebulization.[32] While producing the highest systemic exposure for milrinone, ITA was associated with the lowest animal sensitivity to milrinone. It did however indicate a shorter time to Emax when compared to the other intratracheal method, ITI. Both intratracheal routes showed a relatively small hemodynamic effect on mAP/mPAP.

Hill coefficient parameter was necessary for model convergence in only four of the twelve animals. For comparison purposes, this parameter was included in

the model for all animals, and this may explain why it showed the highest interindividual variability. The estimated values for γ were found to be substantially high, particularly for nebulization administrations, indicating an almost all-or-none effect. Although physiological interpretation of γ values has to be made with caution, some authors suggest that a very high value is indicative of a threshold effect.[39] The presence of such a threshold for phosphodiesterase III inhibition could explain the surprisingly high effect observed at low systemic exposure (SJ) and the relatively small increase in effect at high systemic exposure (ITA). Our results also suggest that once this threshold is reached, there may be no need to increase the concentrations. Doing so might only activate baroreceptor vasoconstriction reflexes as suggested by Hirakawa *et al*[40] thus impeding the intended pulmonary relaxation. Indeed, these authors showed that the capacitance vessels' baroreflex contraction was sufficiently strong as to mask the vasodilation effect generated by a 100µg/kg milrinone IV dose (≈20% of baseline tension). Milrinone doses administered in our study's animals varied from a maximum of 0.78 to as low as 0.08 mg (as per urinary recovery). It is unlikely that the low concentrations observed after SJ administration were high enough to activate baroreflex vasoconstriction however, as higher concentrations were observed for other methods of administration, it cannot be excluded that such a masking effect occurred, potentially have counterbalancing milrinone-induced vasorelaxation. This would be compatible with the twofold higher observed/predicted ΔE_{max}% observed after SJ nebulization in comparison to that of other methods.

Limitations

The major limitations of this exploratory study are related to the small number of animals used per method of administration. Total number of animals took into account the expected variability inherent to the mAP/mPAP ratio in humans, but the difference in PD response to milrinone between administration methods was unknown beforehand. Also, to explore linearity within the therapeutic range of concentrations, each administration group had an animal having received either

a low or high dose, decreasing the number of animals per dose. Finally, the hypercapnia PH model may not reflect completely the reperfusion injury after CPB. As the model is of an acute nature, it cannot describe the morphological changes witnessed in a chronic hypertensive situation.

Conclusions

In summary, this paper compared the PK/PD relationships of four methods of pulmonary administration of milrinone. The intratracheal methods, particularly ITA, showed less hemodynamic effect than nebulizations and, in the case of ITI, unpredictable relationship between drug exposure and effect. Nebulization methods on the other hand, especially SJ, suggest better efficacy and sensitivity but are less fit for emergency situations.

Acknowledgements

This work was supported by a grant from The Fonds de recherche du Québec-Santé (FRQS) in partnership with the Groupe de recherche universitaire sur le médicament (GRUM). The authors would like to thank Marie-Pierre Mathieu and Audrey Denoncourt for their precious technical help and expertise.

Tables

Table 1. Dosing data related to the four methods of pulmonary administration of milrinone lactate in hypertensive swine.

Admin Method	ID	Weight (kg)	Target Dose (µg/kg)	Nominal Administered Dose (mg)	Amount Recovered In Urine (mg)	F* (%)	Neb Time (min)
ITA							
	5	45	50	2.25	1.13	50	-
	6	35	50	1.75	0.53	30	-
	10	29	15	0.45	0.17	37	-
ITI							
	3	71	50	3.47	0.21	6	-
	4	45	50	2.25	0.68	30	-
	11	29	15	0.45	0.24	53	-
SJ							
	8	33	15	1.65	0.12	7	3
	13	33.4	15	1.67	0.12	7	2
	15	33.4	50	5.01	0.60	12	9
VM							
	7	32	50	2.67	0.59	22	15
	9	36	15	0.9	0.14	15	3
	16	30.8	15	0.77	0.12	15	8

Where ITA : intratracheal atomization, ITI : intratracheal instillation, SJ : simple jet nebulization and VM: vibrating mesh nebulization; Admin: administration; Neb: nebulization

* Bioavailability was deduced from milrinone amount recovered in urine

Table 2. Pharmacokinetic/pharmacodynamic modeling of milrinone plasma concentrations and mAP/mPAP ratio under four methods of pulmonary administration in hypertensive swine.

	PHARMACOKINETIC PARAMETERS								PHARMACODYNAMIC PARAMETERS					
	Tlag	**ka**	**Cl/F**	**Cl_{12}/F**	**V_1/F**	**V_2/F**	**V_{DSS}/F**	**$T_{1/2}$**	**E_0**	**EC_{50}**	**Observed Δ Emax**	**Predicted Δ Emax**	**Emax Time**	**Hill coefficient**
	(min)	(1/min)	(ml/min/kg)	(mL/min/kg)	(mL/kg)	(mL/kg)	(mL/kg)	min		(ng/mL)	(% of baseline)	(% of E_0)	min	
ITA	0.52 (37)	0.36 (64)	3.02 (42)	8.91 (10)	169 (60)	303 (23)	473 (32)	130 (69)	2.60 (23)	39 (60)*	23 (22)	17 (36)	6 (66)	16 (53)
ITI	0.47 (78)	0.42 (87)	6.05 (32)	19.79 (131)	345 (65)	264 (64)	609 (26)	70 (9)	3.11 (27)	5.2 (60)	20 (15)	20 (20)	24 (30)**	50 (119)
SJ	0.43 (88)	††-	4.08 (24)	59.89 (115)	395 (15)	492 (79)	887 (45)	150 (34)	2.82 (31)	2.0 (35)	44 (33)	37 (60)	†	105 (92)
VM	0.54 (57)	††--	4.44 (45)	54.64 (80)	184 (39)	603 (73)	786 (55)	120 (28)	2.43 (23)	4.3 (48)	23 (42)	18 (31)	†	246 (84)

†† A zero-order input was used for the duration of nebulization. Values are expressed as mean estimates and coefficients of variation (%).Where Tlag: time to first detectable concentration, ka: absorption rate constant, Cl: central compartment clearance, Cl_{12}: intercompartimental clearance, V: central compartment volume, V_2: second compartment volume, Vdss/F: volume of distribution at steady T½: Elimination half-life, E0: mAP/mPAP ratio, EC50: milrinone concentration producing 50% of the effect, Δ Emax: amplitude of milrinone effect on the mAP/mPAP ratio. ITA: intratracheal atomization, ITI: intratracheal intillation, SJ: simple jet nebulization and VM: vibrating mesh nebulization.* $p<0.05$ versus ITI, SJ and VM;** $p<0.05$ versus ITA;† Similar to nebulization time

Figures

Figure 1. Time flow chart of procedure durations during a typical animal protocol.

Figure 2. Individual full milrinone plasma concentration-time profiles (0-360 min).

Figure 3. Individual milrinone plasma concentration-time profiles (0-20 min) and effect (mean systemic arterial pressures (mAP) over mean pulmonary arterial pressures (mPAP) ratio) versus time profiles (0-60 min).

Figure 4. Pooled individual observed versus predicted plasma concentrations and mAP (mean arterial systemic pressures) over mPAP (mean pulmonary arterial pressures) ratio in swine having received high (50 μg/kg) or low (15 μg/kg) milrinone target doses though intratracheal instillation and atomization and simple jet and ultrasonic mesh nebulization using a potential infusion/first-order absorption two-compartment pharmacokinetic model and a sigmoid Emax pharmacodynamic model.

Figure 5. Pooled right atrium areas and right ventricular dimensions at end-diastole during normotension, pulmonary hypertension and after milrinone maximum effect for intratracheal atomization and simple jet and vibrating mesh nebulizations. Values are expressed as means ± standard deviation (n= 12).

*p<0.05

References

1. Denault AY, Deschamps A, Couture P. Intraoperative hemodynamic instability during and after separation from cardiopulmonary bypass. Seminars in cardiothoracic and vascular anesthesia 2010;14:165-82.
2. Reichert CL, Visser CA, van den Brink RB, Koolen JJ, van Wezel HB, Moulijn AC, Dunning AJ. Prognostic value of biventricular function in hypotensive patients after cardiac surgery as assessed by transesophageal echocardiography. J Cardiothorac Vasc Anesth 1992;6:429-32.
3. Davila-Roman VG, Waggoner AD, Hopkins WE, Barzilai B. Right ventricular dysfunction in low output syndrome after cardiac operations: assessment by transesophageal echocardiography. Ann Thorac Surg 1995;60:1081-6.
4. Denault AY, Pearl RG, Michler RE, Rao V, Tsui SS, Seitelberger R, Cromie M, Lindberg E, D'Armini AM. Tezosentan and right ventricular failure in patients with pulmonary hypertension undergoing cardiac surgery: the TACTICS trial. J Cardiothorac Vasc Anesth 2013;27:1212-7.
5. Denault AY, Bussieres JS, Arellano R, Finegan B, Gavra P, Haddad F, Nguyen AQ, Varin F, Fortier A, Levesque S, Shi Y, Elmi-Sarabi M, Tardif JC, Perrault LP, Lambert J. A multicentre randomized-controlled trial of inhaled milrinone in high-risk cardiac surgical patients. Can J Anaesth 2016.
6. Denault A, Deschamps A, Tardif J-C, Lambert J, Perrault L. Pulmonary hypertension in cardiac surgery. Current cardiology reviews 2010;6:1-14.
7. Buckley MS, Feldman JP. Nebulized milrinone use in a pulmonary hypertensive crisis. Pharmacotherapy 2007;27:1763-6.
8. Lamarche Y, Malo O, Thorin E, Denault A, Carrier M, Roy J, Perrault LP. Inhaled but not intravenous milrinone prevents pulmonary endothelial

dysfunction after cardiopulmonary bypass. J Thorac Cardiovasc Surg 2005;130:83-92.

9. Nguyen AQ, Theoret Y, Chen C, Denault A, Varin F. High performance liquid chromatography using UV detection for the quantification of milrinone in plasma: improved sensitivity for inhalation. J Chromatogr B Analyt Technol Biomed Life Sci 2009;877:657-60.
10. Haraldsson s A, Kieler-Jensen N, Ricksten SE. The additive pulmonary vasodilatory effects of inhaled prostacyclin and inhaled milrinone in postcardiac surgical patients with pulmonary hypertension. Anesth Analg 2001;93:1439-45, table of contents.
11. Gelvez J, Fakioglu H, Olarte JL, Soliz A, Totapally BR, Torbati D. Effect of aerosolized milrinone during drug-induced pulmonary hypertension in lambs. Pharmacol Res 2004;50:87-91.
12. Robitaille A, Denault AY, Couture P, Belisle S, Fortier A, Guertin MC, Carrier M, Martineau R. Importance of relative pulmonary hypertension in cardiac surgery: the mean systemic-to-pulmonary artery pressure ratio. J Cardiothorac Vasc Anesth 2006;20:331-9.
13. Hasegawa-Baba Y, Kubota H, Takata A, Miyagawa M. Intratracheal instillation methods and the distribution of administered material in the lung of the rat. J Toxicol Pathol 2014;27:197-204.
14. Lamarche Y, Perrault LP, Maltais S, Tetreault K, Lambert J, Denault AY. Preliminary experience with inhaled milrinone in cardiac surgery. Eur J Cardiothorac Surg 2007;31:1081-7.
15. Doolan LA, Jones EF, Kalman J, Buxton BF, Tonkin AM. A placebo-controlled trial verifying the efficacy of milrinone in weaning high-risk patients from cardiopulmonary bypass. J Cardiothorac Vasc Anesth 1997;11:37-41.
16. Swindle MM. Swine in the laboratory : surgery, anesthesia, imaging, and experimental techniques. 2nd ed. Boca Raton: CRC Press, 2007.

17. Lee KJ, Hernandez G, Gordon JB. Hypercapnic acidosis and compensated hypercapnia in control and pulmonary hypertensive piglets. Pediatr Pulmonol 2003;36:94-101.
18. Yavuz Y, Ronning K, Bakkelund K, Lyng O, Aadahl P, Marvik R, Gronbech JE. Hemodynamic and tissue blood flow responses to long-term pneumoperitoneum and hypercapnia in the pig. Surg Endosc 2006;20:1394-401.
19. Laffey JG, Engelberts D, Kavanagh BP. Buffering hypercapnic acidosis worsens acute lung injury. Am J Respir Crit Care Med 2000;161:141-6.
20. Gavra P, Laflamme M, Denault AY, Theoret Y, Perrault LP, Varin F. Use of nebulized milrinone in cardiac surgery; Comparison of vibrating mesh and simple jet nebulizers. Pulm Pharmacol Ther 2017;46:20-9.
21. Gavra P, Nguyen AQ, Theoret Y, Litalien C, Denault AY, Varin F. A specific and sensitive HPLC-MS/MS micromethod for milrinone plasma levels determination after inhalation in cardiac patients. Ther Drug Monit 2014;36:663-8.
22. Naeije R, Dewachter L. [Animal models of pulmonary arterial hypertension]. Rev Mal Respir 2007;24:481-96.
23. Halden E, Hedstrand U, Torsner K. Oleic acid lung damage in pigs. Acta Anaesthesiol Scand 1982;26:121-5.
24. Pullamsetti SS, Savai R, Schaefer MB, Wilhelm J, Ghofrani HA, Weissmann N, Schudt C, Fleming I, Mayer K, Leiper J, Seeger W, Grimminger F, Schermuly RT. cAMP phosphodiesterase inhibitors increases nitric oxide production by modulating dimethylarginine dimethylaminohydrolases. Circulation 2011;123:1194-204.
25. Sawamura F, Kato M, Fujita K, Nakazawa T, Beardsworth A. Tadalafil, a Long-Acting Inhibitor of PDE5, Improves Pulmonary Hemodynamics and Survival Rate of Monocrotaline-Induced Pulmonary Artery Hypertension in Rats. Journal of Pharmacological Sciences 2009;111:235-43.
26. Bianco JC, Qizilbash B, Carrier M, Couture P, Fortier A, Tardif JC, Lambert J, Denault AY. Is patient-prosthesis mismatch a perioperative

predictor of long-term mortality after aortic valve replacement? J Cardiothorac Vasc Anesth 2013;27:647-53.

27. Haddad F, Guihaire J, Skhiri M, Denault AY, Mercier O, Al-Halabi S, Vrtovec B, Fadel E, Zamanian RT, Schnittger I. Septal curvature is marker of hemodynamic, anatomical, and electromechanical ventricular interdependence in patients with pulmonary arterial hypertension. Echocardiography 2014;31:699-707.
28. Schreier H, McNicol KJ, Bennett DB, Teitelbaum Z, Derendorf H. Pharmacokinetics of detirelix following intratracheal instillation and aerosol inhalation in the unanesthetized awake sheep. Pharm Res 1994;11:1056-9.
29. Paret G, Mazkereth R, Sella R, Almog S, Mayan H, Lotan D, Ben-Abraham R, Barzilay Z, Ezra D. Atropine pharmacokinetics and pharmacodynamics following endotracheal versus endobronchial administration in dogs. Resuscitation 1999;41:57-62.
30. Bennett DB, Tyson E, Nerenberg CA, Mah S, de Groot JS, Teitelbaum Z. Pulmonary delivery of detirelix by intratracheal instillation and aerosol inhalation in the briefly anesthetized dog. Pharm Res 1994;11:1048-55.
31. Patton JS, Byron PR. Inhaling medicines: delivering drugs to the body through the lungs. Nat Rev Drug Discov 2007;6:67-74.
32. Avram MJ, Henthorn TK, Spyker DA, Krejcie TC, Lloyd PM, Cassella JV, Rabinowitz JD. Recirculatory pharmacokinetic model of the uptake, distribution, and bioavailability of prochlorperazine administered as a thermally generated aerosol in a single breath to dogs. Drug Metab Dispos 2007;35:262-7.
33. Ari A. Jet, Ultrasonic, and Mesh Nebulizers: An Evaluation of Nebulizers for Better Clinical Outcomes. Eurasian Journal of Pulmonology 2014;16:1-7.
34. Gavra P, Laflamme M, Denault AY, Theoret Y, Perrault LP, Varin F. Use of nebulized milrinone in cardiac surgery; comparison of vibrating mesh

and simple jet nebulizers. LID - S1094-5539(16)30174-2 [pii] LID - 10.1016/j.pupt.2017.08.004 [doi].

35. Alousi A. Milrinone. New Drugs Annual: Cardiovascular drugs 1985;3.
36. Butterworth JF, James RL, Hines RL, Royster RL. A Pharmacokinetic and Pharmacodynamic Evaluation Milrinone in Adults Undergoing Cardiac Surgery. Anesthesia & Analgesia 1995:783-92.
37. Ramamoorthy C, Anderson GD, Williams GD, Lynn AM. Pharmacokinetics and side effects of milrinone in infants and children after open heart surgery. Anesth Analg 1998;86:283-9.
38. Agu RU, Ugwoke MI, Armand M, Kinget R, Verbeke N. The lung as a route for systemic delivery of therapeutic proteins and peptides. Respiratory research 2001;2:198-209.
39. Giraudel JM, Diquelou A, Laroute V, Lees P, Toutain PL. Pharmacokinetic/pharmacodynamic modelling of NSAIDs in a model of reversible inflammation in the cat. Br J Pharmacol 2005;146:642-53.
40. Hirakawa S, Ito H, Sahashi T, Takai K, Wada H. Effects of milrinone on systemic capacitance vessels in relation to venous return and right ventricular pump function. Journal of Cardiovascular Pharmacology 1992;19:96-101.

SECTION III: CONCLUSION

CHAPTER 13: General Discussion

The body of works within this thesis aimed at documenting and understanding the relative efficacy and impact of the various pulmonary administration methods for milrinone and hopefully linking milrinone pharmacodynamic effect on the mPAP/mAP ratio to its pharmacokinetic profile for each type of administration. Human data warranted animal backtranslation as it showed pressing issues which could not be resolved in humans. The studies performed in the context of this thesis span many types of research, ranging from pharmaceutical *in vitro, animal in vivo and ex vivo* and in parallel, to clinical.

The first research section involved the identification and quantification of the surgical artefacts affecting PK/PD determination of milrinone. Secondly, a new HPLC-MS/MS method was developed in order to compensate for the lack of specificity the previous method presented. These essential preliminaries were followed by studies that compared the *in vivo* and *ex vivo* efficacy of the simple jet and vibrating mesh nebulizer in a CPB experimental animal model. Lastly and most importantly, a new hypercapnic animal model was developed and was used to determine the PK/PD of milrinone under four types of pulmonary administrations.

13.1 Quantification of surgical artefacts

The first manuscript addressed the surgical artefacts plaguing human pharmacodynamic data. During PD analysis of human data, high fluctuations of the ratio interfered with the creation of a model describing the hemodynamic effects of milrinone (thesis of Dr Anne Nguyen). The surgical manipulations occurring during nebulization were associated with peaks and troughs in the mPAP/mAP ratio, preventing an optimal use of PK/PD modeling. Indeed, a workaround solution was to demonstrate a correlation between AUC of milrinone concentration and AUC of the ratio during nebulization. However, this method

does not allow prediction of plasma and effect at each time point and consequently, simulations are impossible. For the purposes of developing a PK/PD model, data devoid of surgical artefacts was needed. However, such this experimental condition is very difficult to enforce during human cardiac surgery, thus necessitating a return to an animal model.

In this study, the animal model described by Lamarche et al to first show the benefits of inhaled over intravenous milrinone was used [23]. The hemodynamic parameters were closely monitored in absence of milrinone administration, in order to clearly determine the duration and full impact of the hemodynamic artefacts resulting from each surgical manipulation. This paper identified the major artefacts appearing during the CPB preparation phase and quantified effects as high as 30% of baseline on the mAP/mPAP ratio, the biomarker of choice for describing the effects of milrinone. In addition, it was found that these artefacts can last for up to 7 min which amounts to half of the usual nebulizing time for milrinone and as such, potentially inserts a large bias in milrinone effect characterization.

The results of this research were highly variable due to the many factors involved. Firstly, surgeons did not receive specific instructions regarding the expected speed of the CPB preparation that would be representative of an operating room context. In addition, the different surgeons were surgical fellows with different degree of experience and, consequently, the response of each animal to the manipulations varied greatly. For example, recovered suction liquid, which takes into account blood losses, varied between 100 to more than 2000mL. This degree variation for fluid losses could easily affect the mAP/mPAP ratio as they have a direct effect on hemodynamics. These results clearly showed the necessity of a surgical-free animal model.

13.2 Bioanalytical method

Analytical method choice is a paramount factor in the success of a pharmacokinetic study. A major issue that arose in the clinical setting was the concomitant administration of several medications. This issue directly impacts on the success of sample analysis as it affects the specificity of the method. The initial HPLC-UV analytical method developed by Nguyen et al [143] proved to have insufficient selectivity in the isolation of milrinone, showing chromatographical interaction at its retention time with other endogenous or exogenous compounds. A new method was thus required in order to quantify milrinone in clinical samples. Through collaboration with Dr. Yves Théorêt at the clinical pharmacology department of Sainte-Justine hospital, an HPLC tandem mass spectrometry method was developed. The novel method was also meant to offer the possibility of being used in a pediatric context. The scope of this work was to create a method as specific to milrinone while maintaining a low clinical sample volume. The liquid-liquid extraction was downsized from a previous method developed by Gavra and Nguyen et al presented in Annexe I [144]. The mobile phase was also adapted. The HPLC-MS/MS method provided substantial ameliorations such as a 0.3125 ng/mL lower limit of quantification, in comparison to the previous 1.25 ng/mL, a 5 times faster analysis time and a 20 times lower sample volume (50 µl). This new method was subsequently used in the pharmacokinetic analysis (excerpts showed in Annexe II) of a multicenter clinical research trial investigating the effect of inhaled milrinone pre-CPB administration on clinical outcomes [145] and showed no selectivity issues.

Tu en as eu besoin pour la nebulization aussi, compte tenu des très faibles concentrations donc sensibilité

13.3 *In vitro, in vivo and ex vivo* nebulizer studies

Nebulization is a pulmonary administration method offering many advantages, such as good bioavailability, fast effect and non-invasive administration. This

method has seen several generations of devices capable of transforming a volume of liquid into a breathable mist. This mist and the size of particles within it, are important factors to be taken into account when delivering medication to the lung. This information combined with ventilation characteristics and drug physicochemical properties are considered as the major factors in drug deposition [89, 146, 147].

13.3.1 *In vitro* studies

In vitro studies were performed in order to determine the physical properties of the particles generated by the two nebulizers, SJ and VM. Determination of these properties was performed using industry gold NGI Generation Impactor. The breath simulator was required for generating stable ventilation parameters during characterisation of nebulizer emitted dose and determination of particle size distribution for each of the nebulizers. This distribution was thought to play a key role in the target location of deposition of each of nebulizer.

Setting up the methodology for the *in vitro* testing was in itself a challenge. To obtain quantitative recovery of milrinone from nebulizer and impactor components, several solutions were tested in order to identify one that ensures optimal milrinone desorption. These components included ventilation filters during determination of emitted and inhaled doses as well as all impactor sections during particle size determination. Particles being of size of the order of microns, their bouncing off metal components represented an issue which was resolved through the use of silicone. A disadvantage of the Copley breath simulator is that it generates breathing patterns through only one port in a sinusoid push/pull fashion. This particularity sets it apart from operating room ventilators which function using two ports, one for air input and another for output. An additional issue in acquiring i*n vitro* data was choosing temperature and humidity conditions. The characterization of low mean aerodynamic diameter particles requires low temperatures (7°C) in order to prevent droplet

evaporation. These temperatures prevent the use of high humidity as condensation occurs. These factors however affect the hygroscopicity of generated liquid particles and not taking them into account underestimates the determined size [148].

13.3.2 *In vivo and ex vivo* studies

The particle size distribution generated by the SJ and VM nebulizers was believed to have a direct impact on their intrapulmonary deposition and thus, on the amount of milrinone thought to be delivered to the optimal tracheobronchial effect site, up until the sixteenth to nineteenth tracheobronchial tree generations. Although PDEIII is not yet determined, its distribution is known to differ in the bronchial tree. We assumed that this differential deposition pattern would translate into a difference in milrinone efficacy between the two nebulizers and consequently the *in vitro* efficiency in endothelial-dependent relaxation of the pulmonary arteries. To determine this difference between nebulizers, a comparative study with a methodology similar to that used by Lamarche et al's[23] was followed. with the exception that both SJ and VM were used to administer milrinone before CPB. Lungs were subsequently removed and endothelial-dependent relaxation responses to increasing acetylcholine and bradykinin concentrations were recorded *in vivo* and *ex vivo* data collection study was executed by Dr Maxime Laflamme at the Montreal Heart Institute. Data clean-up and PD modeling was performed later in our laboratory.

IN VIVO

Our in vivo study was congruent with literature data showing a prophylactic effect of milrinone on the ratio following weaning from CPB. In our study, the ratio was maintained up 30 min after weaning. Our study also showed improved oxygenation for the groups having received milrinone. Our study was however unable to show a significant difference in hemodynamic parameters and blood gases between types of nebulizations. On the other, taking into account the in

vitro section results from this study, we can affirm that the beneficial effect from SJ administration was executed by half the inhaled dose, implying a better efficacy of the SJ method.

EX VIVO

Relaxation data required a thorough reanalysis to ascertain the accuracy of the proposed baseline. Indeed, certain discrepancies were found pertaining to arterial phenylephrine contractions that serve for the establishment of the 100% value (or I_0). Some arteries were found not having reached full phenylephrine contraction before relaxation with ACh or Bk was begun. For this reason, modeling of the relaxation profiles did not include a fixed I_0 as initially intended for the inhibitory sigmoid Emax model. Similarly, maximum relaxation was sometimes not maintained until the end of the protocol causing a rise in contraction at the end of the sigmoid that added variability in the estimated Emax and required data cleaning.

Endothelial-dependent relaxations of pulmonary arteries were all modeled individually, which generated a great number of individual analyses. However, not all animals provided the same number of data since some arterial rings did not always perform consistently. This inconsistency between the numbers of arteries originating from each animal suggested the need of determining an analysis method normalizing the mean parameters of each animal according to their number of performing arteries. The solution to this issue was a statistical analysis per animal through linear mixed effects modeling including a weight proportional to the number of arteries per animal. This methodology allows for a statistical analysis of animals per nebulization while maintaining the power of the number of individual arteries, thus reducing bias. In comparison with previous analysis methodology, where mean values calculated per animal, linear mixed effects modeling allowed a clear statistical analysis of data and provided a basis upon to compare not only milrinone versus saline but also the two milrinone administration methods themselves.

13.4 PK/PD model

Following the *in vitro, in vivo* and *ex vivo* experimentation, it became clearer that the administration method does indeed have a significant impact on the efficacy of pulmonary milrinone. The SJ and VM nebulizations are not, however, the only pulmonary administration methods used in the clinical setting for milrinone. In emergency cases, milrinone is also instilled intratracheally as a bolus dose using a regular syringue. The latter administration has, nevertheless, the major drawback of a high variability that is mostly related to the physical characteristics of the subject. Depending on the form and shape of the subject's tracheobronchial tree and the positioning, the instilled substance will reach, unpredictably, different sections of the lungs (though preferentially dorsal if the subject in in a horizontal position [120]. To overcome the potential disadvantages of the bolus, an intratracheal atomization administration was proposed as an alternative.

These four methods of pulmonary administration generate very distinct particle size distributions. SJ and VM nebulization show bimodal particle size distributions where nearly 40 and 20% of the dose, respectively, is delivered as large particles to the upper bronchi while the remaining targets the lower bronchi and alveolar regions. Intratracheal methods generate a very different type of distribution. Intratracheal instillation has no defined particle size distribution, since all particles are larger than 14 microns. Alternately, intratracheal atomization using the MADett® generates particles ranging roughly from 10 to 100 microns with a 30 micron average (data kindly provided by Wolfe Tory Medical Inc.). These distinct distribution patterns were thought to be an underlying factor that would potentially result in differences in milrinone pharmacokinetics and, consequently, pharmacodynamics. This hypothesis deserved further investigation.

13.4.1 Animal model

The choice of experimentation animal model for this investigation was based on several factors. Even though our initial choice was the CPB swine model used by Dr. Lamarche, several other options were considered. The CPB model posed the problem of surgical manipulations and added the logistical difficulties and costs of CPB. Pulmonary lung damage models using oleic acid, monocrotaline, embolies and TXA_2 analogues were also considered. These models, for the most part, are time consuming and generate unpredictable effects. The best option was finally considered to be a hypercapnic swine pulmonary hypertension model. This model allowed a titratable pulmonary effect on arterial pressure that caused no physical damage. Adjustments of the ventilation parameters were found to be easily controllable and bore no additional cost. Four animals randomly allocated to different types of administration were used to optimize the protocol when adjustments in blood biochemistry are required to stabilize the hemodynamic status of the animal and, consequently, prevent any impact on milrinone pharmacokinetic or pharmacodynamic parameters. Initially, pH was not controlled, resulting in a reduction of arterial pH, an increase in HCO_3- levels and lactate production. In addition, lack of pH management caused a decrease in systemic pressures and cardiac frequency. Following pH management with tromethamine infusion and, at need, additional bolus administration, hemodynamic parameters and blood biochemistry showed only slight change, in accordance to literature [56] Respiratory acidosis was however not fully controlled as it is necessary to obtain the increase in pulmonary pressures [149].

13.4.2 Pharmacokinetic Modeling

The PK of milrinone is not entirely new as it has been already characterized after intravenous administration. [150-153] However, the choice of PK model to best describe data is still subject to debate. Two studies [151, 153] having characterized the full PK profile in cardiac patients opted for a tri-compartmental

model, the other studies used bi-compartmental. In our animal data, the model offering the best fit after various mode of pulmonary administration was either bi- or mono-compartmental. Two animals out of twelve showed marginally better statistical diagnostics (parameter coefficients of variation and distribution of residuals) for one- rather than two- compartments. For the sake of uniformity, a two-compartment model was selected. In addition, literature supports the use of a bi-compartmental model in determining milrinone PK in a heart failure patient population [154, 155]. Indeed, during the PK analysis of most of our animal data, the two-compartment model described effectively plasma milrinone concentration. Furthermore, addition of a third compartment increased exponentially individual parameter variation coefficients. The estimated pulmonary milrinone PK parameters using the two-compartment model were similar to those obtained previously through non-compartmental analysis and were also similar to those reported for intravenous milrinone in cardiac surgery undergoing CPB [150, 152] and in patients with heart failure.[154-156]

Based on existing literature, we chose to model the absorption using zero-order input for nebulizations [10, 157] and first-order input for intratracheal administrations. When intending to apply a first-order absorption to nebulizations, C_{max} was not accurately fitted. Of the twelve animals, only one following intratracheal instillation showed a substantially slower absorption than other animals as indicated by the 120 min T_{max} and a Ka of 0.009 min^{-1}. The pharmacokinetic protocol for this particular animal had to be interrupted as it exhibit large changes in hemodynamic parameters following the 120 min mark.

Initial dosing used for modeling was the target dose. However, first modeling using these doses revealed a discrepancy between estimated clearance and literature, indicating that bioavailabilty, specifically for intratracheal administrations, was unaccounted for. Subsequent urine analysis then revealed that systemic bioavailability of the latter was substantially lower than first thought. When using amount recovered unchanged in urine instead of inhaled doses, r^2 between dose and plasma AUC increased from 0.17 to 0.88.

Analysis of urine samples was performed at CHU Sainte Justine using a modified methodology based on our previous work.[158] Urine samples analyzed with the unmodified method exhibited fluctuations in the peak height of the internal standard olprinone. This problem was fully solved by diluting urine samples with animal plasma prior to extraction. Modeling revealed high distributional clearances for the nebulizations suggesting a higher pulmonary retention.

.

13.4.3 Pharmacodynamic modeling.

Effect modeling was based on a sigmoid Emax model. Linear and indirect relationships between PK and PD were also tested. When testing the Emax model, an effect compartment was also tried but the estimated Ke_0 values were found high enough to indicate that the compartment was unnecessary. The need for a Hill coefficient was also debated. Four of the twelve animals required γ for the convergence of the model, however this parameter showed the highest interindividual variability.

Analysis of the PK/PD relationship of milrinone was shown to be different between the methods of administration. The maximum determined effect was not linked to the administration method generating the highest plasma concentrations. On the contrary, it was linked to the one showing the lowest, indicating that systemic concentrations are not responsible for the effect that is perhaps local. Our hypothesis was that ITA would provide the best effect as it allows, in theory, an even intrapulmonary coating of the upper tracheobronchial tree. In practice, this form of administration required more active intraoperative volume and pH management due to a higher prevalence of high cardiac frequency spikes. The method having distinguished itself the most was SJ. E_{max} for the latter was the highest out of all methods and it also showed the lowest EC_{50}. These results are congruent with our *ex-vivo* study where SJ milrinone

administration allowed the highest relaxation and sensitivity to ACh. Another common point between the *ex vivo* and PKPD study was the high values of the Hill coefficient. The estimated values were found to be too high to represent a physiological mechanism other than an all-or-nothing effect. This all-or-nothing effect is however of note as the Hill coefficient is indicative of sensitivity and very high values indicate a threshold effect [159]. Once the this effect threshold is reached, there might be no need to increase doses as they might only trigger a baroreflex response [160].

During experimentation, the effect of the oxygen vector was also verified by saline administration at the end of the protocol before sacrifice and none was found. This effect was not analyzed during modeling.

13.5 Conclusions and Perspectives

Applied to the field of cardiac surgery, the use of drugs administered via the lungs has changed considerably in recent years. Methods have evolved and new methods have appeared. Our first in vivo study aimed at exploring the advantages of the initial form of clinical nebulization, by simple jet over a newer version, by vibrating mesh. The main scope of our second study was to further exploring the differences between the two nebulizations at a pharmacokinetic and pharmacodynamic level and comparing these two forms to the intratracheal instillation emergency administration and a possible new method by atomization.

These studies open up new avenues of research as they bring about several questions related to the differential absorption of different pulmonary generations and theories about how to better target them. These hypotheses are however based on an incomplete knowledge of the human lung. Further research is need on the pulmonary retention of milrinone and the pulmonary localisation of its target in human pulmonary arteries in all levels of the tracheobronchial tree.

In addition, these scientific works focus on the acute effect of milrinone. The endothelial relaxation studies indicated a persistent effect however our PK/PD does not address milrinone prophylaxis in cardiac surgery.

These studies show an evolution of the techniques used to administer milrinone to the lungs. It helped to better understand the issues related to the characterization of pulmonary therapies in the context of cardiac surgery. A PK/PD model was developed linking the concentration of plasma milrinone to its effect on measures of the mAP/mPAP ratio, a specific biomarker thus allowing us to identify the administration method providing the highest benefit

The determination of the PK/PD relationship will potentially play a role in predicting the impact of dose changes on drug duration and intensity and, consequently, possibly provide an optimal dosing regimen to improve its clinical use.

13.6 References

1. Buckley, M.S. and J.P. Feldman, *Nebulized milrinone use in a pulmonary hypertensive crisis.* Pharmacotherapy, 2007. **27**: p. 1763-6.
2. Denault, A.Y., A. Deschamps, and P. Couture, *Intraoperative hemodynamic instability during and after separation from cardiopulmonary bypass.* Seminars in cardiothoracic and vascular anesthesia, 2010. **14**: p. 165-82.
3. Denault, A.Y., et al., *Difficult and Complex Separation from Cardiopulmonary Bypass in High-Risk Cardiac Surgical Patients: A Multicenter Study.* Journal of cardiothoracic and vascular anesthesia, 2012. **xx**: p. 1-9.
4. Denault, A., et al., *Pulmonary hypertension in cardiac surgery.* Current cardiology reviews, 2010. **6**: p. 1-14.
5. Scanlon, V.C. and T. Sanders, *Essentials of anatomy and physiology*. 2nd ed. 1995, Philadelphia: F.A. Davis. xvii, 606 p.
6. Marieb, E.N., *Human anatomy and physiology*. 3rd ed. Benjamin/Cummings series in the life sciences. 1995, Redwood City, Calif. ; Don Mills, Ont.: Benjamin/Cummings. xxxii, 1040 , 83 p.
7. Levitzky, M.G., *Pulmonary physiology*. 6th ed. Lange physiology series. 2003, New York Toronto: McGraw-Hill, Medical Pub. Division. x, 278 p.
8. Phalen, R.F., *Inhalation studies : foundations and techniques*. 1984, Boca Raton, Fla.: CRC Press. 277 p.
9. Stuart, B.O., *Deposition and clearance of inhaled particles.* Environ Health Perspect, 1984. **55**: p. 369-90.
10. Patton, J.S. and P.R. Byron, *Inhaling medicines: delivering drugs to the body through the lungs.* Nat Rev Drug Discov, 2007. **6**(1): p. 67-74.
11. Olsson, B., et al., *Pulmonary Drug Metabolism, Clearance, and Absorption.* 2011: p. 21-50.

12. Frazier, A.A., et al., *From the archives of the AFIP: pulmonary vasculature: hypertension and infarction.* Radiographics, 2000. **20**(2): p. 491-524; quiz 530-1, 532.
13. Stenmark, K.R. and S.H. Abman, *Lung vascular development: implications for the pathogenesis of bronchopulmonary dysplasia.* Annu Rev Physiol, 2005. **67**: p. 623-61.
14. Majesky, M.W., et al., *The adventitia: a dynamic interface containing resident progenitor cells.* Arterioscler Thromb Vasc Biol, 2011. **31**(7): p. 1530-9.
15. Webb, R.C., *Smooth muscle contraction and relaxation.* Adv Physiol Educ, 2003. **27**(1-4): p. 201-6.
16. Gravlee, G.P., R.F. Davis, and J.R. Utley, *Cardiopulmonary bypass principles and practices*. 3rd ed. 2007, Philadelphia, Pa. ; London: Lippincott Williams & Wilkins. 1 texte électronique.
17. Alsatli, R.A., *Mini cardiopulmonary bypass: Anesthetic considerations.* Anesth Essays Res, 2012. **6**(1): p. 10-3.
18. Denault, A.Y., et al., *Inhaled milrinone: a new alternative in cardiac surgery?* Seminars in cardiothoracic and vascular anesthesia, 2006. **10**: p. 346-60.
19. Anyanwu, E., et al., *Ultrastructural changes in the human lung following cardiopulmonary bypass.* Basic research in cardiology, 1982. **77**: p. 309-322.
20. Courtney, J.M., et al., *Biomaterials in cardiopulmonary bypass.* Perfusion, 1994. **9**: p. 3-10.
21. Hind, C.R., et al., *Effect of cardiopulmonary bypass on circulating concentrations of leucocyte elastase and free radical activity.* Cardiovasc Res, 1988. **22**(1): p. 37-41.
22. Royston, D., *The inflammatory response and extracorporeal circulation.* J Cardiothorac Vasc Anesth, 1997. **11**(3): p. 341-54.

23. Lamarche, Y., et al., *Inhaled but not intravenous milrinone prevents pulmonary endothelial dysfunction after cardiopulmonary bypass.* J Thorac Cardiovasc Surg, 2005. **130**(1): p. 83-92.
24. Fortier, S., et al., *Inhaled prostacyclin reduces cardiopulmonary bypass-induced pulmonary endothelial dysfunction via increased cyclic adenosine monophosphate levels.* J Thorac Cardiovasc Surg, 2004. **128**(1): p. 109-16.
25. McGoon, M.D. and G.C. Kane, *Pulmonary hypertension: diagnosis and management.* Mayo Clin Proc, 2009. **84**(2): p. 191-207.
26. Klodell, C.T., Jr., *Secondary pulmonary hypertension: a review of the cardiac causes.* J Cardiovasc Nurs, 2005. **20**(2): p. 119-23.
27. Mikhail, G., et al., *An evaluation of nebulized prostacyclin in patients with primary and secondary pulmonary hypertension.* Eur Heart J, 1997. **18**(9): p. 1499-504.
28. Borges, a.C., et al., *Relationship between haemodynamics and morphology in pulmonary hypertension. A quantitative intravascular ultrasound study.* European heart journal, 1997. **18**: p. 1988-1994.
29. Keith, I.M., *The role of endogenous lung neuropeptides in regulation of the pulmonary circulation.* Physiol Res, 2000. **49**(5): p. 519-37.
30. Goldstein, D.J., et al., *Inhaled nitric oxide is not a negative inotropic agent in a porcine model of pulmonary hypertension.* J Thorac Cardiovasc Surg, 1997. **114**(3): p. 461-6.
31. Farber, H.W. and J. Loscalzo, *Pulmonary arterial hypertension.* N Engl J Med, 2004. **351**(16): p. 1655-65.
32. Christman, B.W., et al., *An imbalance between the excretion of thromboxane and prostacyclin metabolites in pulmonary hypertension.* N Engl J Med, 1992. **327**(2): p. 70-5.
33. Hache, M., et al., *Inhaled epoprostenol (prostacyclin) and pulmonary hypertension before cardiac surgery.* J Thorac Cardiovasc Surg, 2003. **125**(3): p. 642-9.

34. Steinhorn, R.H., *Pharmacotherapy for pulmonary hypertension.* Pediatr Clin North Am, 2012. **59**(5): p. 1129-46.
35. Marsboom, G.R. and S.P. Janssens, *Models for pulmonary hypertension.* Drug Discovery Today: Disease Models, 2004. **1**(3): p. 289-296.
36. Geiger, R., et al., *Tezosentan decreases pulmonary artery pressure and improves survival rate in an animal model of meconium aspiration.* Pediatr Res, 2006. **59**(1): p. 147-50.
37. Nicholls, M.G., et al., *Bioactivity of adrenomedullin and proadrenomedullin N-terminal 20 peptide in man.* Peptides, 2001. **22**(11): p. 1745-52.
38. Simonneau, G., et al., *Updated clinical classification of pulmonary hypertension.* J Am Coll Cardiol, 2013. **62**(25 Suppl): p. D34-41.
39. Couture, P., et al., *[La dysfonction ventriculaire diastolique gauche et droite comme prédicteur des difficultés de sevrage de la circulation extracorporelle].* Canadian Journal of Anesthesia, 2006: p. 1-10.
40. Robitaille, A., et al., *Importance of relative pulmonary hypertension in cardiac surgery: the mean systemic-to-pulmonary artery pressure ratio.* J Cardiothorac Vasc Anesth, 2006. **20**(3): p. 331-9.
41. Ocal, A., et al., *Efficiency of prostacyclin in the treatment of protamine-mediated right ventricular failure and acute pulmonary hypertension.* Tohoku J Exp Med, 2005. **207**(1): p. 51-8.
42. Sukernik, M.R., B. Mets, and E. Bennett-Guerrero, *Patent foramen ovale and its significance in the perioperative period.* Anesth Analg, 2001. **93**(5): p. 1137-46.
43. Bubb, K.J., et al., *Inhibition of Phosphodiesterase 2 Augments cGMP and cAMP Signaling to Ameliorate Pulmonary Hypertension.* Circulation, 2014. **130**: p. 496-507.
44. Jaenke, R.S. and A.F. Alexander, *Fine structural alterations of bovine peripheral pulmonary arteries in hypoxia-induced hypertension.* Am J Pathol, 1973. **73**(2): p. 377-98.

45. Naeije, R. and L. Dewachter, *[Animal models of pulmonary arterial hypertension].* Rev Mal Respir, 2007. **24**(4 Pt 1): p. 481-96.
46. Gelvez, J., et al., *Effect of aerosolized milrinone during drug-induced pulmonary hypertension in lambs.* Pharmacol Res, 2004. **50**(1): p. 87-91.
47. Halden, E., U. Hedstrand, and K. Torsner, *Oleic acid lung damage in pigs.* Acta Anaesthesiol Scand, 1982. **26**(2): p. 121-5.
48. Dawson, J.R., R.D. Cressman, and A. Blalock, *Experimental hypertension and pregnancy in dogs.* Am J Pathol, 1941. **17**(1): p. 31-38 3.
49. Chu, D., et al., *A new animal model for pulmonary hypertension based on the overexpression of a single gene, angiopoietin-1.* Ann Thorac Surg, 2004. **77**(2): p. 449-56; discussion 456-7.
50. Balanos, G.M., et al., *Human pulmonary vascular response to 4 h of hypercapnia and hypocapnia measured using Doppler echocardiography.* Journal of applied physiology (Bethesda, Md. : 1985), 2003. **94**: p. 1543-51.
51. Kiely, D.G., R.I. Cargill, and B.J. Lipworth, *Effects of Hypercapnia on Hemodynamic, Inotropic, Lusitropic, and Electrophysiologic Indices in Humans.* Chest, 1996. **109**(5): p. 1215-1221.
52. Auer, L.M. and B.B. Johansson, *Dilatation of pial arterial vessels in hypercapnia and in acute hypertension.* Acta physiologica Scandinavica, 1980. **109**: p. 249-51.
53. Borst, H.G., et al., *Effects of unilateral hypoxia and hypercapnia on pulmonary blood flow distribution in the dog.* Am J Physiol, 1957. **191**(3): p. 446-52.
54. Domkowski, P.W., et al., *Pulmonary hydraulic impedance responses to hypoxia and hypercapnia in newborn pigs.* J Appl Physiol (1985), 1994. **77**(1): p. 386-96.
55. Lee, K.J., G. Hernandez, and J.B. Gordon, *Hypercapnic acidosis and compensated hypercapnia in control and pulmonary hypertensive piglets.* Pediatr Pulmonol, 2003. **36**(2): p. 94-101.

56. Weber, T., et al., *Tromethamine buffer modifies the depressant effect of permissive hypercapnia on myocardial contractility in patients with acute respiratory distress syndrome.* Am J Respir Crit Care Med, 2000. **162**(4 Pt 1): p. 1361-5.
57. Yavuz, Y., et al., *Hemodynamic and tissue blood flow responses to long-term pneumoperitoneum and hypercapnia in the pig.* Surg Endosc, 2006. **20**(9): p. 1394-401.
58. Rothman, A., et al., *Hemodynamic and histologic characterization of a swine (Sus scrofa domestica) model of chronic pulmonary arterial hypertension.* Comp Med, 2011. **61**(3): p. 258-62.
59. Wu, J., et al., *Hemodynamics and right-ventricle functional characteristics of a swine carotid artery-jugular vein shunt model of pulmonary arterial hypertension: An 18-month experimental study.* Exp Biol Med (Maywood), 2015. **240**(10): p. 1362-72.
60. Sundaram, V. and J.C. Fang, *Gastrointestinal and Liver Issues in Heart Failure.* Circulation, 2016. **133**(17): p. 1696.
61. Alousi, A., *Milrinone.* New Drugs Annual: Cardiovascular drugs, 1985. **3**.
62. Farah, A.E., A.A. Alousi, and R.P. Schwarz, Jr., *Positive inotropic agents.* Annu Rev Pharmacol Toxicol, 1984. **24**: p. 275-328.
63. Mylotte, K.M., et al., *Milrinone and thyroid hormone stimulate myocardial membrane Ca2+-ATPase activity and share structural homologies.* Proc Natl Acad Sci U S A, 1985. **82**(23): p. 7974-8.
64. Satoh, K., et al., *Implication of protein kinase A for a hepato-protective mechanism of milrinone pretreatment.* J Surg Res, 2009. **155**(1): p. 32-9.
65. Lamarche, Y., et al., *Preliminary experience with inhaled milrinone in cardiac surgery.* Eur J Cardiothorac Surg, 2007. **31**(6): p. 1081-7.
66. Lakshminrusimha, S., et al., *Milrinone enhances relaxation to prostacyclin and iloprost in pulmonary arteries isolated from lambs with persistent pulmonary hypertension of the newborn.* Pediatr Crit Care Med, 2009. **10**(1): p. 106-12.

67. Rashid, N., et al., *Effects of prostacyclin and milrinone on pulmonary hemodynamics in newborn lambs with persistent pulmonary hypertension induced by ductal ligation.* Pediatr Res, 2006. **60**(5): p. 624-9.
68. Shipley, J.B., et al., *Milrinone: basic and clinical pharmacology and acute and chronic management.* Am J Med Sci, 1996. **311**(6): p. 286-91.
69. Hasei, M., et al., *Correlation between plasma milrinone concentration and renal function in patients with cardiac disease.* Acta Anaesthesiol Scand, 2008. **52**(7): p. 991-6.
70. Joynt, C., et al., *Dose-response effects of milrinone on hemodynamics of newborn pigs with hypoxia-reoxygenation.* Intensive Care Med, 2008. **34**(7): p. 1321-9.
71. Butterworth, J.F., et al., *A Pharmacokinetic and Pharmacodynamic Evaluation Milrinone in Adults Undergoing Cardiac Surgery.* Anesthesia & Analgesia, 1995: p. 783-792.
72. Hardy, J.F. and S. Belisle, *Inotropic support of the heart that fails to successfully wean from cardiopulmonary bypass: the Montreal Heart Institute experience.* J Cardiothorac Vasc Anesth, 1993. **7**(4 Suppl 2): p. 33-9.
73. Wang, H., et al., *Comparison of inhaled and intravenous milrinone in patients with pulmonary hypertension undergoing mitral valve surgery.* Adv Ther, 2009. **26**(4): p. 462-8.
74. Sablotzki, A., et al., *Selective pulmonary vasodilation with inhaled aerosolized milrinone in heart transplant candidates.* Can J Anaesth, 2005. **52**(10): p. 1076-82.
75. Guo, H.W., et al., *[Effect of inhaling specific phosphodiesterase inhibitor on lung injury induced by cardiopulmonary bypass].* Zhonghua Yi Xue Za Zhi, 2011. **91**(20): p. 1401-4.
76. Gong, M., et al., *Preoperative inhalation of milrinone attenuates inflammation in patients undergoing cardiac surgery with cardiopulmonary bypass.* Med Princ Pract, 2012. **21**(1): p. 30-5.

77. Berlinski, A. and J.R. Willis, *Albuterol delivery by 4 different nebulizers placed in 4 different positions in a pediatric ventilator in vitro model.* Respir Care, 2013. **58**(7): p. 1124-33.
78. Ari, A., *Jet, Ultrasonic, and Mesh Nebulizers: An Evaluation of Nebulizers for Better Clinical Outcomes.* Eurasian Journal of Pulmonology, 2014. **16**(1): p. 1-7.
79. Muchao, F.P. and L.V. Filho, *Advances in inhalation therapy in pediatrics.* J Pediatr (Rio J), 2010. **86**(5): p. 367-76.
80. Kleinstreuer, C., Y. Feng, and E. Childress, *Drug-targeting methodologies with applications: A review.* World J Clin Cases, 2014. **2**(12): p. 742-56.
81. Labiris, N.R. and M.B. Dolovich, *Pulmonary drug delivery. Part I: Physiological factors affecting therapeutic effectiveness of aerosolized medications.* British Journal of Clinical Pharmacology, 2003. **56**(6): p. 588-599.
82. Huang, J. and L. Zhang, *Micro-particle deposition and lobar distribution of mass flow in human upper respiratory tract model.* Chinese Science Bulletin, 2011. **56**(4-5): p. 380-385.
83. Hofmann, W., *Modelling particle deposition in human lungs: modelling concepts and comparison with experimental data.* Biomarkers, 2009. **14 Suppl 1**: p. 59-62.
84. Liu, Y., R.M. So, and C.H. Zhang, *Modeling the bifurcating flow in an asymmetric human lung airway.* J Biomech, 2003. **36**(7): p. 951-9.
85. Olschewski, H., et al., *Pharmacodynamics and Pharmacokinetics of Inhaled Iloprost, Aerosolized by Three Different Devices, in Severe Pulmonary Hypertension.* Chest, 2003. **124**(4): p. 1294-1304.
86. Agu, R.U., et al., *The lung as a route for systemic delivery of therapeutic proteins and peptides.* Respiratory research, 2001. **2**: p. 198-209.
87. Stahlhofen, W., J. Gebhart, and J. Heyder, *Experimental determination of the regional deposition of aerosol particles in the human respiratory tract.* Am Ind Hyg Assoc J, 1980. **41**(6): p. 385-98a.

88. Newman, S.P., *Aerosol Deposition Considerations in Inhalation Therapy.* Chest, 1985. **88**(2): p. 152S-160S.
89. Anderson, J.C., et al., *Effect of ventilation rate on instilled surfactant distribution in the pulmonary airways of rats.* Journal of applied physiology (Bethesda, Md. : 1985), 2004. **97**: p. 45-56.
90. Copley, M., *Nebulizer testing.* 2008.
91. Byron, P.R., *Drug delivery devices: issues in drug development.* Proceedings of the American Thoracic Society, 2004. **1**: p. 321-328.
92. Shekunov, B.Y., et al., *Particle size analysis in pharmaceutics: principles, methods and applications.* Pharm Res, 2007. **24**(2): p. 203-27.
93. Abdelrahim, M.E., *Aerodynamic characteristics of nebulized terbutaline sulphate using the Andersen Cascade Impactor compared to the Next Generation Impactor.* Pharmaceutical development and technology, 2011. **16**: p. 137-45.
94. Dunbar, C. and J. Mitchell, *Analysis of cascade impactor mass distributions.*, in *Journal of aerosol medicine : the official journal of the International Society for Aerosols in Medicine*. 2005. p. 439-51.
95. Taki, M., et al., *Aerodynamic deposition of combination dry powder inhaler formulations in vitro: a comparison of three impactors.* Int J Pharm, 2010. **388**(1-2): p. 40-51.
96. Wong, W., et al., *Pharmacopeial methodologies for determining aerodynamic mass distributions of ultra-high dose inhaler medicines.* J Pharm Biomed Anal, 2010. **51**(4): p. 853-7.
97. Mitchell, J.P. and M.W. Nagel, *Cascade impactors for the size characterization of aerosols from medical inhalers: their uses and limitations.* J Aerosol Med, 2003. **16**(4): p. 341-77.
98. Le, J., et al., *Consensus summary of aerosolized antimicrobial agents: application of guideline criteria. Insights from the Society of Infectious Diseases Pharmacists.* Pharmacotherapy, 2010. **30**(6): p. 562-84.
99. Mitchell, J.P., et al., *Aerodynamic particle size analysis of aerosols from pressurized metered-dose inhalers: comparison of Andersen 8-stage*

cascade impactor, next generation pharmaceutical impactor, and model 3321 Aerodynamic Particle Sizer aerosol spectrometer. AAPS PharmSciTech, 2003. **4**(4): p. E54.

100. Snyder, L.R., J.J. Kirkland, and J.L. Glajch, *Practical HPLC method development*, in *Wiley online books UBCM Chemistry 2000*. 1997, Wiley,: New York. p. 1 online resource (xxvi, 765 pages).
101. Meyer, V. and John Wiley & Sons., *Practical high-performance liquid chromatography*, in *Wiley online books UBCM Chemistry 2000*. 2004, John Wiley,: Chichester, England. p. xv, 357 pages.
102. Quintero, A., et al., *Validation of an HPLC method for sildenafil citrate analysis in human plasma samples.* Pharmazie, 2009. **64**(12): p. 796-9.
103. Hoffmann, E.d. and V. Stroobant, *Mass spectrometry : principles and applications*. 2nd ed. 2002, Chichester ; Toronto: Wiley. xii, 407 p.
104. Banerjee, S. and S. Mazumdar, *Electrospray Ionization Mass Spectrometry: A Technique to Access the Information beyond the Molecular Weight of the Analyte.* International Journal of Analytical Chemistry, 2012. **2012**: p. 1-40.
105. Cooper, G.M. and R.E. Hausman, *The cell : a molecular approach*. Sixth edition ed. 2013, Sunderland, Massachusetts: Sinauer Associates. xxv, 832 pages.
106. Mustapha, R.B., et al., *Influence of drug concentration on the diffusion parameters of caffeine.* Indian J Pharmacol, 2011. **43**(2): p. 157-62.
107. Lin, J.H. and M. Yamazaki, *Role of P-glycoprotein in pharmacokinetics: clinical implications.* Clin Pharmacokinet, 2003. **42**(1): p. 59-98.
108. Lin, J.H. and M. Yamazaki, *Clinical relevance of P-glycoprotein in drug therapy.* Drug Metab Rev, 2003. **35**(4): p. 417-54.
109. Aiache, J.M., *Traité de biopharmacie et pharmacocinétique*. 2e éd. ev. et augm. ed. 1990, Paris Montréal: Éditions Vigot ; Presses de l'Université de Montréal. 384 p.
110. Gibaldi, M., *Biopharmaceutics and clinical pharmacokinetics*. 4th ed. 1991, Philadelphia: Lea & Febiger. x, 406 p.

111. Bitonti, A.J., et al., *Pulmonary delivery of an erythropoietin Fc fusion protein in non-human primates through an immunoglobulin transport pathway.* Proc Natl Acad Sci U S A, 2004. **101**(26): p. 9763-8.
112. Low, S.C., et al., *Oral and pulmonary delivery of FSH-Fc fusion proteins via neonatal Fc receptor-mediated transcytosis.* Hum Reprod, 2005. **20**(7): p. 1805-13.
113. Patton, J.S., *Pulmonary Polypeptide and Polynucleic Acid DeliveryMechanisms of macromolecule absorption by the lungs.* Advanced Drug Delivery Reviews, 1996. **19**(1): p. 3-36.
114. Bosquillon, C., *Drug transporters in the lung--do they play a role in the biopharmaceutics of inhaled drugs?* J Pharm Sci, 2010. **99**(5): p. 2240-55.
115. Schreier, H., et al., *Pharmacokinetics of detirelix following intratracheal instillation and aerosol inhalation in the unanesthetized awake sheep.* Pharm Res, 1994. **11**(7): p. 1056-9.
116. Fernandes, C.A. and R. Vanbever, *Preclinical models for pulmonary drug delivery.* Expert Opin Drug Deliv, 2009. **6**(11): p. 1231-45.
117. Brain, J.D., et al., *Pulmonary distribution of particles given by intratracheal instillation or by aerosol inhalation.* Environ Res, 1976. **11**(1): p. 13-33.
118. Osier, M. and G. Oberdorster, *Intratracheal inhalation vs intratracheal instillation: differences in particle effects.* Fundam Appl Toxicol, 1997. **40**(2): p. 220-7.
119. Schanker, L.S., E.W. Mitchell, and R.A. Brown, Jr., *Species comparison of drug absorption from the lung after aerosol inhalation or intratracheal injection.* Drug Metab Dispos, 1986. **14**(1): p. 79-88.
120. Hasegawa-Baba, Y., et al., *Intratracheal instillation methods and the distribution of administered material in the lung of the rat.* J Toxicol Pathol, 2014. **27**(3-4): p. 197-204.
121. Belpaire, F.M., M.G. Bogaert, and M. Rosseneu, *Binding of beta-adrenoceptor blocking drugs to human serum albumin, to alpha 1-acid*

glycoprotein and to human serum. Eur J Clin Pharmacol, 1982. **22**(3): p. 253-6.

122. Israili, Z.H. and P.G. Dayton, *Human alpha-1-glycoprotein and its interactions with drugs.* Drug Metab Rev, 2001. **33**(2): p. 161-235.
123. Belpaire, F.M., et al., *Binding to serum alpha 1-acid glycoprotein and effect of beta-adrenoceptor antagonists in rats with inflammation.* British journal of pharmacology, 1986. **88**: p. 697-705.
124. Suhara, T., et al., *Lung as reservoir for antidepressants in pharmacokinetic drug interactions.* Lancet, 1998. **351**(9099): p. 332-5.
125. International Transporter, C., et al., *Membrane transporters in drug development.* Nat Rev Drug Discov, 2010. **9**(3): p. 215-36.
126. Hines, R.N. and D.G. McCarver, *The ontogeny of human drug-metabolizing enzymes: phase I oxidative enzymes.* J Pharmacol Exp Ther, 2002. **300**(2): p. 355-60.
127. McCarver, D.G. and R.N. Hines, *The ontogeny of human drug-metabolizing enzymes: phase II conjugation enzymes and regulatory mechanisms.* J Pharmacol Exp Ther, 2002. **300**(2): p. 361-6.
128. Yang, J., et al., *Misuse of the well-stirred model of hepatic drug clearance.* Drug Metab Dispos, 2007. **35**(3): p. 501-2.
129. Upton, R.N. and D.J. Doolette, *Kinetic aspects of drug disposition in the lungs.* Clin Exp Pharmacol Physiol, 1999. **26**(5-6): p. 381-91.
130. Anttila, S., et al., *Expression and localization of CYP3A4 and CYP3A5 in human lung.* Am J Respir Cell Mol Biol, 1997. **16**(3): p. 242-9.
131. Krishna, D.R. and U. Klotz, *Extrahepatic metabolism of drugs in humans.* Clin Pharmacokinet, 1994. **26**(2): p. 144-60.
132. de Wet, C. and J. Moss, *METABOLIC FUNCTIONS OF THE LUNG.* Anesthesiology Clinics of North America, 1998. **16**(1): p. 181-199.
133. Boyer, J.L., *Bile formation and secretion.* Compr Physiol, 2013. **3**(3): p. 1035-78.
134. Boroujerdi, M., *Pharmacokinetics : principles and applications*. 2002, New York ; Toronto: McGraw-Hill, Medical Pub. Division. xix, 420 p.

135. Black, K.J., J.M. Koller, and B.D. Miller, *Rapid quantitative pharmacodynamic imaging by a novel method: theory, simulation testing and proof of principle.* PeerJ, 2013. **1**: p. e117.
136. Kumar, V.H., et al., *Prostacyclin and milrinone by aerosolization improve pulmonary hemodynamics in newborn lambs with experimental pulmonary hypertension.* J Appl Physiol (1985), 2010. **109**(3): p. 677-84.
137. Cortínez, L.I., *What is the ke0 and what does it tell me about propofol?* Anaesthesia, 2014. **69**(5): p. 399-402.
138. Ghoneim, M.M., *Drugs and human memory (part 2). Clinical, theoretical, and methodologic issues.* Anesthesiology, 2004. **100**(5): p. 1277-97.
139. Gabrielsson, J. and D. Weiner, *Non-compartmental analysis.* Methods Mol Biol, 2012. **929**: p. 377-89.
140. Gabrielsson, J. and D. Weiner, *Pharmacokinetic & pharmacodynamic data analysis : concepts and applications*. 4th ed. 2006, Stockholm, Sweden: Swedish Pharmaceutical Society. xiv, 1254 p.
141. Toutain, P.L. and A. Bousquet-Melou, *Plasma terminal half-life.* J Vet Pharmacol Ther, 2004. **27**(6): p. 427-39.
142. Bonate, P.L., *Pharmacokinetic-pharmacodynamic modeling and simulation*. 2006, New York: Springer. xii, 387 p.
143. Nguyen, A.Q., et al., *High performance liquid chromatography using UV detection for the quantification of milrinone in plasma: improved sensitivity for inhalation.* J Chromatogr B Analyt Technol Biomed Life Sci, 2009. **877**(7): p. 657-60.
144. Gavra, P., et al., *High-performance liquid chromatography assay using ultraviolet detection for urinary quantification of milrinone concentrations in cardiac surgery patients undergoing cardiopulmonary bypass.* Biomed Chromatogr, 2014. **28**(8): p. 1084-9.
145. Denault, A.Y., et al., *A multicentre randomized-controlled trial of inhaled milrinone in high-risk cardiac surgical patients.* Can J Anaesth, 2016.
146. Dhand, R., *Inhalation therapy in invasive and noninvasive mechanical ventilation.* Current opinion in critical care, 2007. **13**: p. 27-38.

147. Gurses, B.K. and G.C. Smaldone, *Effect of tubing deposition, breathing pattern, and temperature on aerosol mass distribution measured by cascade impactor.* J Aerosol Med, 2003. **16**(4): p. 387-94.
148. Hegg, D.A., et al., *An Instrument for Measuring Size-Resolved Aerosol Hygroscopicity at both Sub- and Super-Micron Sizes.* Aerosol Science and Technology, 2007. **41**(9): p. 873-883.
149. Bueltmann, M., et al., *Inhaled milrinone attenuates experimental acute lung injury.* Intensive care medicine, 2009. **35**: p. 171-8.
150. Das, P.A., et al., *Disposition of milrinone in patients after cardiac surgery.* Br J Anaesth, 1994. **72**(4): p. 426-9.
151. Bailey, J.M., et al., *Pharmacokinetics of intravenous milrinone in patients undergoing cardiac surgery.* Anesthesiology, 1994. **81**(3): p. 616-22.
152. De Hert, S.G., et al., *Comparison of two different loading doses of milrinone for weaning from cardiopulmonary bypass.* J Cardiothorac Vasc Anesth, 1995. **9**(3): p. 264-71.
153. Butterworth, J.F., et al., *A pharmacokinetic and pharmacodynamic evaluation of milrinone in adults undergoing cardiac surgery.* Anesth Analg, 1995. **81**(4): p. 783-92.
154. Benotti, J.R., et al., *Pharmacokinetics and pharmacodynamics of milrinone in chronic congestive heart failure.* Am J Cardiol, 1985. **56**(10): p. 685-9.
155. Edelson, J., et al., *Pharmacokinetics of the bipyridines amrinone and milrinone.* Circulation, 1986. **73**(3 Pt 2): p. III145-52.
156. Stroshane, R.M., et al., *Oral and intravenous pharmacokinetics of milrinone in human volunteers.* J Pharm Sci, 1984. **73**(10): p. 1438-41.
157. Patton, J.S., C.S. Fishburn, and J.G. Weers, *The lungs as a portal of entry for systemic drug delivery.* Proc Am Thorac Soc, 2004. **1**(4): p. 338-44.
158. Gavra, P., et al., *A specific and sensitive HPLC-MS/MS micromethod for milrinone plasma levels determination after inhalation in cardiac patients.* Ther Drug Monit, 2014. **36**(5): p. 663-8.

159. Giraudel, J.M., et al., *Pharmacokinetic/pharmacodynamic modelling of NSAIDs in a model of reversible inflammation in the cat.* Br J Pharmacol, 2005. **146**(5): p. 642-53.
160. Ito, H., et al., *Baroreflex Modifies the Effect of Vasodilators on Systemic Capacitance Vessel in Dogs*, in *Veins: Their Functional Role in the Circulation*, S. Hirakawa, et al., Editors. 1993, Springer Japan: Tokyo. p. 79-89.

Annexe I. Manuscript #5 (co-first author): High-performance liquid chromatography assay using ultraviolet detection for urinary quantification of milrinone concentrations in cardiac surgery patients undergoing cardiopulmonary bypass

Paul Gavra[a†], Anne QN. Nguyen[a†], Natasha Beauregard[a], André Y. Denault[b] and France Varin[a*]

[a] Faculté de pharmacie, Université de Montréal, Montréal, Canada

[b] Montreal Heart Institute, Montréal, Canada

[†] These authors contributed equally to this work.

Short title: HPLC method for urinary milrinone

* **Correspondence to:**

France Varin, Faculté de pharmacie, Université de Montréal, C.P. 6128, Succursale Centre-Ville, Montréal, QC, Canada H3C 3J7.

E-mail : france.varin@umontreal.ca

Telephone: 514 343-7016

Current status: Published in Biomedical Chromatography

Abbreviations used

CPB, cardiopulmonary bypass; CV, coefficient of variation; LLOQ, lower limit of quantification; QC, quality control; SPE, solid phase extraction.

Keywords

Milrinone; HPLC; Inhalation; Urine; Pharmacokinetics

Abstract

An analytical assay using liquid-liquid extraction and high-performance liquid chromatography with ultraviolet detection was developed for the quantification of total (conjugated and unconjugated) urinary concentrations of milrinone after the inhalation of a 5 mg dose in 15 cardiac patients undergoing cardiopulmonary bypass (CPB). Urine samples (700 µl) were extracted with ethyl-acetate and subsequently underwent acid back-extraction before and after deconjugation by mild acid hydrolysis. Milrinone was separated on a strong cation exchange analytical column. The mobile phase consisted of a constant mixture of acetonitrile: tetrahydrofurane-NaH_2PO_4 buffer (40:60 v/v, pH 3.0). Thirteen calibration curves were linear in the concentration range of 31.25-4000 ng/ml, using olprinone as the internal standard (r^2 range: 0.9911-0.9999, n = 13). Mean milrinone recovery and accuracy were respectively 85.2 ± 3.1% and ≥ 93%. Intra- and inter-day precisions (coefficients of variation, %) were ≤ 5% and ≤ 8%, respectively. Over a 24 h collection period, the cumulative urinary milrinone recovered from 15 patients was 26.1±7.7% of the nominal 5 mg dose administered. The relative amount of milrinone glucuronic acid conjugate was negligible in the urine of patients undergoing CPB This method proved to be reliable, specific and accurate to determine the cumulative amount of total milrinone recovered in urine after inhalation.

Introduction

Milrinone is a phosphodiesterase 3 inhibitor commonly used for its vasodilator effect in patients undergoing cardiac surgery to facilitate weaning from cardiopulmonary bypass (CPB) (Denault et al, 2006; Haddad et al, 2009). The pulmonary reperfusion syndrome often occurs during and after weaning from CPB and would result in pulmonary hypertension and right heart complications (Shafique et al, 1993). Intravenous milrinone is generally used as a treatment following CPB but its main drawback is the presence of systemic hypotension. Inhalation of milrinone using a nebulizer before CPB has been suggested as an alternative route of administration to reduce pulmonary pressure after CPB while avoiding systemic hypotension (Denault et al, 2006). Preliminary results from our laboratory indicate that the estimated delivered dose and systemic exposure after inhaled milrinone may vary up to twofold according to the type of nebulizer used (Nguyen et al, 2010). However, the cumulative amount of milrinone recovered in urine after inhalation in cardiac surgical patients undergoing CPB has not been characterized.

In healthy subjects, milrinone has been reported to be mainly excreted in the urine in two forms: unchanged (83%) and as an O-glucuronic acid conjugate (12%) (Primacor®). Alousi et al (1985), reported a similar mean extent of glucuronidation in dogs using radioactive compounds and separation by HPLC (15 %). Therefore, determination of the total amount of milrinone excreted in urine after nebulization would allow us to assess the systemic bioavailability after this highly variable route of administration. To the best of our knowledge, only three analytical methods have been published for the determination of milrinone in urine for studies in dogs (Edelson et al, 1983) and humans (Baranowska et al, 2011; Magiera et al, 2012). However, most of the reported assays have not been fully validated, were not reproducible under similar conditions, and used an internal standard that was commercially unavailable (Edelson et al, 1983). No validated method has been reported for the determination of milrinone in human urine.

The scope of this paper is to provide a validated high performance liquid chromatography (HPLC) assay using ultraviolet (UV) detection for the quantification of milrinone total urinary concentration after inhalation and determine the relative amount of its O-glucuronic acid conjugate form in cardiac surgical patients undergoing CPB.

Methods

Chemicals and reagents

Milrinone standard (99.2 % pure) was kindly provided by Sandoz (Boucherville, QC, CAN). The internal standard, olprinone, was purchased from Toronto Research Chemicals (Toronto, Ont, CAN). An O-glucuronic acid reference standard for milrinone was not available. Chemical structures are illustrated in Fig. 1. All solvents and reagents used were of HPLC grade. The mobile phase was filtered through a 0.22 µm type HVLP membrane before use (Millipore, Billerica, MA, USA). Ultrahigh purified water was obtained from Milli-Q water dispensing system by Millipore Corporation (Billerica, MA, USA).

Chromatographic conditions

The HPLC analysis was performed on an Agilent HP1200 series HPLC system (Agilent Technologies, Santa-Clara, CA, USA) equipped with a multiple solvent delivery system and a variable wavelength UV/visible detector. Chromatographic separations were carried on a Waters Spherisorb strong cation exchange column (150 mm X 4.6 mm I.D., 5 µm HiChrom Ltd., Reading, Berkshire, UK) protected by a security filter system. The mobile phase consisted of a mixture of acetonitrile and tetrahydrofurane-NaH_2PO_4 buffer (40:60 v/v) delivered at 1.6 ml/min with a run time of 5.5 min. Tetrahydrofurane was added to 0.05M NaH_2PO_4 buffer (pH 3.0) immediately before HPLC analysis to obtain the final tetrahydrofurane-NaH_2PO_4 buffer (5:218, v/v). The chromatography was performed at ambient temperature. Injection volume was 120 µl and UV detection at 325 nm. Chromatographic peaks were integrated by the ChemStation software (Agilent Technologies, Santa-Clara, CA, USA).

Stock and working standard solutions

Stock solutions (1 mg/ml) of milrinone were prepared in methanol and stored at -20˚C. A stock solution of olprinone (1 mg/ml) was aliquoted in water and stored

at -20˚C. Working solutions of both stock solutions were prepared in water. The phosphate buffer used for sample preparation was adjusted to pH 7.4 by mixing stock 0.5M KH_2PO4 and 0.5M Na_2HPO_4 solutions. The neutralizing solution used for ending incubation and neutralising after the acid back-extraction was prepared by adding 0.6 ml 10N NaOH to 9.4 ml of phosphate buffer (0.5M, pH 7.0).

Calibration and quality control samples

Eight milrinone calibration standards, 31.25 (lower limit of quantification, LLOQ), 62.5, 125, 250, 500, 1000, 2000 and 4000 ng/ml were used to establish calibration curves in urine. Calibration samples were prepared by serial 1:1 dilutions with previously screened blank healthy subject urine. Calibration curves were generated by plotting the analyte/internal standard peak-height ratio against nominal milrinone concentration. Quality control (QC) samples were prepared by spiking blank healthy subject urine with milrinone stock solutions to obtain final concentrations of 160 and 1600 ng/ml. Prior to extracted-sample analysis, milrinone and internal standard daily retention times were assessed by injecting *in vitro* samples containing each standard.

Urine samples preparation

Acid deglucuronidation. Since no O-glucuronic acid conjugate was available for milrinone, we established the optimal conditions for hydrolysis using urine samples collected from several end-stage renal failure patients having received inhaled milrinone before CPB. These patients were expected to have higher levels of the conjugate and acted as positive controls. We compared the results obtained at 65°C after various incubation times (up to 24 h) under mild acid conditions (pH ≈ 1.5) with those obtained using *Helix pomatia* β-glucuronidase (Sigma Chemicals, St-Louis, Mo, USA) enzymatic hydrolysis. A duration of 24 h for mild acid hydrolysis yielded the same results as the optimal enzymatic hydrolysis conditions (5,000 Units, 6 h, 45°C). Stability of both milrinone and olprinone under these mild acid hydrolysis conditions was then verified. ANOVA

analysis showed that the effects of temperature and/or acidity were not statistically significant.

Urine samples (700 µl) obtained from patients treated with milrinone (please refer to clinical application) and calibration standards were added 100 µl of internal standard and 200 µl of HCL 0.5N before incubation at 65˚C for 24 hours. Incubation was ended by placing samples on ice and transferring 600 µl in a glass vial containing 50 µl of neutralising solution. For non-incubated samples, the 0.5N HCL and neutralising solutions were replaced with purified water for a similar preparation of samples prior to extraction.

Extraction. Following incubation 500 µl of sample was pipetted into 250 µl of phosphate buffer, 100 µl of internal standard and 5 ml of ethyl acetate. The samples were then shaken for 15 min, centrifuged (*IEC Centra-8R* centrifuge) at 3200 rpm (1280 g) for 15 min and placed at -70˚C for 20 min. The ethyl acetate layer was transferred in a clean 15 ml conical tube containing 400 µl of HCl 0.1N. The samples were vortexed for 1 min, centrifuged (*IEC Centra-8R* centrifuge) for 10 min at 3200 rpm (1280 g) and the ethyl acetate was subsequently discarded. Thus 25 µl of neutralising solution were added to 300 µl of the acidified phase and 120 µl was injected in the HPLC.

Method validation. The analytical method was validated for selectivity, linearity, sensitivity, extraction recovery, precision, accuracy, matrix effects and stability according to US Food and Drug Administration (FDA) guidance for bioanalytical method validation (2001).

Selectivity. Blank drug-free urine samples were obtained from two healthy subjects and 28 urine samples were obtained immediately before inhalation of milrinone (pre-dose) in patients undergoing cardiac surgery. Matrix effects for analytes were evaluated through comparison of samples from direct injections of standard solutions, known-concentration spiked healthy subject samples and patient samples. Samples were assayed to determine whether endogenous

urine components or anesthesia medication cause interferences at the retention times of the analyte or internal standard. To this end, chromatograms of blank samples (healthy subjects and patients) were compared to milrinone and olprinone-containing samples.

Linearity. Eight calibration standards (31.25 – 4000 ng/ml) covering the expected clinical range were prepared in urine. Linearity was assessed using a weighted least square linear regression ($1/x^2$ nominal).

Sensitivity. Milrinone was spiked at a concentration of 31.25 ng/ml (LLOQ) in healthy subject urine and was extracted and injected on 8 different days (inter-day).

Recovery. Four replicate sets of samples spiked at 60, 160 and 1600 ng/ml were prepared. Recovery was assessed by comparing the peak height ratio of milrinone spiked prior and after extraction. Recovery of the internal standard was also determined by comparing the peak heights of four extracted samples with the internal standard spiked prior and after extraction.

Precision and accuracy. The intra-assay precision and accuracy were assessed in urine as follows: 60, 160 and 1600 ng/ml QC concentrations were assayed in replicates of four. All samples were assayed on the same day and their back-calculated concentration determined from a calibration curve prepared the same day. Inter-assay precision and accuracy were assessed as follows: 60, 160 and 1600 ng/ml QC concentrations were assayed in duplicate for each calibration curve. One curve with its respective QC samples was assayed per day for a total of 13 calibration curves over 13 different days. Precision was expressed as the coefficient of variation (CV, %) and accuracy as the percent bias (%). Accuracy was determined by comparing the calculated concentration of the extracted milrinone urine standard with the nominal concentration of milrinone.

Stability. Short-term bench stability was verified in four replicates of urine standards (160 and 1600 ng/ml) thawed at room temperature for 24h before analysis. For the freeze-thaw cycle stability studies, four aliquots (160 and 1600 ng/ml) were prepared and frozen at -70˚C for 24h. The samples were thawed unassisted at room temperature and analyzed alongside fresh samples of the same concentration. The samples were refrozen for 24h under the same conditions and the freeze-thaw cycle was repeated one more time before reanalysis. Processed samples stability was also tested for extracts (160 and 1600 ng/ml) stored in the refrigerator for 24h and remained in the autosampler for 24h. Results were compared with those obtained for the freshly prepared samples.

Clinical application

Following permission from Health Canada (clinical trial application) and approval by the local ethics committee, informed consent was obtained from all participating subjects. As part of the protocol, milrinone concentrations in urine were determined for 15 patients having inhaled 5 mg of the study drug prior to initiation of CPB and cardiac surgery. Urine was collected over different intervals (n = 4-7), before drug administration, before CPB, post CPB, post-surgery and for a period of 24 hours post-nebulization and samples were stored at -70˚C until analysis. Pre-dose urine samples were verified to be free of endogenous or drug interferences under the anesthetic and surgical procedure. In order to determine the relative amount of milrinone's O-glucuronic acid conjugate form in cardiac surgical patients undergoing CPB, the amount of milrinone (total and free) was quantified in urine collected after milrinone administration by analysing all samples, once with and once without incubation, alongside their respective and similarly treated standard curves. Systemic bioavailability after inhaled milrinone was estimated by comparing the dose recovered in urine after 24 hours with the nominal dose (5 mg) initially administered to the patient.

Results and Discussion

Method optimization

The bioavailability and pharmacokinetics of inhaled milrinone have never been described but are expected to be highly variable due to the inherent losses of the drug delivery method. In pharmacokinetic studies involving inhaled drugs, due to these losses, an estimation of the percentage of the nominal dose actually being delivered to patients is required. In the case of milrinone, the molecule being excreted mostly unchanged or conjugated, measurement of total urinary excretion allows for a realistic approximation of the delivered dose. The purpose of this paper was to provide a low-cost, rapid and validated method for the quantification of total amount of milrinone in human urine.

A few analytical methods were available for determination of milrinone in urine. Recently, Magiera et al (Magiera et al, 2012) and Baranowska (Baranowska et al, 2011) described metamethods using solid-phase extraction (SPE) followed by UHPLC-UV and liquid-liquid extraction followed by UHPLC–ESI-MS/MS quantification, respectively. These methods required highly specialized and expensive equipment that offered a sensitivity level considered unnecessary to determine milrinone urine levels after commonly administered dose (50-80 µg/kg). Furthermore, being metamethods, they are not focused on the milrinone determination, resulting in longer running times. The HPLC-UV method described by Edelson et al (Edelson et al, 1983) for their pharmacokinetic study consisted of a liquid-liquid extraction followed by an acid back-extraction and separation on a C18 analytical column. The latter method was used as a starting point for our method optimization. A major drawback of the Edelson et al (Edelson et al, 1983) assay was their internal standard (1,6-dihydro-2-ethyl-6-oxo-(3,4'-bypiridine)-5-carbonitrile) that, to our knowledge, is not commercially available.

Several potential candidates for our internal standard were screened: carbamazepine, amrinone, propranolol and finally olprinone. The mobile phase

composition that allowed adequate separation of carbamazepine from the solvent front drastically reduced milrinone sensitivity. During validation procedures, patient samples spiked with amrinone showed a systematic bias when compared to calibration standards prepared in subjects' blank urine. Although propranolol recovery was 63.5 ± 1.8 %, its absorbance signal at 325 nm was found too low compared to that of milrinone (optimal propranolol concentration for acceptable signal was 100 000 ng/ml of diluted urine). Olprinone had no interferences and showed consistency in absorbance signal at 325 nm between subjects and patients. Thus, with its sufficient recovery, olprinone was considered the most reliable and suitable internal standard. As the urinary concentrations of milrinone were expected to be relatively high after a dose of 5 mg, sensitivity was not deemed an issue and the volume of sample used for extraction was reduced to use less ethyl acetate and facilitate manipulation. In order to shorten the analysis time, our extraction method does not concentrate the sample, which resulted in a slightly lower recovery of milrinone but saved an hour of manipulation time while reducing baseline signal noise. When compared to Edelson et al (Edelson et al, 1983), our assay is fully validated using a commercially available internal standard, presents a shorter run time (5.5 versus 8 min), a slightly lower recovery (85 % vs 90 %), and an increased sensitivity (LLOQ = 31.25 vs 50 ng/ml).

Assay validation

Selectivity. Chromatograms of a healthy subject blank sample, a cardiac patient blank, a healthy subject blank spiked at 31.25 ng/ml (calibration standard, LLOQ) and a cardiac patient sample are shown in Fig. 2. The blank healthy subject urine used for each calibration curve (not necessarily in the fasted state) and urine sampled from each patient undergoing cardiac surgery (prior to milrinone administration) were analyzed and shown to be free of any interference. No matrix effects for milrinone and olprinone were observed. Variations in day-to-day elution times were the following: between 2.4 and 2.7 min for milrinone and between 4.4 and 4.6 min for the internal standard.

Linearity. Calibration curves of milrinone in urine were linear from 31.25 to 4000 ng/ml with a mean coefficient of determination (r^2) of 0.9964 (n = 8; range: 0.9911-0.9999).

Sensitivity. Mean inter-assay precision and accuracy for the LLOQ (31.25 ng/ml) were 2.3 % and 99 %, respectively (n = 13). The LLOQ's signal amplitude was found to be more than 10 times that of the baseline noise.

Recovery. Mean recoveries of milrinone for the 60, 160 and 1600 ng/ml concentrations were 86.3, 84.1 and 84.8 % (n = 4), respectively. The mean recovery of the internal standard was 63.5 % (n = 4).

Precision and accuracy. Intra and inter-assay precision and accuracy results are summarized in Table 1. Intra-assay precision study revealed a CV < 5 % (n = 4) for milrinone concentrations and accuracy ranged from 94 to 99 %. Inter-assay precision study revealed a CV < 8 % (n = 16) for milrinone concentrations and accuracy ranged from 92 to 100 %.

Stability. For the short-term stability, accuracy ranged from 97 to 102 %. Accuracy ranged from 93 to 102 % after two freeze-thaw cycles. For the processed samples stability, accuracy following storage of extracts in the refrigerator and in the autosampler varied between 100 and 103 %.

Clinical application

Deglucuronidation. A mean cumulative amount of 1.103 mg ± 0.426 and 1.099 mg ± 0.403 were determined for free and total urinary milrinone, respectively. Individual percentages of glucuronic acid conjugate varied between - 8.9 % and 19 % (mean: - 0.6%) of the cumulative total amount measured. These results indicate that the amount of milrinone O-glucuronic acid conjugate in urine was negligible in our cardiac patients A mean extent of 12 % for O-glucuronidation has been reported in healthy volunteers (Primacor®). Alousi et al (Alousi et al,

1985) reported using a mild acid hydrolysis without providing neither a description of the incubation conditions nor of the between subject variability in the content of the glucuronic acid conjugate.

In some of our patients, negative deconjugation results were obtained which, in our opinion, could be explained by the experimental error of our analytical assay. Furthermore, it has been reported that lysosomal enzyme release occurs during cardiopulmonary bypass in man, resulting in an increase of 35% in the activity of β-glucuronidase (Gnanadurai et al, 1977). This release of lysosomal enzymes originates from damaged renal cells (Hashimoto et al, 1993). This factor may also have contributed in reducing the O-glucuronic acid conjugate fraction in our cardiac patients undergoing CPB.

Urinary pharmacokinetics. In our 15 patients, the mean cumulative amount of milrinone recovered in urine was 26.1 ± 7.7% of the nominal 5 mg dose administered. The urinary pharmacokinetic profiles of free and total (free and conjugated) milrinone obtained from a patient having received 5 mg of milrinone inhaled over 20 min is shown in Fig. 3. In this patient, the free and total amount of milrinone recovered in urine over the 24 hour period were 1.128 and 1.238 mg, respectively; corresponding to 24.8 % of the initially nebulized dose (5 mg). In a previous *in vitro* study (Nguyen et al, 2009), our group tested the performance of the mesh nebulizer and quantified the overall loss of drug in the apparatus. In this study, the mean amount of milrinone delivered at the end of the endotracheal tube was estimated at 40 % of the initially nebulized dose (5mg). Although estimation of overall loss is not feasible *in vivo*, these results are compatible with the low percentage of milrinone recovered (relative to nominal dose) from the urine in our patients. Combined urinary and plasma pharmacokinetics are essential to shed light on this highly variable route of administration. In future pharmacokinetic studies, this method will prove helpful to assess the absolute or relative bioavailability after milrinone inhalation.

Conclusion

A highly selective, rapid and low-cost HPLC assay with UV detection has been optimized and validated for the determination of total amount of milrinone in human urine. The method is simple and uses a commercially available internal standard. It was successfully applied to determine the systemic bioavailability and urinary pharmacokinetic profile of milrinone after inhalation in cardiac surgical patients undergoing CPB.

Acknowledgements

This study was supported by the Fonds de la Recherche en Santé du Québec (FRSQ) and Groupe de Recherche Universitaire sur le Médicament de l'Université de Montréal (GRUM). A doctoral award (Frederick Banting and Charles Best Canada Graduate Scholarships) was granted to Anne QN Nguyen by the Canadian Institutes of Health Research.

Tables

Table 1. Intra and inter-assay precision and accuracy results. C.V.

	Intra-assay		Inter-assay	
	160 ng/ml	**1600 ng/ml**	**160 ng/ml**	**1600 ng/ml**
n	4	4	21	20
Mean ± S.D. (ng/ml)	151.0 ± 6.8	1587.6 ± 35.8	170.1 ± 12.9	1599.5 ± 115.8
C.V. (%)	4.5	2.3	7.6	7.2
% bias	- 5.6	-0.8	6.3	0.0

Figures

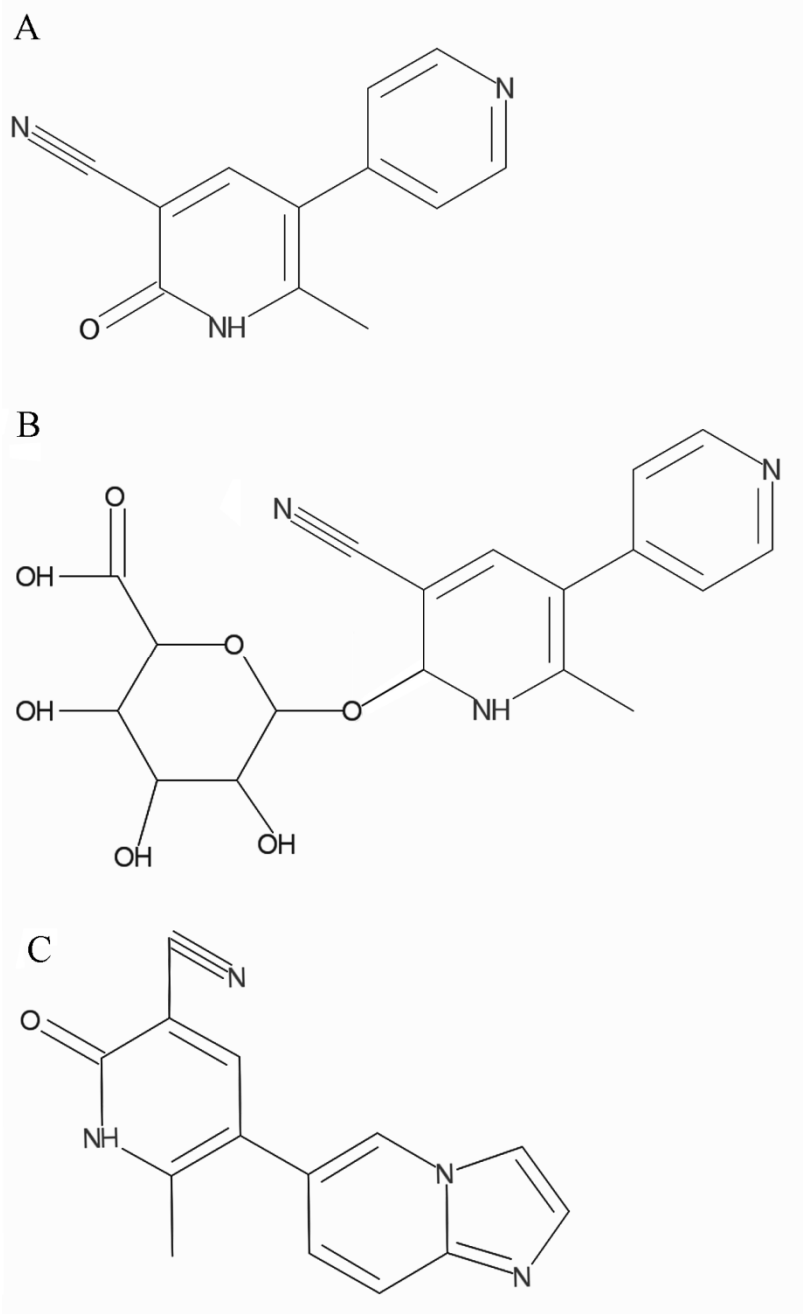

Fig 1. Chemical structures of A, milrinone, B, the O-glucuronic acid milrinone conjugate and C, the internal standard olprinone.

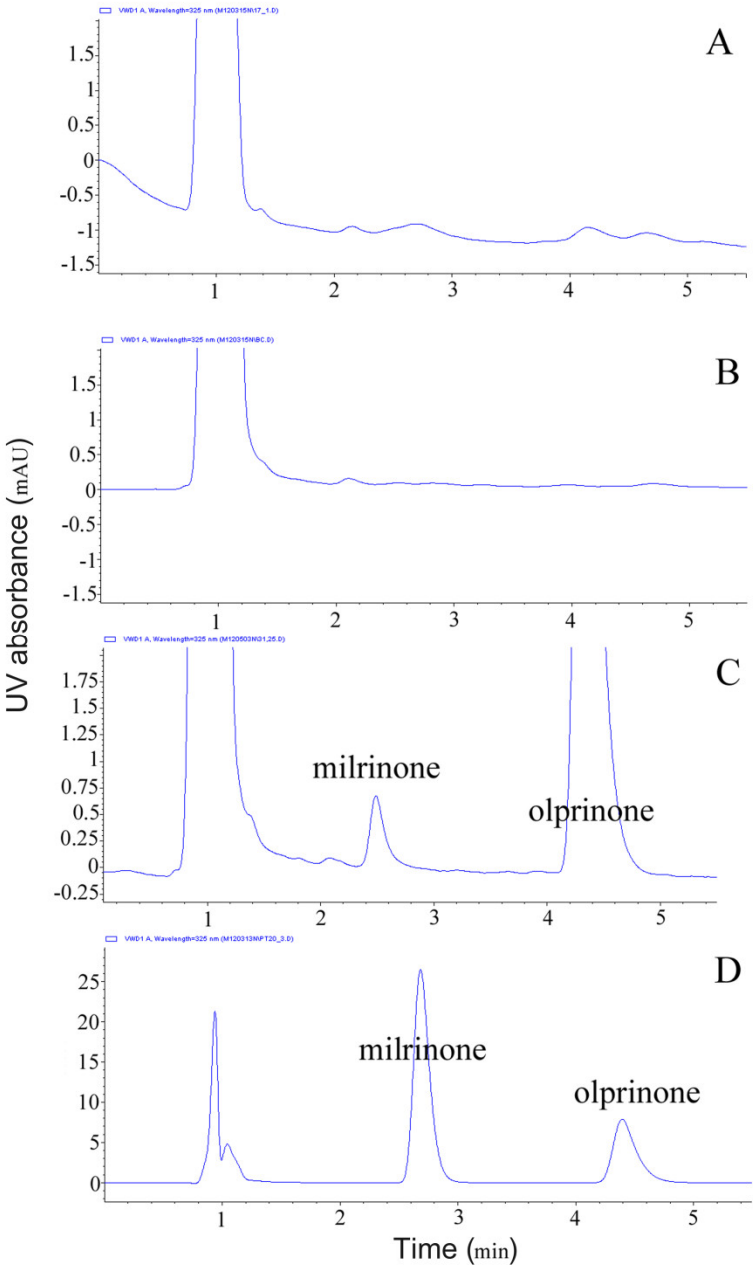

Fig 2. Typical HPLC chromatograms of urinary extracts from (a) blank subject sample, (b) blank cardiac patient sample, (c) milrinone-spiked (31.21 ng/ml, LLOQ) urine calibration standard (d) cardiac patient sample after inhalation of a 5 mg milrinone dose over 20 minutes (1278.5 ng/ml).

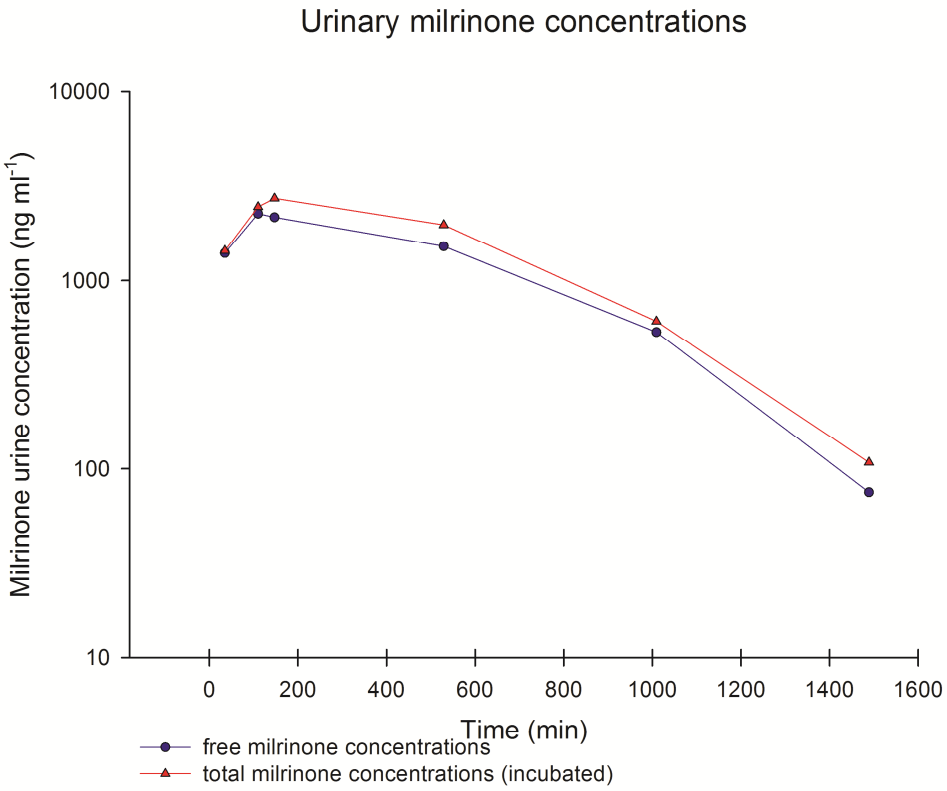

Fig. 3. Urinary pharmacokinetic profile of a patient having received 5 mg of milrinone inhaled over 20 min.

References

Alousi AA, Fabian JR, Baker FJ, Stroshane MR. Milrinone. New Drugs Annual: Cardiovascular Drugs. 1985;3:39.

Baranowska I, Magiera S, Baranowski J. UHPLC method for the simultaneous determination of beta-blockers, isoflavones, and flavonoids in human urine. Journal of chromatographic science. 2011 Nov-Dec;49(10):764-73.

Denault AY, Lamarche Y, Couture P, Haddad F, Lambert J, Tardif JC, et al. Inhaled milrinone: a new alternative in cardiac surgery? Seminars in cardiothoracic and vascular anesthesia. 2006 Dec;10(4):346-60. 10.1177/1089253206294400

Edelson J, Koss RF, Baker JF, Park GB. High-performance liquid chromatographic analysis of milrinone in plasma and urine. Intravenous pharmacokinetics in the dog. Journal of chromatography. 1983 Sep 9;276(2):456-62.

Gnanadurai TV, Branthwaite MA, Colbeck JF, Welman E. Lysosomal enzyme release during cardiopulmonary bypass. Anaesthesia. 1977 Sep;32(8):743-8.

Haddad F, Couture P, Tousignant C, Denault AY. The right ventricle in cardiac surgery, a perioperative perspective: II. Pathophysiology, clinical importance, and management. Anesthesia and analgesia. 2009 Feb;108(2):422-33. 10.1213/ane.0b013e31818d8b92

Hashimoto K, Nomura K, Nakano M, Sasaki T, Kurosawa H. Pharmacological intervention for renal protection during cardiopulmonary bypass. Heart and vessels. 1993;8(4):203-10

Magiera S, Baranowska I, Kusa J. Development and validation of UHPLC-ESI-MS/MS method for the determination of selected cardiovascular drugs, polyphenols and their metabolites in human urine. Talanta. 2012 Jan 30;89:47-56. 10.1016/j.talanta.2011.11.055

Nguyen AQN, Denault AY, Perrault LP, Varin F. Exploratory PK/PD study after inhaled milrinone in cardiac patients. Canadian Journal of Anesthesia/Journal canadien d'anesthésie. 2010;57(S1):19. 10.1007/s12630-010-9415-0

Nguyen AQN, Denault AY, Perrault LP, Varin F, editors. In vivo-in vitro correlation between early systemic exposure and delivered dose of inhaled milrinone using two types of nebulizers. American Conference on Pharmacometrics; 2009 2009. The AAPS Journal: The AAPS Journal; 2009.

Nguyen AQN, Théorêt Y, Chen C, Denault AY, Varin F. High performance liquid chromatography using UV detection for the quantification of milrinone in plasma: improved sensitivity for inhalation. Journal of chromatography B, Analytical technologies in the biomedical and life sciences. 2009 Mar 1;877(7):657-60. 10.1016/j.jchromb.2009.01.024

Primacor® Product Information [Internet]. Primacor® [cited 2013 nov 07]. Available from: http://products.sanofi.com.au/aus_pi_primacor.pdf

Shafique T, Johnson RG, Dai HB, Weintraub RM, Sellke FW. Altered pulmonary microvascular reactivity after total cardiopulmonary bypass. The Journal of thoracic and cardiovascular surgery. 1993 Sep;106(3):479-86.

US Food and Drug Administration. FDA Guidance for Industry: Bioanalytical Method Validation. US Department of Health and Human Services, Food and Drug Administration, Center for Drug Evaluation and Research: Rockvile, MD, 2001

Annexe II. Excerpt of manuscript #6: Multicentered Randomized Controlled Trial of Inhaled Milrinone in High-Risk Cardiac Surgical Patients

André Y. Denault, MD PhD,[a] Jean S. Bussières MD,[b] Ramiro Arellano MD MSc,[c] Barry Finegan,[d] Paul Gavra, François Haddad, MD,[e] Anne Q.N. Nguyen,[f] France Varin, PhD,[f] Annick Fortier, MSc,[g] Sylvie Levesque, MSc,[g] Yanfen Shi, MD,[h] Masha Elmi-Sarabi,[a] Jean-Claude Tardif, MD,[h] Louis P. Perrault, MD, PhD,[i] and Jean Lambert, PhD[g]

From the Departments of [a]Anesthesia, [h]Medicine, [i]Cardiac Surgery, Montreal Heart Institute; [f] Faculty of Pharmacy, Université de Montréal; the [g]Montreal Health Innovations Coordinating Center (MHICC), Montreal, Canada; [b]Department of Anesthesiology, Institut Universitaire de Cardiologie et de Pneumologie de Québec, Canada; [c]Department of Anesthesiology, Kingston Hospital, Queens University, Canada; [d] Department of Anesthesiology, Edmonton Heart Institute, University of Alberta, Edmonton, Canada; [e]Department of Cardiology, Stanford Cardiovascular Institute,
Stanford USA

Methods excerpt

Pharmacokinetic and pharmacodynamics sub-study.

This sub-study involved patients from only one of the four centers, The Montreal Heart Institute (n=45).In order to study the milrinone blood concentration, six arterial blood samples (5 mL) were collected into heparinized tubes from patients having received either milrinone (n=22) or saline (n=23). Samples were drawn before drug administration (0 min) and at approximately 10, 15, 20, 25 and 30 min after the start of milrinone or saline nebulization. Samples were kept in an ice-water bath until centrifugation (15 min, 1900g). Plasma was frozen at -70°C until HPLC-MS/MS analysis (Gavra et al, 2014) after the completion of the study. Hemodynamic parameters (MAP and mPAP) were taken at times corresponding to blood collection and the MAP/mPAP ratio was calculated. Non-compartmental analysis (NCA) was subsequently performed on pharmacokinetic (PK) and pharmacodynamics (PD) data using Phoenix™ (Certara, St. Louis, MO). NCA was executed using, respectively plasma, (200 – 202) and drug effect (220) models with uniform weighting and intravenous infusion dosing. Peak concentration (C_{max}) and their corresponding time (T_{max}) were determined. To calculate areas under the curve (AUC), a linear-linear trapezoidal method was used for both PK and PD data beginning at the start of nebulization until the time point corresponding to maximum concentration ($AUC_{0\text{-}Tmax}$). For the calculation of AUC for the PD data, both positive and negative fluctuations from the predetermined baseline response (R0; reference value) were taken into account during integration, yielding a net AUC. The relationship between corresponding individual AUCs and AUC was then investigated.

AUC analysis was also performed in the same fashion for the PD data of the control group from beginning to end of nebulization time.

Results excerpt

Pharmacokinetic and pharmacodynamics sub-study.

Pharmacokinetic and pharmacodynamic data were available for 19 and 18 patients of the milrinone sub-group respectively. Average C_{max} and T_{max} were 86.8±38.8 ng/ml and 20.5±6.5 minutes respectively (n=19). Pharmacodynamic data (hemodynamic parameters) was available for 18 patients of the milrinone sub-group. The mean area under the curve between time 0 (beginning of nebulization) and T_{max} (AUC0- T_{max}) for plasma concentrations and MAP/MPAP ratio were 1258±559 ng*min/ml (n=19) and 3.94±2.06 (n=18) respectively. During this time period, a positive correlation was found between the AUC0- T_{max} of plasma concentrations and the AUC of the ratio (r2= 0.414, p= 0.004, Fig). In 10 patients, an increase of more than 20% of their MAP/MPAP ratio was observed. An example of two different patients is shown in figure 3. The mean AUC0- T_{max} for the ratio of the control group was -0.287±2.93 (n=18) which was significantly lower ($p<0.0001$) than that of the milrinone group.

Figures

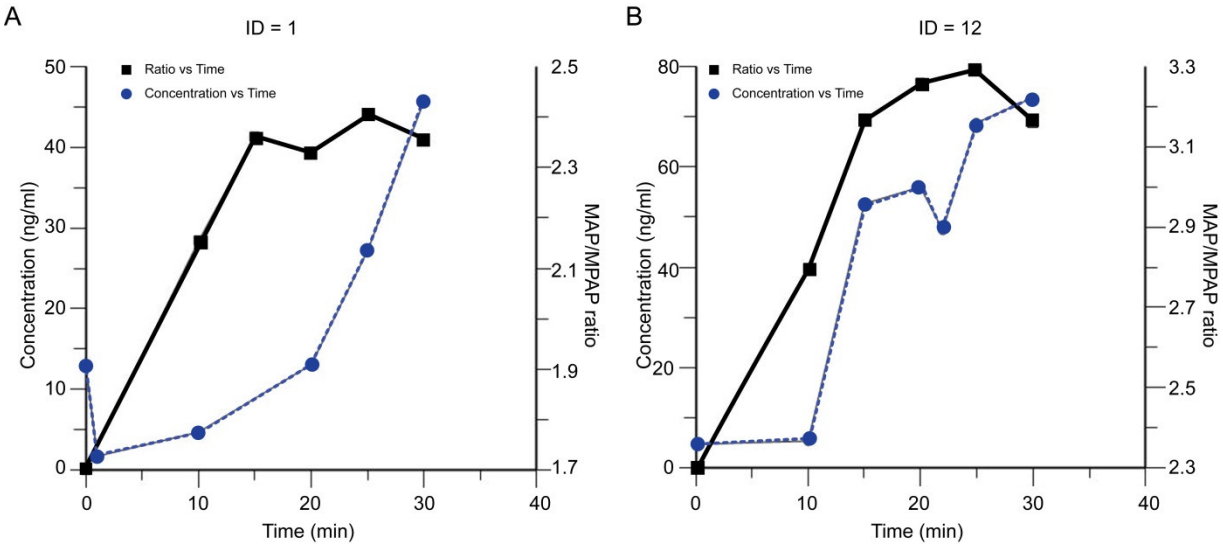

Figure 3 Patient #1 and #12 concentration on the X axis in relation to the mean arterial pressure (MAP) over the mean pulmonary artery (MPAP) ratio on the Y axis.